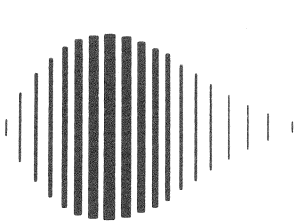

NATIONAL CENTER FOR EARTHQUAKE
ENGINEERING RESEARCH
State University of New York at Buffalo

Experimental and Analytical Investigation of Seismic Response of Structures with Supplemental Fluid Viscous Dampers

by

M. C. Constantinou and M. D. Symans
State University of New York at Buffalo
Department of Civil Engineering
Buffalo, New York 14260

Technical Report NCEER-92-0032

December 21, 1992

This research was conducted at the State University of New York at Buffalo and was partially supported by the National Science Foundation under Grant No. BCS 90-25010 and the New York State Science and Technology Foundation under Grant No. NEC-91029.

NOTICE

This report was prepared by the State University of New York at Buffalo as a result of research sponsored by the National Center for Earthquake Engineering Research (NCEER) through grants from the National Science Foundation, the New York State Science and Technology Foundation, and other sponsors. Neither NCEER, associates of NCEER, its sponsors, the State University of New York at Buffalo, nor any person acting on their behalf:

a. makes any warranty, express or implied, with respect to the use of any information, apparatus, method, or process disclosed in this report or that such use may not infringe upon privately owned rights; or

b. assumes any liabilities of whatsoever kind with respect to the use of, or the damage resulting from the use of, any information, apparatus, method or process disclosed in this report.

Any opinions, findings, and conclusions or recommendations expressed in this publication are those of the author(s) and do not necessarily reflect the views of the National Science Foundation, the New York State Science and Technology Foundation, or other sponsors.

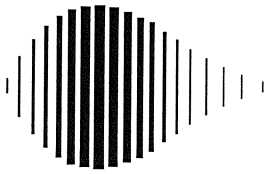

Experimental and Analytical Investigation of Seismic Response of Structures with Supplemental Fluid Viscous Dampers

by

M.C. Constantinou[1] and M.D. Symans[2]

December 21, 1992

Technical Report NCEER-92-0032

NCEER Project Number 90-2101

NSF Master Contract Number BCS 90-25010
and
NYSSTF Grant Number NEC-91029
and
NSF Grant Number BCS 88-57080

1 Associate Professor, Department of Civil Engineering, State University of New York at Buffalo
2 Graduate Student, Department of Civil Engineering, State University of New York at Buffalo

NATIONAL CENTER FOR EARTHQUAKE ENGINEERING RESEARCH
State University of New York at Buffalo
Red Jacket Quadrangle, Buffalo, NY 14261

PREFACE

The National Center for Earthquake Engineering Research (NCEER) was established to expand and disseminate knowledge about earthquakes, improve earthquake-resistant design, and implement seismic hazard mitigation procedures to minimize loss of lives and property. The emphasis is on structures in the eastern and central United States and lifelines throughout the country that are found in zones of low, moderate, and high seismicity.

NCEER's research and implementation plan in years six through ten (1991-1996) comprises four interlocked elements, as shown in the figure below. Element I, Basic Research, is carried out to support projects in the Applied Research area. Element II, Applied Research, is the major focus of work for years six through ten. Element III, Demonstration Projects, have been planned to support Applied Research projects, and will be either case studies or regional studies. Element IV, Implementation, will result from activity in the four Applied Research projects, and from Demonstration Projects.

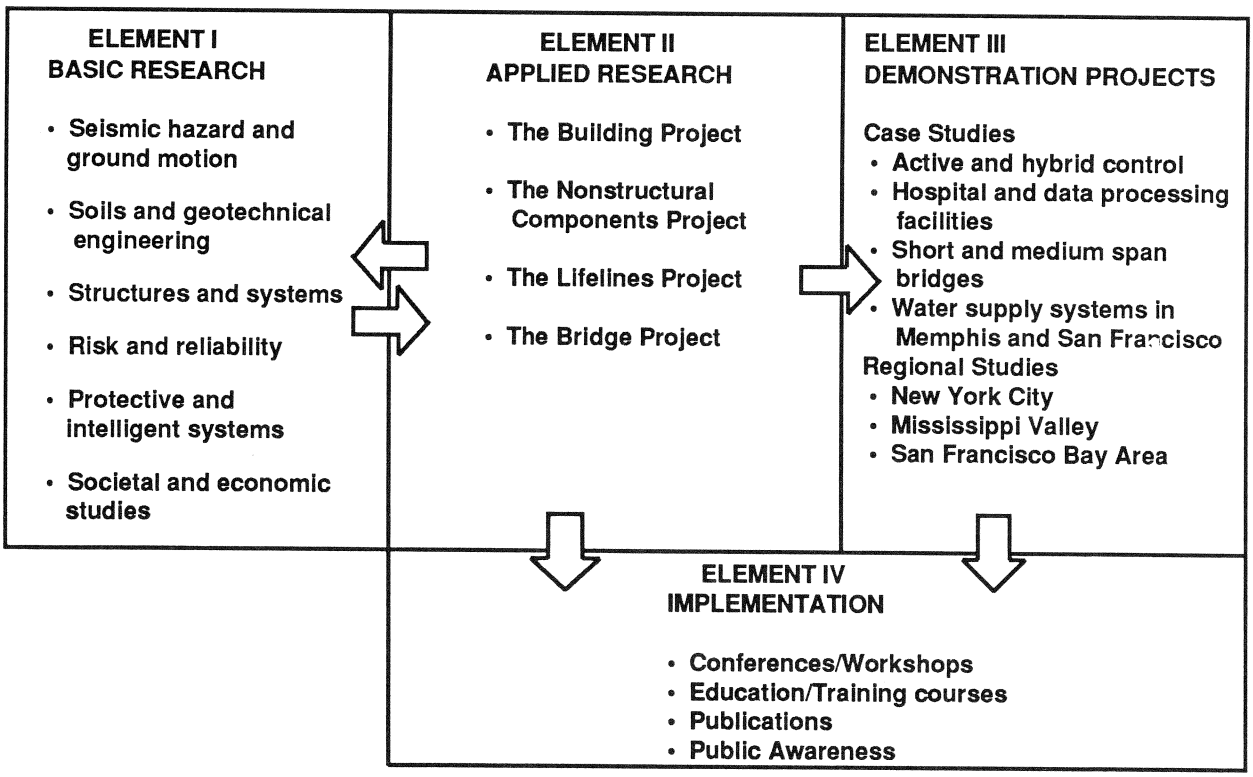

Research in the **Building Project** focuses on the evaluation and retrofit of buildings in regions of moderate seismicity. Emphasis is on lightly reinforced concrete buildings, steel semi-rigid frames, and masonry walls or infills. The research involves small- and medium-scale shake table tests and full-scale component tests at several institutions. In a parallel effort, analytical models and computer programs are being developed to aid in the prediction of the response of these buildings to various types of ground motion.

Two of the short-term products of the **Building Project** will be a monograph on the evaluation of lightly reinforced concrete buildings and a state-of-the-art report on unreinforced masonry.

The **protective and intelligent systems program** constitutes one of the important areas of research in the **Building Project**. Current tasks include the following:

1. Evaluate the performance of full-scale active bracing and active mass dampers already in place in terms of performance, power requirements, maintenance, reliability and cost.
2. Compare passive and active control strategies in terms of structural type, degree of effectiveness, cost and long-term reliability.
3. Perform fundamental studies of hybrid control.
4. Develop and test hybrid control systems.

Recently, a number of innovative passive damping devices have been studied analytically and experimentally, both at NCEER and elsewhere, for structural applications in order to improve their seismic response performance. In this report, the performance of a fluid viscous damper has been investigated through component tests and earthquake simulation tests performed on one-story and three-story steel structures both with and without dampers. It is shown that the addition of supplemental dampers significantly reduces the structural response in terms of both interstory drifts and shear forces.

ABSTRACT

Many different supplemental energy dissipating devices have been proposed to assist in mitigating the harmful effects of earthquakes on structures. This report presents the results of a study on fluid viscous dampers.

A series of component tests with various dynamic inputs have been performed to determine the mechanical characteristics and frequency dependencies of the damper. In addition, temperature dependencies have been considered by varying the ambient temperature of the damper during component testing. Based on the component tests, a mathematical model has been developed to describe the macroscopic behavior of the damper.

Earthquake simulation tests have been performed on one-story and three-story steel structures both with and without dampers. The addition of supplemental dampers significantly reduces the response of the structure in terms of both interstory drifts and shear forces. The experimental response has been compared with the analytical response where the mathematical model of the damper is used to develop the equations of motion. The comparisons show very good agreement.

ACKNOWLEDGEMENTS

Financial support for this project has been provided by the National Center for Earthquake Engineering Research (Project No. 90-2101) and the National Science Foundation (Grant No. BCS 8857080). Taylor Devices, Inc., N. Tonawanda, NY, manufactured and donated the dampers used in the experiments. Special thanks are given to Mr. Douglas Taylor, President of Taylor Devices, Inc., for his invaluable assistance.

TABLE OF CONTENTS

TABLE OF CONTENTS (Cont'd)

LIST OF ILLUSTRATIONS

LIST OF ILLUSTRATIONS (Cont'd)

LIST OF ILLUSTRATIONS (Cont'd)

LIST OF ILLUSTRATIONS (Cont'd)

LIST OF ILLUSTRATIONS (Cont'd)

LIST OF TABLES

LIST OF TABLES (Cont'd)

SECTION 1
INTRODUCTION

Many methods have been proposed for achieving optimum performance of structures subjected to earthquake excitation. The conventional approach requires that structures passively resist earthquakes through a combination of strength, deformability, and energy absorption. The level of damping in these structures is typically very low and therefore the amount of energy dissipated during elastic behavior is very low. During strong earthquakes, these structures deform well beyond the elastic limit and remain intact only due to their ability to deform inelastically. The inelastic deformation takes the form of localized plastic hinges which results in increased flexibility and energy dissipation. Therefore, much of the earthquake energy is absorbed by the structure through localized damage of the lateral force resisting system. This is somewhat of a paradox in that the effects of earthquakes (i.e., structural damage) are counteracted by allowing structural damage.

An alternative approach to mitigating the hazardous effects of earthquakes begins with the consideration of the distribution of energy within a structure. During a seismic event, a finite quantity of energy is input into a structure. This input energy is transformed into both kinetic and potential (strain) energy which must be either absorbed or dissipated through heat. If there were no damping, vibrations would exist for all time. However, there is always some level of inherent damping which withdraws energy from the system and therefore reduces the amplitude of vibration until the motion ceases. The structural performance can be improved if a portion of the input energy can be absorbed, not by the structure itself, but by some type of supplemental "device". This is made clear by considering the conservation of energy relationship (Uang 1988)

$$E = E_k + E_s + E_h + E_d \qquad (1\text{-}1)$$

where E is the absolute energy input from the earthquake motion, E_k is the absolute kinetic energy, E_s is the recoverable elastic strain energy, E_h is the irrecoverable energy dissipated by the structural system through inelastic or other forms of action, and E_d is the energy dissipated by supplemental damping devices. The absolute energy input, E, represents the work done by the total base shear force at the foundation on the ground (foundation) displacement. It, thus, contains the effect of the inertia forces of the structure.

In the conventional design approach, acceptable structural performance is accomplished by the occurrence of inelastic deformations. This has the direct effect of increasing energy E_h. It also has an indirect effect. The occurrence of inelastic deformations results in softening of the structural system which itself modifies the absolute input energy. In effect, the increased flexibility acts as a filter which reflects a portion of the earthquake energy.

The recently applied technique of seismic isolation (e.g., Buckle 1990, Kelly 1991, Mokha 1991, Constantinou 1991b) accomplishes the same task by the introduction, at the foundation of a structure, of a system which is characterized by flexibility and energy absorption capability. The flexibility alone, typically expressed by a period of the order of 2 seconds, is sufficient to reflect a major portion of the earthquake energy so that inelastic action does not occur. Energy dissipation in the isolation system is then useful in limiting the displacement response and in avoiding resonances. However, in earthquakes rich in long period components, it is not possible to provide sufficient flexibility

for the reflection of the earthquake energy. In this case, energy absorption plays an important role (Constantinou 1991b).

Modern seismic isolation systems incorporate energy dissipating mechanisms. Examples are high damping elastomeric bearings, lead plugs in elastomeric bearings, mild steel dampers, fluid viscous dampers, and friction in sliding bearings (Buckle 1990, Mokha 1991).

Another approach to improved earthquake response performance and damage control is that of supplemental damping systems. In these systems, mechanical devices are incorporated in the frame of the structure and dissipate energy throughout the height of the structure. The means by which energy is dissipated is either: yielding of mild steel, sliding friction, motion of a piston within a viscous fluid, orificing of fluid, or viscoelastic action in rubber-like materials. These systems represent the topic of this report. A review of these systems follows.

1.1 Friction Devices

A frictional device located at the intersection of cross bracing has been proposed by Pall (1982, 1987) and used in a building in Canada. Figure 1-1 illustrates the design of this device. When seismic load is applied, the compression brace buckles while the tension brace induces slippage at the friction joint. This, in turn, activates the four links which force the compression brace to slip. In this manner, energy is dissipated in both braces while they are designed to be effective in tension only.

Experimental studies by Filiatrault (1985) and Aiken (1988) confirmed that these friction devices could enhance the seismic performance of structures. The devices provided a substantial increase in energy dissipation capacity and reduced drifts in comparison to moment resisting frames. Reductions in story shear

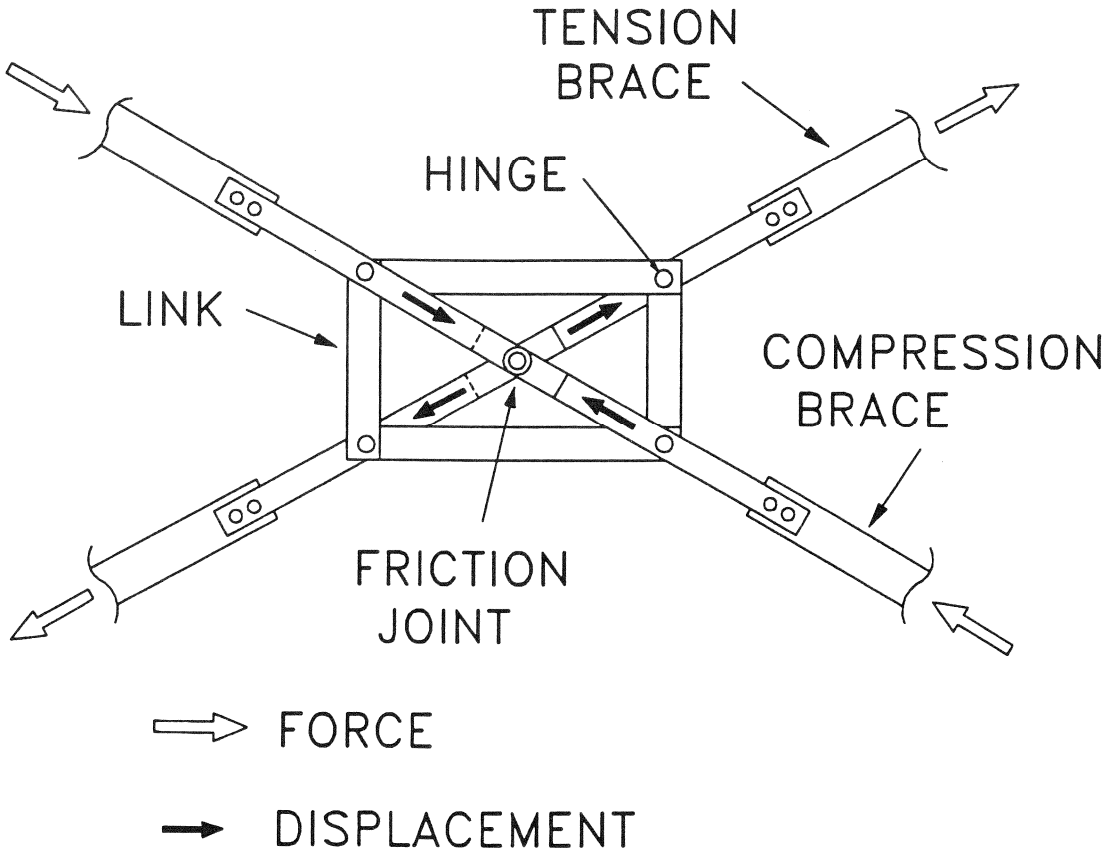

FIGURE 1-1 Friction Damping Device of Pall (1982)

forces were moderate. However, these forces are primarily resisted by the braces in a controlled manner and only indirectly resisted by the primary structural elements. This subject is further discussed in Subsection 1.6.

Sumitomo Metal Industries of Japan developed, and for a number of years, manufactured, friction dampers for railway applications. Recently, the application of these dampers was extended to structural engineering. Two tall structures in Japan, the Sonic City Office Building in Omiya City and the Asahi Beer Azumabashi Building in Tokyo, incorporate the Sumitomo friction dampers for reduction of the response to ground-borne vibrations and minor earthquakes. These structures are, respectively, 31- and 22-story steel frames. Furthermore, a 6-story seismically isolated building in Tokyo incorporates these dampers in the isolation system as energy-absorption devices.

Figure 1-2 shows the construction of a typical Sumitomo friction damper. The device consists of copper pads impregnated with graphite in contact with the steel casing of the device. The load on the contact surface is developed by a series of wedges which act under the compression of belleville washer springs. The graphite serves the purpose of lubricating the contact and ensuring a stable coefficient of friction and silent operation.

The Sumitomo friction device bears a similarity to a displacement control device described by Constantinou (1991a, 1991b) for applications in bridge seismic isolation. These devices utilize a frictional interface consisting of graphite impregnated copper in contact with steel (Sumitomo device) or in contact with stainless steel (displacement control device). A difference exists in the use of stainless steel which is known not to suffer any additional corrosion when in contact with copper. In contrast, carbon and low alloy steels will suffer moderate to severe corrosion (BSI 1979).

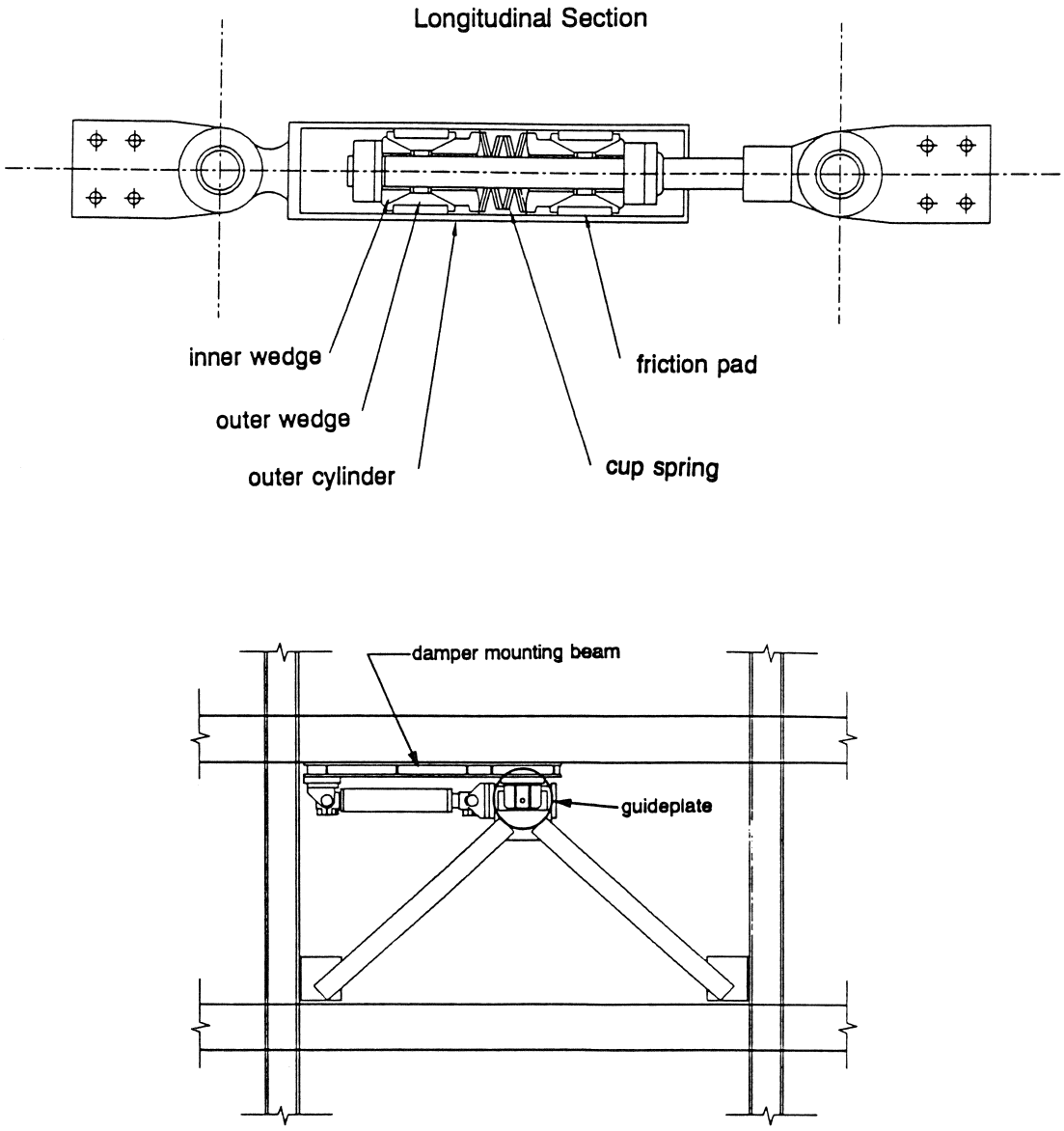

FIGURE 1-2 **Sumitomo Friction Damper and Installation Detail (from Aiken 1990)**

An experimental study of the Sumitomo damper was reported by Aiken (1990). Dampers were installed in a 9-story model structure and tested on a shake table. The dampers were not installed diagonally as braces. Rather, they were placed parallel to the floor beams, with one of their ends attached to a floor beam above and the other end attached to a chevron brace arrangement which was attached to the floor beam below. The chevron braces were designed to be very stiff. Furthermore, a special arrangement was used at the connection of each damper to the chevron brace to prevent lateral loading of the device. Figure 1-2 demonstrates the installation.

The experimental study resulted in conclusions which are similar to those of the study of the friction bracing devices of Pall (1982). In general, displacements were reduced in comparison to moment resisting frames. However, this reduction depended on the input motion. For example, in tests with the Japanese Miyagiken earthquake, ratios of interstory drift in the friction damped structure to interstory drift in the moment resisting structure of about 0.5 were recorded. In tests with the 1940 El Centro and 1952 Taft earthquakes, the ratio of interstory drifts was typically around 0.9. Furthermore, recorded base shear forces were, in general, of the same order as those of the moment resisting frame. However, the friction damped structure absorbed earthquake energy by mechanical means. This energy would have otherwise been absorbed by inelastic action in the frame.

An interesting outcome of the study is that, for optimum performance, the friction force at each level should be carefully selected based on the results of nonlinear dynamic analyses. The tested structure had a friction force of about 0.12W (W = model weight) at the first story and it reduced to about 0.05W at the top story.

Another friction device, proposed by Fitzgerald (1989), utilizes

slotted bolted connections in concentrically braced connections. Component tests demonstrated stable frictional behavior.

1.2 Yielding Steel Elements

The reliable yielding properties of mild steel have been explored in a variety of ways for improving the seismic performance of structures. The eccentrically-braced frame (Roeder 1978) represents a widely accepted concept. Energy dissipation is primarily concentrated at specifically detailed shear links of eccentrically-braced frames. These links represent part of the structural system which is likely to suffer localized damage in severe earthquakes.

A number of mild steel devices have been developed in New Zealand (Tyler 1978, Skinner 1980). Some of these devices were tested at U.C. Berkeley as parts of seismic isolation systems (Kelly 1980) and similar ones were widely used in seismic isolation applications in Japan (Kelly 1988).

Tyler (1985) described tests on a steel element fabricated from round steel bar and incorporated in the bracing of frames. Figure 1-3 shows details of a similar bracing system which was installed in a building in New Zealand. An important characteristic of the element is that the compression brace disconnects from the rectangular steel frame so that buckling is prevented and pinched hysteretic behavior does not occur. Energy is dissipated by inelastic deformation of the rectangular steel frame in the diagonal direction of the tension brace.

Another element, called "Added Damping and Stiffness" or ADAS device has been studied by Whittaker (1989). The device consists of multiple X-steel plates of the shape shown in Figure 1-4 and installed as illustrated in the same figure. The similarity of the device to that of Tyler (1978) and Kelly (1980) is apparent. The

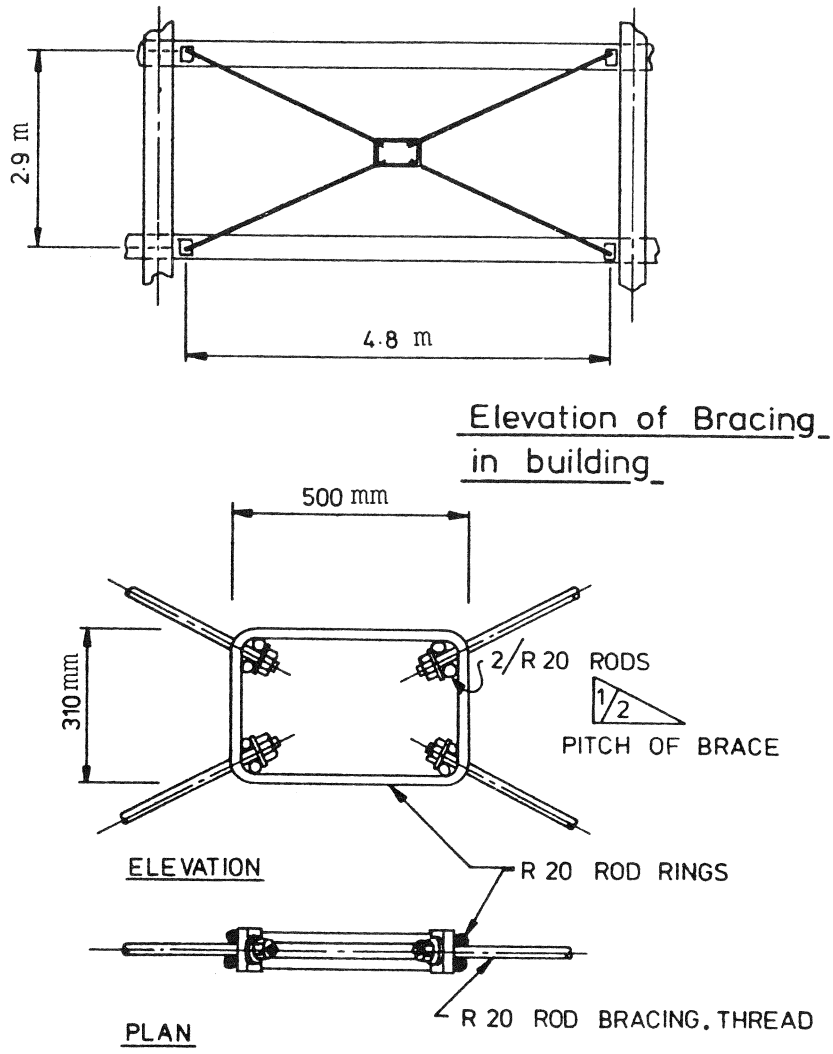

FIGURE 1-3 **Details of a Yielding Steel Bracing System in a Building in New Zealand (from Tyler 1985)**

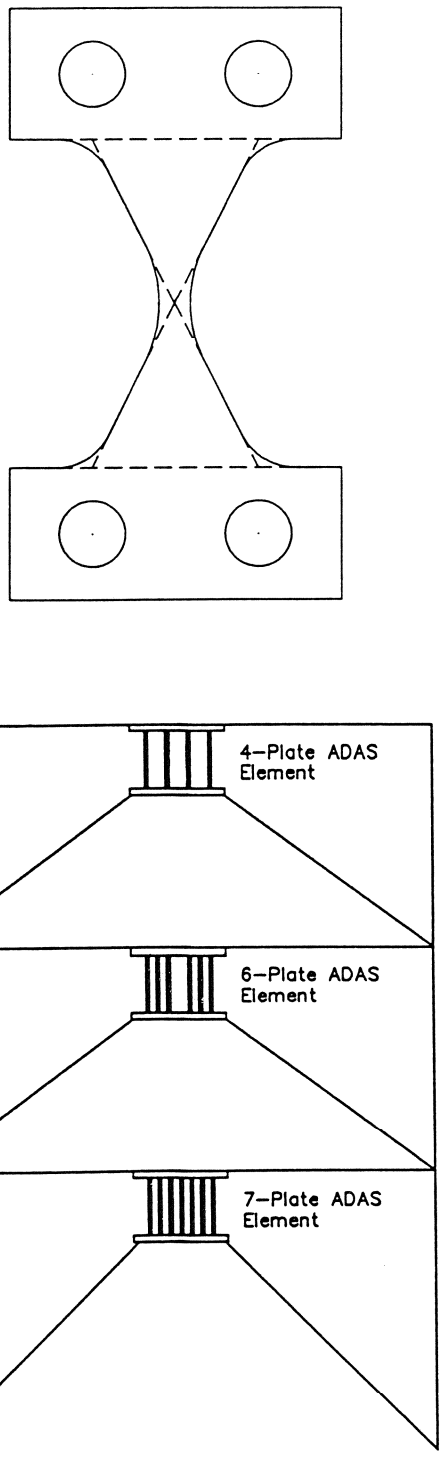

FIGURE 1-4 **ADAS X-shaped Steel Plate and Installation Detail (from Whittaker 1989)**

shape of the device is such that yielding occurs over the entire length of the device. This is accomplished by the use of rigid boundary members so that the X-plates are deformed in double curvature.

Shake table tests of a 3-story steel model structure by Whittaker (1989) demonstrated that the ADAS elements improved the behavior of the moment-resisting frame to which they were installed by a) increasing its stiffness, b) increasing its strength and c) increasing its ability to dissipate energy. Ratios of recorded interstory drifts in the structure with ADAS elements to interstory drifts in the moment-resisting frame were typically in the range of 0.3 to 0.7. This reduction is primarily an effect of the increased stiffness of the structure by the ADAS elements.

Ratios of recorded base shears in the structure with ADAS elements to base shears in the moment-resisting frame were in the range of 0.6 to 1.25. Thus, the base shear in the ADAS frame was in some tests larger than the shear in the moment frame. However, it should be noted again that, as in the case of friction braced structures, the structure shear forces are primarily resisted by the ADAS elements and their supporting chevron braces (see Figure 1-4). The ADAS elements yield in a pre-determined manner and relieve the moment frame from excessive ductility demands. ADAS elements have been very recently used in the seismic retrofitting of the Wells Fargo Bank, a 2-story concrete building in San Francisco.

Various devices whose behavior is based on the yielding properties of mild steel have been implemented in Japan (Fujita 1991).

Kajima Corporation developed bell-shaped steel devices which serve as added stiffness and damping elements. These dampers were installed in the connecting corridors between a 5-story and a 9-story building in Japan. The same company developed another steel

device, called the Honeycomb Damper, for use as walls in buildings. They were installed in the 15-story Oujiseishi Headquarters Building in Tokyo.

Obayashi Corporation developed a steel plate device which is installed in a manner similar to the ADAS elements (Figure 1-4). The plate is subjected to shearing action. It has been installed in the Sumitomo Irufine Office Building, a 14-story steel structure in Tokyo.

1.3 Viscoelastic Dampers

Viscoelastic dampers, made of bonded viscoelastic layers (acrylic polymers), have been developed by 3M Company and used in wind vibration control applications. Examples are the World Trade Center in New York City (110 stories), the Columbia SeaFirst Building in Seattle (73 stories) and the Number Two Union Square Building in Seattle (60 stories).

The suitability of the viscoelastic dampers for enhancing the earthquake resistance of structures has been experimentally studied by Lin (1988), Aiken (1990) and Chang (1991). Figure 1-5 illustrates a viscoelastic damper and its installation as part of the bracing system in a structure.

The behavior of viscoelastic dampers is controlled by the behavior in shear of the viscoelastic layers. In general, this material exhibits viscoelastic solid behavior with both its storage and loss moduli being dependent on frequency and temperature.

Typical viscoelastic material properties were reported by Chang (1991). At a temperature of 70°F (21°C) and shear strain of 0.05, the properties of storage and loss shear moduli were both approximately equal to 55 psi (0.38 MPa) at a frequency of 0.1 Hz and equal to about 450 psi (3.11 MPa) at a frequency of 4 Hz. At

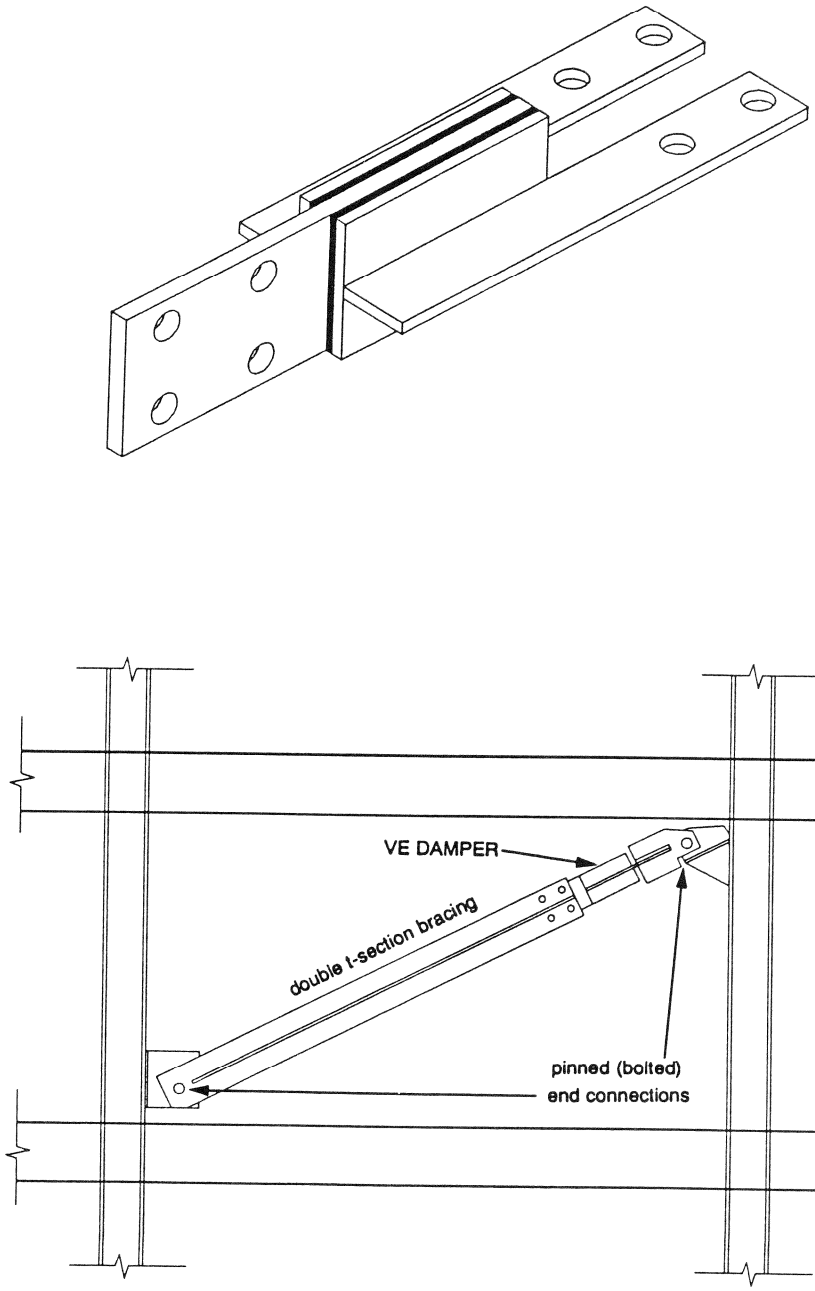

FIGURE 1-5 **Viscoelastic Damper and Installation Detail (from Aiken 1990)**

a temperature of 90°F (32°C), the values reduced to about 30 psi (0.21 MPa) at a frequency of 0.1 Hz and 185 psi (1.28 MPa) at a frequency of 4 Hz. Furthermore, these values reduced by an additional 10 to 20 percent at shear strains of 0.20.

The shake table tests of Lin (1988), Aiken (1990) and Chang (1991) demonstrated that significant benefits could be gained by the use of viscoelastic dampers. The tests of Aiken (1990) showed interstory drift reductions in comparison to those of the moment resisting frame which were slightly better than those of the friction (Sumitomo damper) damped structure. The ratio of interstory drift in the viscoelastically damped structure to the interstory drift in the moment resisting frame was between 0.5 and 0.9. Base shear forces in the viscoelastically damped structure were about the same as in the moment resisting frame.

The results of Chang (1991) are particularly interesting because tests were performed in a range of temperatures between 77 and 108°F (25 and 42°C). The addition of viscoelastic dampers resulted in increases of the natural frequency and corresponding damping ratio of the 5-story model structure from 3.17 Hz to 3.64 Hz and from 0.0125 to 0.15, respectively, at a temperature of 77°F (25°C). At 108°F (42°C) temperature, the increases were from 3.17 Hz to 3.26 Hz and from 0.0125 to 0.053, respectively.

The modification of the structural damping at the temperature of 108°F (42°C) is rather small. Yet, recorded interstory drifts in the viscoelastically damped structure were typically about 60 percent of those in the moment resisting frame. However, this substantial reduction is merely a result of the very low damping capacity of the moment resisting frame. If the moment resisting frame had a realistic damping ratio, the reduction would have been less dramatic.

The temperature dependency of viscoelastic dampers appears to be a major concern which needs to be addressed at the design stage. An interesting problem may arise in a symmetric viscoelastically damped structure in which either the dampers on one face of the structure or the dampers in the upper floors are at a higher temperature. In effect, the viscoelastically damped structure now exhibits either asymmetry in plan or vertical irregularity.

Aiken (1990) reported several delamination failures of viscoelastic dampers during testing. The failures were attributed to the development of tensile stresses. It was recommended that the dampers should not be constructed as shown in Figure 1-5, but rather be fitted with a bolt directly through the damper which prevents spreading of the steel plates.

Viscoelastic devices have been developed by the Lorant Group which may be used either at beam-column connections or as parts of a bracing system. Experimental and analytical studies have been very recently reported by Hsu (1992). These devices have been installed in a 2-story steel structure in Phoenix, Arizona.

Hazama Corporation of Japan developed a viscoelastic device whose construction and installation is similar to the 3M viscoelastic device with the exception that several layers of material are used (Fujita 1991). The material used in the Hazama device also exhibits temperature dependent properties. Typical results on the storage and loss shear moduli at a frequency of 1 Hz and shear strain of 0.5 are: 355 psi (2.45 MPa) and 412 psi (2.85 MPa), respectively at 32°F (0°C) and 14 psi (0.1 MPa) and 8 psi (0.055 MPa), respectively at 113°F (45°C). Thus, the ability of the device to dissipate energy (expressed by the loss shear modulus) reduces by a factor of 50 in the temperature range of 32 to 113°F (0 to 45°C).

Another viscoelastic device in the form of walls has been developed by Shimizu Corporation (Fujita 1991). The device consists of sheets of thermo-plastic rubber sandwiched between steel plates. It has been installed in the Shimizu Head Office Building, a 24-story structure in Tokyo.

1.4 Viscous Walls

The Building Research Institute in Japan tested and installed viscous damping walls in a test structure for earthquake response observation. The walls were developed by Sumitomo Construction Company (Arima 1988) and consist of a moving plate within a highly viscous fluid which is contained within a wall container. The device exhibits strong viscoelastic fluid behavior which is similar to that of the GERB viscodampers which have been used in applications of vibration and seismic isolation (Makris 1992).

Observations of seismic response of a 4-story prototype building with viscous damping walls demonstrated a marked improvement in the response as compared to that of the building without the walls.

1.5 Fluid Viscous Dampers

Fluid viscous dampers, which operate on the principle of fluid flow through orifices, are the subject of this study. A detailed description of these devices follows in Section 2.

These devices originated in the early 1960's for use in steel mills as energy absorbing buffers on overhead cranes. Variations of these devices were used as canal lock buffers, offshore oil rig leg suspensions, and mostly in shock isolation systems of aerospace and military hardware. Some large scale applications of these devices include:

a) The West Seattle Swing Bridge. Fluid dampers with a built-in hydraulic logic system could provide damping at two pre-

determined levels. The logic system can determine if the bridge condition is normal or faulted. Under normal conditions, damping is very low. When a fault occurs, due to motor runaway, excessive current or wave loadings, or earthquakes, the device senses the higher than normal velocity and absorbs significant energy.

b) The New York Power Indian Point 3 Nuclear Power Plant. Each nuclear generator is connected to the containment building walls by eight 300 Kip (1.34 MN) capacity fluid dampers. The dampers are specifically designed for seismic pulse attenuation.

c) The Virginia Power North Ana Nuclear Station. This is an application similar to that of the Indian Point 3 Plant, except that the dampers have 2000 Kip (8.92 MN) capacity.

d) Suppression of wind induced vibration of launching platforms such as those of the Space Shuttle and the Atlas Missile.

The particular fluid viscous damper used in this study originated in a classified application on the U.S. Air Force B-2 Stealth Bomber. Thus, the device includes performance characteristics considered as current state of the art in hydraulic technology. Two of these characteristics, which are of interest in applications of earthquake engineering, are essentially linear viscous behavior and capability to operate over a wide temperature range (typically -40°F to 160°F or -40°C to 70°C).

1.6 Considerations in the Design of Energy Absorbing Systems

The preceding review of energy absorbing systems demonstrates that these systems are capable of producing significant reductions of interstory drifts in moment-resisting frames to which they are installed. Accordingly, they are all suitable for applications of seismic retrofit of existing buildings.

Let us consider the implications of the use of energy absorbing systems in an existing moment-resisting frame building. In general, the gravity load-carrying elements of the structural system have sufficient stiffness and strength to carry the gravity loads and seismic forces in a moderate earthquake. The energy absorbing devices are installed in new bracing systems and assuming that they are capable of reducing drifts to half of those of the original system in a severe earthquake, one can immediately observe that the reduction of drift will result in a proportional reduction in bending moment in the columns, which will now undergo limited rather than excessive yielding.

However, the behavior of the retrofitted structure has changed from that of a moment-resisting frame to that of a braced frame. The forces which develop in the energy absorbing elements will induce additional axial forces in the columns. Depending on the type of energy absorbing device used, this additional axial force may be in-phase with the peak drift and, thus, may affect the safety of the loaded column.

Figure 1-6 shows idealized force-displacement loops of various energy absorbing devices. In the friction and steel yielding devices, the peak brace force occurs at the time of peak displacement. Accordingly, the additional column force, which is equal to $F\sin\theta$ (θ = brace angle with respect to horizontal), is in-phase with the bending moment due to column drift. Similarly, in the viscoelastic device a major portion of the additional column force is in-phase with the bending moment. In contrast, in the viscous device the additional column force is out-of-phase with the bending moment.

The implications of this difference in behavior of energy absorbing devices are illustrated in Figure 1-7. We assume that the energy absorbing devices are installed in the interior columns of a reinforced concrete frame. The nominal axial force - bending

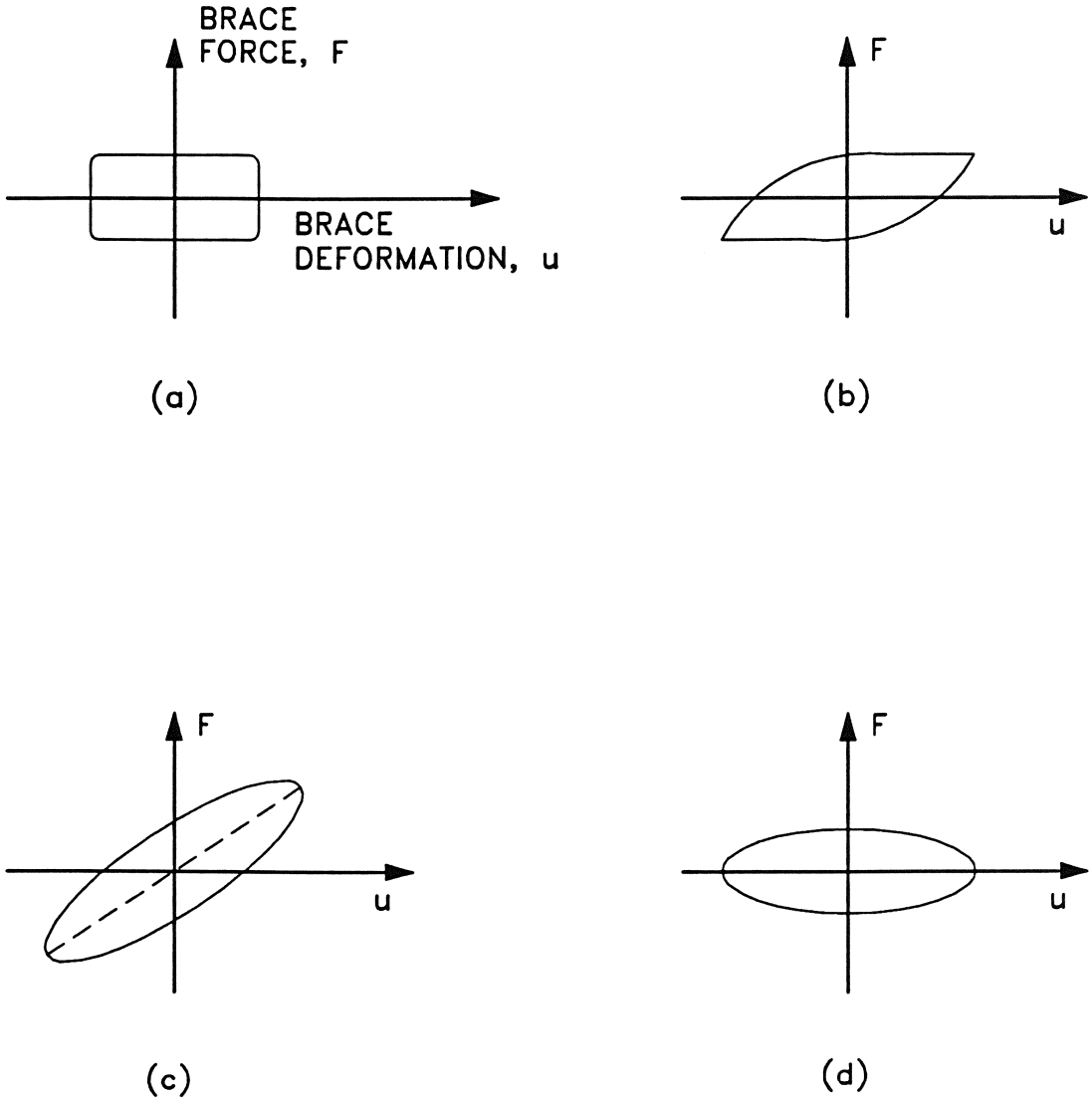

FIGURE 1-6 **Force - Displacement Relation in (a) Friction Device, (b) Steel Yielding Device, (c) Viscoelastic Device, and (d) Viscous Device**

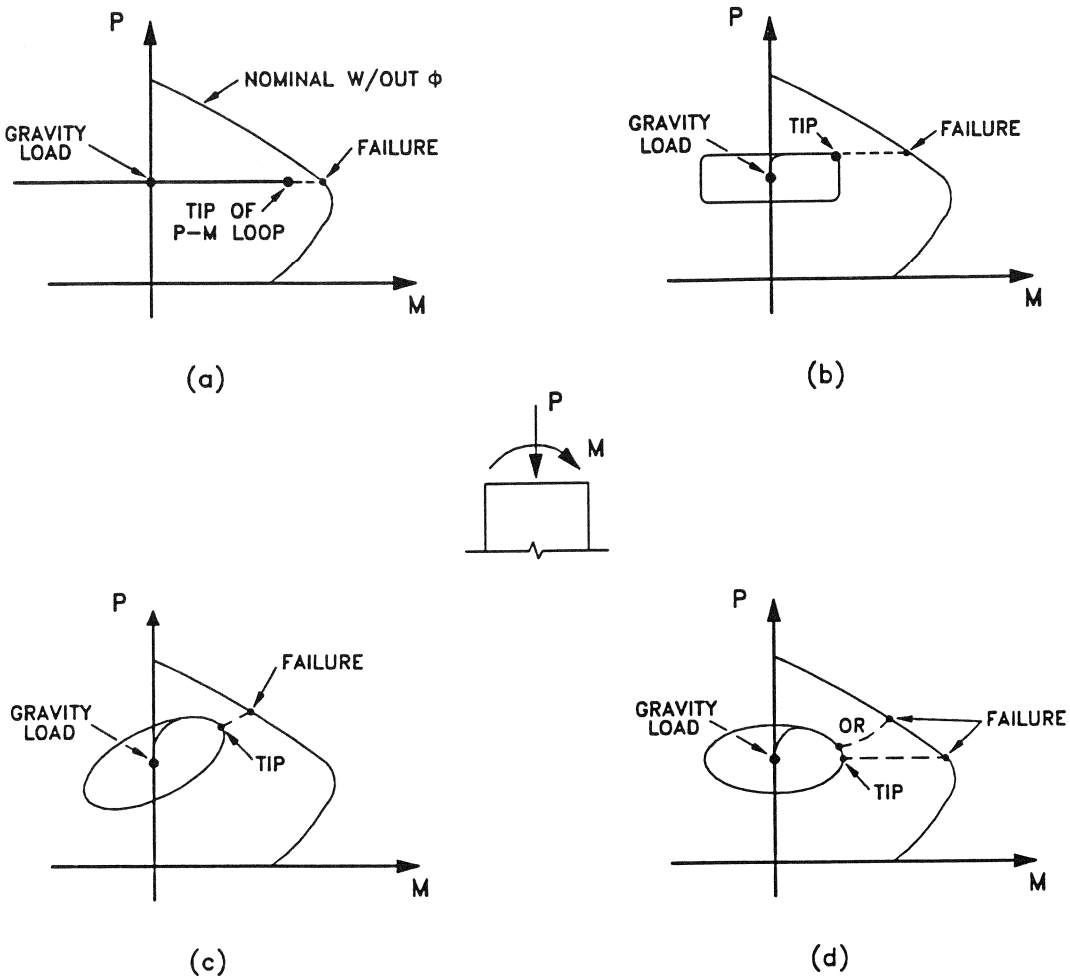

FIGURE 1-7 **Column Interaction Diagrams and Axial Force - Bending Moment Loops during Seismic Excitation for (a) Moment-resisting Frame, (b) Friction Damped Frame, (c) Visco-elastically Damped Frame, and (d) Viscously Damped Frame**

moment interaction diagram of a column is shown. It is assumed that the column was designed to be in the compression controlled range of the diagram. During seismic excitation, the moment-resisting frame undergoes large drifts and column bending moments but axial load remains practically unchanged. Failure will occur when the tip of the P-M loop reaches the nominal curve as illustrated in Figure 1-7(a). The available capacity of the column is related to the distance between the tip of the P-M loop and the nominal curve (shown as a dashed line in Figure 1-7).

In the frame with added energy dissipating devices, the P-M loops show less bending moment. Despite this, the available capacity of the column may not have increased since the distance between the tip of the P-M loop and the nominal curve may have remained about the same. An exception to this behavior can be found in the viscous device.

The conclusion of the preceding discussion is that drift is not the only concern in design. Energy absorbing devices may reduce drift and thus reduce inelastic action. However, depending on their force-displacement characteristics, they may induce significant axial column forces which may lead to column compression failure. This concern is particularly important in the seismic retrofitting of structures which suffered damage in previous earthquakes. After all, it may not always be possible to upgrade the seismic resistance of such structures by the addition of energy absorbing devices alone. It may also be necessary to strengthen the columns.

The experimental results of Aiken (1990) on the Sumitomo friction dampers can be utilized to illustrate the significance of additional axial forces induced by energy absorbing devices. The structure tested was 9 stories tall with two identical frames as shown in Figure 1-8. The forces in the elements, braces and columns are depicted in Figure 1-8 with the assumption that all friction dampers experience sliding. The additional interior 1st

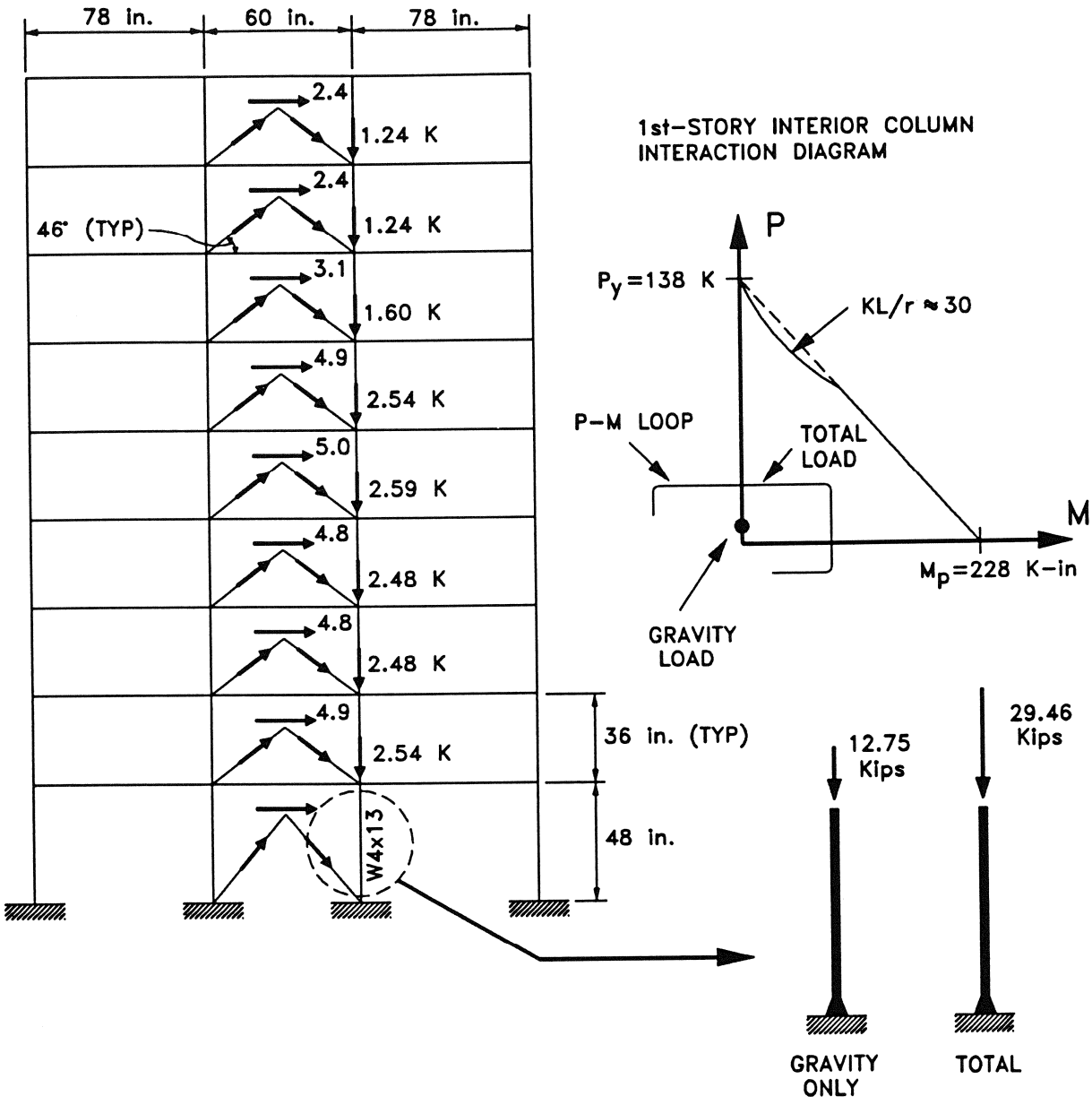

FIGURE 1-8 Gravity and Additional Axial Load in Interior Column of 9-story Model Structure with Added Friction Dampers tested by Aiken (1990) (1 in. = 25.4 mm, 1 Kip = 4.46 KN)

story column axial force adds up to 16.71 Kips (74.5 KN). The force in the column due to the weight of the structure is 12.75 Kips (56.9 KN). The substantial additional axial load may be regarded as a result of the height of the structure (9-stories). Similar calculations with the 3-story model structure with ADAS elements tested by Whittaker (1989), resulted in additional axial load of only 14 percent of the gravity load.

The relation of the gravity load and total load in the 1st story interior column of the 9-story model to the capacity of the column is illustrated in the upper right corner of Figure 1-8. It may be observed that the gravity load amounts to only 9.2 percent of the column yield force and 16.8 percent of the allowable concentric axial load ($F_a=0.55F_y$). Furthermore, it should be noted that the column has a very low slenderness ratio so that almost maximum column capacity is available.

1.7 Code Provisions for Design of Structures Incorporating Passive Energy Dissipating Devices

The existence of design specifications is significant in the implementation of the technology of energy dissipating devices. Currently, such specifications do not exist. The absence of such specifications, while not a deterrent to the use of the technology, may prevent widespread use of the technology. This is equivalent to the experience in the United States with the use of the technology of seismic isolation (Mayes 1990).

Efforts for the development of regulations for the design and construction of structures incorporating passive energy dissipating devices are currently in progress by the Structural Engineers Association of California and by the Technical Subcommittee 12 of the Building Seismic Safety Council. When developed, these regulations are expected to eventually become part of the Uniform Building Code and the NEHRP (National Earthquake Hazards Reduction

Program) Recommended Provisions for the Development of Seismic Regulations for New Buildings, respectively.

1.8 Objectives

In order to analytically predict the response of a structure containing some type of supplemental damping device, the dynamic characteristics of the damping device must be determined. In particular, the behavior of such devices is often dependent on the frequency of motion and the ambient temperature. Therefore, the initial objective is to investigate the mechanical characteristics of the damper so as to obtain a mathematical model describing the behavior of the device.

To verify the proposed mathematical model, a series of earthquake simulator tests on a model structure can be performed. From the experimental response of various structural configurations (i.e., with and without dampers), the analytical response can be verified and the benefit of supplemental dampers can be determined. In addition, the response obtained with the use of fluid viscous dampers can be compared with the response obtained from the use of other devices.

1.9 Scope

To achieve the objectives stated above, the following tasks were performed:

a) Selection of the devices for component testing.

b) Component testing of a single damper under a variety of dynamic inputs and under different ambient temperatures.

c) Development of a mathematical model based on mechanical properties.

d) Design of a lateral bracing system to incorporate dampers in the test structure.

e) Identification of various structural configurations (see Figures 3-2 and 3-3).

f) Earthquake simulation testing of various structural configurations using selected ground motions.

g) Comparison of experimental results and results obtained by time-history analysis.

h) Development of rigorous and approximate approaches to obtaining modal properties.

i) Perform response spectrum analysis using approximate modal properties.

j) Comparison of experimental, time-history analysis, and response spectrum results.

k) Determine effectiveness of incorporating dampers in test structure.

l) Compare performance of fluid viscous dampers with performance of other devices.

SECTION 2
MECHANICAL PROPERTIES OF FLUID DAMPERS

2.1 Description of Dampers

Damping devices which utilize fluid flow through orifices were originally developed for the shock isolation of military hardware. To appreciate the level of technology involved in these shock isolation systems, note that the so-called weapons grade shock usually has free field input wave forms with peak velocities in excess of 180 in/sec (4572 mm/sec), rise times of less than 2 msecs and peak accelerations of the order of 200g (Clements 1972).

The fluid dampers under investigation evolved from these shock isolation damping devices. The construction of the tested device is shown in Figure 2-1. It consists of a stainless steel piston, with a bronze orifice head and an accumulator. It is filled with silicone oil. The orifice flow is compensated by a passive bi-metallic thermostat that allows operation of the device over a temperature range of -40°F to 160°F (-40°C to 70°C). The orifice configuration, mechanical construction, fluid and thermostat used in this device originated within a device used in a classified application on the U.S. Air Force B-2 Stealth Bomber. Thus, the device includes performance characteristics considered as state of the art in hydraulic technology.

2.2 Operation of Dampers

The force that is generated by the fluid damper is due to a pressure differential across the piston head. Consider that the piston moves from left to right in Figure 2-1 (device subjected to compression force). Fluid flows from chamber 2 towards chamber 1. Accordingly, the damping force is proportional to the pressure differential in these two chambers. However, the fluid volume is reduced by the product of travel and piston rod area. Since the

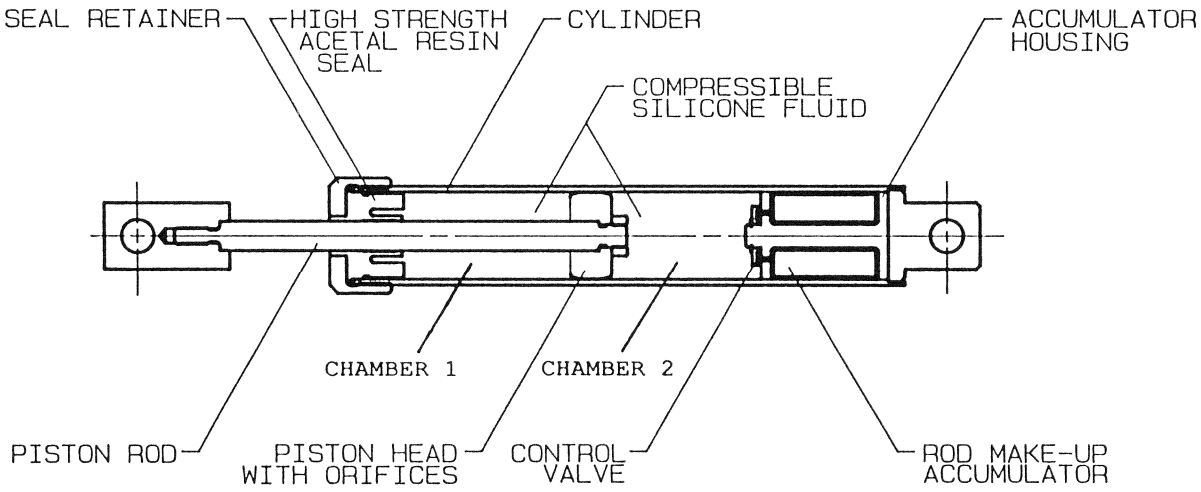

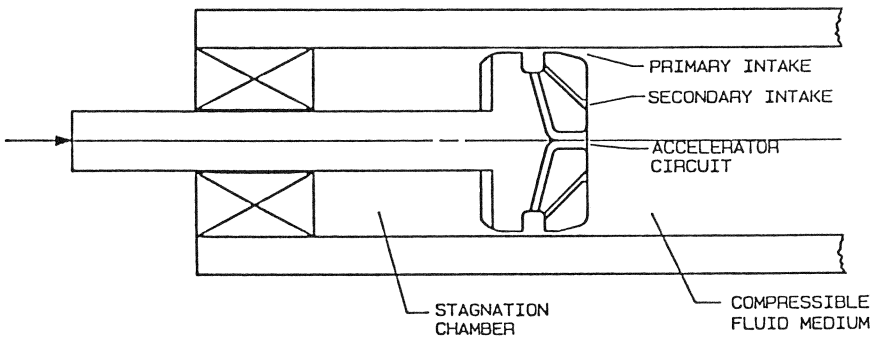

Fluidic Control Orifice

FIGURE 2-1 Construction of Fluid Viscous Damper

fluid is compressible, this reduction in fluid volume is accompanied by the development of a restoring (spring like) force. This is prevented by the use of the accumulator. The tested device showed no measurable stiffness for piston motions with frequency less than about 4 Hz. In general, this cutoff frequency depends on the design of the accumulator and may be specified in the design.

The existence of the aforementioned cutoff frequency is a desirable property. The devices may provide additional viscous type damping to the fundamental mode of the structure (typically with a frequency less than the cutoff frequency) and additional damping and stiffness to the higher modes. This may, in effect, completely suppress the contribution of the higher modes of vibration.

The force in the fluid damper may be expressed as

$$P = bp_{12} \tag{2-1}$$

where p_{12} is the pressure differential in chambers 1 and 2. Constant b is a function of the piston head area, A_p, piston rod area, A_r, area of orifice, A_1, number of orifices, n, area of control valves, A_2 and the discharge coefficient of the orifice, C_{d1} and control valve, C_{d2}.

The pressure differential across the piston for cylindrical orifices is given by

$$p_{12} = \frac{\rho}{2n^2 C_{d1}^2}\left(\frac{A_p}{A_1}\right)^2 \dot{u}^2\, sgn\,(\dot{u}) \tag{2-2}$$

where ρ is the fluid density and $\dot{u}$ is the velocity of the piston with respect to the housing.

In cylindrically-shaped orifices, the pressure differential is proportional to the piston velocity squared. Such orifices are

termed "square law" or "Bernoullian" orifices since Equation 2-2 is predicted by Bernoulli's equation. Bernoullian orifices produce damper forces which are proportional to velocity squared, a usually unacceptable performance in shock isolation.

The orifice design in the tested fluid damper produces a force that is not proportional to velocity squared. The orifice utilizes a series of specially shaped passages to alter flow characteristics with fluid speed. A schematic of this orifice is shown in Figure 2-1. It is known as Fluidic Control Orifice. It provides forces which are proportional to $|\dot{u}|^{\alpha}$, where α is a predetermined coefficient in the range of 0.5 to 1.2. A design with coefficient α equal to 0.5 is useful in applications involving extremely high velocity shocks. They are typically used in the shock isolation of military hardware. In applications of earthquake engineering, a design with α = 1 appears to be the most desired one. It results in essentially linear viscous behavior. The devices utilized in this testing program were designed to have this behavior.

2.3 Testing Arrangement and Procedure

The mechanical characteristics of the dampers have been determined using the testing arrangement shown in Figures 2-2 and 2-3. A hydraulic actuator applies a dynamic force along the axis of the damper. The force in the damper is measured using a load cell which is connected between the damper and the reaction frame. The displacement of the damper is measured using an LVDT (Linear Variable Differential Transformer) which is located within the actuator. The force-displacement relationship can now be obtained and used to extract the mechanical characteristics of the dampers.

Figure 2-4 and Table 2-I show dimensional and other characteristics of the tested damper and other commercially available dampers. It

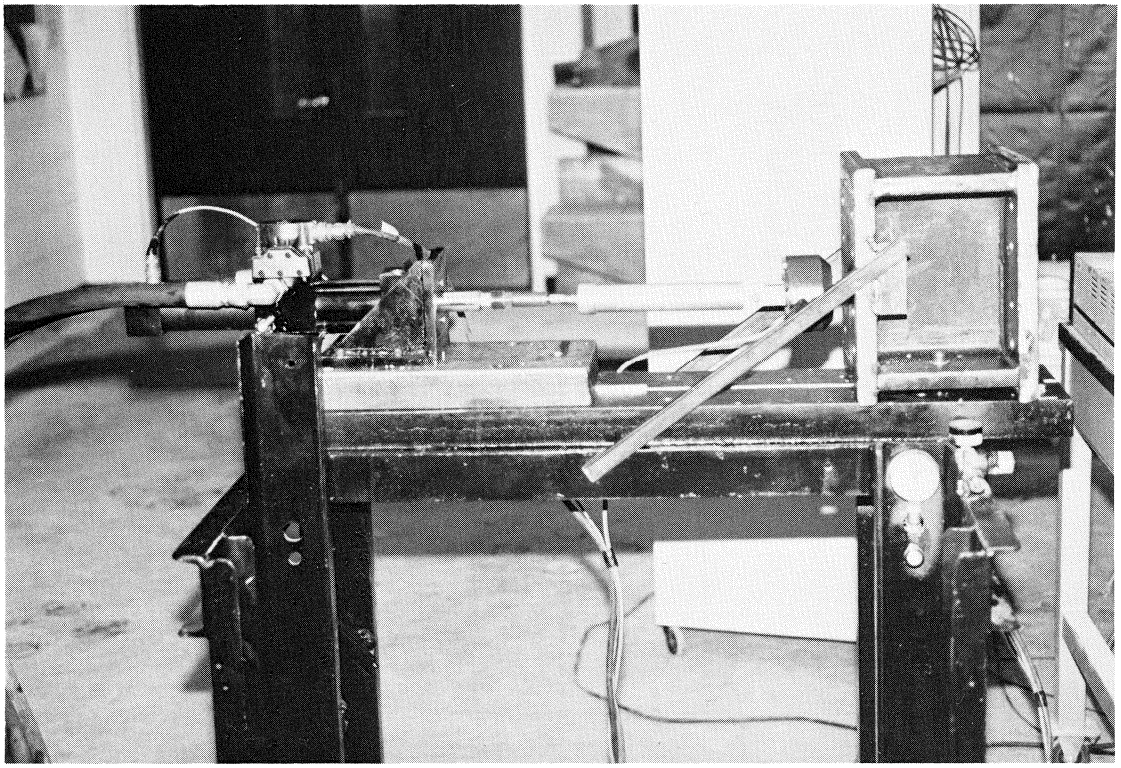

FIGURE 2-2 View of Testing Arrangement

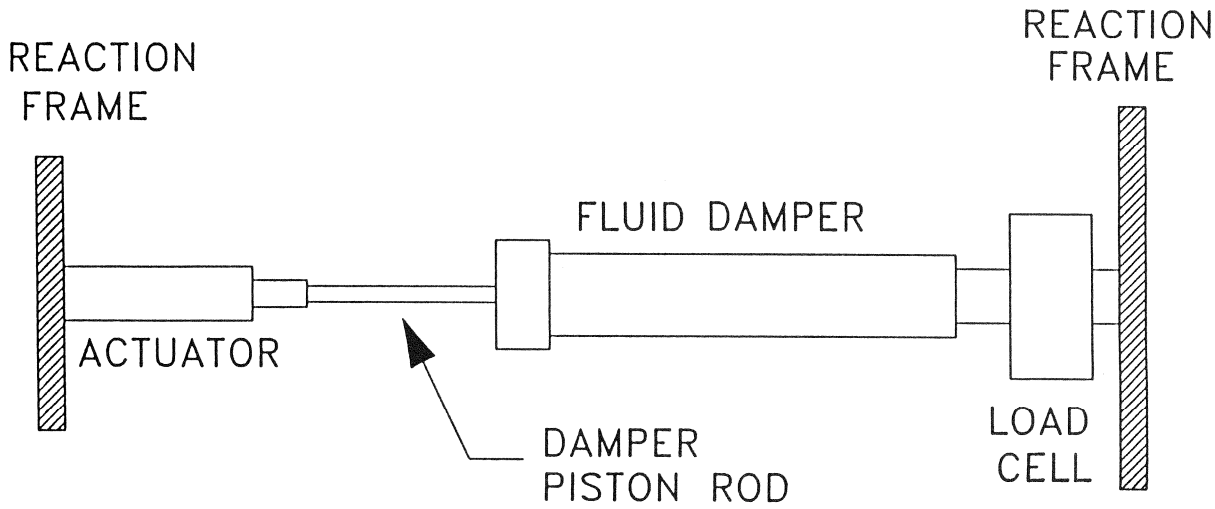

FIGURE 2-3 Schematic of Testing Arrangement

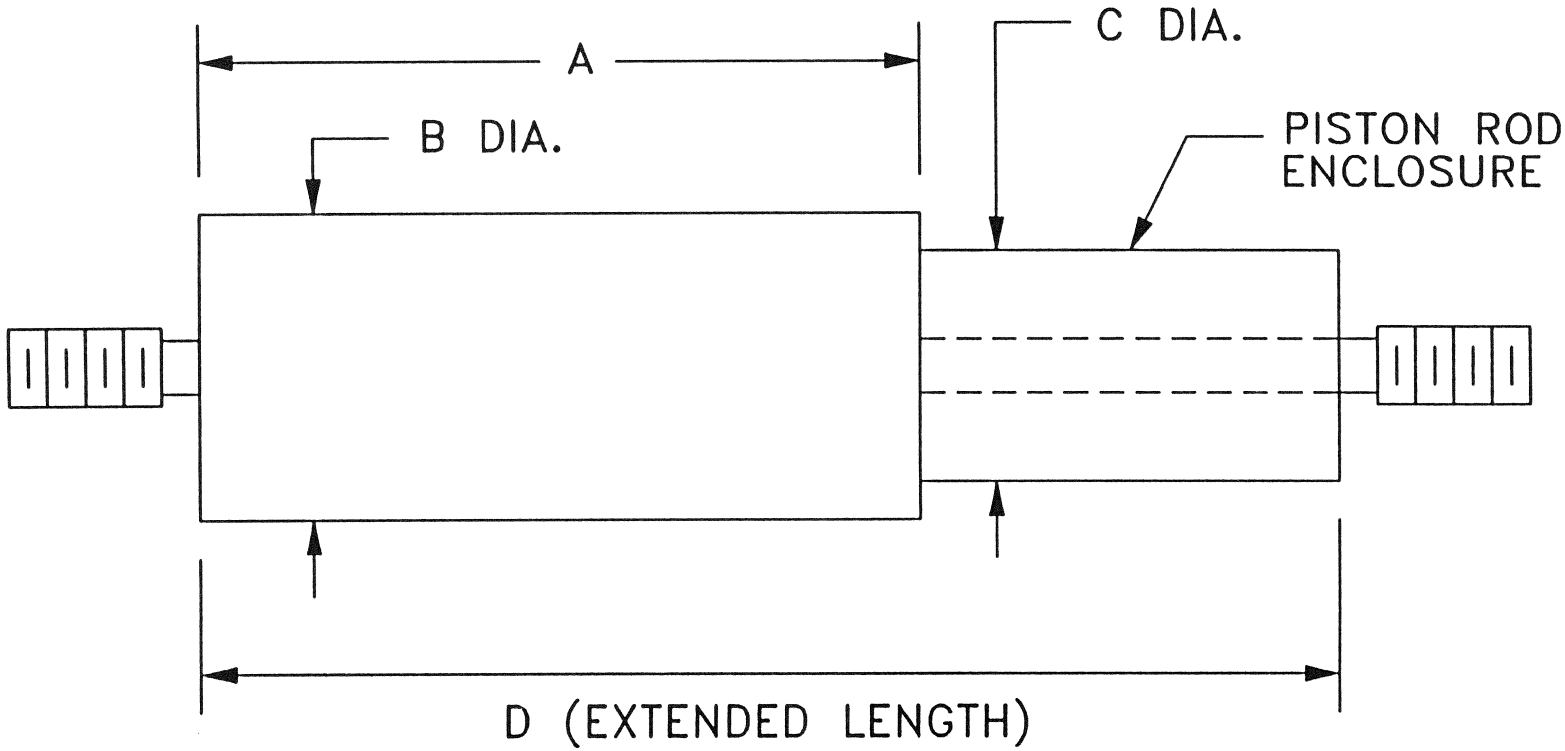

FIGURE 2-4 **Geometrical Characteristics of Fluid Viscous Dampers (Refer to Table 2-I)**

TABLE 2-I Characteristics of Fluid Viscous Dampers
(1 in. = 25.4 mm, 1 Kip = 4.46 KN, 1 lb = 4.46 N)

MODEL	MAX. FORCE (Kips)	STROKE (in.)	WEIGHT (lbs)	A (in.)	B (in.)	C (in.)	D (in.)
1.5 X 4 *	2	4	2.33	9.0	1.50	w/out enclosure	13.0
3 X 4	10	4	20	11.9	3.00	2.59	17.5
4 X 5	20	5	40	12.7	4.00	3.38	20.5
5 X 5	30	5	50	14.1	5.00	4.38	22.5

Weight is for all steel construction.
* = Tested Damper

may be noted that commercially available dampers are capable of producing significant force output while having small dimensions.

2.4 Mechanical Properties

2.4.1 General Equations

The frequency and amplitude of the motion of the damper piston was specified for each test. The actuator was run under displacement control such that the resulting motion of the damper piston was sinusoidal. The damper motion is given by

$$u = u_0 \sin(\omega t) \tag{2-3}$$

where u_o is the amplitude of the displacement, ω is the frequency of motion, and t is the time. For steady-state conditions, the force needed to maintain this motion is

$$P = P_o \sin(\omega t + \delta) \tag{2-4}$$

where P_o is the amplitude of the force, and δ is the phase angle. The area within the recorded force-displacement loops can be measured to determine the energy dissipated in a single cycle of motion

$$W_d = \oint P\,du = \pi P_o u_o \sin(\delta) \tag{2-5}$$

Rewriting Equation 2-4,

$$P = P_o \sin(\omega t)\cos(\delta) + P_o \cos(\omega t)\sin(\delta) \tag{2-6}$$

and introducing the quantities

$$K_1 = \frac{P_o}{u_o}\cos(\delta) \quad , \quad K_2 = \frac{P_o}{u_o}\sin(\delta) \tag{2-7}$$

where K_1 is the storage stiffness and K_2 is the loss stiffness, one obtains

$$P = K_1 u_o \sin(\omega t) + K_2 u_o \cos(\omega t) \qquad (2\text{-}8)$$

Equation 2-8 may also be written the form

$$P = K_1 u + \frac{K_2}{\omega} \dot{u} \qquad (2\text{-}9)$$

where it is clear that the first term represents the force due to the stiffness of the damper which is in-phase with the motion and the second term represents the force in the damper due to the viscosity of the damper which is 90° out-of-phase with the motion. The damping coefficient is given by

$$C = \frac{K_2}{\omega} \qquad (2\text{-}10)$$

Combining Equations 2-5 and 2-7,

$$K_2 = \frac{W_d}{\pi u_o^2} \qquad (2\text{-}11)$$

$$\delta = \sin^{-1}\left(\frac{K_2 u_o}{P_o}\right) \qquad (2\text{-}12)$$

Equations 2-7 and 2-10 through 2-12 can now be used to obtain the mechanical properties of the damper from experimentally measured values of W_d , P_o , and u_o. First the loss stiffness is determined from Equation 2-11. Knowing the imposed frequency, ω, the damping coefficient is determined from Equation 2-10. Equation 2-12 is used to compute the phase angle. Finally, the storage stiffness is computed using Equation 2-7.

2.4.2 Experimental Results

A total of 58 tests were conducted in the frequency range of 0.1 to 25 Hz, peak velocity range of 0.65 in/sec to 18.2 in/sec (16.5 to 462.3 mm/sec) and at three temperatures: about 0°C, room

temperature (about 22°C), and about 50°C. In all tests, 5 cycles were completed. Table 2-II summarizes the results.

The low temperature tests were conducted with the arrangement of Figure 2-5 in which the damper was encased in a plastic cylindrical tube containing a pack of ice with alcohol to lower the temperature. The high temperature tests were conducted with the arrangement of Figure 2-6 in which the damper was encased in a cardboard cylindrical tube wrapped with teflon tape with a temperature adjustable heating unit wrapped around it several times. The heating unit generated heat which was transferred to the space between the damper and the cylindrical tube. In all cases, a thermocouple monitored the surface temperature of the housing of the device.

Typical recorded force-displacement loops are presented in Figure 2-7 at temperatures of 1°C, 23°C and 47°C and frequencies of 1, 2 and 4 Hz. In this range of frequency of motion, the device exhibits insignificant storage stiffness and its behavior is essentially linear viscous. One should compare the peak force in the tests with frequency of 2 and 4 Hz (amplitude is such that the peak velocity is the same). The recorded peak forces in the two tests are almost identical.

At frequencies above about 4 Hz, the device exhibited storage stiffness which reached values approximately equal to the loss stiffness at frequencies exceeding 20 Hz. Figure 2-8 demonstrates this behavior in a test at frequency of 20 Hz and amplitude of 0.05 in (1.27 mm).

The mechanical properties of the device were almost completely independent of the amplitude of motion. This was confirmed in tests conducted at the same frequency and different amplitude. For example, one should compare the results of tests 32 and 33 and tests 39 and 40 in Table 2-II. Further confirmation of this

TABLE 2-II Summary of Component Tests and Mechanical Properties (1 in = 25.4 mm, 1 lb = 4.46 N)

TEST	FREQUENCY (Hz)	AMPLITUDE (in)	PEAK VELOCITY (in/sec)	PEAK FORCE (lb)	DISSIPATED ENERGY (lb-in)	STORAGE STIFFNESS (lb/in)	LOSS STIFFNESS (lb/in)	DAMPING COEFFICIENT (lb-sec/in)	PHASE ANGLE (degrees)	TEMPERATURE (°C)
1	0.1	1.03	0.647	71.3	229.1	0	68.7	109.3	90	23
2	0.1	1.03	0.647	71.0	236.2	0	70.9	112.8	90	23
3	0.1	1.03	0.647	80.7	263.5	0	79.1	125.9	90	23
4	0.1	1.03	0.647	85.4	291.6	0	87.5	139.3	90	22
5	0.1	1.03	0.647	85.2	290.8	0	87.3	138.9	90	23
6	0.1	1.03	0.647	59.2	202.4	0	60.7	96.6	90	48
7	0.2	0.51	0.646	106.7	168.4	0	202.9	161.5	90	2
8	0.2	0.51	0.646	69.5	113.8	0	1137.1	109.1	90	23
9	0.2	1.03	1.294	201.9	660.0	0	198.0	157.6	90	2
10	0.2	1.03	1.294	145.2	471.2	0	141.4	112.5	90	23
11	0.4	0.26	0.646	66.5	54.9	0	264.6	105.3	90	23
12	0.4	0.26	0.651	66.5	52.8	0	250.5	99.7	90	23
13	0.4	0.26	0.643	105.0	70.4	0	341.9	136.0	90	2
14	0.6	1.03	3.883	385.9	1240.7	0	372.3	98.8	90	23
15	1.0	0.99	6.220	576.0	1756.7	0	570.5	90.8	90	26
16	1.0	1.02	6.409	624.1	1985.7	0	607.5	96.7	90	23
17	1.0	1.03	6.472	604.1	1990.2	0	597.1	95.0	90	23
18	1.0	1.03	6.472	609.2	1938.7	0	581.7	92.6	90	22
19	1.0	1.03	6.472	848.0	2672.4	0	801.8	127.6	90	2
20	1.0	1.03	6.472	434.6	1399.1	0	419.8	66.8	90	47
21	1.5	1.01	9.519	871.4	2777.8	0	866.8	92.0	90	23

TABLE 2-II Continued

TEST	FREQUENCY (Hz)	AMPLITUDE (in)	PEAK VELOCITY (in/sec)	PEAK FORCE (lb)	DISSIPATED ENERGY (lb-in)	STORAGE STIFFNESS (lb/in)	LOSS STIFFNESS (lb/in)	DAMPING COEFFICIENT (lb-sec/in)	PHASE ANGLE (degrees)	TEMPERATURE (°C)
22	2.0	0.26	3.242	308.7	225.5	0	1078.3	85.8	90	23
23	2.0	0.26	3.217	312.0	220.2	0	1069.5	85.1	90	23
24	2.0	0.26	3.242	282.2	213.6	0	1021.4	81.3	90	23
25	2.0	0.26	3.217	332.3	224.2	0	1088.9	86.7	90	23
26	2.0	0.26	3.242	328.3	240.0	0	1147.7	91.3	90	22
27	2.0	0.26	3.230	489.6	292.0	0	1407.2	112.0	90	2
28	2.0	0.26	3.230	224.6	178.2	0	858.8	68.3	90	46
29	2.0	0.51	6.434	587.6	886.6	0	1076.6	85.7	90	23
30	2.0	0.51	6.421	624.0	943.9	0	1150.6	91.6	90	23
31	2.0	0.51	6.434	896.0	1245.7	0	1512.6	120.4	90	2
32	2.0	0.52	6.472	551.0	851.4	0	1021.8	81.3	90	23
33	2.0	1.02	12.818	1083.0	3472.2	0	1062.3	84.5	90	23
34	2.0	1.02	12.818	1136.5	3638.9	0	1113.3	88.6	90	23
35	2.0	1.03	12.943	1083.0	3415.7	0	1024.8	81.6	90	23
36	2.0	1.03	12.943	1488.0	4754.3	0	1426.5	113.5	90	1
37	4.0	0.26	6.434	597.5	443.3	444.4	2153.1	85.7	79.0	23
38	4.0	0.26	6.434	864.0	571.0	773.0	2773.3	110.3	76.8	2
39	4.0	0.26	6.434	624.6	439.1	492.3	2132.7	84.9	78.3	23
40	4.0	0.51	12.918	1182.7	1811.0	423.0	2181.9	86.8	79.4	23
41	4.0	0.51	12.893	1175.0	1824.5	612.1	2206.8	87.8	74.5	23
42	4.0	0.52	12.994	1120.3	1744.4	416.7	2077.4	82.7	78.9	23

TABLE 2-II Continued

TEST	FREQUENCY (Hz)	AMPLITUDE (in)	PEAK VELOCITY (in/sec)	PEAK FORCE (lb)	DISSIPATED ENERGY (lb-in)	STORAGE STIFFNESS (lb/in)	LOSS STIFFNESS (lb/in)	DAMPING COEFFICIENT (lb-sec/in)	PHASE ANGLE (degrees)	TEMPERATURE (°C)
43	4.0	0.52	12.969	995.9	1600.0	333.3	1912.8	76.1	80.1	23
44	4.0	0.52	13.044	1552.0	2419.3	640.0	2858.9	113.8	77.6	2
45	4.0	0.52	12.943	858.3	1373.3	246.3	1648.2	65.6	81.5	47
46	6.0	0.10	3.597	345.6	86.1	798.6	3011.3	79.9	77.3	25
47	6.0	0.44	16.738	1840.0	2470.3	1000.0	3988.7	105.8	67.3	2
48	6.0	0.47	17.530	1410.8	2036.6	666.7	2998.1	79.5	77.3	23
49	6.0	0.48	18.209	1538.5	2297.6	707.8	3134.9	83.2	77.2	23
50	8.0	0.10	4.785	451.2	114.6	1284.0	4025.0	80.1	74.3	25
51	8.0	0.26	12.818	1095.4	757.3	1250.0	3707.1	73.8	73.0	23
52	8.0	0.26	12.969	1045.6	801.8	1312.7	3834.2	76.3	71.1	23
53	8.0	0.26	12.818	1153.8	795.4	1307.7	3893.6	77.5	73.2	24
54	20.0	0.04	5.027	385.2	35.6	6530.7	7082.4	56.4	47.3	27
55	20.0	0.05	6.522	535.4	63.9	6365.3	7551.2	60.1	51.9	23
56	20.0	0.08	10.430	876.0	192.6	5670.8	8899.2	70.8	57.5	27
57	25.0	0.04	6.707	521.8	47.3	9008.0	8257.6	52.6	40.4	23
58	25.0	0.07	11.357	921.9	164.8	8328.5	10035.3	63.9	49.2	23

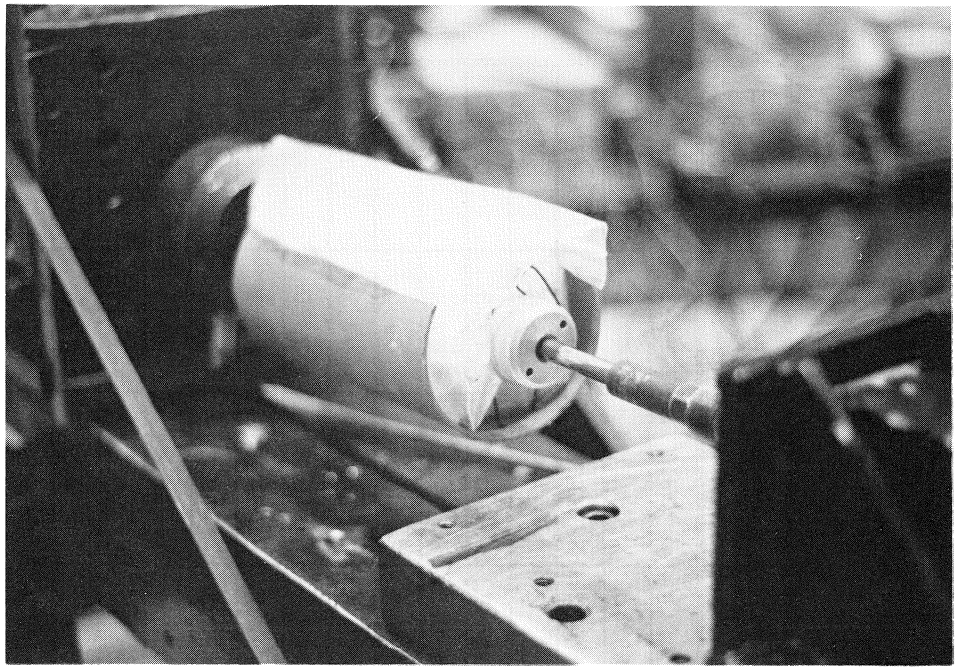

FIGURE 2-5 View of Testing Arrangement in Low Temperature Tests

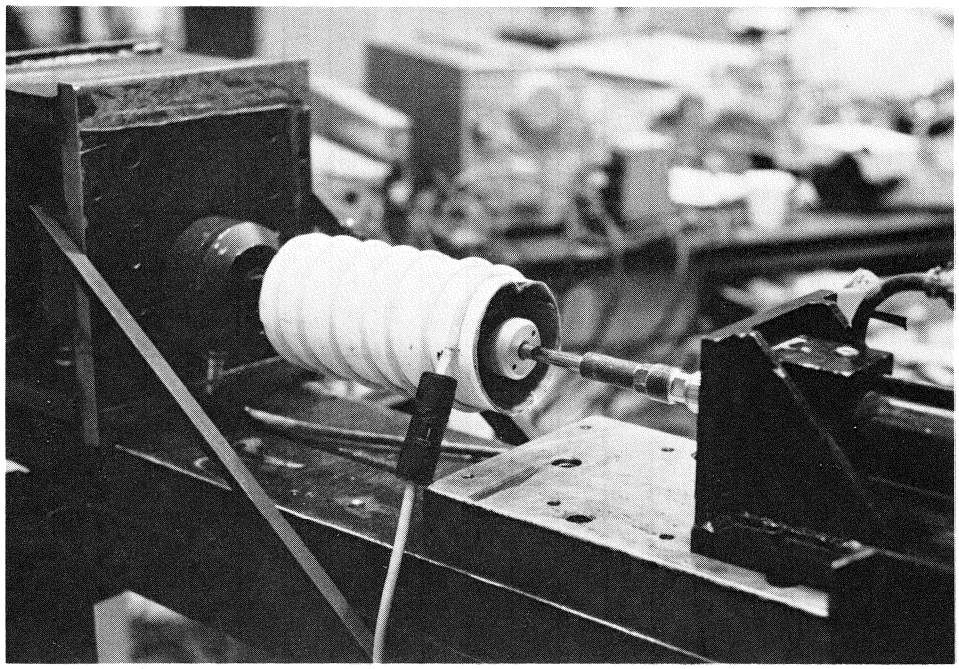

FIGURE 2-6 View of Testing Arrangement in High Temperature Tests

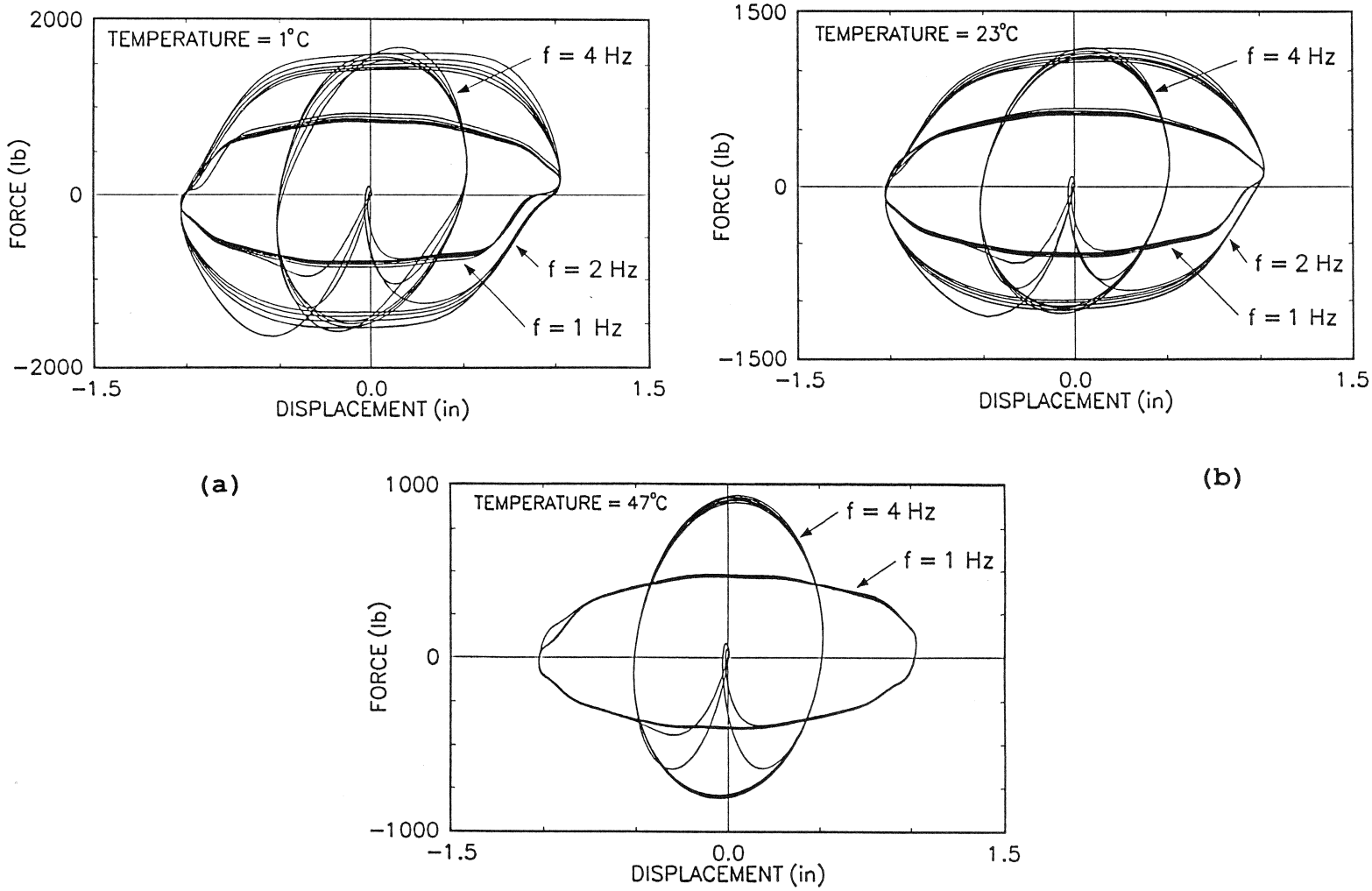

FIGURE 2-7 Recorded Force - Displacement Loops at (a) Low Temperature, (b) Room Temperature, and (c) High Temperature (1 in. = 25.4 mm, 1 lb = 4.46 N)

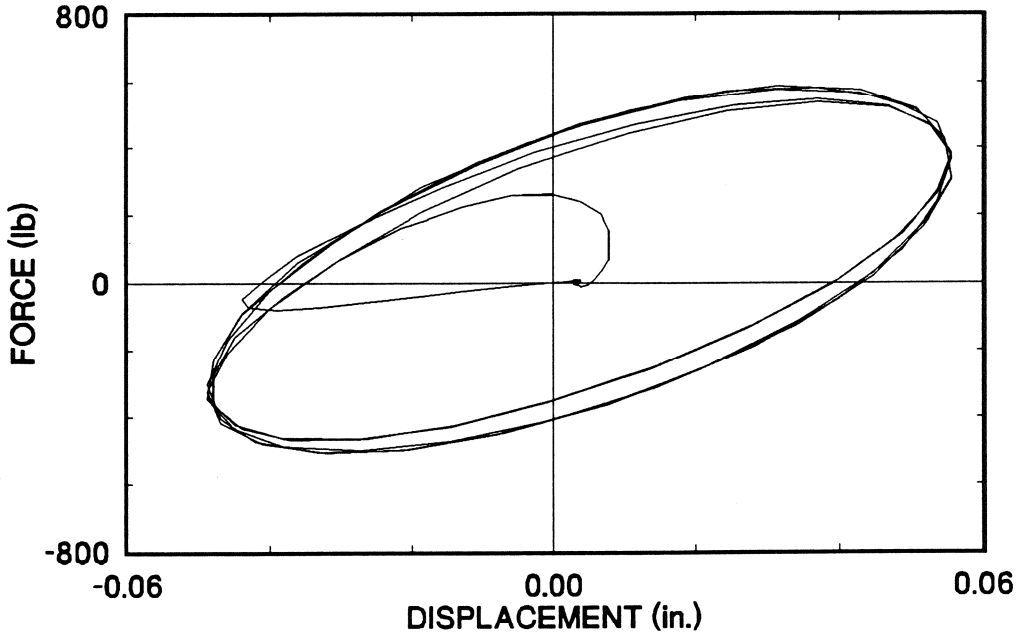

FIGURE 2-8 Recorded Force - Displacement Loop at Frequency of 20 Hz and Temperature of 23°C (1 in. = 25.4 mm, 1 lb = 4.46 N)

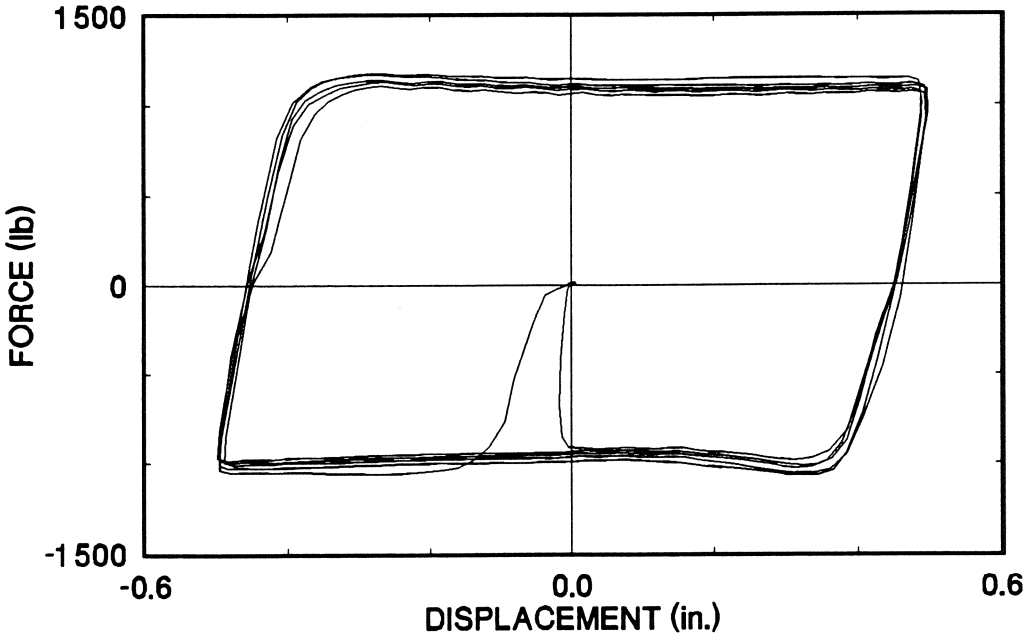

FIGURE 2-9 Recorded Force - Displacement Loop in Constant Velocity Test at Velocity of 12.6 in/sec and Temperature of 23°C (1 in. = 25.4 mm, 1 lb = 4.46 N)

property was obtained in additional tests with constant velocity motion (sawtooth displacement). Figure 2-9 shows the recorded force-displacement loop in one such test with amplitude of 0.5 in (12.7 mm) and constant velocity of 12.6 in/sec (320 mm/sec). Evidently, the output force is independent of amplitude.

Within the temperature range of about 0°C to 50°C, the device apparently exhibits a dependency of its mechanical properties on temperature. This dependency is discussed in detail in the next subsection. However, it is worthy of mentioning that this dependency is not significant. The reader may confirm in the results of Table 2-II (tests 16 to 20) that within the aforementioned range of temperatures, the loss stiffness of the damper reduces by a factor of less than 2. For comparison, viscoelastic material dampers exhibit a close to 50-fold decrease in about the same range of temperatures (see discussion in Section 1.3).

2.5 Mathematical Modeling

Over a large frequency range, the damper exhibits viscoelastic fluid behavior. The simplest model to account for this behavior is the Maxwell model (Bird 1987).

The Maxwell model is defined at the macroscopic level as

$$P + \lambda \dot{P} = C_o \dot{u} \tag{2-13}$$

where λ is the relaxation time, and C_o is the damping constant at zero frequency. A more general Maxwell model may also be considered in which the derivatives are of fractional order (Makris 1991)

$$P + \lambda D^r[P] = C_o D^q[u] \tag{2-14}$$

where $D^r[f(t)]$ is the fractional derivative of order r of the time dependent function f. For complex viscoelastic fluid behavior, Equation 2-14 may offer more control than Equation 2-13 in modeling the behavior.

The generalized Maxwell model was initially considered. The parameter q was set equal to unity based on the assumption that the damping coefficient of the device is independent of the velocity over a wide range of values. For $q = 1$, the parameter C_o becomes the damping constant at zero frequency. Parameters λ and r were then determined by curve fitting of experimental values of C and K_1 versus the frequency of motion. Analytical expressions for the mechanical properties are given by

$$K_1 = \frac{C_o \lambda \omega^{1+r} \sin\left(\frac{\pi r}{2}\right)}{d} \tag{2-15}$$

$$C = \frac{K_2}{\omega} = \frac{C_o \left[1 + \lambda \omega^r \cos\left(\frac{\pi r}{2}\right)\right]}{d} \tag{2-16}$$

$$d = 1 + \lambda^2 \omega^{2r} + 2\lambda \omega^r \cos\left(\frac{\pi r}{2}\right) \tag{2-17}$$

$$\delta = \tan^{-1}\left(\frac{K_2}{K_1}\right) \tag{2-18}$$

The calibration of the model of Equation 2-14 was performed for the case of room temperature, for which experimental data over a wide frequency range were available. The calibration resulted in

parameters $r = 1$, $q = 1$, $\lambda = 0.006$ secs and $C_o = 88$ lb-sec/in (15.45 N-sec/mm). Interestingly, the calibrated model is the classical Maxwell model. A comparison of experimental and analytically derived properties of storage stiffness, damping coefficient and phase angle is presented in Figure 2-10. The comparison is very good except for frequencies above 20 Hz, where the model underpredicts the storage stiffness. Such frequencies are typically not considered in seismic analysis.

Furthermore, the model predicts nonzero storage stiffness in the low frequency range (< 2 Hz). The predicted storage stiffness is insignificant for practical purposes.

The damper exhibits a relaxation time of only 6 msec. This indicates that for low rates of damper force, the term $\lambda \dot{P}$ in Equation 2-13 is insignificant. This occurs for frequencies below a cutoff value of about 4 Hz. Accordingly, for typical structural applications the term $\lambda \dot{P}$ may be neglected. This will be confirmed in a subsequent section where shake table results are compared to analytical results.

The model of the damper below the cutoff frequency is simply

$$P = C_o \dot{u} \qquad (2\text{-}19)$$

and, thus, for most practical purposes the damper behaves as a linear viscous dashpot.

The effect that temperature has on the single parameter of the model, C_o, is investigated in Figure 2-11. The recorded peak force in each test is plotted against the imposed peak velocity for the three values of temperature. It may be seen that the experimental results may be fitted with straight lines with slope equal to C_o.

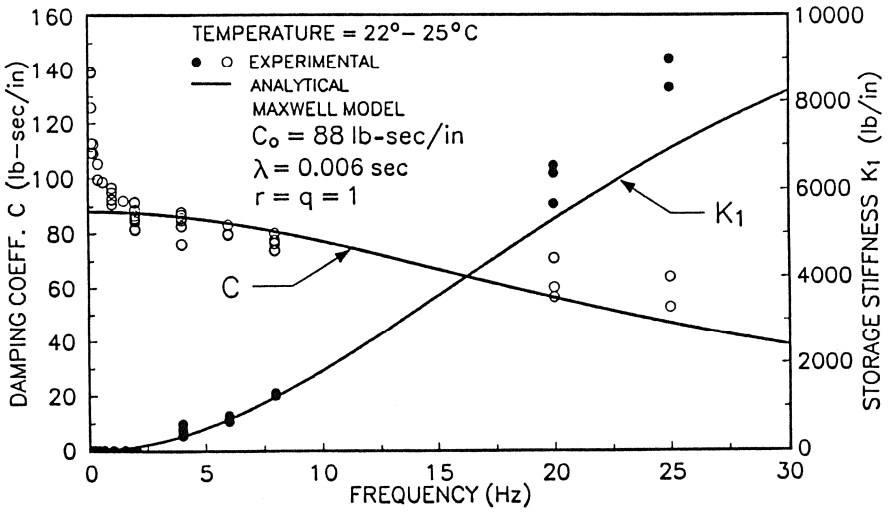

(a)

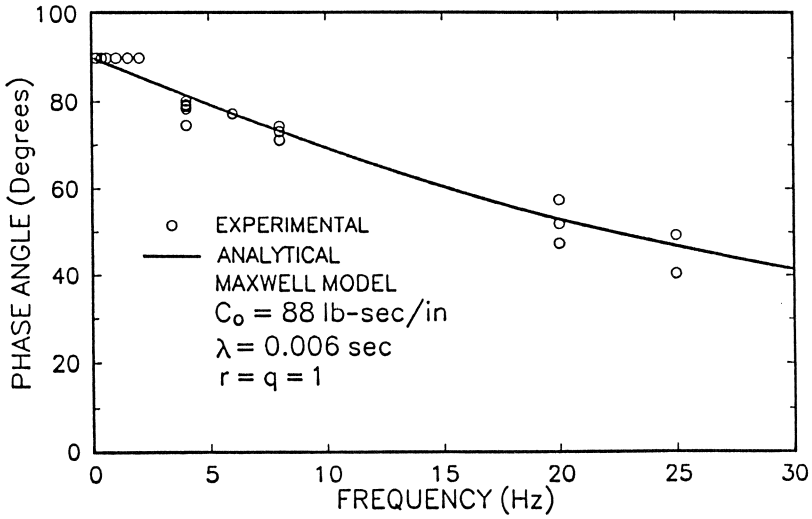

(b)

FIGURE 2-10 **Comparison of Experimental and Analytically Derived Values of (a) Storage Stiffness and Damping Coefficient at Room Temperature and (b) Phase Angle at Room Temperature (1 in. = 25.4 mm, 1 lb = 4.46 N)**

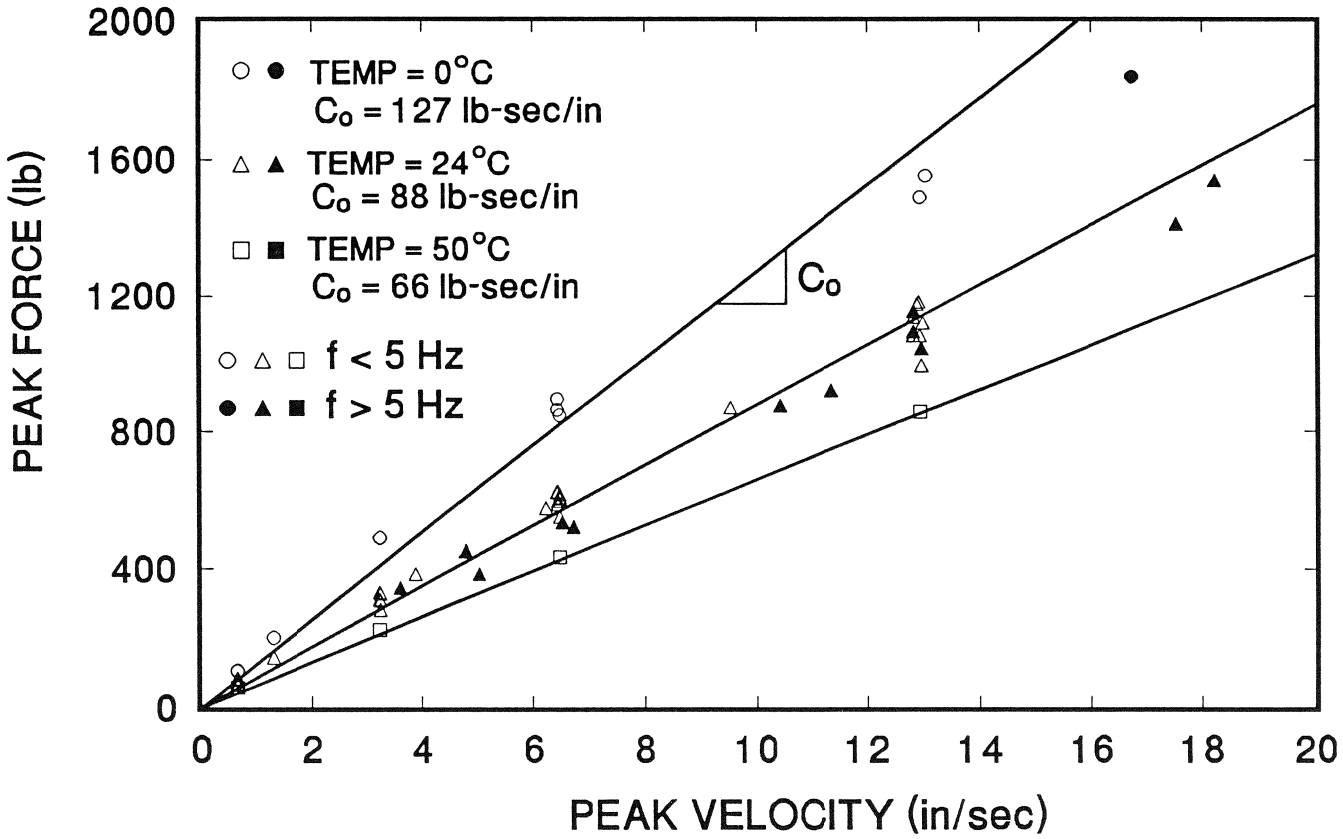

FIGURE 2-11 Recorded Values of Peak Force Versus Peak Velocity for Low, Room and High Temperature Tests (1 in. = 25.4 mm, 1 lb = 4.46 N)

For room temperature (24°C) and above, the behavior is indeed linear viscous to velocities of about 20 in/sec (508 mm/sec) and beyond. As temperature drops, the experimental results deviate from linearity at a lower velocity.

The values of constant C_o in Figure 2-11 demonstrate that the damper exhibits a stable behavior over a wide range of temperatures. Between about 0°C and 50°C, constant C_o reduces by a factor of less than 2. Assuming that a design for a building application will be anchored at a temperature of about 24°C, variations of temperature in the range of 0°C to 50°C will result in variations of the damping ratio of +44% to -25%. That is, if a design calls for a damping ratio of 20% of critical, extreme temperature variations will alter the damping ratio in the range of 15% to 29% of critical.

SECTION 3
MODEL FOR EARTHQUAKE SIMULATOR TESTING

3.1 One-story and Three-story Steel Structures

A series of 66 earthquake simulation tests were performed on a model structure (see Figure 3-1). The structure was a three-story 1:4 scale steel frame which modeled a shear building by the method of artificial mass simulation (Soong 1987). The model does not represent a similitude-scaled replica of a full-scale building. Rather, the test structure was designed as a small structural system. The model has been used in a number of previous earthquake simulation studies. The mass of each floor of the three-story model was 5.46 lb-sec^2/in (958 Kg) for a total mass of 16.38 lb-sec^2/in (2874 Kg). For some of the tests, the structure was modified by rigidly bracing the second and third stories so that the frame would act as a one-story structure. The one-story model had a total mass of 16.7 lb-sec^2/in (2930 Kg).

The model was bolted to the center of a concrete block which was in turn bolted to the shaking table in such a way that the main frames of the model were parallel to the motion of the table. Note that an out-of-plane diagonal bracing system exists perpendicular to the direction of excitation (see Figure 3-1). This out-of-plane bracing was in place during all tests and ensured that there was no motion perpendicular to the direction of table motion and thus the model was effectively reduced to a planar frame.

For the one-story structure, the dampers were placed at the first story and consisted of either two or four damping units (see Figure 3-2). For the three-story structure, the dampers were placed at the first story for the two and four damper cases and at all three stories for the six damper case (see Figure 3-3). The dampers were attached to the structure as shown schematically in Figure 3-4. A close-up view of a damper installed in the first story is shown in

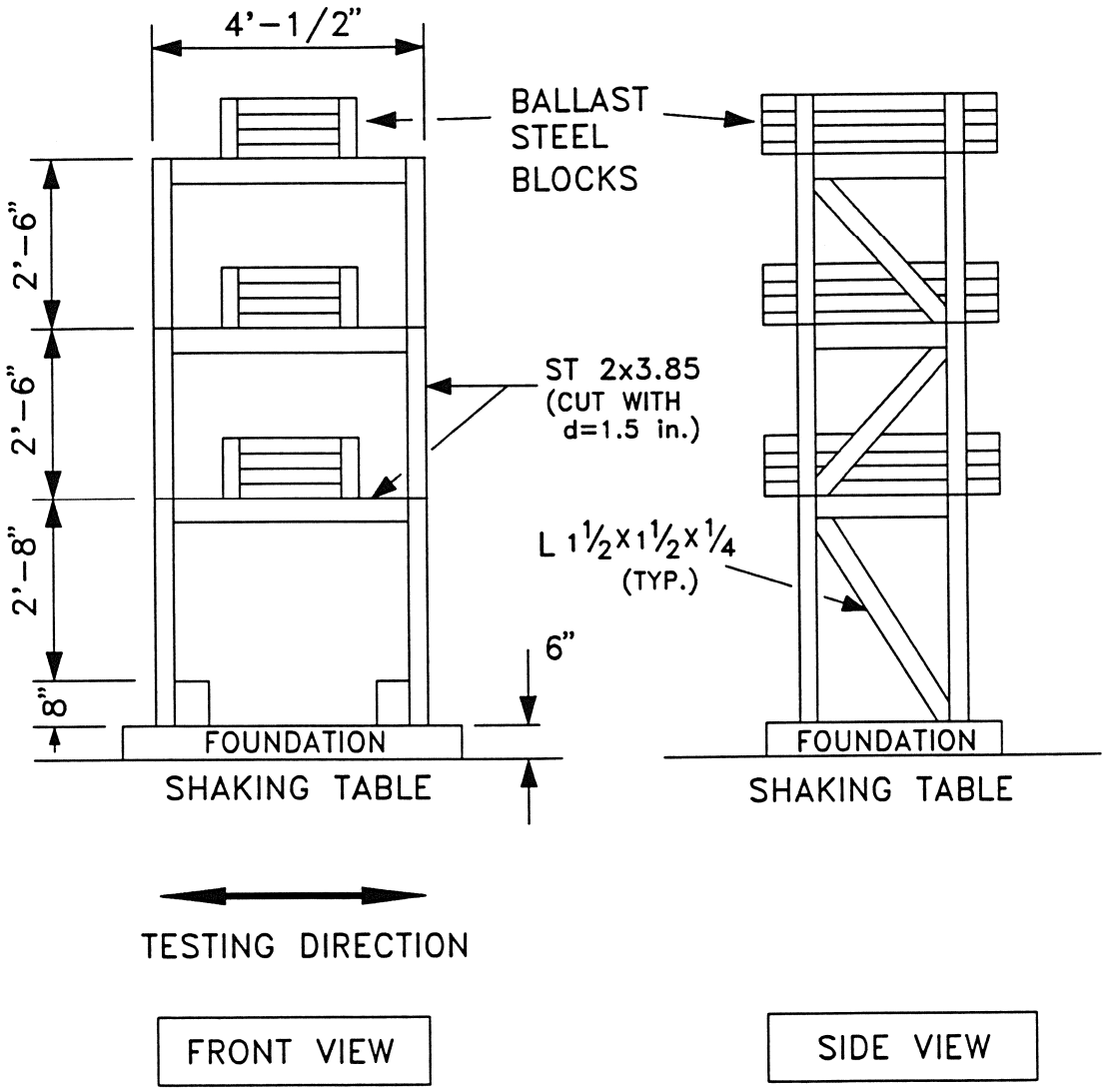

FIGURE 3-1 **Schematic of Model Structure (1 in. = 25.4 mm)**

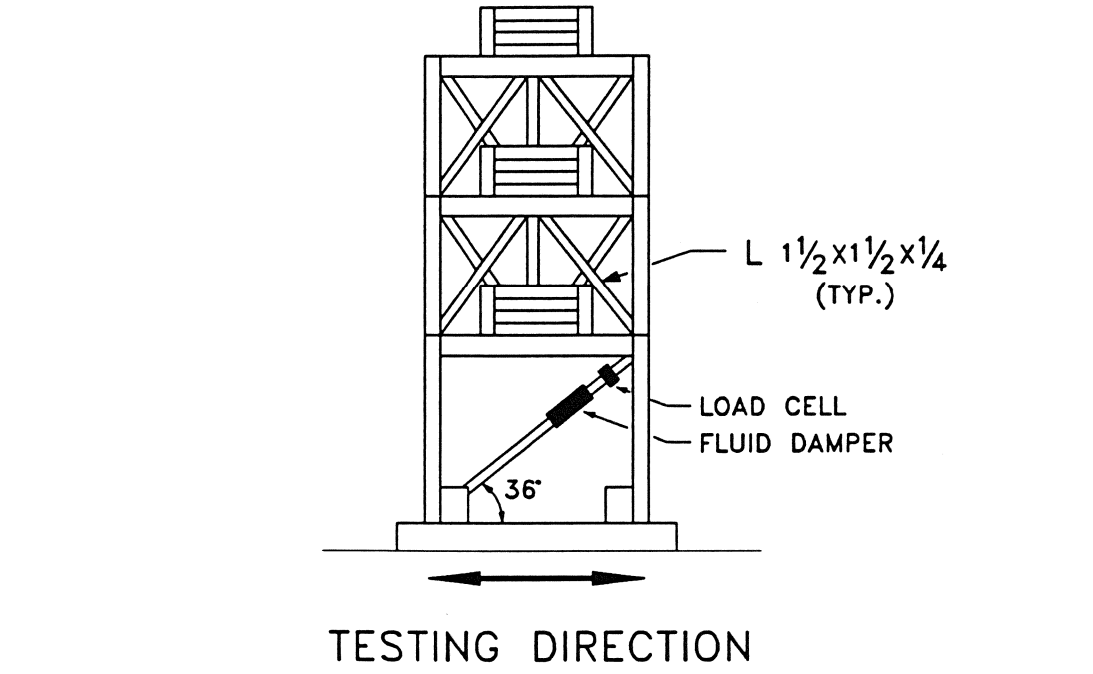

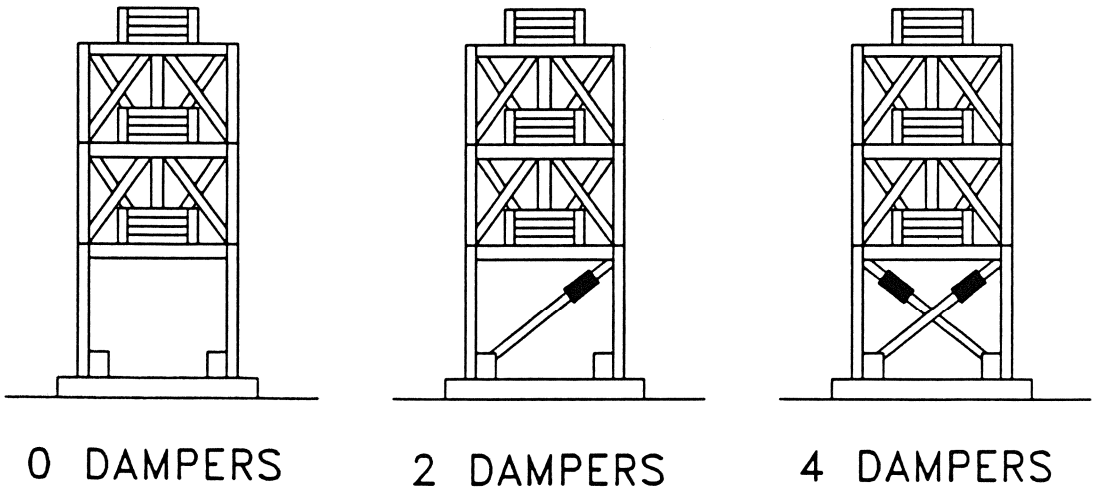

FIGURE 3-2 **Damper Configurations for One-story Structure (1 in. = 25.4 mm)**

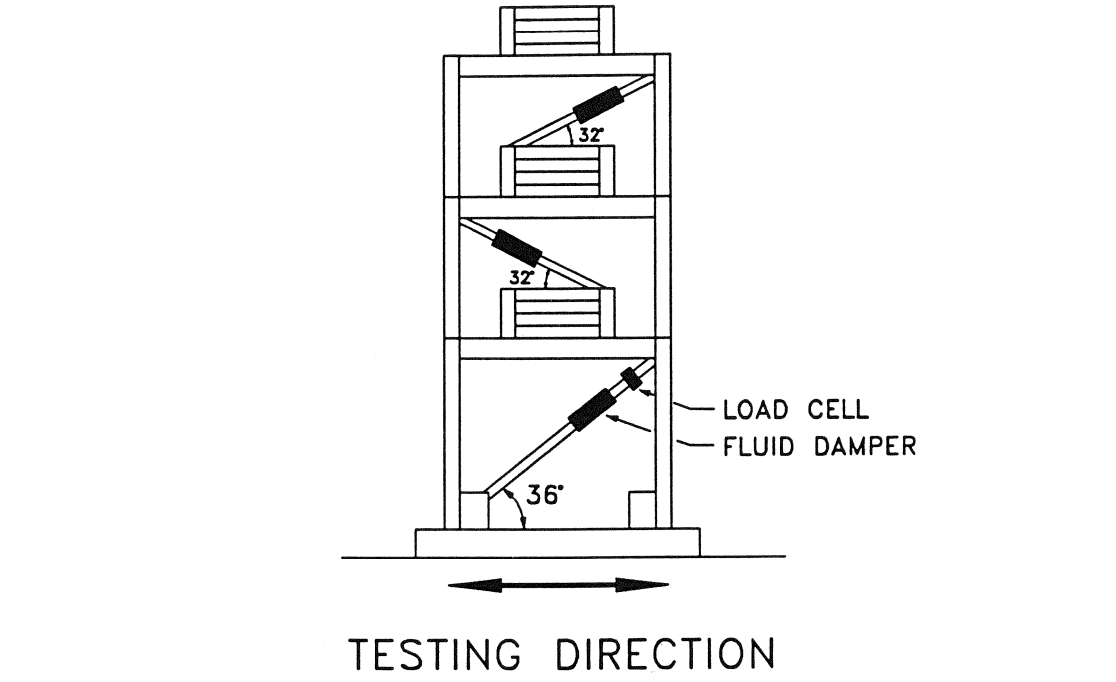

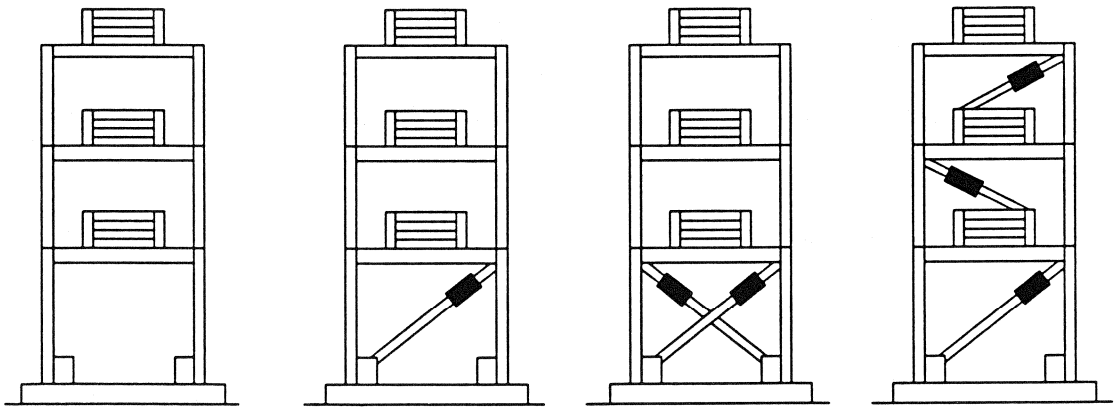

FIGURE 3-3 Damper Configurations for 3-story Structure

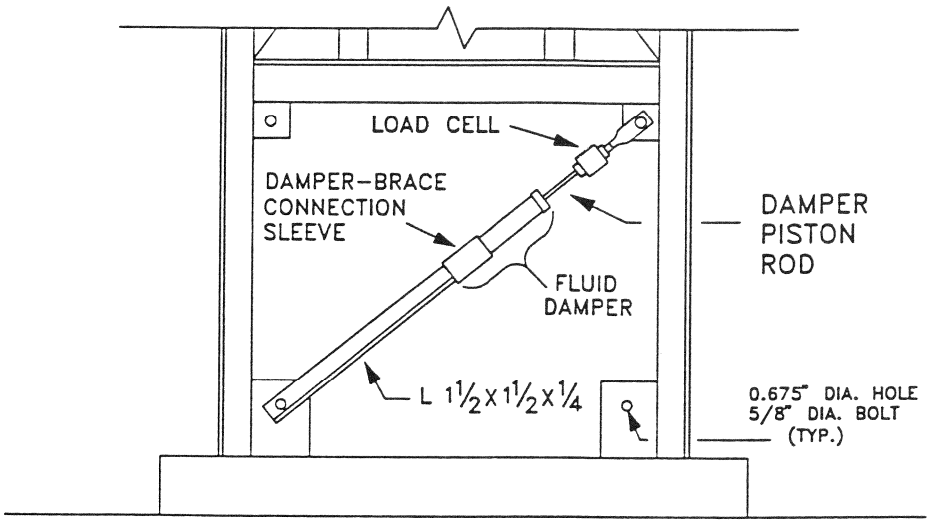

FIGURE 3-4 **Schematic of Damper Connection Details (1 in. = 25.4 mm)**

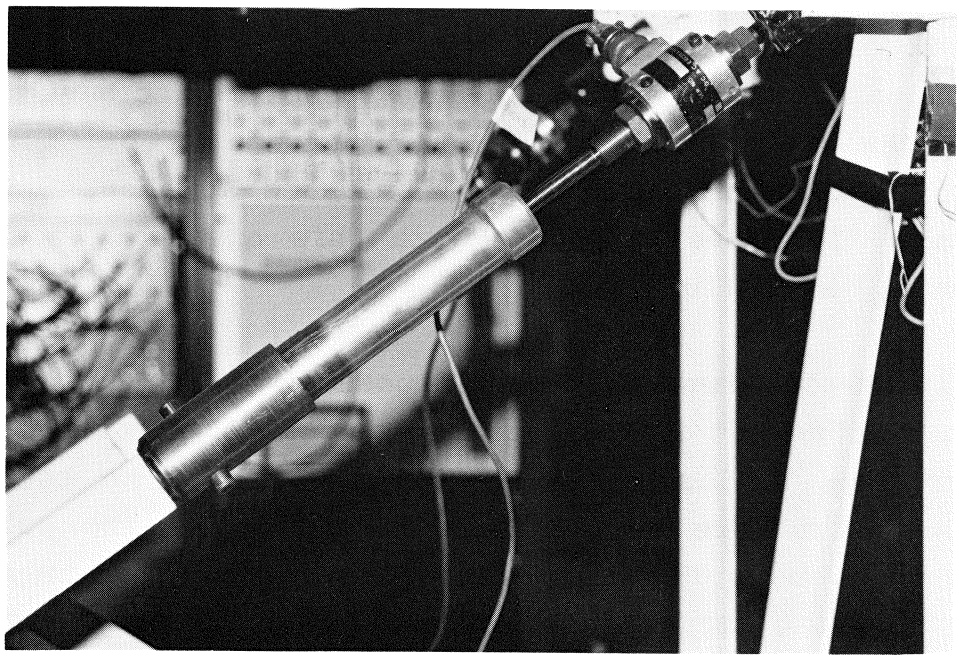

FIGURE 3-5 **Close-up View of Two Dampers in the Model Structure at the First Story**

Figure 3-5. A view of the one-story structure with four dampers and a close-up view of the structure with two dampers in the first story is presented in Figures 3-6 and 3-7, respectively.

Testing proceeded in the following sequence. First the one-story configuration without and with fluid dampers was tested. The structure suffered damage in previous testing and exhibited both low stiffness and strength. Cracks existed on the webs of the structural tees forming the first story columns. Propagation of the cracks was prevented by drilling small holes at the tip of each crack. In this condition, the one-story structure was identified to have, at small amplitudes of vibration, a frequency of 2 Hz and damping ratio of 0.55 percent of critical. In seismic excitation, damping was estimated to be about 2 percent of critical.

Subsequently, the one-story structure was tested in a stiffer configuration. Steel plate stiffeners were welded at the top and bottom of each first story column. The properties of the structure at small amplitude of vibration were identified to have a frequency of 3.13 Hz and damping ratio of 2 percent of critical. Under seismic excitation, damping was estimated at about 3 percent of critical. Tests were conducted in this one-story configuration without and with fluid dampers.

Recognizing that damping in the structure without fluid dampers may be low, a different configuration was created and tested. A system of wire rope cables and pulleys was attached to the one-story stiffened structure as shown in Figure 3-8. The pulleys were locked so that during deformation the cables slid on the pulley guides. During motion, the cables did not change length so that they introduced frictional damping without increasing the stiffness. In seismic excitation, this damping was estimated to be about 5 percent of critical. In this configuration, tests were conducted without fluid dampers.

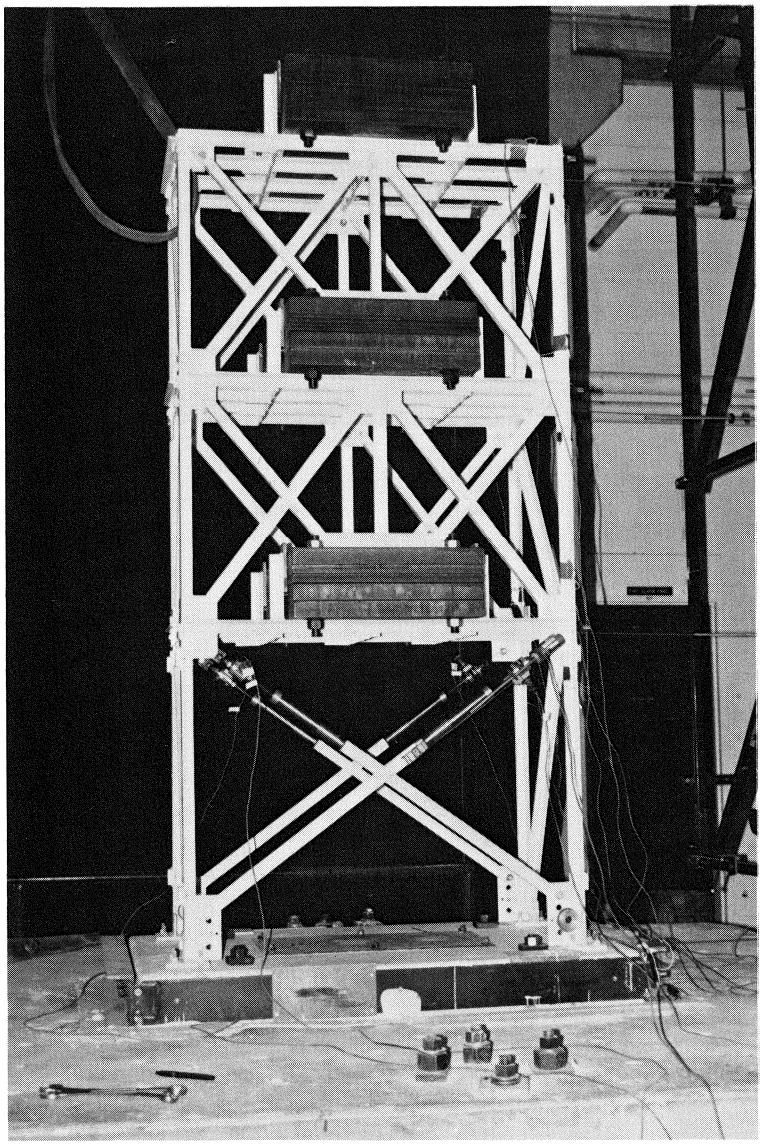

FIGURE 3-6 **View of One-story Model Structure with Four Dampers**

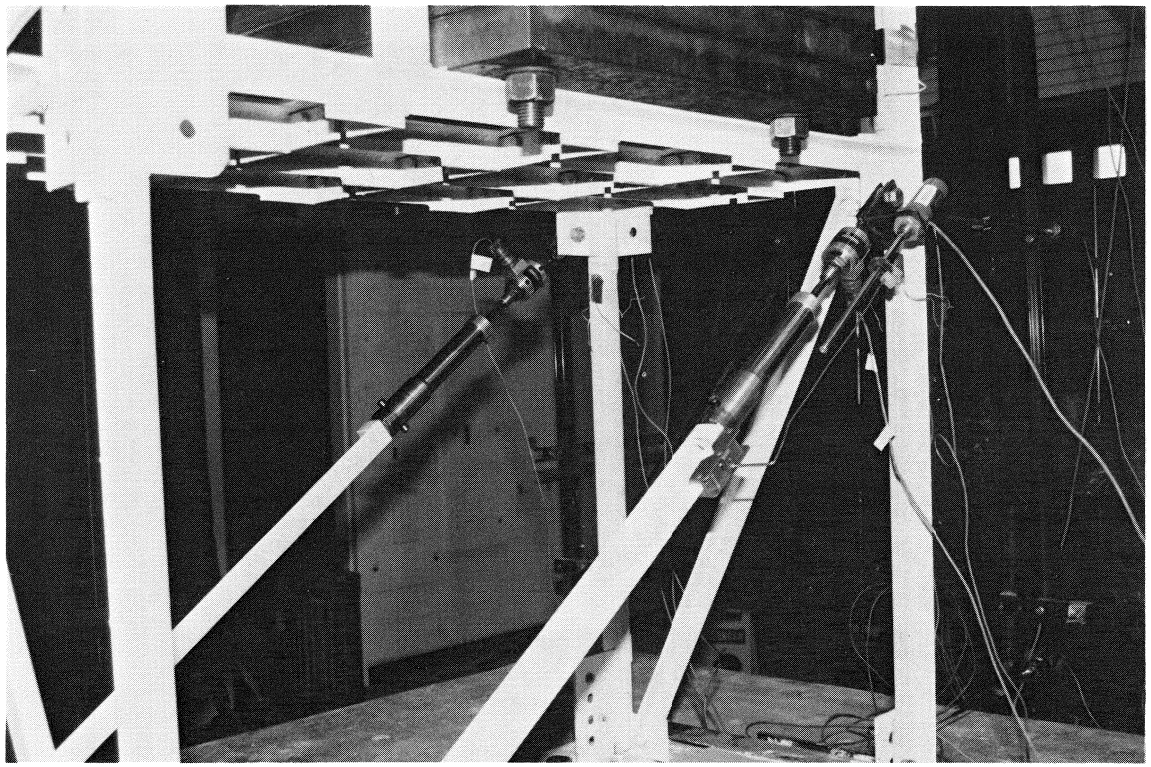

FIGURE 3-7 Close-up View of Two Dampers in the Model Structure at the First Story

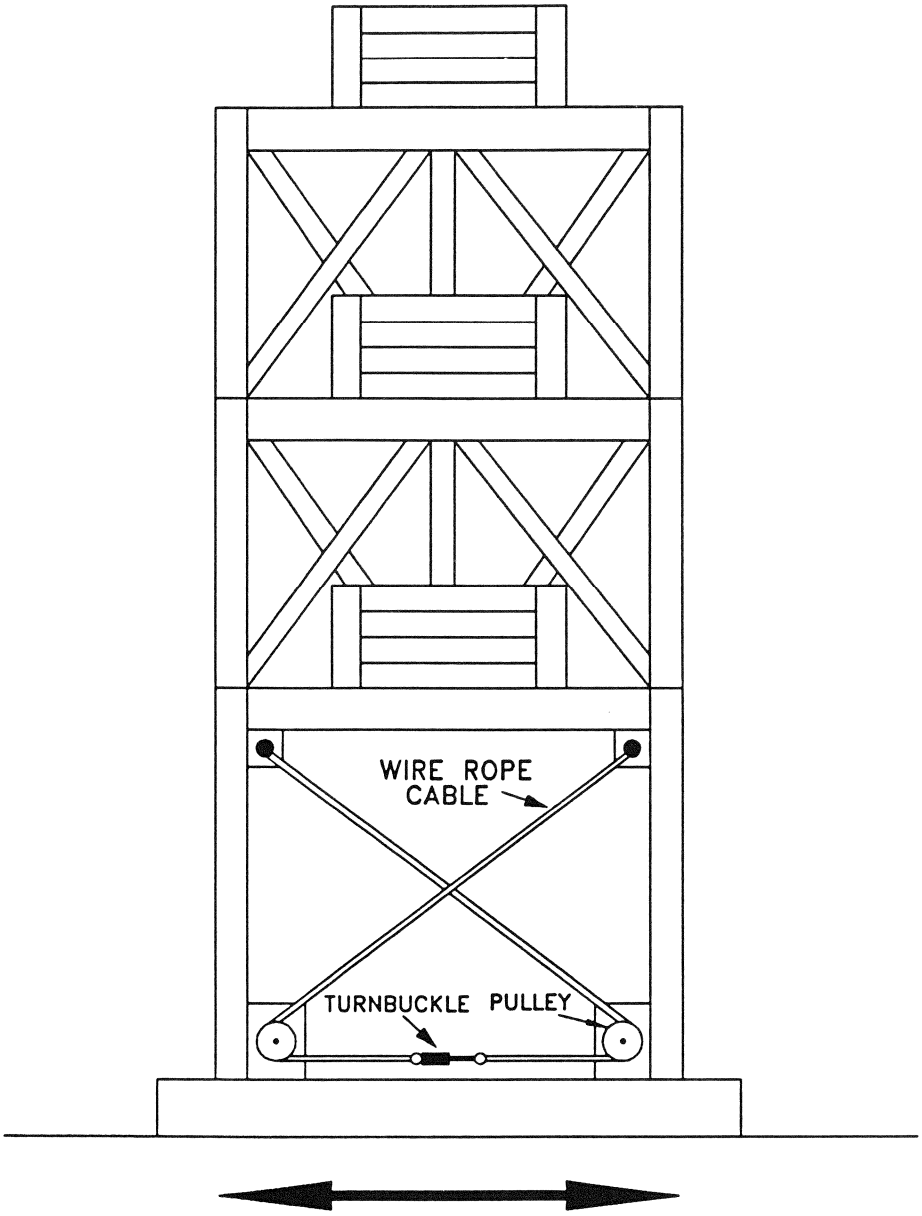

FIGURE 3-8 Schematic of Structure with Wire Rope Cables

In the three-story configuration, the bracing of the top two stories was removed. A view of the three-story structure with six dampers is shown in Figure 3-9. Note the presence of the stiffener plates at the top and bottom of each first story column (compare with Figure 3-6 wherein the stiffener plates have not been attached). The structure was identified at small amplitude of motion to have a fundamental frequency of 2 Hz and a corresponding damping ratio equal to 1.74 percent of critical. Tests were conducted without and with dampers.

3.2 Test Program

A total of 66 earthquake simulation tests were performed on the model structure. The earthquake signals and their characteristics are listed in Table 3-I. Each record was compressed in time by a factor of 2 to satisfy the similitude requirements of the quarter length scale model. Figures 3-10 to 3-14 show recorded time histories of the table motion in tests with input being the earthquake signals of Table 3-I. The acceleration and displacement records were directly measured, whereas the velocity record was obtained by numerical differentiation of the displacement record. It may be observed that the peak ground motion was reproduced well, but not exactly, by the table generated motion.

Figures 3-10 to 3-14 also show the response spectra of displacement and acceleration (exact, not pseudo-acceleration) of the table motions. The 5-percent damped acceleration spectra is compared to the spectra of the actual record to demonstrate the good reproduction of the motion of the table. The spectra at larger values of damping will be useful in analytical calculations to be presented later in this report.

A list of the earthquake simulation tests together with the structural system conditions is presented in Table 3-II. The

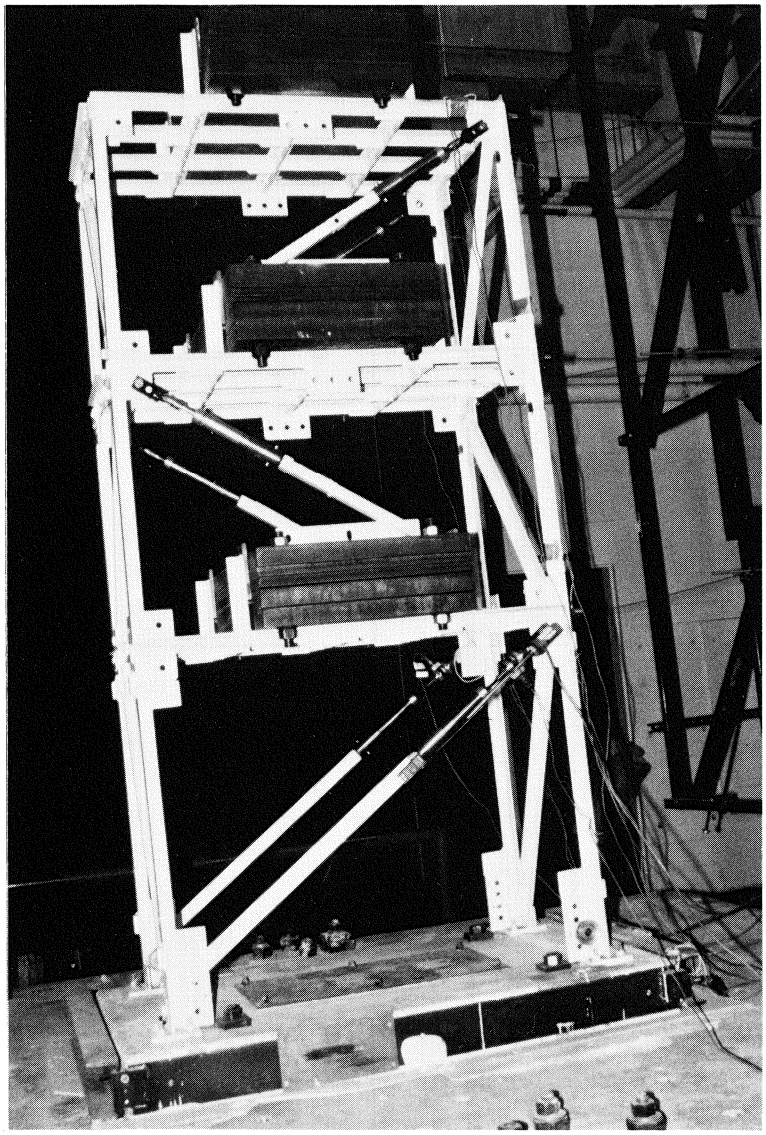

FIGURE 3-9 **View of 3-story Model Structure with Six Dampers**

TABLE 3-I Earthquake Motions Used in Test Program and Characteristics in Prototype Scale (1 in. = 25.4 mm)

NOTATION	RECORD	MAGNITUDE	PREDOMINANT FREQUENCY RANGE (Hz)	PEAK ACCELERATION (g's)	PEAK VELOCITY (in./sec)	PEAK DISPL. (in.)
El Centro S00E	Imperial Valley, May 18, 1940, component S00E	6.7	1-4	0.34	13.17	4.28
Taft N21E	Kern County, July 21, 1952, component N21E	7.2	0.5-5	0.16	6.19	2.64
Pacoima S74W	San Fernando, February 9, 1971, component S74W	6.4	0.25-2	1.08	22.73	4.26
Miyagi-Ken-Oki	Tohoku University, Sendai, Japan, June 12, 1978, component EW	7.4	0.5-5	0.16	5.55	2.00
Hachinohe	Tokachi-Oki earthquake, Japan, May 16, 1968, component NS	7.9	0.25-1.5	0.23	14.06	4.68

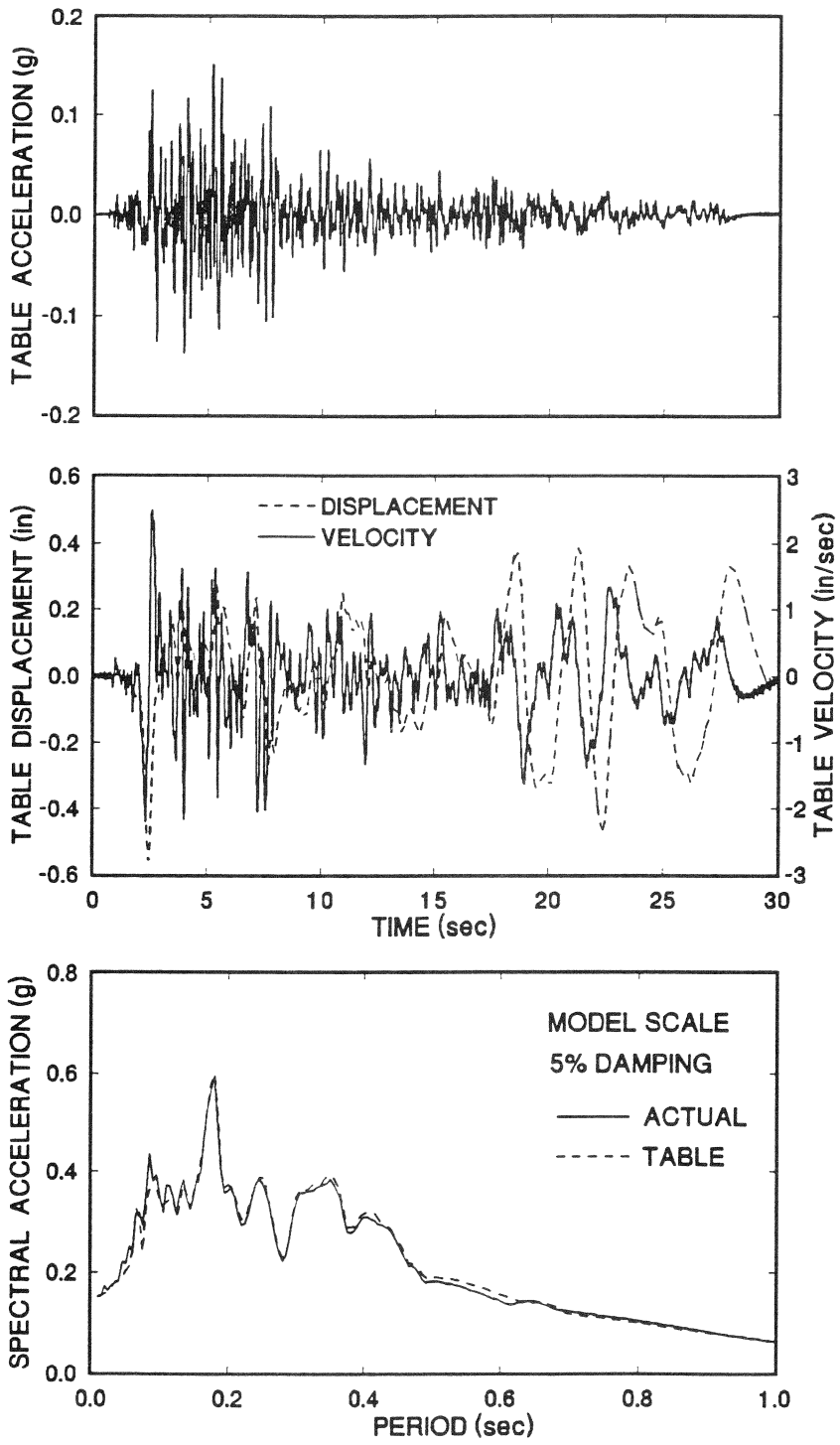

FIGURE 3-10 **Time Histories of Displacement, Velocity and Acceleration and Spectral Acceleration and Displacement of Shaking Table Excited with Taft 100% Motion (1 in. = 25.4 mm)**

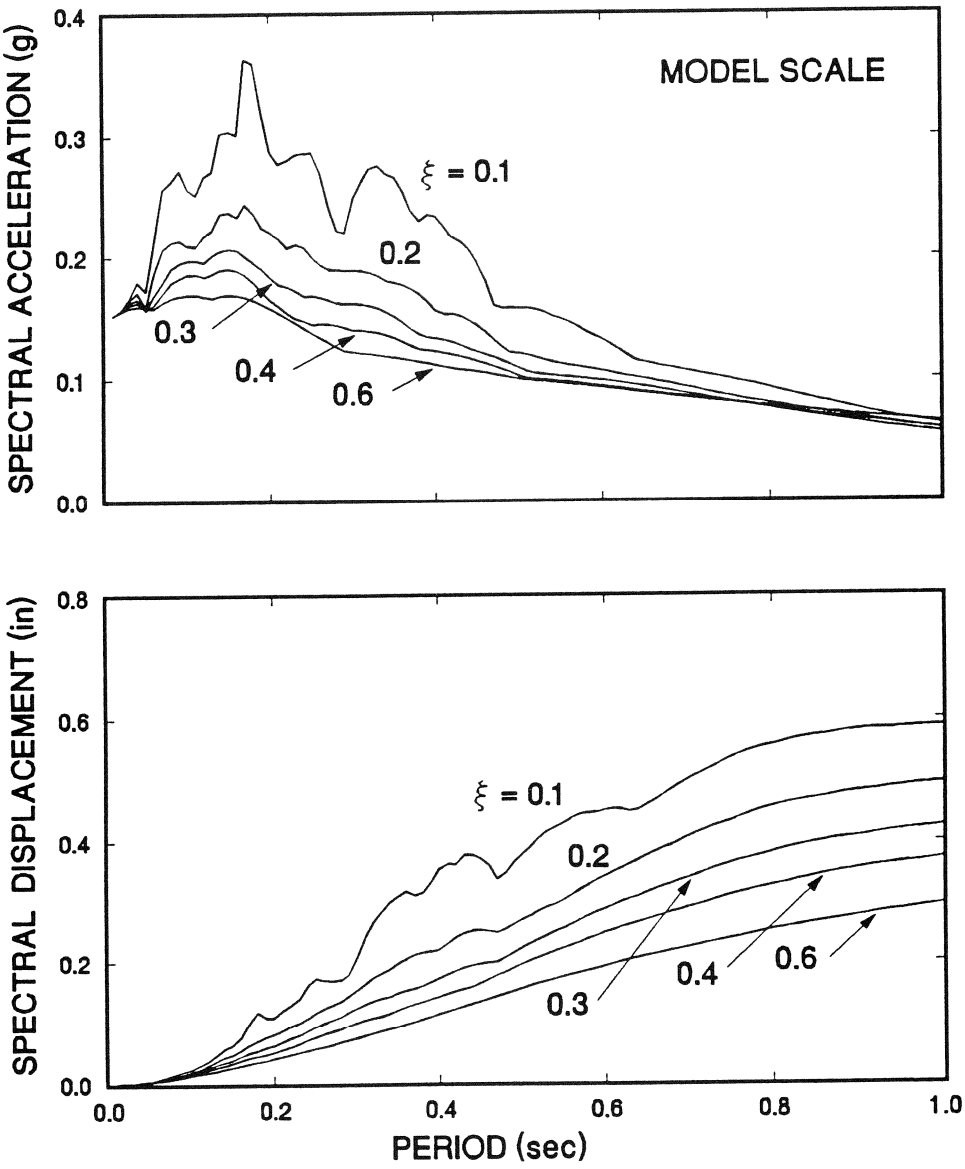

FIGURE 3-10 Continued

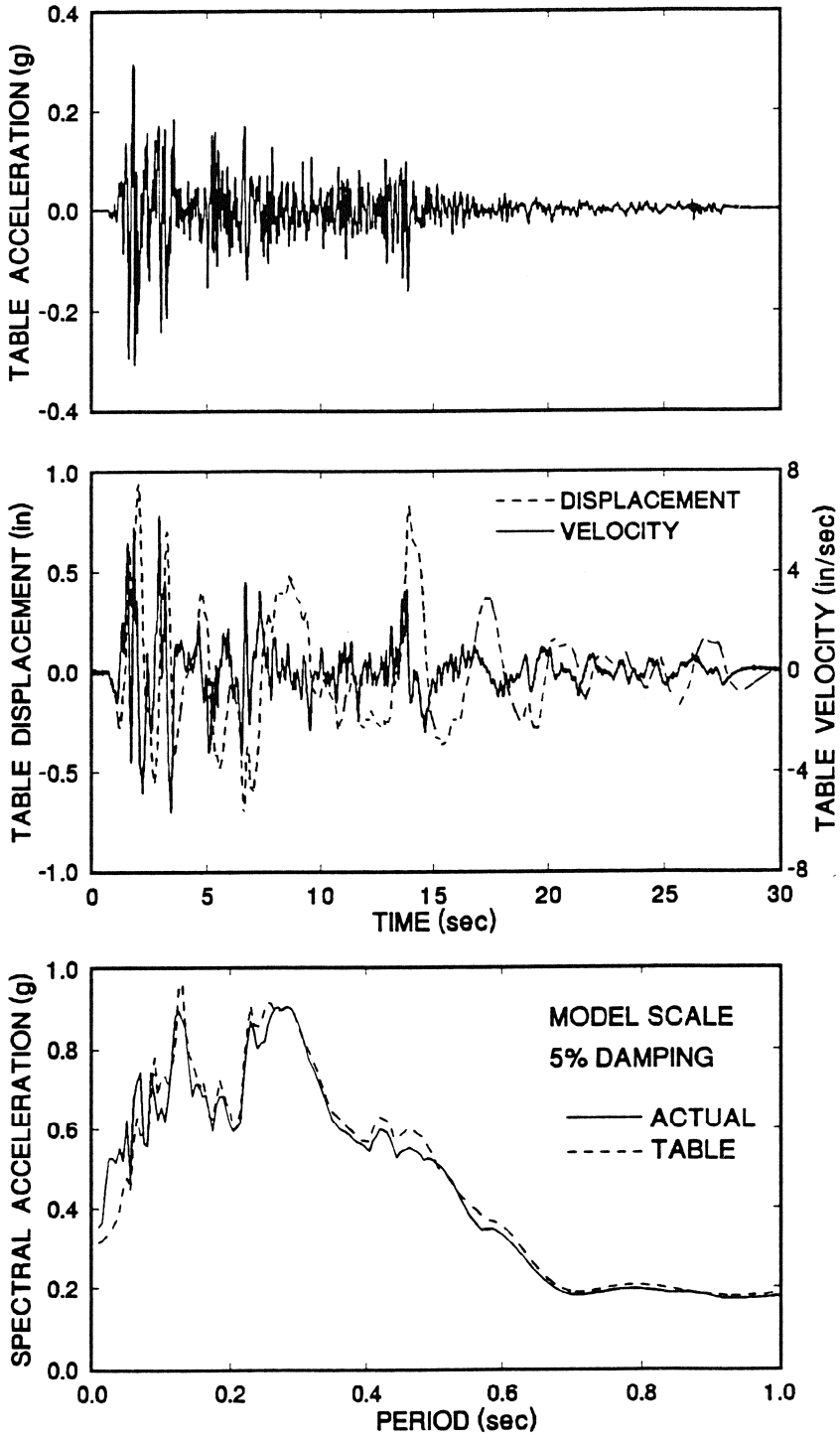

FIGURE 3-11 **Time Histories of Displacement, Velocity and Acceleration and Spectral Acceleration and Displacement of Shaking Table Excited with El Centro 100% Motion (1 in. = 25.4 mm)**

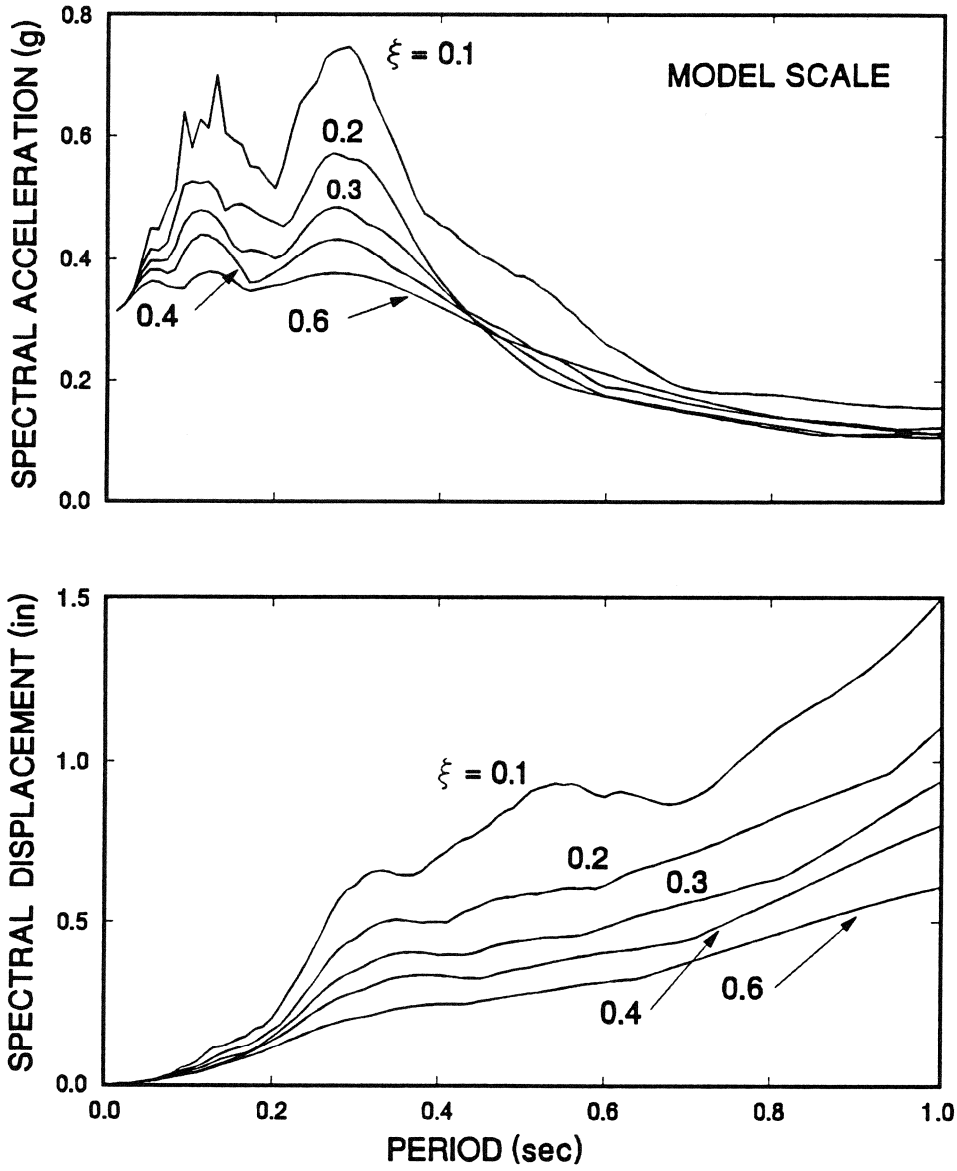

FIGURE 3-11 Continued

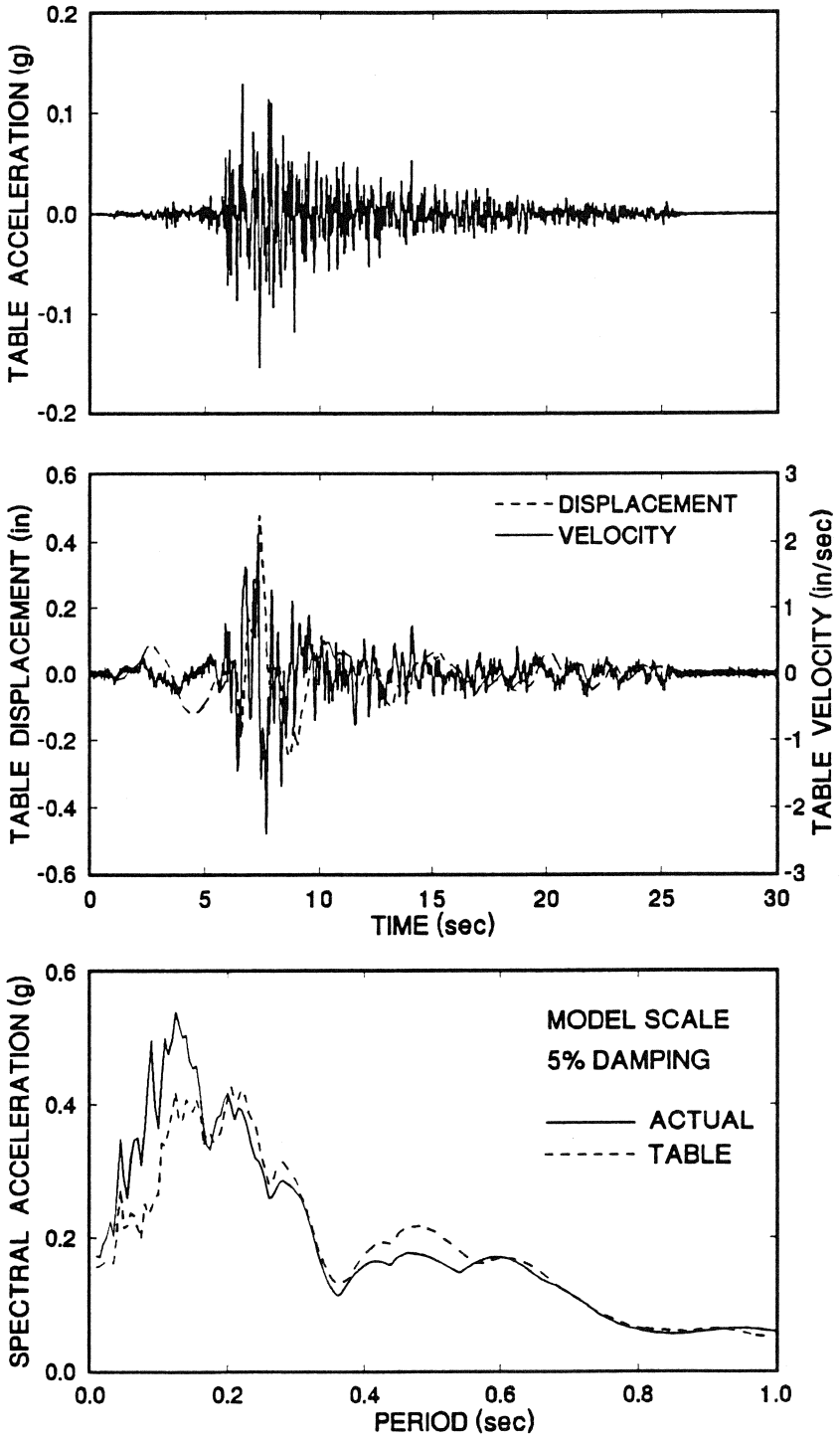

FIGURE 3-12 **Time Histories of Displacement, Velocity and Acceleration and Spectral Acceleration and Displacement of Shaking Table Excited with Miyagiken 100% Motion (1 in. = 25.4 mm)**

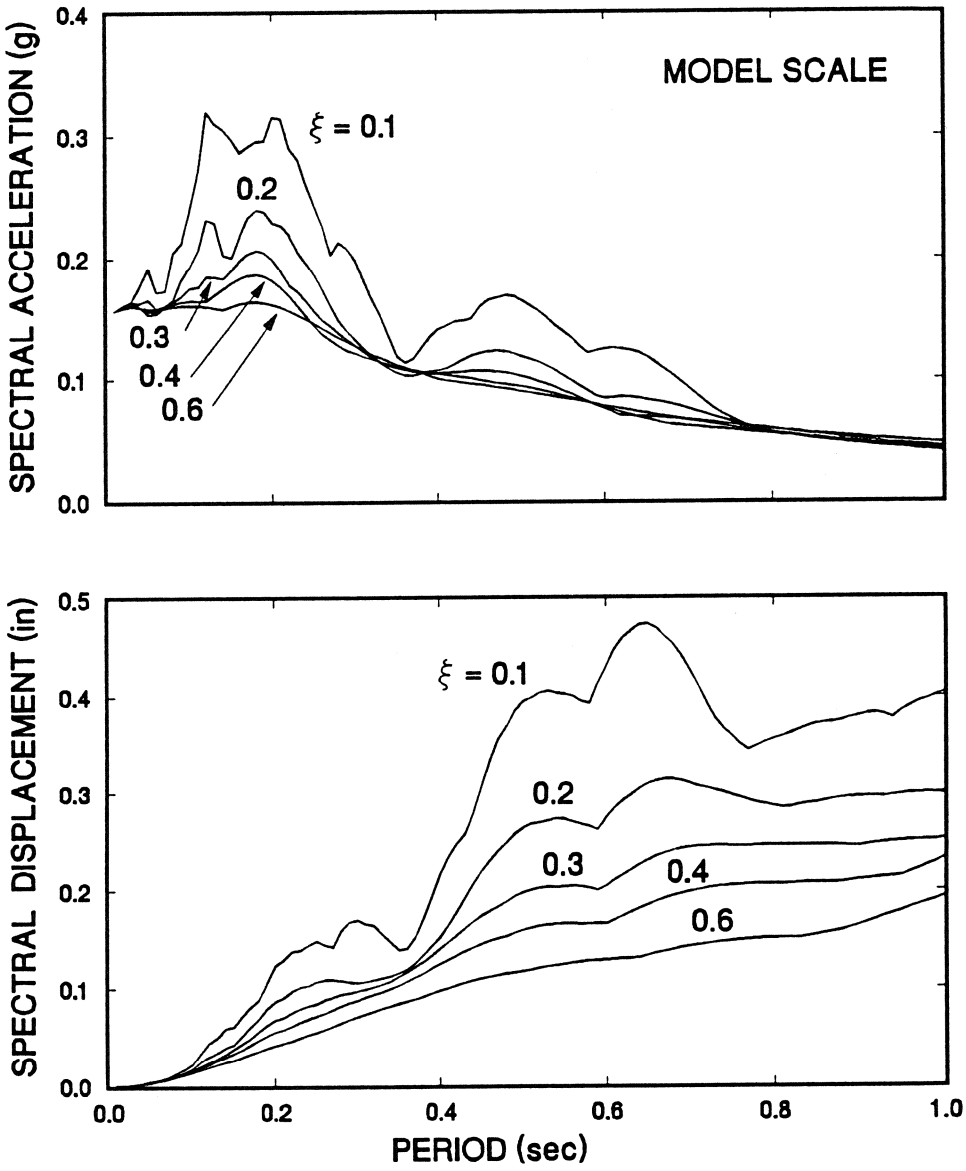

FIGURE 3-12 Continued

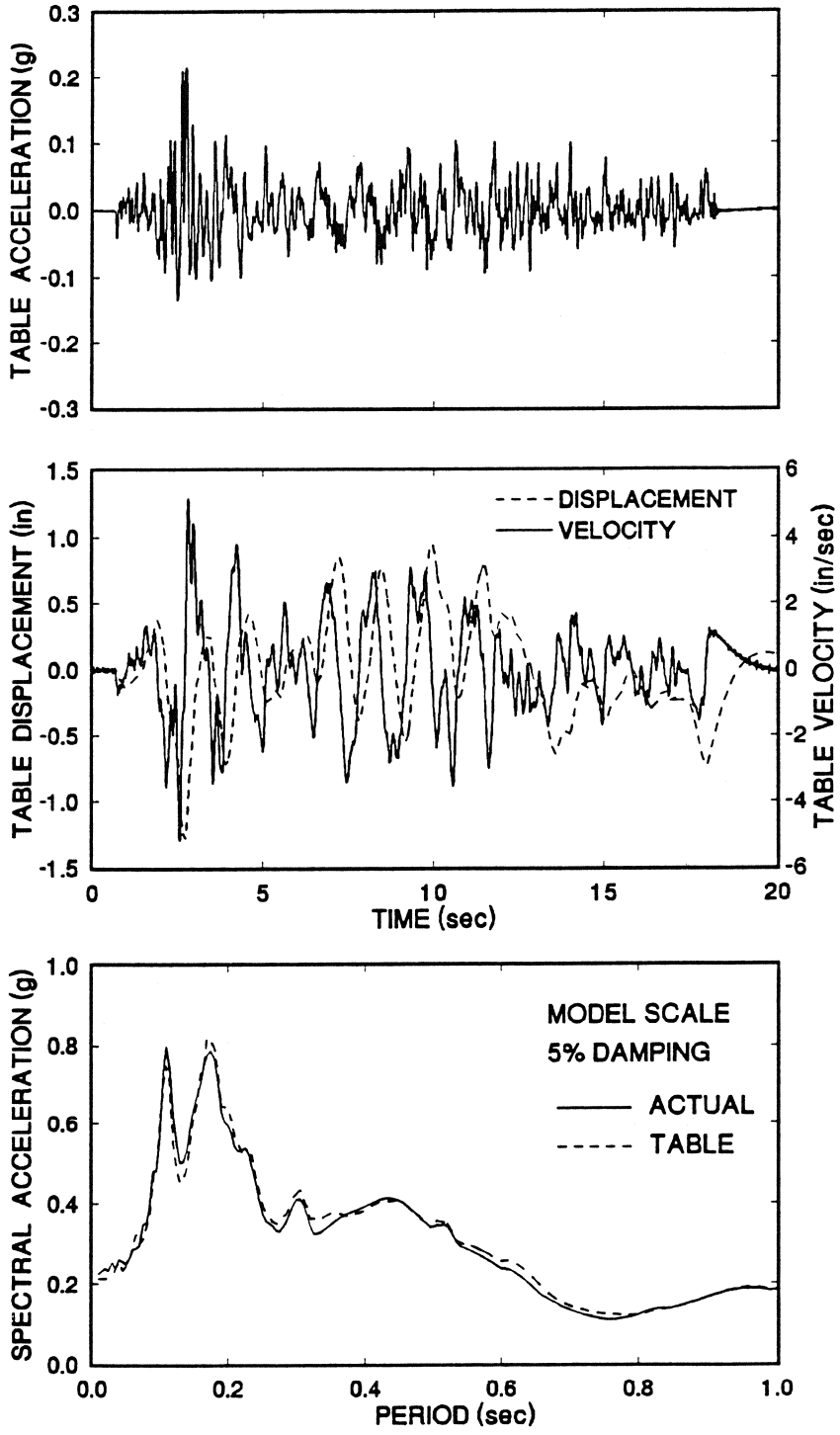

FIGURE 3-13 **Time Histories of Displacement, Velocity and Acceleration and Spectral Acceleration and Displacement of Shaking Table Excited with Hachinohe 100% Motion (1 in. = 25.4 mm)**

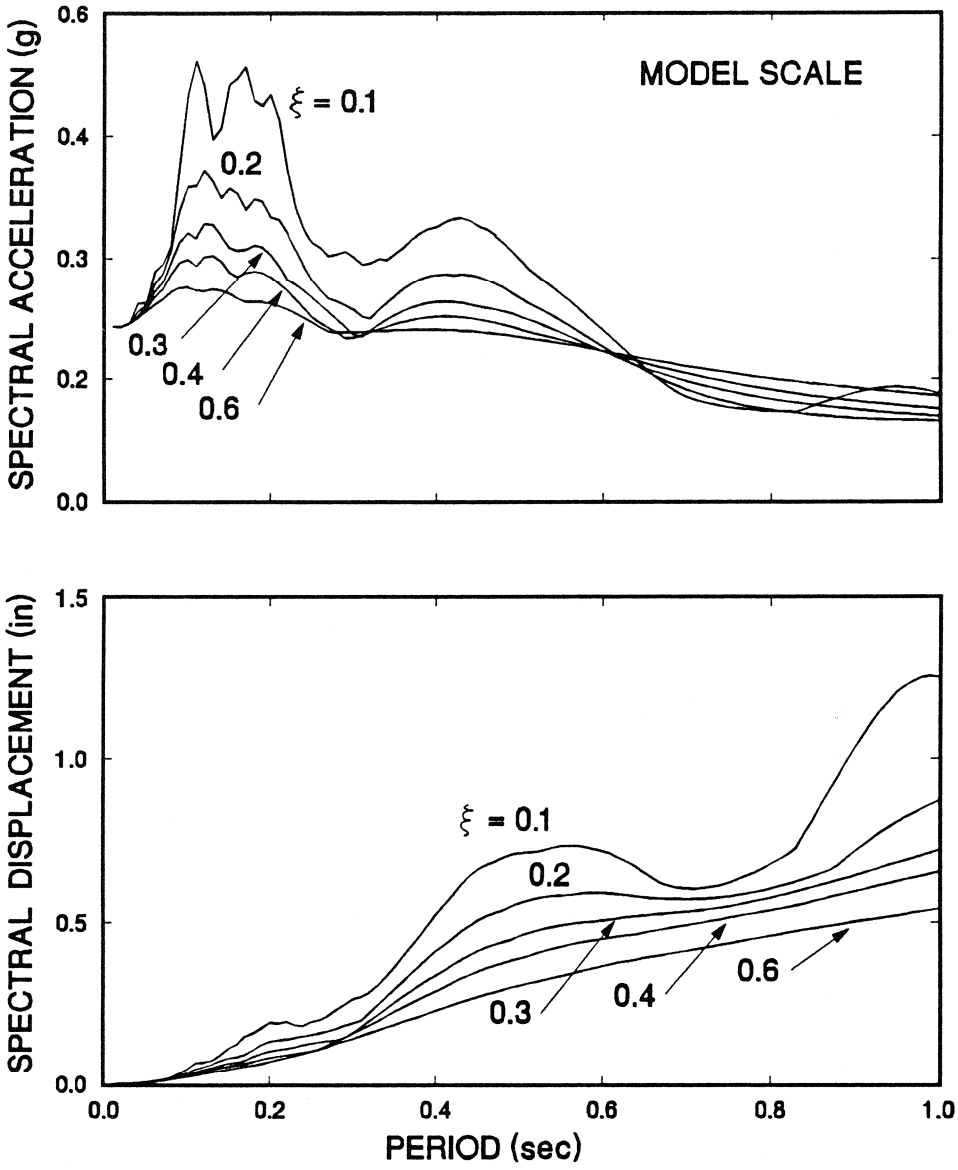

FIGURE 3-13 Continued

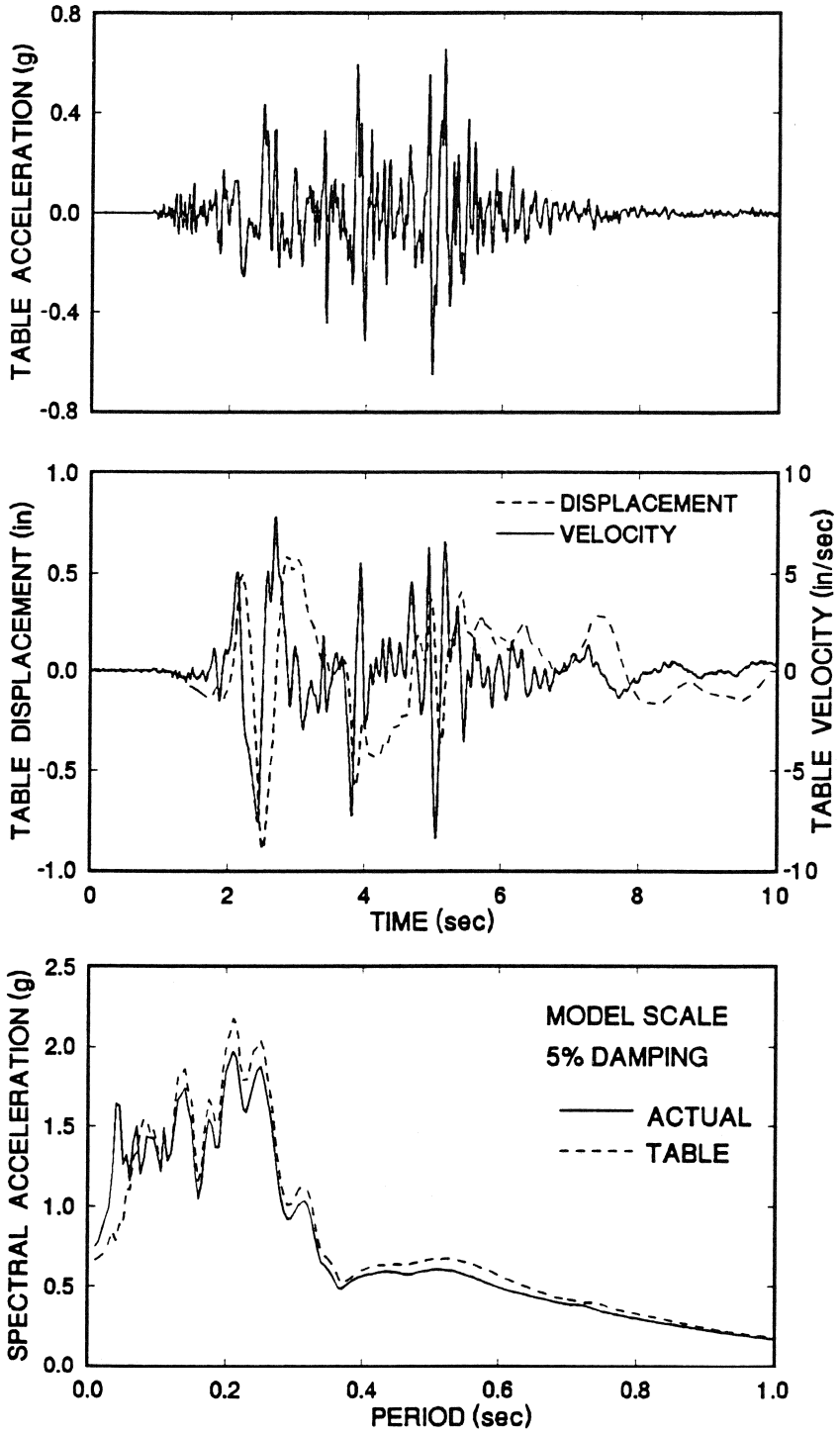

FIGURE 3-14 **Time Histories of Displacement, Velocity and Acceleration and Spectral Acceleration and Displacement of Shaking Table Excited with Pacoima 75% Motion (1 in. = 25.4 mm)**

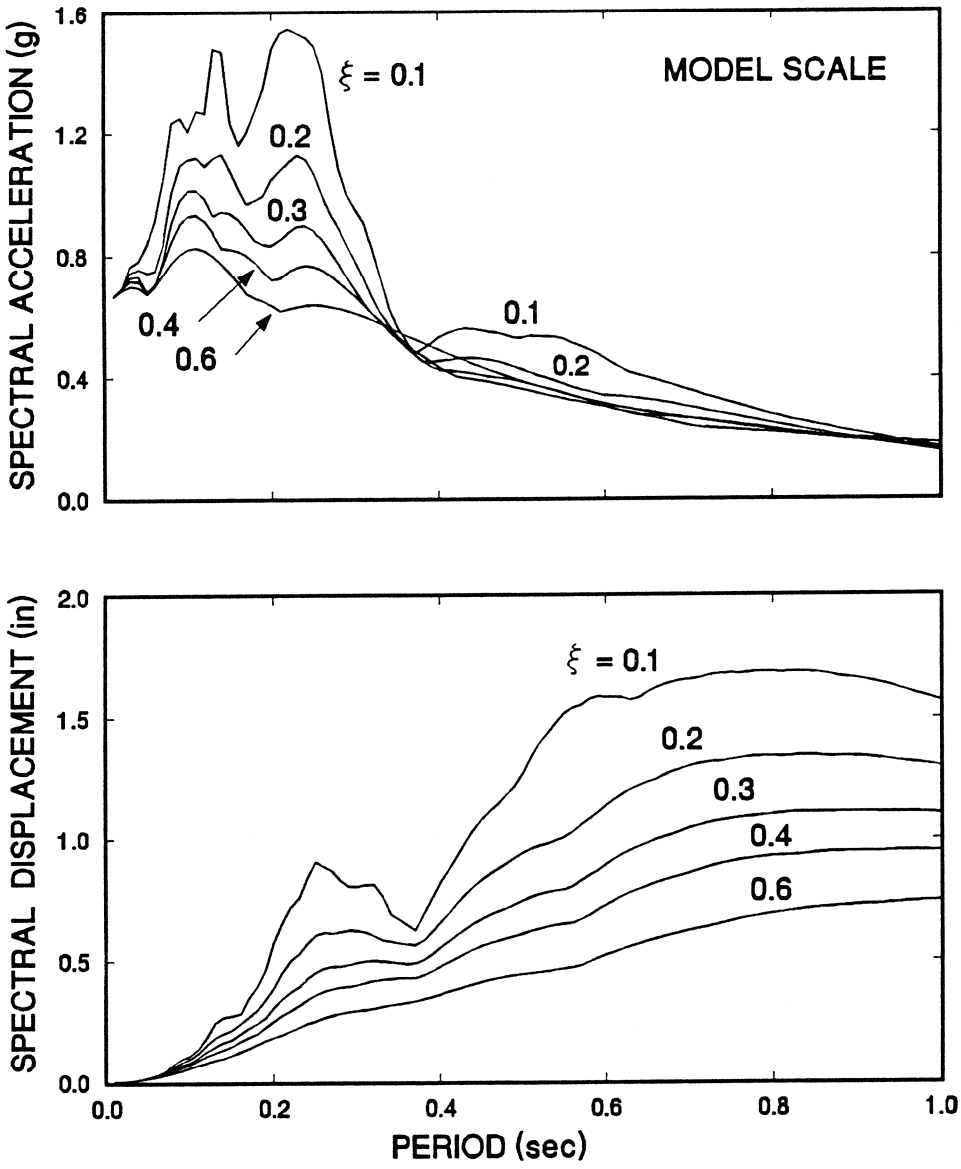

FIGURE 3-14 Continued

TABLE 3-II List of Earthquake Simulation Tests

TEST	STRUCTURE	DAMPERS	EXCITATION
1	1-story	0	El Centro 10%
2	1-story	0	El Centro 20%
3	1-story	0	El Centro 33.3%
4	1-story	0	Taft 33.3%
5	1-story	0	Taft 66.7%
6	1-story	0	Taft 100%
7	1-story	2	Taft 100%
8	1-story	2	Taft 100% (H&V)
9	1-story	2	El Centro 33.3%
10	1-story	2	El Centro 66.7%
11	1-story	2	El Centro 100%
12	1-story	2	Miyagiken 100%
13	1-story	2	Miyagiken 200%
14	1-story	2	Hachinohe 50%
15	1-story	2	Hachinohe 100%
16	1-story	4	El Centro 100%
17	1-story	4	Taft 100%
18	1-story	4	Miyagiken 200%
19	1-story	4	Hachinohe 100%
20	1-story	4	Taft 200%
21	1-story	4	Taft 300%
22	1-story	4	El Centro 150%
23	1-story	4	Miyagiken 320%
24	1-story	4	Hachinohe 150%
25	1-story	4	Pacoima Dam 50%
26	1-story	4	Pacoima Dam 75%
Stiffener Plates Added to Structure			
27	3-story	0	El Centro 33.3%
28	3-story	0	El Centro 50%
29	3-story	0	Taft 100%

H&V = Horizontal and Vertical Components

TABLE 3-II Continued

TEST	STRUCTURE	DAMPERS	EXCITATION
30	3-story	6	El Centro 50%
31	3-story	6	El Centro 100%
32	3-story	6	El Centro 150%
33	3-story	6	Taft 100%
34	3-story	6	Taft 200%
35	3-story	6	Taft 300%
36	3-story	6	Hachinohe 100%
37	3-story	6	Miyagiken 200%
38	3-story	6	Pacoima Dam 50%
39	3-story	6	Pacoima Dam 50% (H&V)
40	3-story	6	El Centro 100% (H&V)
41	3-story	6	Taft 200% (H&V)
42	3-story	2	El Centro 50%
43	3-story	2	El Centro 75%
44	3-story	2	Taft 100%
45	3-story	2	Taft 200%
46	3-story	4	El Centro 50%
47	3-story	4	El Centro 100%
48	3-story	4	Taft 100%
49	3-story	4	Taft 200%
50	1-story	0	El Centro 33.3%
51	1-story	0	Taft 100%
52	1-story *	0	El Centro 33.3%
53	1-story *	0	Taft 100%
54	1-story	2	El Centro 33.3%
55	1-story	2	El Centro 66.7%
56	1-story	2	Taft 100%
57	1-story	2	Taft 200%
58	1-story	2	Hachinohe 100%
59	1-story	2	Hachinohe 150%

H&V = Horizontal and Vertical Components
* = Wire Rope Cable System Attached

TABLE 3-II Continued

TEST	STRUCTURE	DAMPERS	EXCITATION
60	1-story	4	El Centro 33.3%
61	1-story	4	El Centro 66.7%
62	1-story	4	El Centro 100%
63	1-story	4	Taft 100%
64	1-story	4	Taft 200%
65	1-story	4	Taft 300%
66	1-story	4	Hachinohe 150%

excitation is identified with a percentage figure which represents a scaling factor on the acceleration, velocity and displacement of the actual record. For example, the figure 200% denotes a motion scaled up by a factor of two in comparison to the actual record.

3.3 Instrumentation

A list of channels monitored and their corresponding descriptions are given in Table 3-III. A schematic of the structure showing the location of the instrumentation is presented in Figure 3-15. The acceleration of each floor was measured at both the east and west frame so that the effect of torsion could be evaluated. Note that the axial damper force (channels 17 through 20) was only measured for dampers used in the first story. In addition, the axial damper displacement (channel 21) was measured by a displacement transducer placed along the axis of a single damper at the first story. This displacement transducer measured relative displacement of one end of the damper with respect to the other end. All other displacement transducers measured displacements with respect to a non-moving frame.

The measured signals were filtered using a low pass filter with a cutoff frequency of 25 Hz in the D/A output and A/D input.

TABLE 3-III List of Channels (with reference to Figure 3-15)

CHANNEL	INSTRUMENT	NOTATION	RESPONSE MEASURED
1	ACCL	AFHE	Foundation Horiz. Accel. - East
2	ACCL	AFHW	Foundation Horiz. Accel. - West
3	ACCL	A1HE	1st Floor Horiz. Accel. - East
4	ACCL	A1HW	1st Floor Horiz. Accel. - West
5	ACCL	A2HE	2nd Floor Horiz. Accel. - East
6	ACCL	A2HW	2nd Floor Horiz. Accel. - West
7	ACCL	A3HE	3rd Floor Horiz. Accel. - East
8	ACCL	A3HW	3rd Floor Horiz. Accel. - West
9	LDT	DFHC	Foundation Horiz. Displ. - Center
10	LDT	D1HC	1st Floor Horiz. Displ. - Center
11	LDT	D2HC	2nd Floor Horiz. Displ. - Center
12	LDT	D3HC	3rd Floor Horiz. Displ. - Center
13	ACCL	AFAV	Foundation Average Horiz. Accel.
14	ACCL	A1AV	1st Floor Average Horiz. Accel.
15	ACCL	A2AV	2nd Floor Average Horiz. Accel.
16	ACCL	A3AV	3rd Floor Average Horiz. Accel.
17	LOAD CELL	LC01	Axial Force in Damper 1
18	LOAD CELL	LC02	Axial Force in Damper 2
19	LOAD CELL	LC03	Axial Force in Damper 3
20	LOAD CELL	LC04	Axial Force in Damper 4
21	LDT	DDSP	Axial Displ. of Damper 1
22 *	LVDT	DLAT	Table Horiz. Displ.
23 *	ACCL	ALAT	Table Horiz. Accel.
24 *	LVDT	DROL	Table Roll Displ.
25 *	ACCL	AROL	Table Roll Accel.

ACCL = Accelerometer
LDT = Linear Displacement Transducer
LVDT = Linear Variable Differential Transformer
* = Table Controls

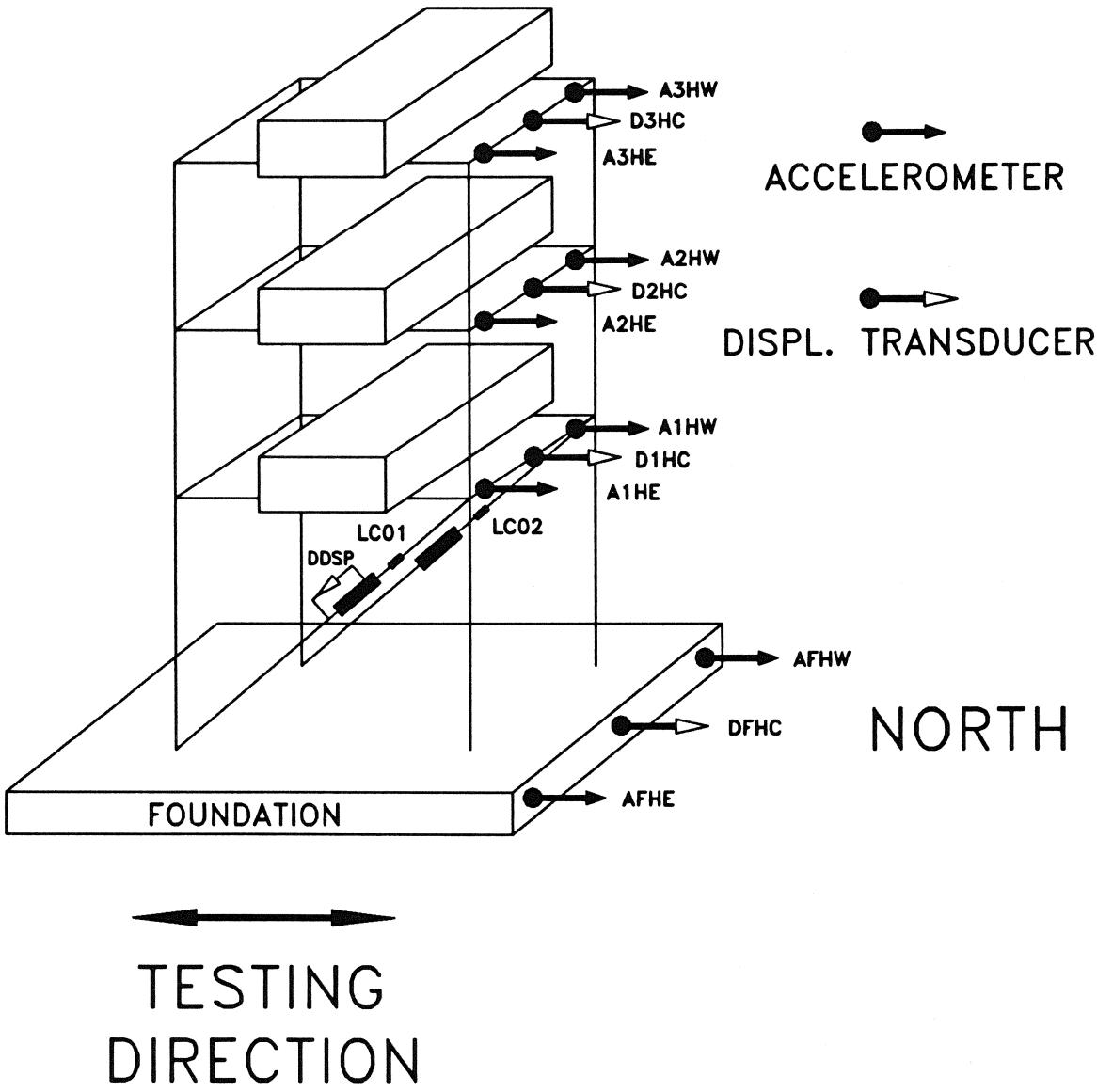

FIGURE 3-15 Instrumentation Diagram

SECTION 4
IDENTIFICATION OF STRUCTURAL PROPERTIES

4.1 Introduction

The identification of the properties of the structure without fluid dampers was easily accomplished by established procedures. The amplitudes of transfer functions of total acceleration under white noise excitation of lightly damped structures contain sharp and narrow peaks which reveal frequencies, damping ratios and mode shapes.

However, the transfer functions of highly damped structures do not usually contain well defined peaks and identification of the structural properties is not directly possible.

The approach followed herein for the identification of the damped structure was based on a calibrated analytical model of the structure. The analytical model was constructed from the properties of the undamped structure and with the effect of fluid dampers included. For this, the constitutive model of Section 2 was utilized. The analytical model was then verified by comparison of analytical to experimental transfer functions. The structural properties were then determined by solution of the eigenvalue problem of the damped structure.

4.2 Identification of One-story Structure

The structural properties of the one-story structure with supplemental dampers can be determined from the equation of motion

$$m\ddot{u} + c_u\dot{u} + ku + \eta P_d = -m\ddot{u}_g \qquad (4\text{-}1)$$

where m is the mass of the structure, k is the stiffness of the undamped structure, c_u is the damping constant of the structure without dampers, η is the number of dampers, P_d is the horizontal

component of force in a single damper, $\ddot{u}_g$ is the ground acceleration; and $\ddot{u}$, $\dot{u}$, and u are the relative acceleration, velocity, and displacement, respectively, of the mass. The constitutive equation of the dampers has been given previously in its most general form by Equation 2-13. For a damper inclined at an angle θ with respect to the horizontal axis, the equation in the horizontal direction becomes

$$P_d + \lambda \dot{P}_d = C_o \dot{u} \cos^2\theta \qquad (4\text{-}2)$$

The amplitude of the total acceleration transfer function or absolute transmissibility, T (Harris 1987), is defined as the ratio of the steady-state total acceleration ($\ddot{u} + \ddot{u}_g$) amplitude to the amplitude of the harmonic ground motion. It may be derived by application of Fourier transform to Equations 4-1 and 4-2:

$$T = \left| 1 + \omega^2 \left[-\omega^2 + \omega_n^2 + 2i\omega\omega_n\xi_u + \frac{i\eta\omega C_o \cos^2\theta}{m(1 + i\omega\lambda)} \right]^{-1} \right| \qquad (4\text{-}3)$$

where ω_n is the natural frequency of the structure without dampers, i is the imaginary unit, and ξ_u is the damping ratio of the undamped structure. Furthermore, in Equation 4-3, the vertical lines stand for the modulus of the contained complex quantity.

Experimental transfer functions are obtained in exactly the same manner. The structure is excited by stationary banded white noise excitation and records of the total acceleration are obtained. The transfer function is then calculated as the ratio of the Fourier amplitude of the recorded total acceleration to the Fourier amplitude of the ground acceleration.

In the case of a structure without fluid dampers, $\eta = 0$ and Equation 4-3 assumes a simple form involving the structural properties of natural frequency, ω_n, and damping ratio, ξ_u. For

lightly damped structures ($\xi_u < 0.1$), the position and magnitude of the single sharp peak in the transfer function determines the structural properties.

The eigenvalue problem of the structure with fluid dampers requires a numerical procedure. Equations 4-1 and 4-2, with $\ddot{u}_g$ set equal to zero, are written in matrix form, having first introduced a new vector $\{Z\}$:

$$\{Z\} = \lfloor \dot{u} \quad u \quad P_d \rfloor \tag{4-4}$$

$$[B]\{\dot{Z}\} + [A]\{Z\} = \{0\} \tag{4-5}$$

where

$$[B] = \begin{bmatrix} 1 & 0 & 0 \\ 0 & 1 & 0 \\ 0 & 0 & \lambda \end{bmatrix} \tag{4-6}$$

$$[A] = \begin{bmatrix} 2\xi_u\omega_n & \omega_n^2 & m^{-1} \\ -1 & 0 & 0 \\ -\eta C_o \cos^2\theta & 0 & 1 \end{bmatrix} \tag{4-7}$$

For a solution of the form

$$\{Z\} = \{Z_o\}\, e^{\mu t} \tag{4-8}$$

Equation 4-5 reduces to

$$[A]\{Z_o\} = -\mu\,[B]\{Z_o\} \tag{4-9}$$

Equation 4-9 describes a generalized eigenvalue problem. The solution of this problem (e.g., IMSL 1987) will result in values of the eigenvalue μ.

The frequency, ω_1, and damping ratio, ξ_1, are determined by recalling the expression for the characteristic roots of the

equation of free vibration of a viscously damped single degree of freedom system:

$$\mu = -\xi_1\omega_1 \pm i\omega_1 \ (1 - \xi_1^2)^{1/2} \tag{4-10}$$

Accordingly,

$$\omega_1 = | \ \mu \ | \tag{4-11}$$

$$\xi_1 = - \frac{\mathbb{R}(\mu)}{\omega_1} \tag{4-12}$$

where | | stands for the modulus and $\mathbb{R}$ for the real part of μ.

4.3 Identification of Multistory Structure

4.3.1 Structure without Fluid Dampers

The equations of motion of a base excited multi-degree of freedom lumped mass structure may be written in the following form

$$[M]\{\ddot{u}\} + [C_u]\{\dot{u}\} + [K]\{u\} = -[M]\{R\}\ \ddot{u}_g \tag{4-13}$$

where $[M]$ is the mass matrix, $[C_u]$ is the damping matrix, $[K]$ is the stiffness matrix; $\{\ddot{u}\}$, $\{\dot{u}\}$, and $\{u\}$ are the vectors of relative acceleration, velocity, and displacement of the degrees of freedom, respectively. Furthermore, $\{R\}$ is a vector which, for a structure with one degree of freedom per floor, contains units.

Expressing the displacement vector in terms of modal coordinates, Y_k:

$$\{u\} = \sum_{k=1}^{K} \{\phi_k\}\ Y_k \tag{4-14}$$

where $\{\phi_k\}$ is the k-th modal vector (or mode shape), and k is the number of degrees of freedom.

The amplitude of the transfer function of degree of freedom j may be obtained by application of Fourier transform:

$$T_j = \left| \sum_{k=1}^{K} \frac{-\Gamma_k \ (2\, i\omega\xi_k\omega_k + \omega_k^2)}{\omega_k^2 - \omega^2 + 2\, i\, \xi_k\omega\omega_k} \ \phi_{jk} \right| \qquad (4\text{-}15)$$

where ω_k and ξ_k are the k-th mode frequency and damping ratio, ϕ_{jk} is the component of mode shape $\{\phi_k\}$ corresponding to degree of freedom j and Γ_k is the k-th modal participation factor given by

$$\Gamma_k = \frac{-\{\phi_k\}^T\ [M]\ \{R\}}{\{\phi_k\}^T\ [M]\ \{\phi_k\}} \qquad (4\text{-}16)$$

For a lightly damped structure ($\xi_k < 0.1$), the k-th peak of the amplitude of the transfer function, T_j, occurs at frequency ω_k. Furthermore, if we assume well separated modes, the term in front of $\{\phi_{jk}\}$ in Equation 4-15 is equal to a negligible value for all frequencies $\omega \neq \omega_k$. Accordingly, Equation 4-15 simplifies to

$$T_j(\omega_k) \approx \frac{\Gamma_k \ (1 + 4\xi_k^2)}{2\xi_k} \ \phi_{jk} \qquad (4\text{-}17)$$

It should be noted that the term in front of ϕ_{jk} in Equation 4-17 is a constant. Therefore, the magnitude of the peak at frequency ω_k of function T_j is proportional to the magnitude of the k-th mode shape corresponding to the j-th degree of freedom. Thus, the position and magnitude of the peaks of experimental transfer functions of all degrees of freedom directly yield the frequencies and mode shapes. Use of Equations 4-16 and 4-17 determines the corresponding damping ratios.

4.3.2 Construction of Stiffness and Damping Matrices

The stiffness matrix, $[K]$, and the damping matrix, $[C_u]$, are constructed from the experimentally determined frequencies, damping ratios, and mode shapes using a procedure described by Clough (1975). The undamped eigenvalue equation is given by

$$\omega_k^2 [M]\{\phi_k\} = [K]\{\phi_k\} \tag{4-18}$$

where ω_k is the frequency corresponding to the k-th mode of vibration, and $\{\phi_k\}$ is the mode shape. The generalized mass and stiffness matrices are given by

$$[M^*] = [\phi]^T [M][\phi] \tag{4-19}$$

$$[K^*] = [\phi]^T [K][\phi] \tag{4-20}$$

where $[\phi]$ is the mode shape matrix containing the mode shapes $\{\phi_k\}$. The orthogonality of the mode shapes relative to the mass matrix can be used to obtain the following relationship

$$[\phi]^{-1} = [M^*]^{-1} [\phi]^T [M] \tag{4-21}$$

Using Equations 4-20 and 4-21, the stiffness matrix, $[K]$, can be determined as

$$[K] = [M][\phi][M^*]^{-1}[K^*][M^*]^{-1}[\phi]^T[M] \tag{4-22}$$

The matrix $[M^*]$ is diagonal with elements m_k^* given by

$$m_k^* = \{\phi_k\}^T [M]\{\phi_k\} \tag{4-23}$$

Equations 4-22 and 4-23 are combined to give

$$[K] = [M] \left(\sum_{k=1}^{K} \frac{\omega_k^2}{m_k^*} \{\phi_k\}\{\phi_k\}^T \right) [M] \tag{4-24}$$

where k is the number of modes.

In a similar way, the damping matrix is evaluated as

$$[C_u] = [M]\left(\sum_{k=1}^{K} \frac{2\xi_k \omega_k}{m_k^*}\{\phi_k\}\{\phi_k\}^T\right)[M] \qquad (4\text{-}25)$$

where ξ_k is the damping ratio corresponding to the k-th mode.

4.3.3 Equations of Motion of Structure with Fluid Dampers

The equations of motion of the structure without dampers (Equation 4-13) are augmented by the vector $\{P_d\}$ which contains the horizontal components of damper forces acting on the floors. For a structure modeled with one degree of freedom per floor, the equation of motion is

$$[M]\{\ddot{u}\} + [C_u]\{\dot{u}\} + [K]\{u\} + \{P_d\} = -[M]\{1\}\,\ddot{u}_g \qquad (4\text{-}26)$$

$$\{P_d\} = \begin{Bmatrix} \eta_N P_N \\ \vdots \\ \eta_j P_j - \eta_{j+1} P_{j+1} \\ \vdots \\ \eta_1 P_1 - \eta_2 P_2 \end{Bmatrix} \qquad (4\text{-}27)$$

where η_j is the number of dampers at the j-th story and P_j is the horizontal component of force in a damper at the j-th story. It is assumed here that all dampers at a story are identical.

The general constitutive equation describing the damper force P_j is

$$P_j + \lambda \frac{dP_j}{dt} = C_o \cos^2\theta_j \frac{d}{dt}(u_j - u_{j-1}) \qquad (4\text{-}28)$$

in which θ_j is the angle of placement of damper j with respect to the horizontal and $u_o = 0$ $(j = 1)$.

Application of Fourier transform to Equations 4-26 to 4-28 results in

$$[S(\omega)]\{\overline{u}\} = -[M]\{1\}\,\overline{\ddot{u}}_g \qquad (4\text{-}29)$$

in which the overbar denotes the Fourier transform and matrix $[S]$ represents the dynamic stiffness matrix:

$$S(\omega) = -\omega^2[M] + i\omega[C_u] + [K] + [D(\omega)] \qquad (4\text{-}30)$$

Matrix $[D]$ contains the contribution of the damper forces to the dynamic stiffness matrix.

The construction of matrix $[D]$ is given below for two of the three tested configurations which are depicted in Figure 3-3. It should be noted that all dampers are identical.

$$[D] = \frac{i\omega}{1 + i\omega\lambda}\,[C] \qquad (4\text{-}31)$$

where for the case of two dampers at the first story

$$[C] = \begin{bmatrix} 0 & 0 & 0 \\ 0 & 0 & 0 \\ 0 & 0 & C_1 \end{bmatrix} \qquad (4\text{-}32)$$

and for the case of six dampers

$$[C] = \begin{bmatrix} C_3 & -C_3 & 0 \\ -C_3 & C_2 + C_3 & -C_2 \\ 0 & -C_2 & C_1 + C_2 \end{bmatrix} \qquad (4\text{-}33)$$

In the above equations,

$$C_i = 2C_o\cos^2\theta_i \;; \qquad i = 1,\ 2 \text{ and } 3 \qquad (4\text{-}34)$$

4.3.4 Transfer Functions of Structure with Fluid Dampers

Defining the inverse of matrix $[S]$ as $[H]$, Equation 4-29 may be solved for $\{\overline{u}\}$. Upon multiplication by $-\omega^2$, the Fourier transform of the relative acceleration vector is obtained:

$$\{\overline{\ddot{u}}\} = \omega^2 [H] [M] \{1\} \overline{\ddot{u}}_g \tag{4-35}$$

The amplitude of the transfer function of the j-th degree of freedom is by definition

$$T_j = \left| \frac{\overline{\ddot{u}}_g + \overline{\ddot{u}}_j}{\overline{\ddot{u}}_g} \right| \tag{4-36}$$

or

$$T_j = \left| 1 + \omega^2 \sum_{k=1}^{K} H_{jk}(\omega)\, m_k \right| \tag{4-37}$$

where H_{jk} are elements of matrix $[H]$ and m_k is the lumped mass at the k-th floor.

4.3.5 Eigenvalue Problem of Structure with Fluid Dampers

The eigenvalue problem is formulated and solved in the same way as that of the one story structure (Section 4.2).

Vector $\{Z\}$ is defined as

$$\{Z\} = \begin{Bmatrix} \{\dot{u}\} \\ \{u\} \\ \{P_d\} \end{Bmatrix} \tag{4-38}$$

Equation 4-5 is valid with matrix $[A]$ and $[B]$ given, in the case of the tested structure, by

$$[B] = \begin{bmatrix} [M] & [0] & [0] \\ [0] & [I] & [0] \\ [0] & [0] & \lambda[I] \end{bmatrix} \tag{4-39}$$

$$[A] = \begin{bmatrix} [C_u] & [K] & [I] \\ -[I] & [0] & [0] \\ -[C] & [0] & [I] \end{bmatrix} \tag{4-40}$$

where $[I]$ is the identity matrix.

It should be noted that the solution of Equation 4-5 will result in the eigenvectors $\{Z_o\}$, a portion of which contains the complex-valued mode shapes.

4.4 Identification Tests

Identification tests were conducted by exciting the base of the model structure with a banded, 0 to 20 Hz white noise of peak acceleration equal to 0.05g. In the case of the structures without fluid dampers, the structural properties were identified by the procedure of Section 4.3. In the case of the structures with fluid dampers, the properties were analytically determined using the procedures of Sections 4.2 and 4.3 and utilizing the identified properties of the bare frame and the calibrated model of the fluid dampers (at room temperature).

The properties are presented in Tables 4-I and 4-II. In the case of the one-story structure, Table 4-I includes properties identified in the seismic tests. Recorded base shear - drift loops were used to obtain the stiffness, energy dissipated in a full cycle, W_d, and elastic energy stored at maximum drift, W_s. The damping was then calculated according to Clough (1975):

TABLE 4-I Properties of One-Story Model Structure

UNSTIFFENED STRUCTURE	0 DAMPERS Small Amplitude Vibration	0 DAMPERS Seismic Motion	2 DAMPERS	4 DAMPERS
Frequency (Hz)	2.00	1.94	2.04	2.10
Damping Ratio (%)	0.55	2.2	28.4	57.7

STIFFENED STRUCTURE	0 DAMPERS Small Amplitude Vibration	0 DAMPERS Seismic Motion	2 DAMPERS	4 DAMPERS
Frequency (Hz)	3.13	2.99	3.27	3.35
Damping Ratio (%)	2.0	2.9	19.3	37.4

STIFFENED STRUCTURE WITH CABLES	0 DAMPERS Small Amplitude Vibration	0 DAMPERS Seismic Motion	2 DAMPERS	4 DAMPERS
Frequency (Hz)	---	3.17	---	---
Damping Ratio (%)	---	5.1	---	---

TABLE 4-II Properties of 3-story Model Structure at Small Amplitude of Vibration

		0 DAMPERS			2 DAMPERS			4 DAMPERS			6 DAMPERS		
	MODE	1	2	3	1	2	3	1	2	3	1	2	3
Frequency (Hz)		2.00	6.60	12.20	2.03	6.88	12.34	2.11	7.52	12.16	2.03	7.64	16.99
Damping Ratio (%)		1.74	0.76	0.34	9.90	14.72	5.02	17.7	31.85	11.33	19.40	44.70	38.04
Mode Shape	Floor 1	0.417	-1.306	1.810									
	Floor 2	0.765	-0.595	-2.293									
	Floor 3	1.000	1.000	1.000									

$$\xi = \frac{W_d}{4\pi W_s} \qquad (4\text{-}41)$$

while the frequency was calculated from the measured stiffness and known mass.

The results in Tables 4-I and 4-II demonstrate the following:

a) The structure without fluid dampers exhibits, under seismic motion, damping in the range of 2 to 5 percent of critical. This shows that the structure was realistically damped.

b) The fluid dampers had a primary effect of increasing damping. The effect on the fundamental frequency is, as expected, small and amounts to an increase of stiffness of generally less than 10 percent.

c) The effect of fluid dampers on the higher mode frequencies is important. This was expected since these frequencies are above 4 Hz, the range in which the dampers develop significant stiffness.

d) The addition of fluid dampers in only the first story of the 3-story model resulted in significant modification of the modal damping properties. This interesting observation will be further discussed in Sections 5 and 6.

e) The one-story structure in its stiffened configuration without dampers experienced some inelastic action during seismic testing. This is evident in its reduction of frequency and increase in damping in comparison to tests at small amplitude vibration. If one assumes elastoplastic behavior, the observed reduction of frequency corresponds to a displacement ductility of about 1.2.

The accuracy of the analytical model of Sections 4.2 and 4.3 is demonstrated in Figures 4-1 to 4-3, which compare analytical and experimental amplitudes of transfer functions. The comparison is

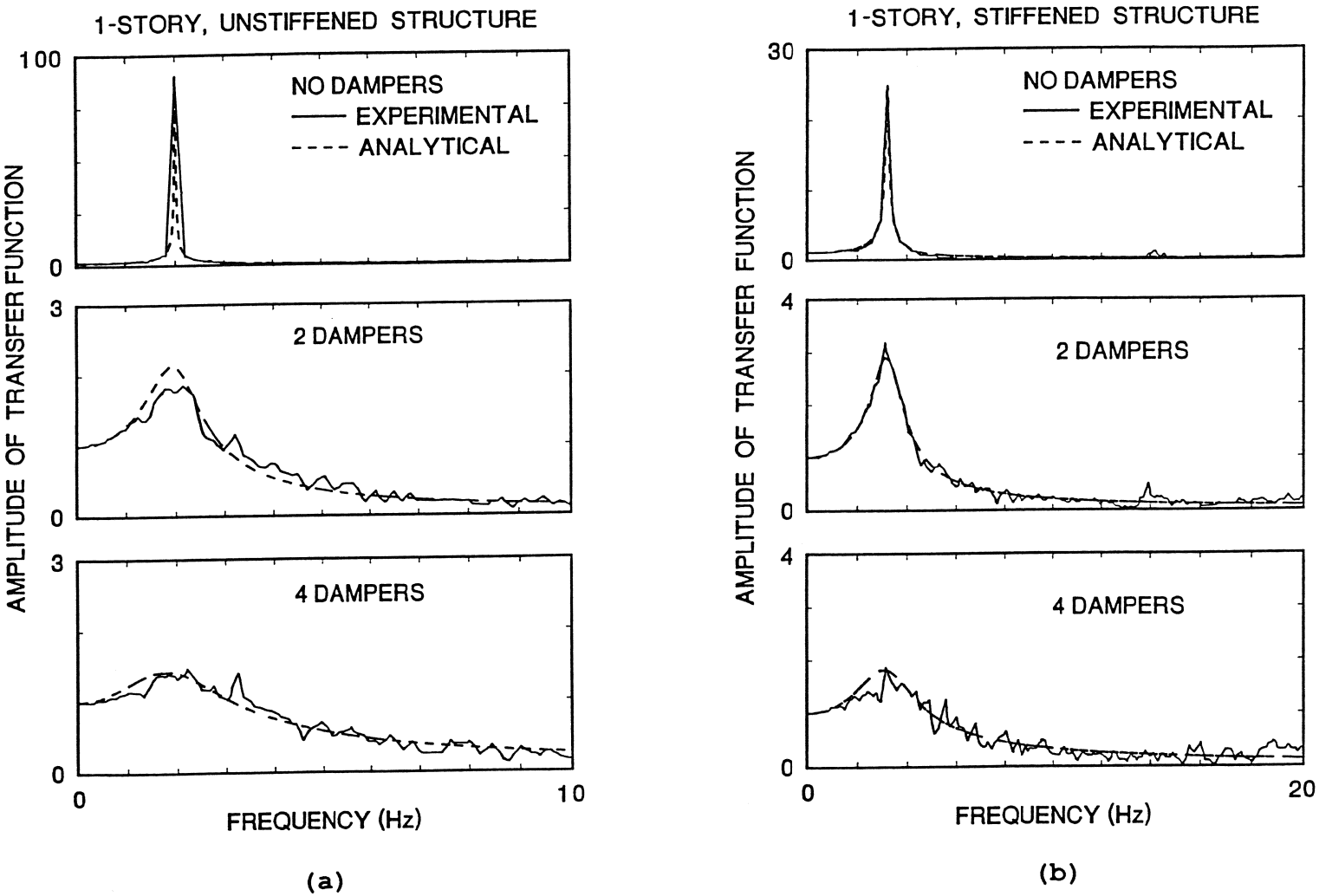

FIGURE 4-1 Comparison of Analytical and Experimental Amplitudes of Transfer Functions of One-story (a) Unstiffened Structure and (b) Stiffened Structure

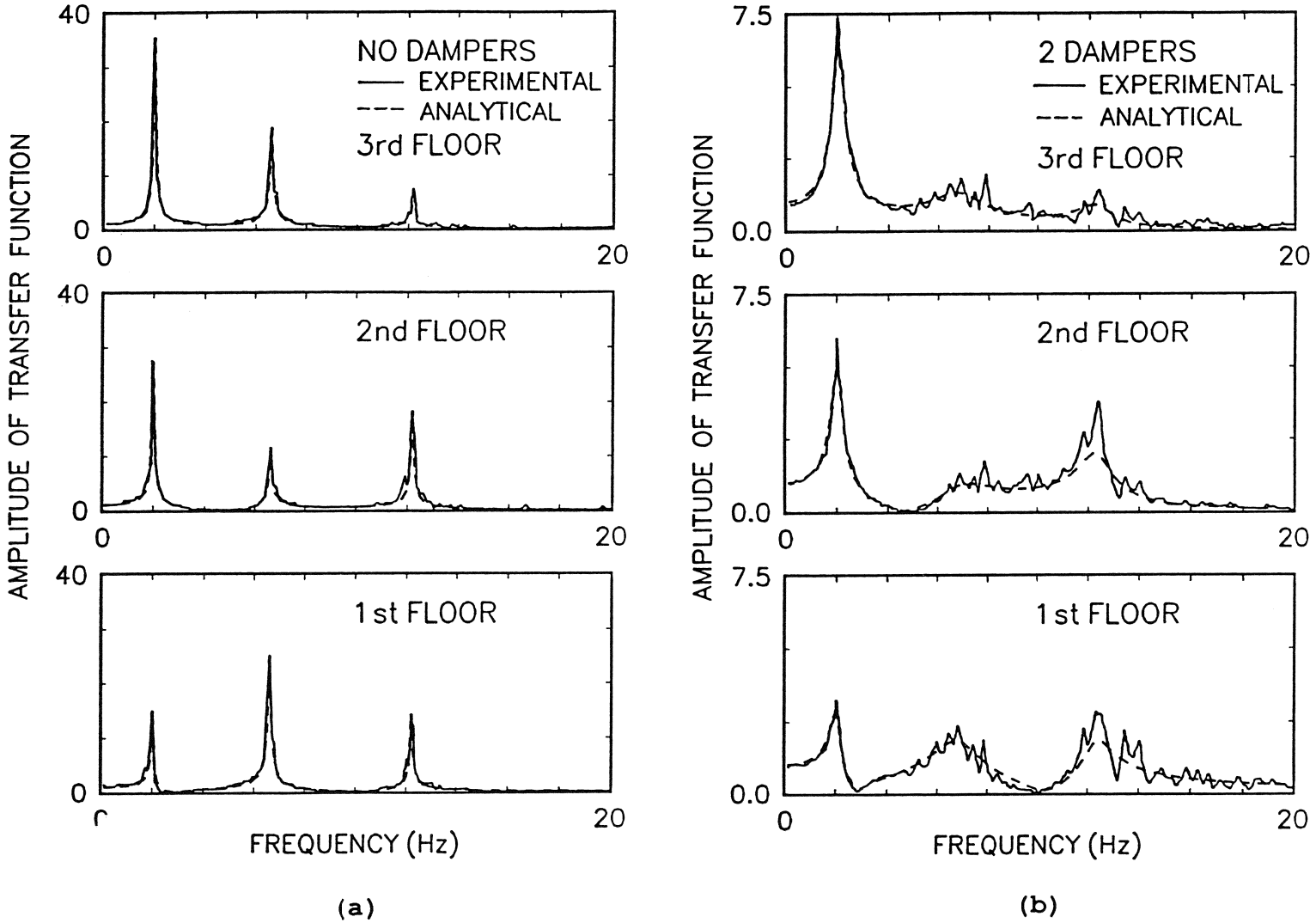

FIGURE 4-2 Comparison of Analytical and Experimental Amplitudes of Transfer Functions of 3-story Structure with (a) No Dampers and (b) Two Dampers

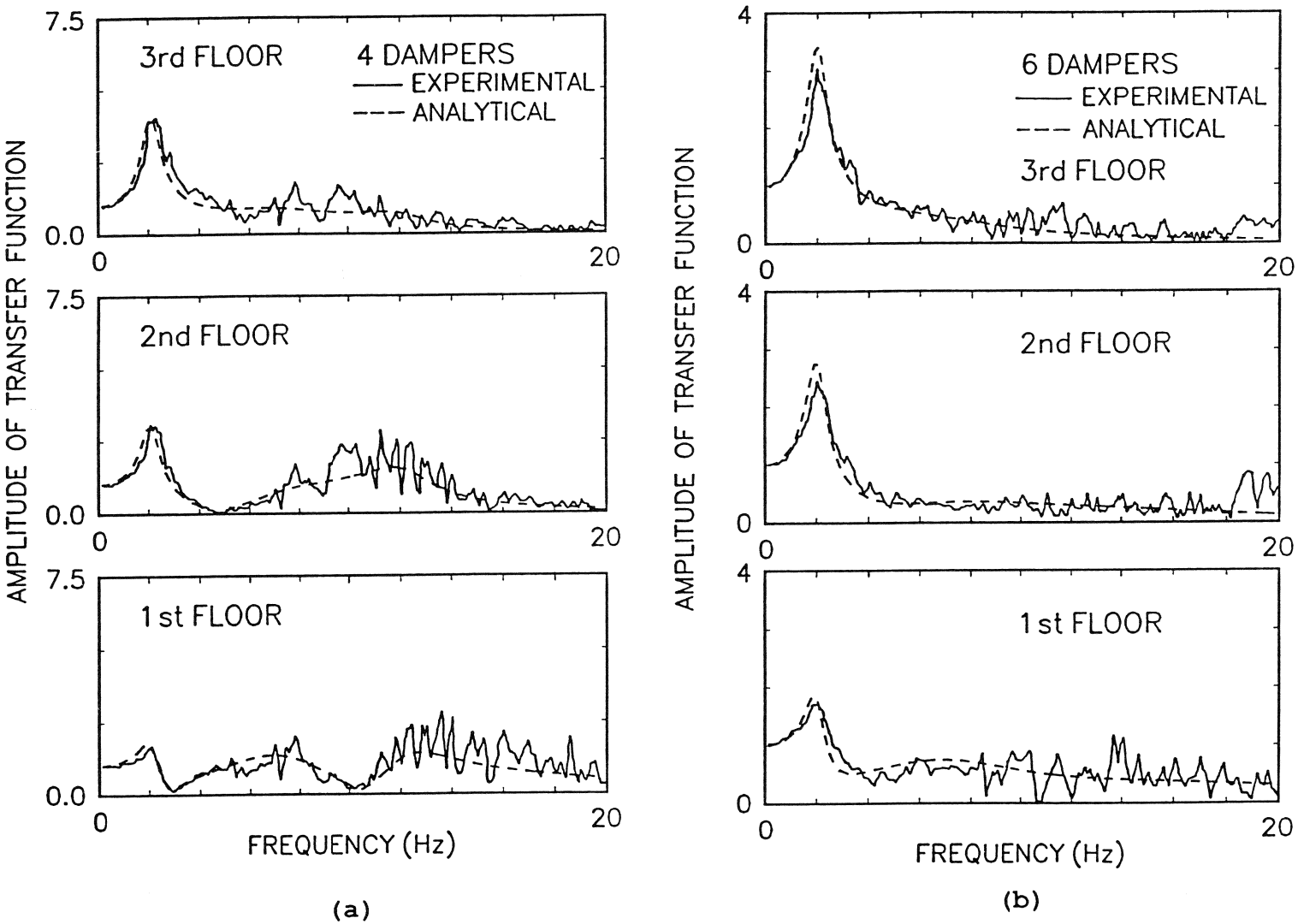

FIGURE 4-3 Comparison of Analytical and Experimental Amplitudes of Transfer Functions of 3-story Structure with (a) Four Dampers and (b) Six Dampers

very good. This indicates that the calculated properties are indeed very good estimates of the true properties.

In Figure 4-3(b), it is particularly interesting to note that the amplitude of the transfer functions of the 3-story structure with dampers at every story contains a single peak close to the fundamental frequency. The higher modes are completely suppressed. Therefore, the structure may be analyzed as a single degree of freedom system.

Finally, Figure 4-4 compares the amplitudes of transfer functions of the 3-story structure with two fluid dampers installed at the first story as calculated using the general Maxwell model of Equation 2-13 and the simple viscous model of Equation 2-19. The latter case is produced in Equation 4-31 by setting $\lambda = 0$. The difference between the two models consists of a minor shift in the frequency position of the higher mode peaks.

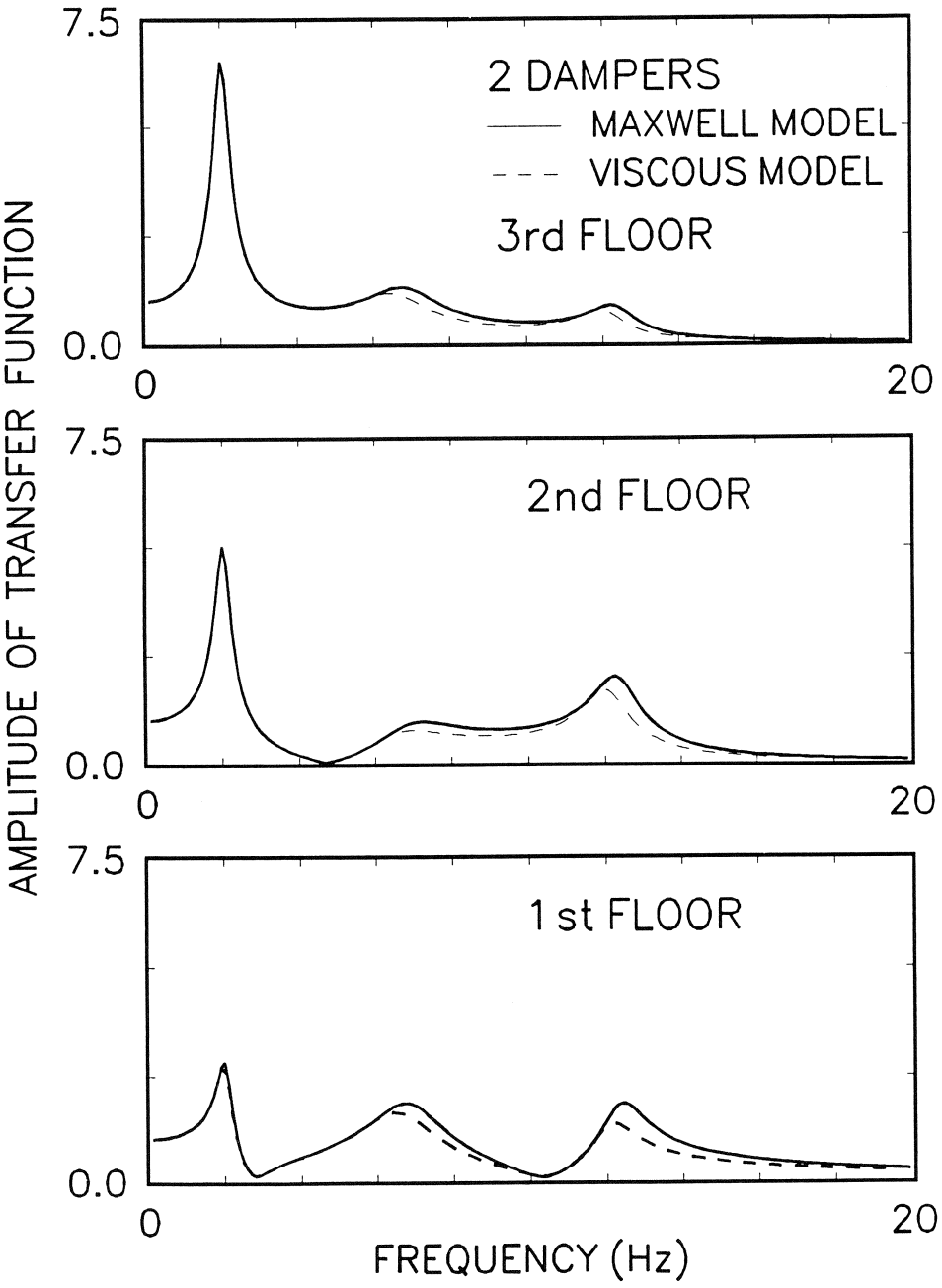

FIGURE 4-4 **Comparisons of Amplitudes of Transfer Functions of 3-story Structure with Two Dampers Based on Analytical Maxwell Model and Analytical Viscous Model**

SECTION 5
EARTHQUAKE SIMULATOR TEST RESULTS

5.1 One-story Structure

The experimental results for the unstiffened and stiffened structure are summarized in Tables 5-I and 5-II, respectively. For each test, the peak values of the table motion in the horizontal direction are given. The displacement and acceleration were directly measured whereas the velocity was determined by numerical differentiation of the displacement record. The peak drift is given as a percentage of the story height which was 32 inches (813 mm). In addition, the peak drift has been determined based upon the horizontal component of the damper displacement. There is a quantitative difference between the two values of the peak drift which has been attributed to slipping at the bolted connections between the structural frame and the lateral bracing. The peak base shear was calculated from the known masses and recorded accelerations and is given as a fraction of the total weight (6446 lb or 28743 N) of the structure.

Results in graphical form for all tests are presented in Appendix A. The graphs present recorded loops of base shear force over weight ratio versus the first story drift. Furthermore, for each test, the graphs of Appendix A present the contributions to the base shear from the fluid dampers and the columns. It is evident in these graphs that the contribution from the fluid dampers to the base shear - drift loops is purely of a viscous nature and accordingly the dampers display no stiffness. This confirms that the additional column axial load due to the damper forces occurs out-of-phase with the peak drift so that column compression failure is not a concern (see also Section 1 and Figure 1-7).

TABLE 5-I Summary of Experimental Results for Unstiffened One-story Structure (1 in. = 25.4 mm)

TEST	EXCITATION	DMP	SYSTEM PARAMETERS		PEAK TABLE MOTION (Horiz)			$\frac{\text{PEAK BASE SHEAR}}{\text{WEIGHT}}$	$\frac{\text{PEAK DRIFT}}{\text{HEIGHT}}$ (%)	$\frac{\text{PEAK DRIFT}^{\star}}{\text{HEIGHT}}$ (%)
			f (Hz)	ξ (%)	DISPL. (in)	VELOC. (in/sec)	ACCEL. (g's)			
1	El Centro 10%	0	2.00 [1]	0.55 [2]	0.093	0.656	0.038	0.085	0.623	---
2	El Centro 20%	0	2.00 [1]	0.55 [2]	0.188	1.259	0.071	0.160	1.205	---
3	El Centro 33.3%	0	2.00 [1]	0.55 [2]	0.310	2.022	0.107	0.228	1.842	---
4	Taft 33.3%	0	2.00 [1]	0.55 [2]	0.185	0.838	0.044	0.091	0.688	---
5	Taft 66.7%	0	2.00 [1]	0.55 [2]	0.374	1.666	0.097	0.153	1.134	---
6	Taft 100%	0	2.00 [1]	0.55 [2]	0.562	2.475	0.144	0.224	1.740	---
7	Taft 100%	2	2.04	28.4	0.563	2.491	0.151	0.129	0.724	0.689
8	Taft 100% (H&V)	2	2.04	28.4	0.566	2.491	0.148	0.130	0.775	0.702
9	El Centro 33.3%	2	2.04	28.4	0.309	2.125	0.106	0.087	0.500	0.469
10	El Centro 66.7%	2	2.04	28.4	0.618	4.009	0.197	0.168	1.071	0.997
11	El Centro 100%	2	2.04	28.4	0.947	6.275	0.310	0.259	1.693	1.576
12	Miyagiken 100%	2	2.04	28.4	0.479	2.403	0.155	0.115	0.636	0.754
13	Miyagiken 200%	2	2.04	28.4	0.961	4.622	0.308	0.234	1.459	1.688
14	Hachinohe 50%	2	2.04	28.4	0.644	2.625	0.116	0.122	0.806	0.930
15	Hachinohe 100%	2	2.04	28.4	1.291	5.172	0.215	0.247	1.645	1.808

DMP = Number of Dampers
f = Undamped Frequency
* = Measured from Component of Damper Displacement
H&V = Horizontal and Vertical Components
Note 1: 2.00 to 1.94 Hz Depending on the Amplitude of Motion
Note 2: 0.55 to 2.2% Depending on the Amplitude of Motion

TABLE 5-I Continued

TEST	EXCITATION	DMP	SYSTEM PARAMETERS		PEAK TABLE MOTION (Horiz)			PEAK BASE SHEAR / WEIGHT	PEAK DRIFT / HEIGHT (%)	PEAK DRIFT * / HEIGHT (%)
			f (Hz)	ξ (%)	DISPL. (in)	VELOC. (in/sec)	ACCEL. (g's)			
16	El Centro 100%	4	2.10	57.7	0.947	6.244	0.298	0.301	1.031	1.002
17	Taft 100%	4	2.10	57.7	0.562	2.491	0.145	0.115	0.504	0.467
18	Miyagiken 200%	4	2.10	57.7	0.962	4.613	0.305	0.200	0.870	0.815
19	Hachinohe 100%	4	2.10	57.7	1.290	5.272	0.216	0.214	1.114	1.026
20	Taft 200%	4	2.10	57.7	1.132	4.900	0.301	0.226	1.067	0.966
21	Taft 300%	4	2.10	57.7	1.700	7.428	0.476	0.342	1.667	1.514
22	El Centro 150%	4	2.10	57.7	1.418	9.509	0.487	0.456	1.563	1.402
23	Miyagiken 320%	4	2.10	57.7	1.635	7.822	0.536	0.338	1.564	1.307
24	Hachinohe 150%	4	2.10	57.7	1.938	7.959	0.319	0.321	1.742	1.490
25	Pacoima Dam 50%	4	2.10	57.7	0.598	5.556	0.452	0.278	1.155	0.993
26	Pacoima Dam 75%	4	2.10	57.7	0.897	8.409	0.658	0.412	1.755	1.626

DMP = Number of Dampers
f = Undamped Frequency
* = Measured From Component of Damper Displacement

TABLE 5-II Summary of Experimental Results for Stiffened One-story Structure (1 in. = 25.4 mm)

TEST	EXCITATION	DMP	SYSTEM PARAMETERS		PEAK TABLE MOTION (Horiz)			*PEAK BASE SHEAR / WEIGHT*	*PEAK DRIFT / HEIGHT* (%)	*PEAK DRIFT* ★ */ HEIGHT* (%)
			f (Hz)	ξ (%)	DISPL. (in)	VELOC. (in/sec)	ACCEL. (g's)			
50	El Centro 33.3%	0	3.13 [1]	2.0 [1]	0.318	2.138	0.110	0.300	0.970	---
51	Taft 100%	0	2.99 [1]	2.9 [1]	0.561	2.484	0.144	0.431	1.479	---
52	El Centro 33.3%	0 [2]	3.15 [1]	4.8 [1]	0.318	2.134	0.112	0.276	0.853	---
53	Taft 100%	0 [2]	3.17 [1]	5.1 [1]	0.561	2.516	0.147	0.307	0.944	---
54	El Centro 33.3%	2	3.27	19.3	0.318	2.094	0.110	0.203	0.635	0.547
55	El Centro 66.7%	2	3.27	19.3	0.632	4.222	0.199	0.393	1.230	1.101
56	Taft 100%	2	3.27	19.3	0.563	2.494	0.145	0.226	0.667	0.594
57	Taft 200%	2	3.27	19.3	1.129	4.912	0.300	0.424	1.362	1.228
58	Hachinohe 100%	2	3.27	19.3	1.289	5.234	0.215	0.263	0.858	0.725
59	Hachinohe 150%	2	3.27	19.3	1.935	7.900	0.324	0.383	1.262	1.118
60	El Centro 33.3%	4	3.35	37.4	0.320	2.084	0.114	0.173	0.441	0.372
61	El Centro 66.7%	4	3.35	37.4	0.632	4.178	0.201	0.335	0.874	0.779
62	El Centro 100%	4	3.35	37.4	0.947	6.281	0.304	0.485	1.305	1.186
63	Taft 100%	4	3.35	37.4	0.561	2.556	0.148	0.180	0.437	0.410
64	Taft 200%	4	3.35	37.4	1.129	4.972	0.304	0.342	0.920	0.819
65	Taft 300%	4	3.35	37.4	1.695	7.425	0.487	0.504	1.405	1.247
66	Hachinohe 150%	4	3.35	37.4	1.934	7.878	0.326	0.330	0.979	0.862

DMP = Number of Dampers
f = Undamped Frequency
* = Measured from Component of Damper Displacement
Note 1: Measured From Hysteresis Loop under Seismic Excitation
Note 2: Wire Rope Cables Attached to Increase Energy Dissipation

5.2 Three-story Structure

The experimental results for the three-story tests are given in Table 5-III. For each test, the peak values of the table motion in the horizontal direction are given. The peak drift is given as a percentage of the story height which was 32 inches (813 mm) for the first story and 30 inches (762 mm) for the second and third story. In addition, the peak drift of the first story has been determined based upon the horizontal component of the damper displacement. The quantitative difference between the two values is again a result of slipping at the bolted connections between the structural frame and the lateral bracing. The peak acceleration at each floor is given and the peak shear force at each story is given as a fraction of the total weight (6332 lb or 28235 N) of the structure.

Plots of recorded story shear force over total weight ratio versus story drift for all tests are presented in Appendix B.

5.3 Effectiveness of Dampers

A number of observations related to the effectiveness of fluid dampers are made from the results of Tables 5-I through 5-III and from Appendices A and B.

5.3.1 Reduction of Response

A comparison of responses between the one-story structure without and with fluid dampers reveals ratios of peak story drift in the damped structure to peak story drift in the undamped moment-resisting frame structure, RD, in the range of 0.3 to 0.7 and ratios of peak base shear force in the damped structure to peak base shear force in the undamped structure, RBS, in the range of 0.4 to 0.7. These significant reductions in response are a result of the increased ability to dissipate energy and are not a result of changes in stiffness.

TABLE 5-III Summary of Experimental Results for 3-story Structure (1 in. = 25.4 mm)

TEST	EXCITATION	DMP	SYSTEM PARAMETERS		PEAK TABLE MOTION (Horiz)			PEAK ACCELERATION (g's)		
			f (Hz)	ξ (%)	DISPL. (in)	VELOC. (in/sec)	ACCEL. (g's)	1st Floor	2nd Floor	3rd Floor
27	El Centro 33.3%	0	2.00 [1]	1.74 [1]	0.317	2.138	0.109	0.275	0.308	0.417
28	El Centro 50%	0	2.00 [1]	1.74 [1]	0.477	3.169	0.157	0.389	0.410	0.585
29	Taft 100%	0	2.00 [1]	1.74 [1]	0.562	2.472	0.146	0.424	0.403	0.555
30	El Centro 50%	6	2.03	19.4	0.475	3.134	0.152	0.127	0.152	0.205
31	El Centro 100%	6	2.03	19.4	0.949	6.322	0.312	0.205	0.286	0.368
32	El Centro 150%	6	2.03	19.4	1.419	9.447	0.485	0.340	0.402	0.534
33	Taft 100%	6	2.03	19.4	0.562	2.516	0.145	0.140	0.136	0.178
34	Taft 200%	6	2.03	19.4	1.131	4.994	0.300	0.253	0.264	0.348
35	Taft 300%	6	2.03	19.4	1.700	7.416	0.465	0.362	0.379	0.513
36	Hachinohe 100%	6	2.03	19.4	1.290	5.325	0.215	0.248	0.276	0.334
37	Miyagiken 200%	6	2.03	19.4	1.036	5.003	0.326	0.247	0.271	0.342
38	Pacoima Dam 50%	6	2.03	19.4	0.596	5.538	0.455	0.282	0.308	0.376
39	Pacoima Dam 50% (H&V)	6	2.03	19.4	0.555	5.244	0.419	0.273	0.314	0.377
40	El Centro 100% (H&V)	6	2.03	19.4	0.938	6.147	0.298	0.239	0.293	0.390
41	Taft 200% (H&V)	6	2.03	19.4	1.133	5.013	0.316	0.243	0.283	0.352
42	El Centro 50%	2	2.03	9.9	0.471	3.116	0.156	0.220	0.286	0.301
43	El Centro 75%	2	2.03	9.9	0.710	4.663	0.225	0.316	0.391	0.427
44	Taft 100%	2	2.03	9.9	0.563	2.541	0.147	0.172	0.218	0.271
45	Taft 200%	2	2.03	9.9	1.129	4.975	0.298	0.345	0.426	0.545
46	El Centro 50%	4	2.11	17.7	0.474	3.209	0.156	0.170	0.221	0.282
47	El Centro 100%	4	2.11	17.7	0.948	6.447	0.304	0.346	0.476	0.591
48	Taft 100%	4	2.11	17.7	0.561	2.494	0.145	0.161	0.208	0.246
49	Taft 200%	4	2.11	17.7	1.130	4.947	0.299	0.324	0.383	0.464

TABLE 5-III Continued

TEST	EXCITATION	DMP	SYSTEM PARAMETERS		PEAK SHEAR FORCE / WEIGHT			PEAK DRIFT / HEIGHT (%)			PEAK DRIFT * / HEIGHT (%)
			f (Hz)	ξ (%)	1st Story	2nd Story	3rd Story	1st Story	2nd Story	3rd Story	1st Story
27	El Centro 33.3%	0	2.00 [1]	1.74 [1]	0.220	0.199	0.139	0.976	1.069	0.769	---
28	El Centro 50%	0	2.00 [1]	1.74 [1]	0.295	0.272	0.195	1.386	1.498	1.073	---
29	Taft 100%	0	2.00 [1]	1.74 [1]	0.255	0.200	0.185	1.161	1.077	0.911	---
30	El Centro 50%	6	2.03	19.4	0.138	0.108	0.068	0.489	0.510	0.281	0.471
31	El Centro 100%	6	2.03	19.4	0.261	0.208	0.123	0.993	0.998	0.600	0.943
32	El Centro 150%	6	2.03	19.4	0.368	0.298	0.178	1.436	1.492	0.852	1.382
33	Taft 100%	6	2.03	19.4	0.120	0.104	0.059	0.425	0.463	0.253	0.399
34	Taft 200%	6	2.03	19.4	0.235	0.198	0.116	0.900	0.921	0.546	0.830
35	Taft 300%	6	2.03	19.4	0.343	0.288	0.171	1.407	1.369	0.819	1.270
36	Hachinohe 100%	6	2.03	19.4	0.256	0.201	0.111	1.036	0.963	0.575	0.957
37	Miyagiken 200%	6	2.03	19.4	0.254	0.202	0.114	0.947	0.963	0.610	0.890
38	Pacoima Dam 50%	6	2.03	19.4	0.275	0.224	0.125	1.106	1.017	0.629	1.003
39	Pacoima Dam 50% (H&V)	6	2.03	19.4	0.260	0.214	0.126	1.021	0.956	0.652	0.951
40	El Centro 100% (H&V)	6	2.03	19.4	0.260	0.202	0.130	0.998	1.029	0.588	0.941
41	Taft 200% (H&V)	6	2.03	19.4	0.236	0.195	0.117	0.929	0.931	0.531	0.829
42	El Centro 50%	2	2.03	9.9	0.196	0.159	0.100	0.806	0.865	0.548	0.750
43	El Centro 75%	2	2.03	9.9	0.282	0.233	0.142	1.210	1.292	0.785	1.124
44	Taft 100%	2	2.03	9.9	0.150	0.148	0.090	0.626	0.696	0.500	0.574
45	Taft 200%	2	2.03	9.9	0.296	0.279	0.182	1.247	1.431	0.983	1.181
46	El Centro 50%	4	2.11	17.7	0.159	0.132	0.094	0.540	0.660	0.465	0.520
47	El Centro 100%	4	2.11	17.7	0.314	0.256	0.197	1.142	1.279	0.933	1.081
48	Taft 100%	4	2.11	17.7	0.118	0.130	0.082	0.411	0.638	0.465	0.388
49	Taft 200%	4	2.11	17.7	0.253	0.249	0.155	0.949	1.208	0.829	0.887

DMP = Number of Dampers, f = Undamped Frequency, * = Measured from Component of Damper Displacement
Note 1: For Small Amplitude of Vibration, H&V = Horizontal and Vertical Components

The corresponding ratios of story drift and story shear force in the 3-story structure are lower and typically in the range of 0.3 to 0.5. The lower values of these ratios in the 3-story structure in comparison to the one-story structure is merely the result of lower damping in the bare frame of the 3-story structure. For this, the reader should recall the results of Tables 4-I and 4-II.

A comparison of responses of the 3-story structure without and with fluid dampers is presented in Figure 5-1. Clearly, the addition of fluid dampers resulted in overall significant reduction of accelerations, story shear forces and interstory drifts.

A different comparison of responses is presented in Figure 5-2, which presents profiles of response of the 3-story structure without and with dampers at two different levels of the same earthquake. Evidently, the responses of the two systems are approximately the same for two significantly different levels of the same earthquake. It may be stated that, for this particular earthquake, the addition of fluid dampers has increased the earthquake resistance of the moment resisting bare frame by three-fold. Of course, this is not generally the case. An inspection of the acceleration spectra in Figures 3-10 to 3-14, shows that the reduction achieved by increasing damping from 5 to 20% of critical depends on the period of the structure and the content in frequency of the excitation.

It is interesting to note in Figure 5-2 that the base shear force in the damped structure is larger than that of the undamped structure despite the overall lower accelerations. This is explained by considering the differences in the contribution of the higher modes of the two systems. In the undamped structure, the peak values of floor accelerations occur at different times as a result of contributions from the higher modes. In the damped structure, higher modes are almost completely suppressed and the peak values of floor accelerations occur at almost identical times.

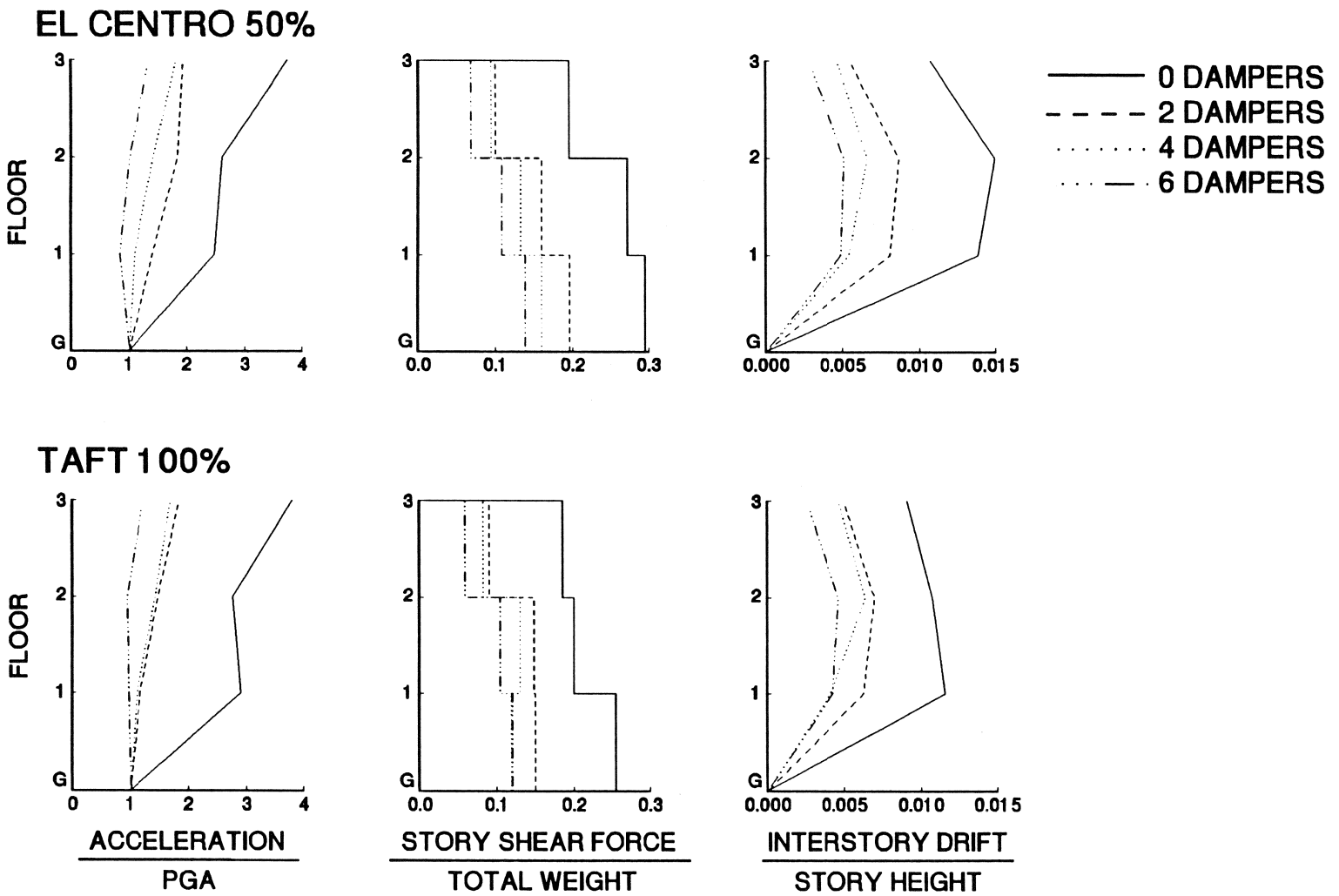

FIGURE 5-1 **Acceleration, Story Shear and Interstory Drift Profiles of 3-story Structure**

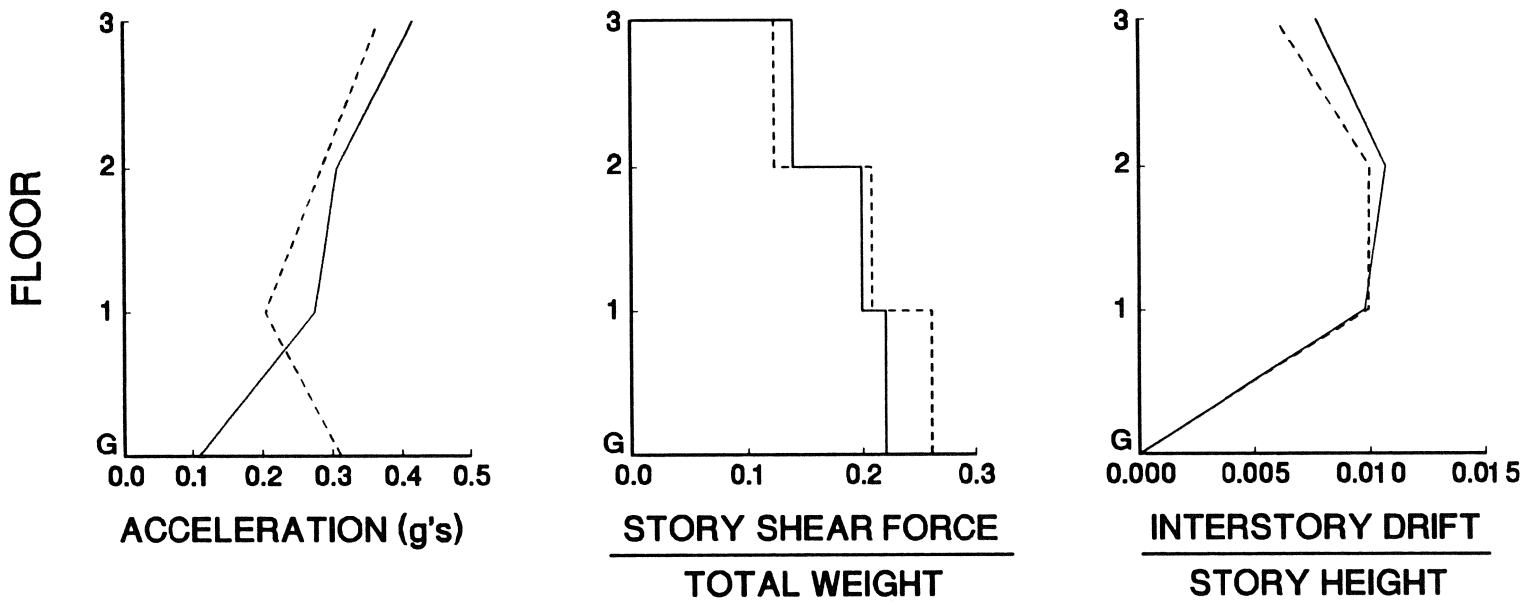

FIGURE 5-2 **Comparison of Response Profiles for Two Different Levels of the Same Earthquake**

5.3.2 Effect of Vertical Ground Motion

An observation to be made from Tables 5-I and 5-III is the effect that the vertical ground motion has on the response of the damped structure. The response, in terms of story drifts and shear forces, is affected. The effect is either a minor mixed increase and decrease of various response quantities or a minor net reduction of response. In general, this effect appears to be negligible.

5.3.3 Energy Dissipation

The effect of fluid dampers on the behavior of a structural system to which they are attached is vividly illustrated in graphs of the time history of the energy dissipated by various mechanisms in the structure. Figure 5-3 shows energy time histories for the one-story structure subjected to the Taft 100% motion. The energies were calculated from the equation of motion (Equation 4-1) after multiplication by du and integration over the time interval 0 to t. The result is (see also Section 1)

$$E = E_k + E_s + E_h + E_d \tag{5-1}$$

where

$$E = \int_0^t m\,(\ddot{u} + \ddot{u}_g)\,du_g \tag{5-2}$$

is the absolute energy input,

$$E_k = \frac{1}{2}\,m\,(\dot{u} + \dot{u}_g)^2 \tag{5-3}$$

is the kinetic energy,

$$E_s = \frac{1}{2}\,k u^2 \tag{5-4}$$

is the recoverable strain energy,

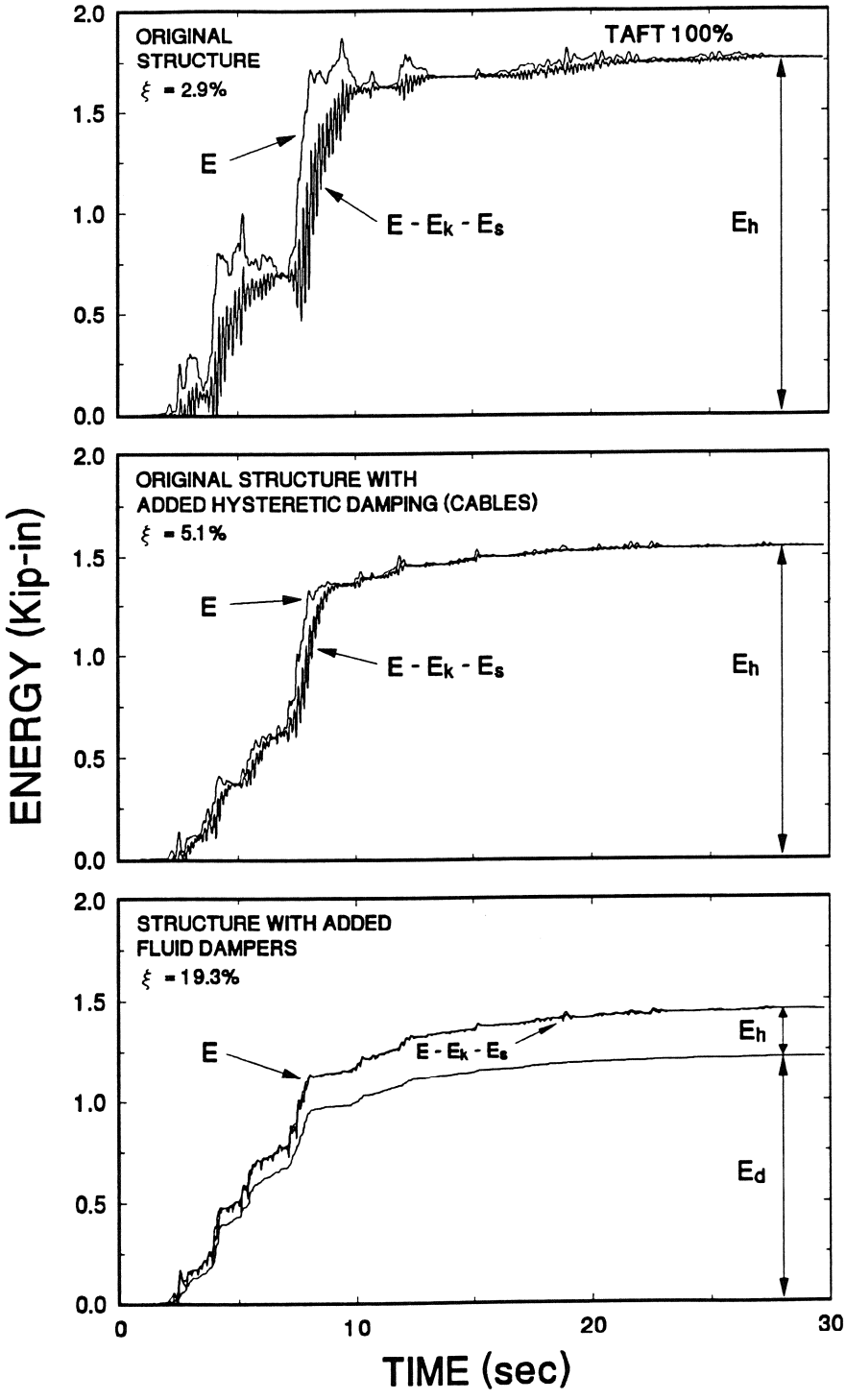

FIGURE 5-3 **Energy Time Histories in One-story Stiffened Structure Subjected to Taft 100% Motion (1 Kip = 4.46 KN, 1 in. = 25.4 mm)**

$$E_d = \int_0^t \eta P_d \, du \qquad (5\text{-}5)$$

is the energy dissipated by the fluid dampers, and E_h is the energy dissipated by other mechanisms in the structural frame (by viscous and hysteretic actions).

Figure 5-3 demonstrates a reduction of the absolute input energy with the addition of fluid dampers. Furthermore, the kinetic and strain energies are reduced. This demonstrates the reduction of structural deformation. However, the most beneficial effect is the significant reduction of the energy dissipated in the structural frame in exchange for energy dissipation by the fluid dampers.

5.3.4 Effect of Position of Fluid Dampers

The 3-story structure was tested in two different configurations. In the first, fluid dampers were placed at all stories (case of 6 dampers). In the second, fluid dampers were placed only at the first story (cases of 2 and 4 dampers). The primary effect of the difference in configuration was that damping in the fundamental mode varied from 9.9% (2 dampers) to 17.7% (4 dampers) to 19.4% of critical (6 dampers). The secondary effect was substantial differences in the higher mode characteristics of the three systems (see Table 4-II).

In terms of response of the three systems, Figure 5-1 provides a comparison of the systems for two earthquakes. Evidently, the concentration of the fluid dampers at one level did not have any adverse effect. The observed differences in the response of the three systems is just a result of a difference in the damping of the fundamental mode.

It should be noted that, in general, this behavior can be achieved by placing fluid dampers at those stories where the largest interstory velocity is expected. For response primarily in the first mode, this occurs at the story with maximum drift in the mode shape.

In effect, increases in damping may be achieved either by distribution of several fluid dampers over the height of the structure, or by strategically placing larger dampers at few locations. The only drawback of such an approach is the development of larger forces at a few joints and the reduction in damper redundancy.

5.4 Comparison with Other Energy Absorbing Systems

Direct comparison of responses of different structural systems to earthquakes is very difficult. Typically, a relatively small difference in the period of the structure may lead to dramatic changes in the response when the spectrum of the excitation exhibits significant changes in the range of periods containing the respective fundamental periods.

However, comparisons of indirect response quantities, such as ratios of a particular response quantity in the damped structure to the same quantity in the undamped structure, may provide some limited insight into the behavior of various energy absorbing systems.

For this, we utilize recorded ratios of peak drift responses, RD, and peak base shear force, RBS. Table 5-IV provides a comparison of these quantities for various energy absorbing systems.

The results in Table 5-IV demonstrate that all systems may produce reductions in drift which are comparable. Furthermore, fluid dampers produce reductions in base shear force which are not

TABLE 5-IV Comparison of Drift (RD) and Base Shear Force (RBS) Response Ratios of Various Energy Absorbing Systems

SYSTEM	RD	RBS	REFERENCE
Viscoelastic Dampers	0.5 - 0.9	~ 1	Aiken, 1990
Friction Dampers	0.5 - 0.9	~ 1	Aiken, 1990
Yielding Steel Dampers	0.3 - 0.7	0.6 - 1.25	Whittaker, 1989
Fluid Dampers	0.3 - 0.7	0.4 - 0.7	This Study

realized in the other energy absorbing systems. The reason for this behavior is the effectively viscous nature of fluid dampers. As stated earlier, this behavior has a further advantage in that the additional column axial forces are out-of-phase with the peak drift (see Figure 1-7).

In summary, the addition of fluid dampers significantly reduced both the peak base shear and peak drift in all tests performed. The simultaneous reduction of both of these response quantities is desirable in that the shear forces transmitted to the supporting columns are reduced and, at the same time, the non-structural elements are subjected to lower levels of relative displacement. With currently available seismic protection techniques, other than seismic isolation, it is often difficult to simultaneously reduce both of these response quantities.

5.5 Comparison with Active Control

Active control systems are based on the development of external forces (e.g., developed by actuators or actively moving masses) and have been extensively studied. Soong (1990) demonstrated that the effect of the active control is to primarily modify the structural properties of stiffness and damping. In fact, successful experimental studies with an active tendon system (Chung 1989 and Soong 1990) demonstrated that the primary effect of active control was to increase damping of the tested system with only minor or insignificant modification of stiffness.

In this respect, the achievements of active control may be reproduced and exceeded by fluid viscous dampers with the following additional advantages:

a) Low Cost. Low cost is primarily achieved by utilizing the motion of the structure itself to generate the required damping forces rather than using other means which are external to the structural system (e.g., actuators).

b) Reliability. Fluid dampers have demonstrated good performance over the last twenty years in military applications.

c) Power Requirements. Fluid dampers do not have external power requirements.

d) Longevity. Fluid dampers have been subjected to many years of continuous use in the harsh environment of military applications.

In Table 5-V, the experimental results obtained with the 3-story model structure are compared against the results obtained with the same structure and an active control system (Chung 1989 and Soong 1990). This table compares the recorded response of the structure subjected to the 1940 El Centro, component S00E excitation when uncontrolled and when controlled by either an active tendon system or by fluid dampers. It is evident in this table that the effect of the active tendon system is to only modify damping, an effect which can be reliably produced by fluid dampers. Actually, the level of damping achieved by the fluid dampers is such that, for this particular structure and excitation, the fluid dampers exhibit a clearly superior performance to that of active control.

TABLE 5-V Comparison of Response of Tested 3-Story Model Structure

CONTROL METHOD	SYSTEM PARAMETERS		EXCITATION	FLOOR OR STORY	PEAK FLOOR ACCEL. (g's)	*PEAK INTERSTORY DRIFT / HEIGHT* (%)
	f (Hz)	ξ (%)				
Uncontrolled	2.24 6.83 11.53	1.62 0.39 0.36	El Centro S00E PGA=0.085g	3 2 1	0.322 0.221 0.158	0.596 0.874 0.667
Active Tendon System	2.28 6.94 11.56	12.77 12.27 5.45	El Centro S00E PGA=0.085g	3 2 1	0.200 0.138 0.139	0.405 0.592 0.392
Uncontrolled	2.00 6.60 12.20	1.74 0.76 0.34	El Centro S00E PGA=0.157g	3 2 1	0.585 0.410 0.389	1.073 1.498 1.386
Six Fluid Dampers Placed at all Stories	2.03 7.64 16.99	19.40 44.70 38.04	El Centro S00E PGA=0.152g	3 2 1	0.205 0.152 0.127	0.281 0.510 0.489
Four Fluid Dampers Placed at First Story	2.11 7.52 12.16	17.70 31.85 11.33	El Centro S00E PGA=0.156g	3 2 1	0.282 0.221 0.170	0.465 0.660 0.540

SECTION 6
ANALYTICAL PREDICTION OF RESPONSE

6.1 Time History Response Analysis

The time history analysis of a multi-degree-of-freedom structure subjected to earthquake excitation begins with the equations of motion for the lumped mass model which have been given previously as Equations 4-26 to 4-28. The mass matrix, $[M]$, is diagonal. The stiffness matrix, $[K]$, and damping matrix, $[C_u]$, are constructed either analytically or, as in the case of a model structure, from experimentally determined values of frequencies, damping ratios, and mode shapes (see Equations 4-24 and 4-25).

Application of Fourier Transform to Equations 4-26 to 4-28 results in

$$\{\bar{u}\} = - [S]^{-1} [M] \{1\} \bar{\ddot{u}}_g \tag{6-1}$$

and

$$\bar{P}_j = \frac{i\omega C_{oj} \cos^2 \theta_j}{1 + i\omega\lambda} (\bar{u}_j - \bar{u}_{j-1}) \tag{6-2}$$

Matrix $[S]$ is given by Equations 4-30 to 4-34. Equations 6-1 and 6-2 can be solved numerically for the relative displacement vector, $\{u\}$, and horizontal component of damper force, P_j, by employing the discrete Fourier transform in combination with the Fast Fourier transform (Veletsos and Ventura 1985):

$$\{u(t)\} = \frac{-1}{2\pi} \int_{-\infty}^{\infty} [S]^{-1} [M] \{1\} \bar{\ddot{u}}_g e^{i\omega t} d\omega \tag{6-3}$$

$$P_j(t) = \frac{1}{2\pi} \int_{-\infty}^{\infty} \bar{P}_j e^{i\omega t} d\omega \tag{6-4}$$

Relative acceleration vectors are determined by an expression identical to Equation 6-3 but with the term $-\omega^2$ multiplying the inverse of the dynamic stiffness matrix, $[S]^{-1}$. The total acceleration vector, $\{\ddot{u}_t\}$, is then obtained from

$$\{\ddot{u}_t\} = \{\ddot{u}\} + \{1\}\ddot{u}_g \qquad (6\text{-}5)$$

The computed total acceleration histories are used in the calculation of the story shear forces.

The time-history analysis for a single-degree-of-freedom structure is similar to the above development but with some simplifications.

6.2 Comparison of Experimental and Analytical Time History Responses

Experimental results are compared with the analytical results for the one-story unstiffened and stiffened structures in Figures 6-1 through 6-3 and Figures 6-4 through 6-5, respectively. The base shear force versus drift and the total axial damper force versus axial damper displacement are plotted for selected tests. The comparisons show good agreement.

It should be noted that, in general, the damper force - damper displacement loops (e.g., see Figures 6-2(b) and 6-4(b) are predicted very well from the analytical model. However, the analytical model tends to underpredict the story drift. The reader should recall that the two displacements were directly measured by different instruments which recorded a difference between the two quantities (see Tables 5-I and 5-II). The difference was caused by slippage in the joints of the braces. This slippage was not accounted for in the analytical model.

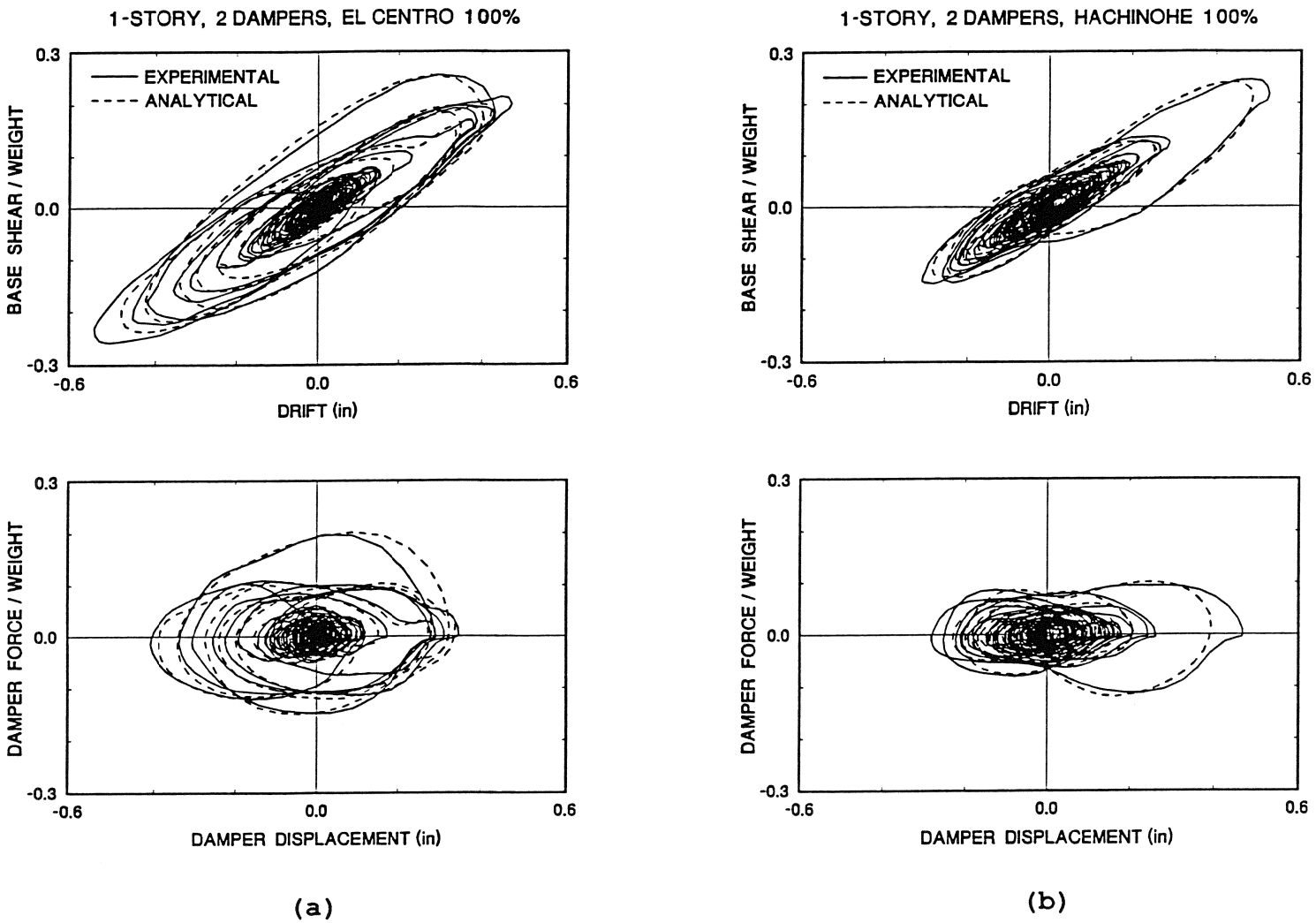

FIGURE 6-1 Comparison of Experimental and Analytical Results for the One-story Unstiffened Structure with Two Dampers Subjected to (a) El Centro 100% Motion and (b) Hachinohe 100% Motion (1 in. = 25.4 mm)

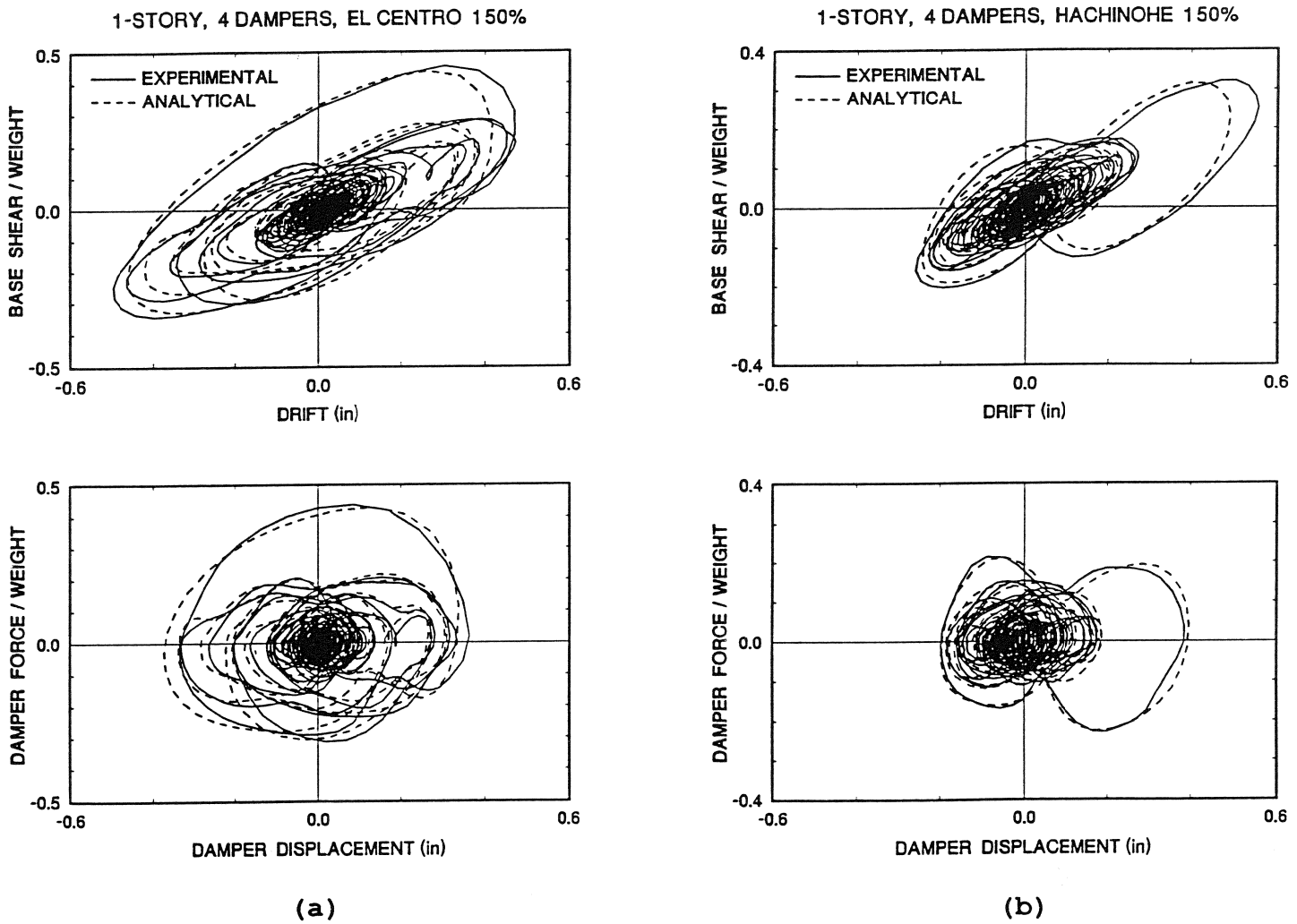

FIGURE 6-2 Comparison of Experimental and Analytical Results for the One-story Unstiffened Structure with Four Dampers Subjected to (a) El Centro 150% Motion and (b) Hachinohe 150% Motion (1 in. = 25.4 mm)

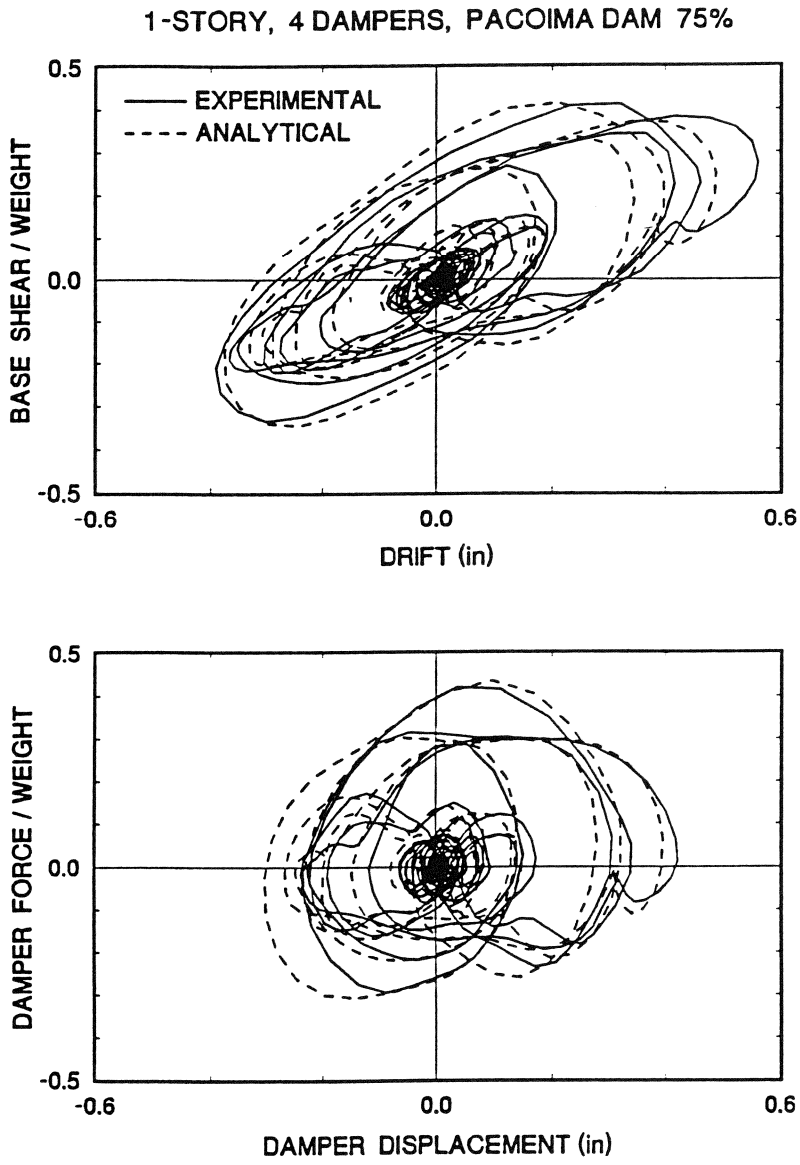

FIGURE 6-3 Comparison of Experimental and Analytical Results for the One-story Unstiffened Structure with Four Dampers Subjected to Pacoima 75% Motion (1 in. = 25.4 mm)

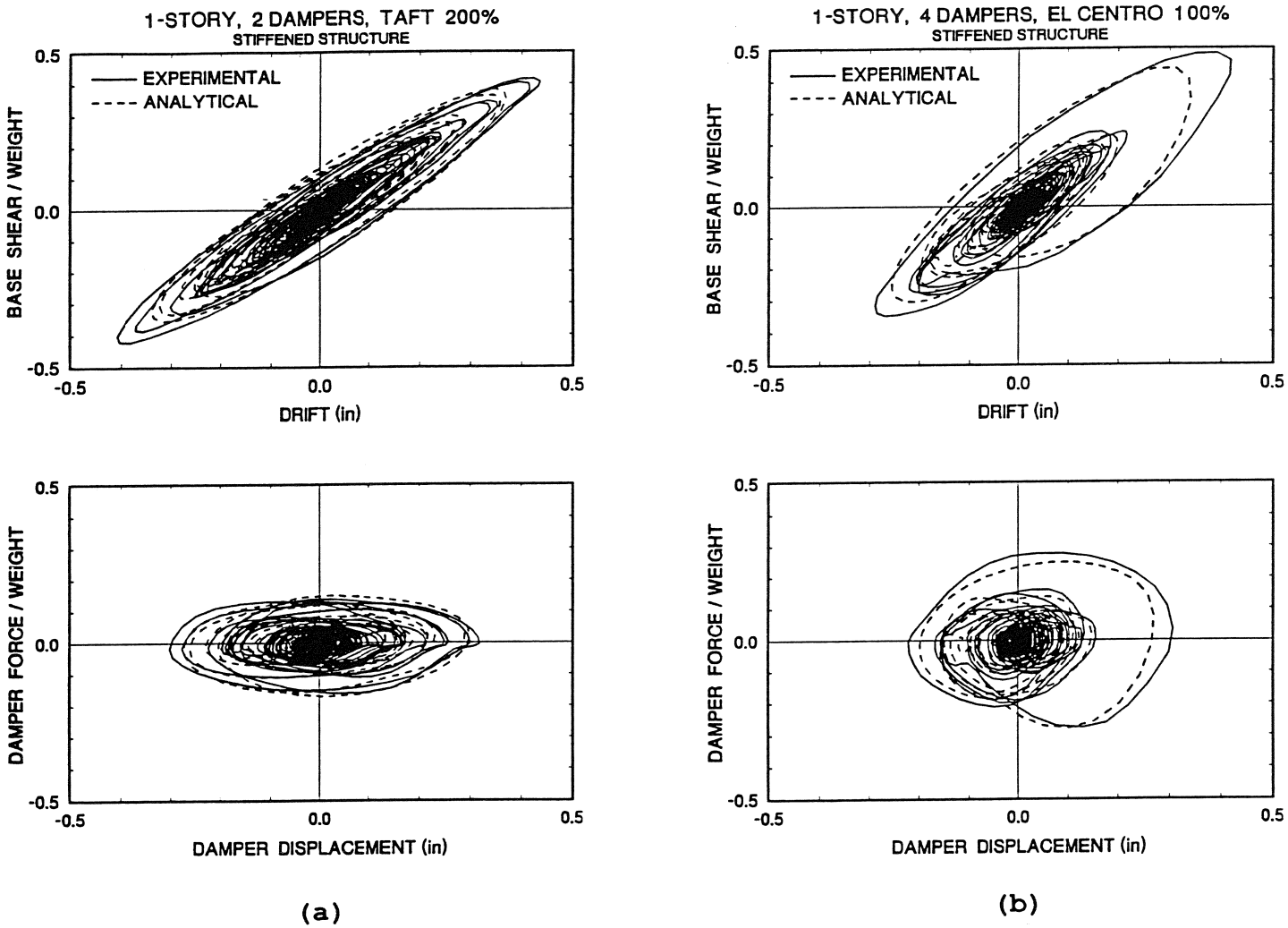

FIGURE 6-4 Comparison of Experimental and Analytical Results for the One-story Stiffened Structure with (a) Two Dampers Subjected to Taft 200% Motion and (b) Four Dampers Subjected to El Centro 100% Motion (1 in. = 25.4 mm)

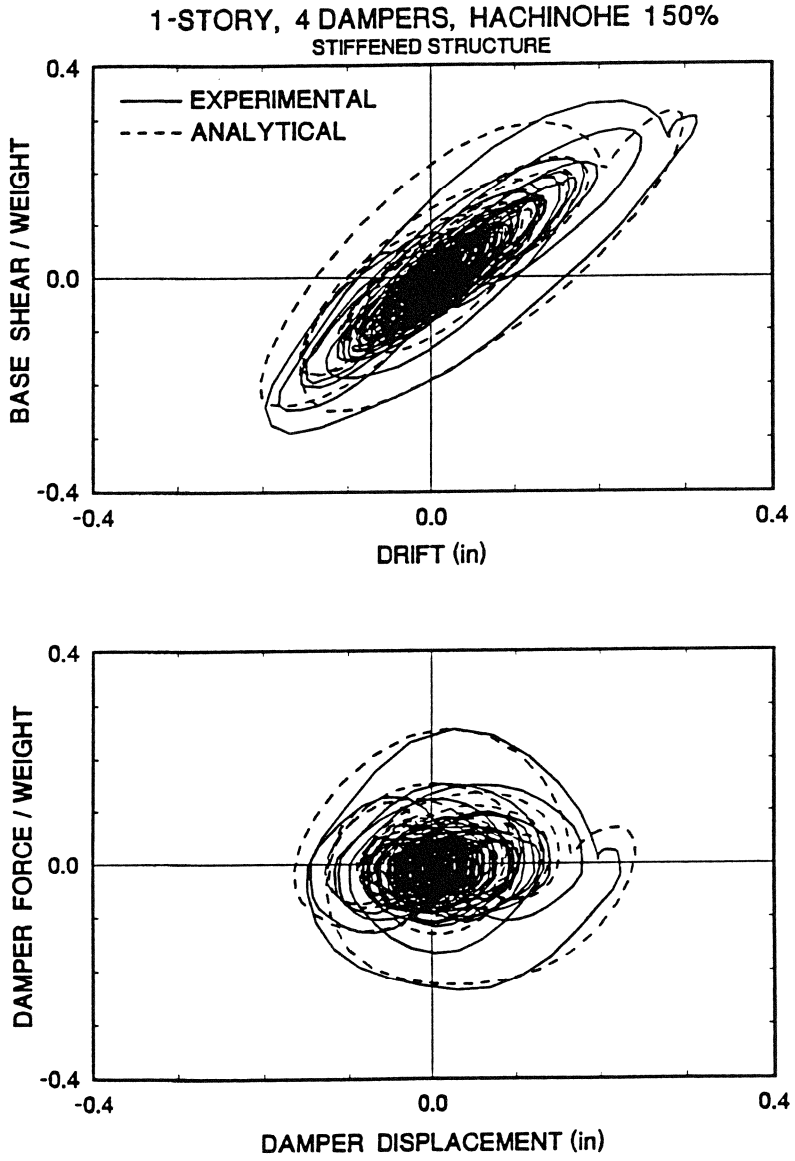

FIGURE 6-5 Comparison of Experimental and Analytical Results for the One-story Stiffened Structure with Four Dampers Subjected to Hachinohe 150% Motion (1 in. = 25.4 mm)

The analytical response is compared for the cases of $\lambda = 0$ (viscous model) and $\lambda = 0.006$ secs (Maxwell model) in Figures 6-6 and 6-7. The base shear force versus drift and the total axial damper force versus the axial damper displacement are plotted for selected tests. The comparisons show that approximating the damper behavior as purely viscous ($\lambda = 0$) will give nearly identical results to the more accurate viscoelastic behavior.

Comparisons of analytical and experimental story shear force versus story drift loops of the 3-story structure are presented in Figures 6-8 through 6-11. Furthermore, Figures 6-12 and 6-13 compare loops of the total axial damper force at the first story versus axial damper displacement in the 3-story structure. Again, the comparison shows good agreement.

Finally, Figures 6-14 and 6-15 compare analytical results obtained with the Maxwell model ($\lambda = 0.006$ secs) and the simple viscous model ($\lambda = 0$) representing the behavior of the fluid dampers. The first story shear versus drift and the total axial damper force at the first story versus the axial damper displacement are plotted for selected tests. These figures confirm that the simple viscous model is appropriate for analysis.

6.3 Response Spectrum Analysis Method

The comparison of analytical to experimental results in Section 6.2 demonstrated that the simple viscous model for fluid dampers is sufficiently accurate. In this respect, a structure with added fluid dampers may be modeled as a non-proportionally viscously damped system. This enables the development of an approximate method of analysis using response spectra. The advantage of this method over a time history analysis is that it directly gives the peak response by use of the usual design specification (i.e., the design spectrum).

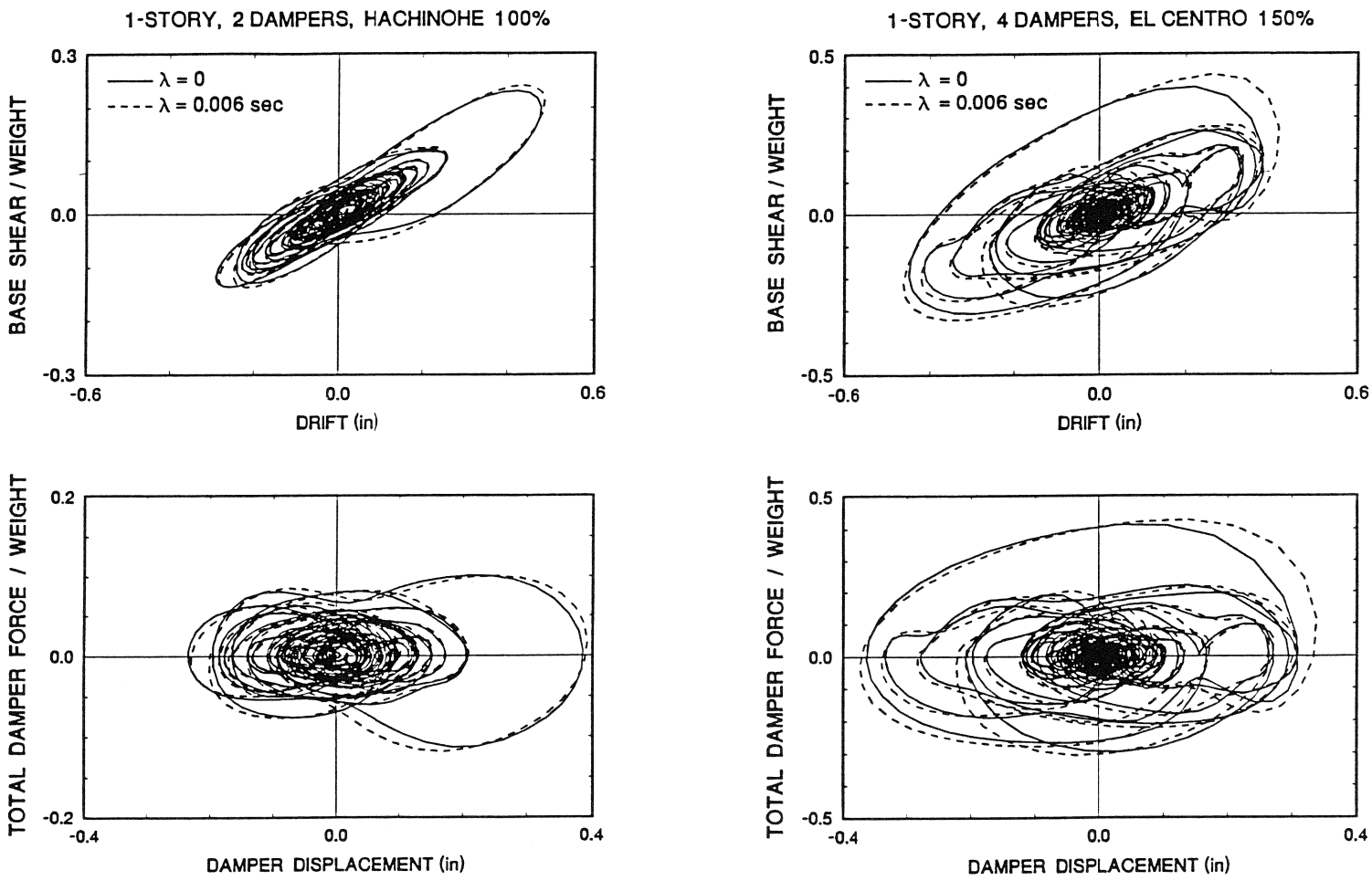

(a) (b)

FIGURE 6-6 Comparison of Analytical Results with the Viscous (λ = 0) and Maxwell (λ = 0.006 secs) Models for the One-story Unstiffened Structure with (a) Two Dampers Subjected to Hachinohe 100% Motion and (b) Four Dampers Subjected to El Centro 150% Motion (1 in. = 25.4 mm)

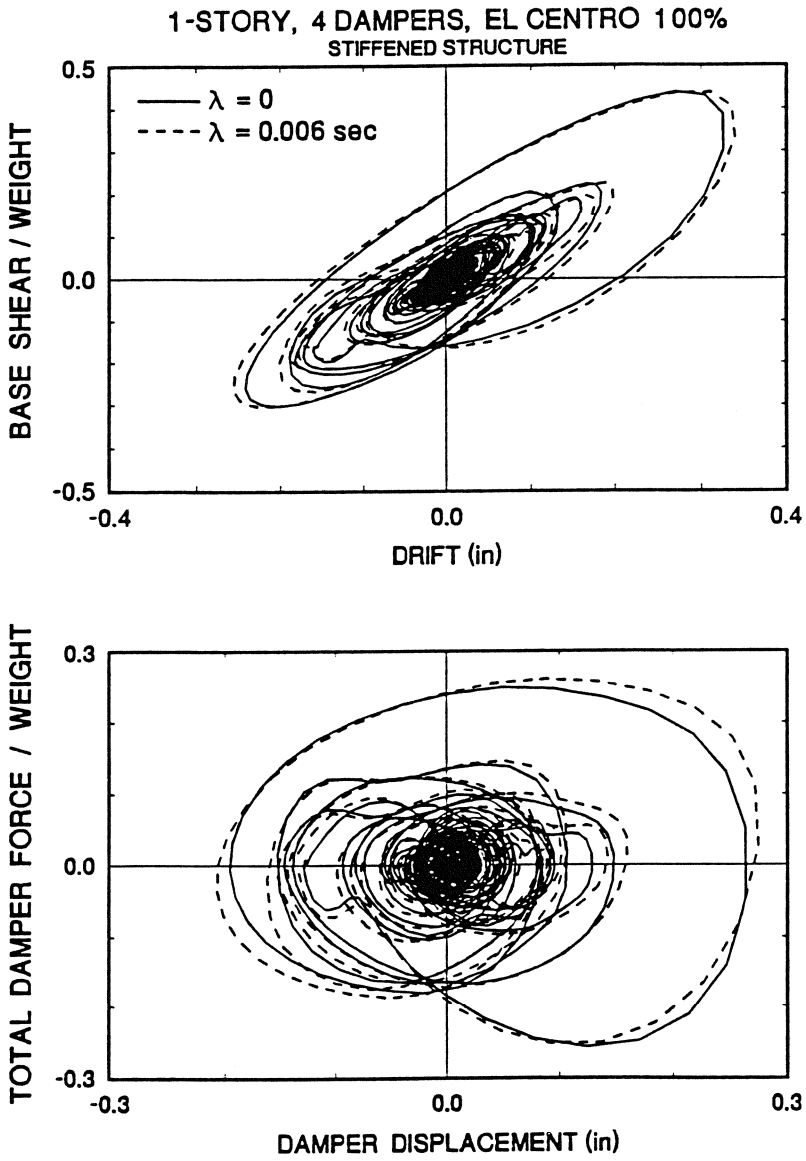

FIGURE 6-7 Comparison of Analytical Results with the Viscous (λ = 0) and Maxwell (λ = 0.006 secs) Models for the One-story Stiffened Structure with Four Dampers Subjected to El Centro 100% Motion (1 in. = 25.4 mm)

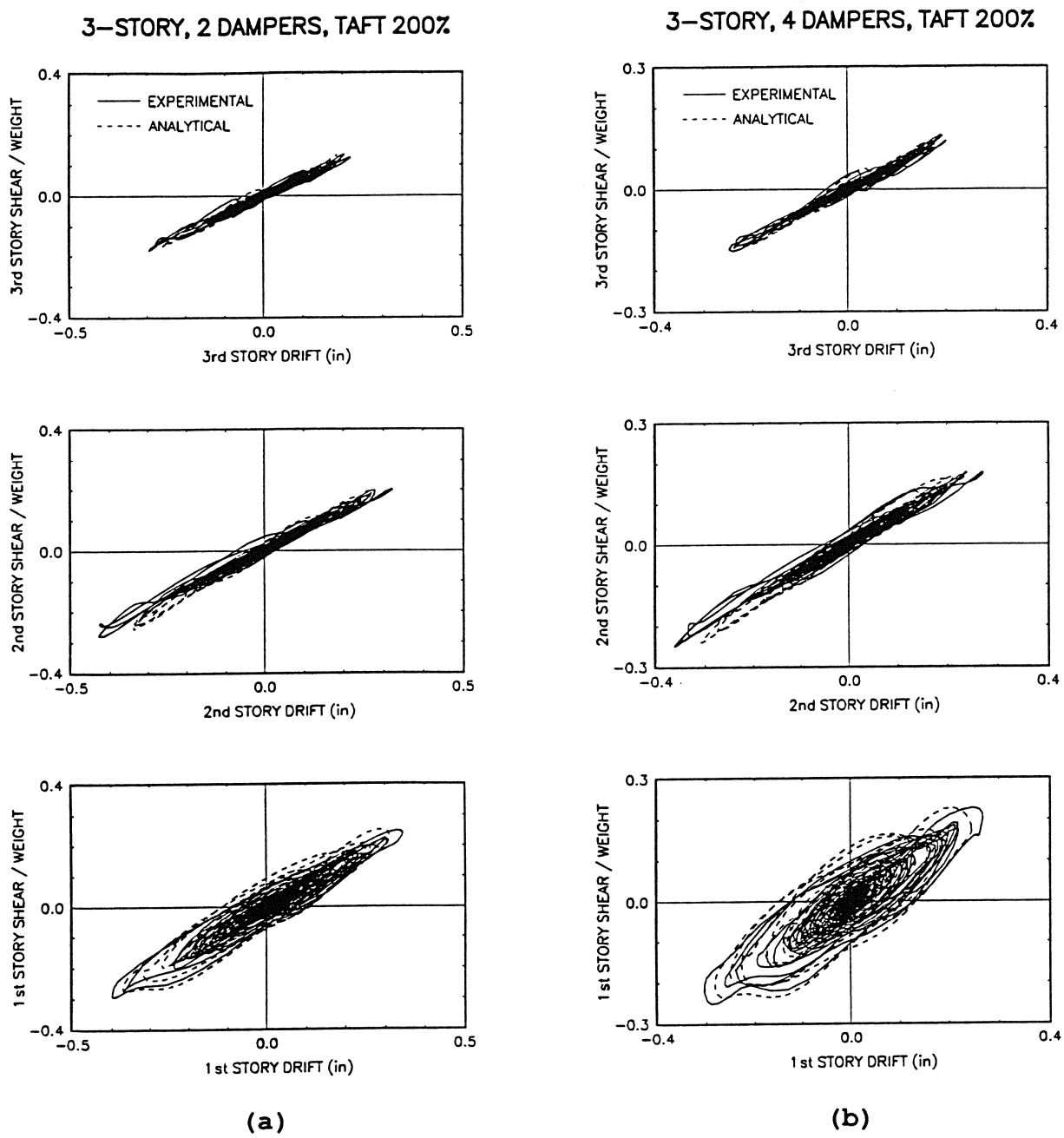

FIGURE 6-8 Comparison of Experimental and Analytical Results for the 3-story Structure Subjected to Taft 200% Motion with (a) Two Dampers and (b) Four Dampers (1 in. = 25.4 mm)

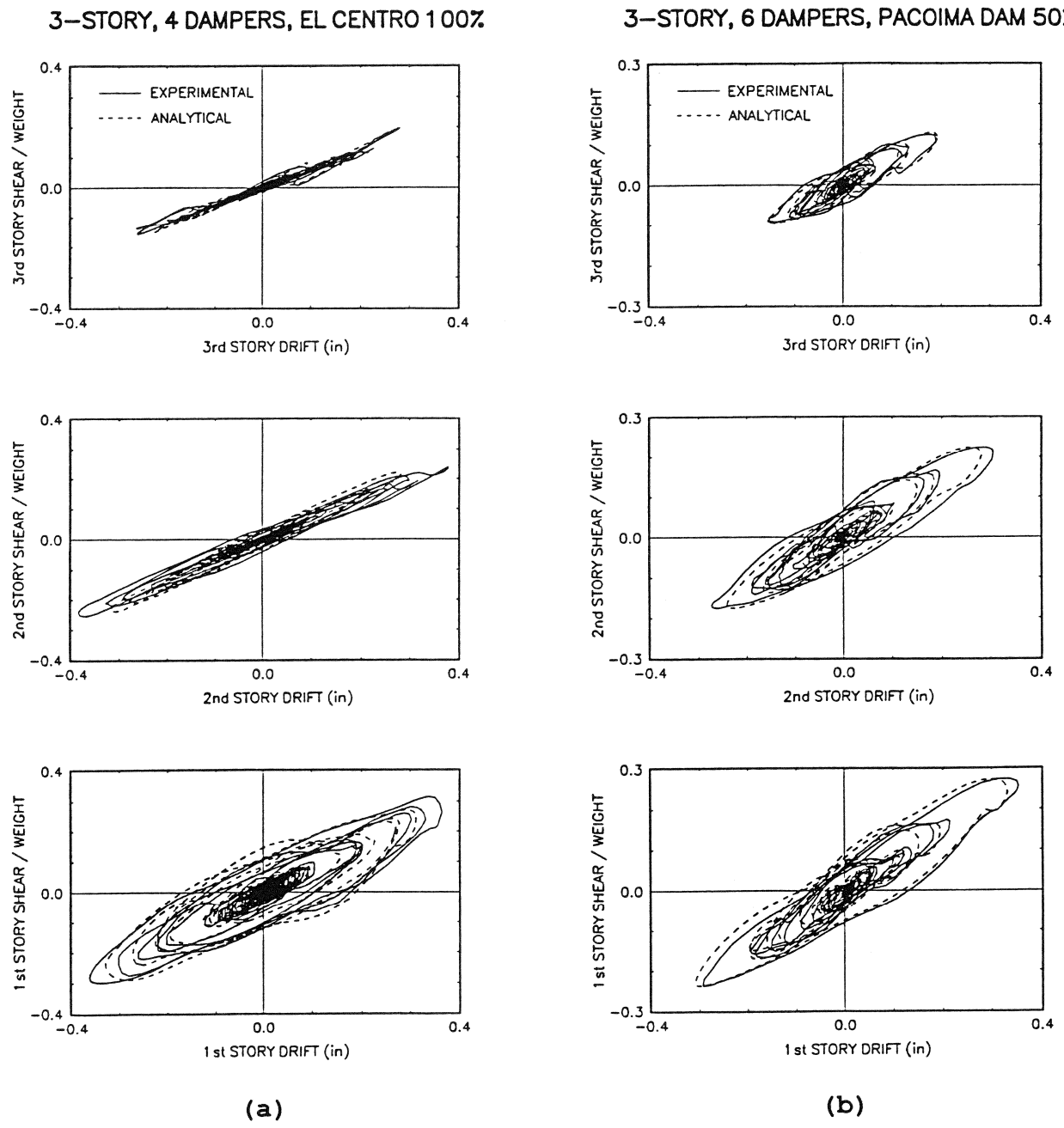

FIGURE 6-9 Comparison of Experimental and Analytical Results for the 3-story Structure with (a) Four Dampers Subjected to El Centro 100% Motion and (b) Six Dampers Subjected to Pacoima 50% Motion (1 in. = 25.4 mm)

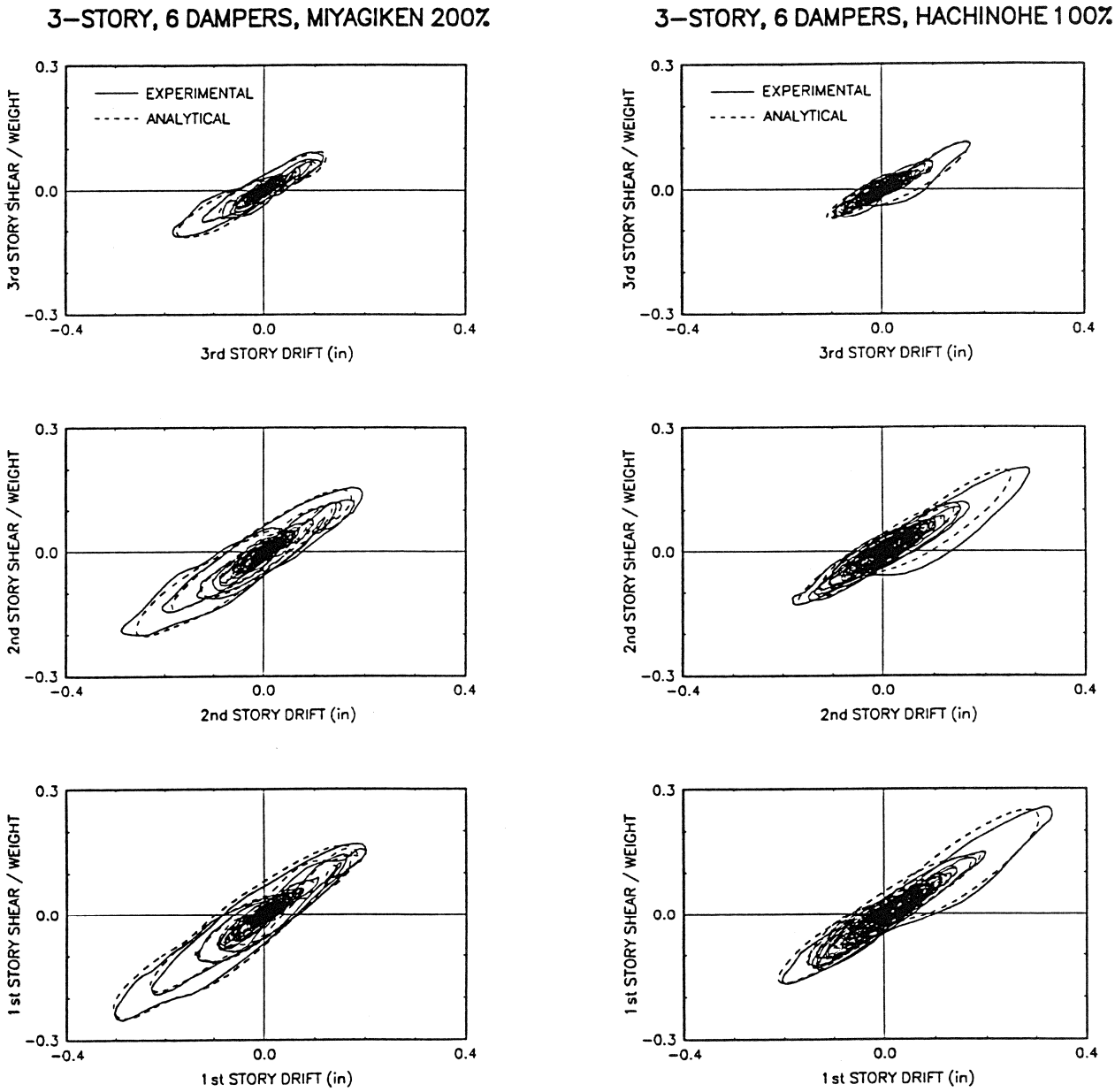

FIGURE 6-10 Comparison of Experimental and Analytical Results for the 3-story Structure with Six Dampers Subjected to (a) Miyagiken 200% Motion and (b) Hachinohe 100% Motion (1 in. = 25.4 mm)

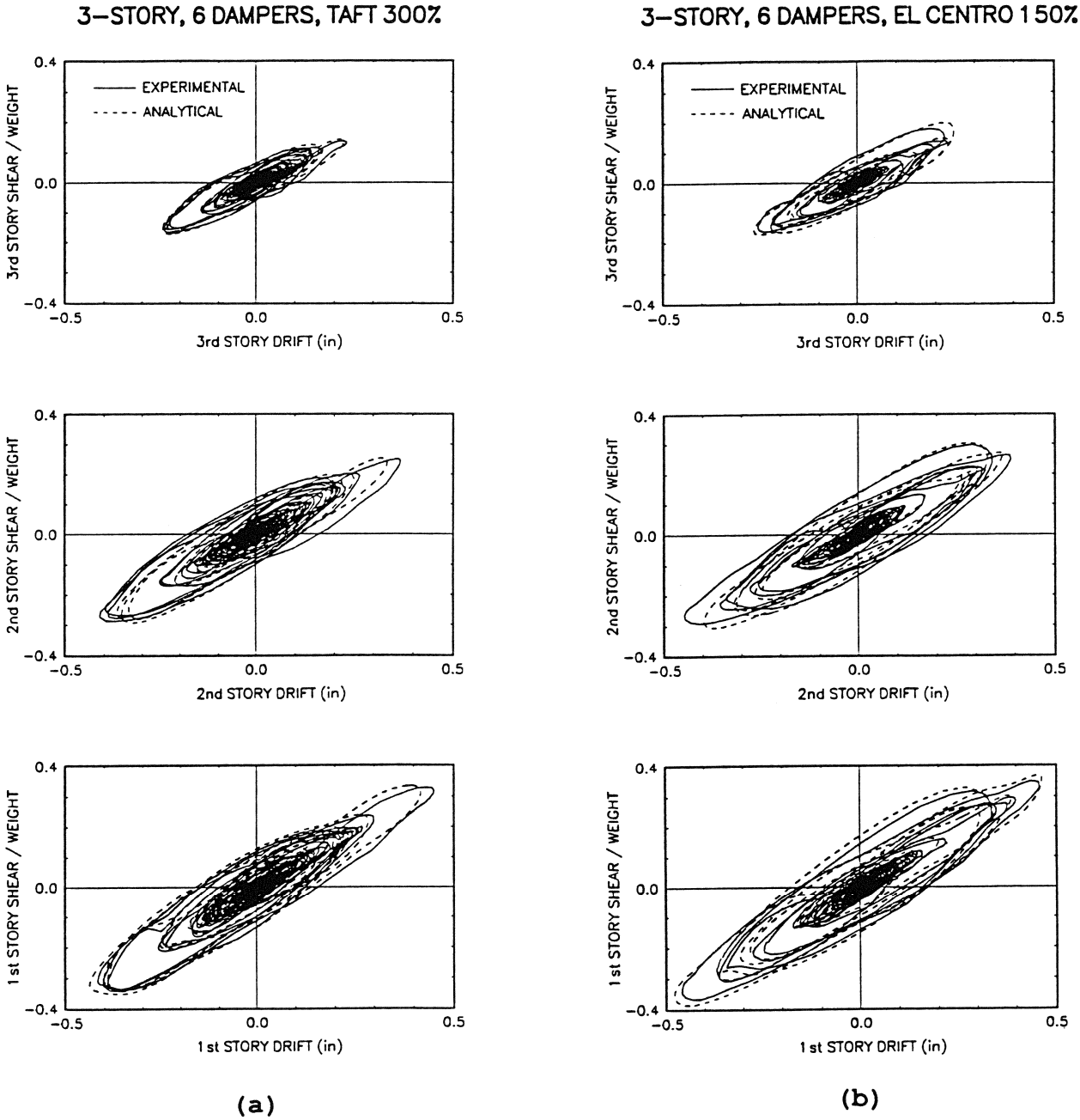

FIGURE 6–11 Comparison of Experimental and Analytical Results for the 3-story Structure with Six Dampers Subjected to (a) Taft 300% Motion and (b) El Centro 150% Motion (1 in. = 25.4 mm)

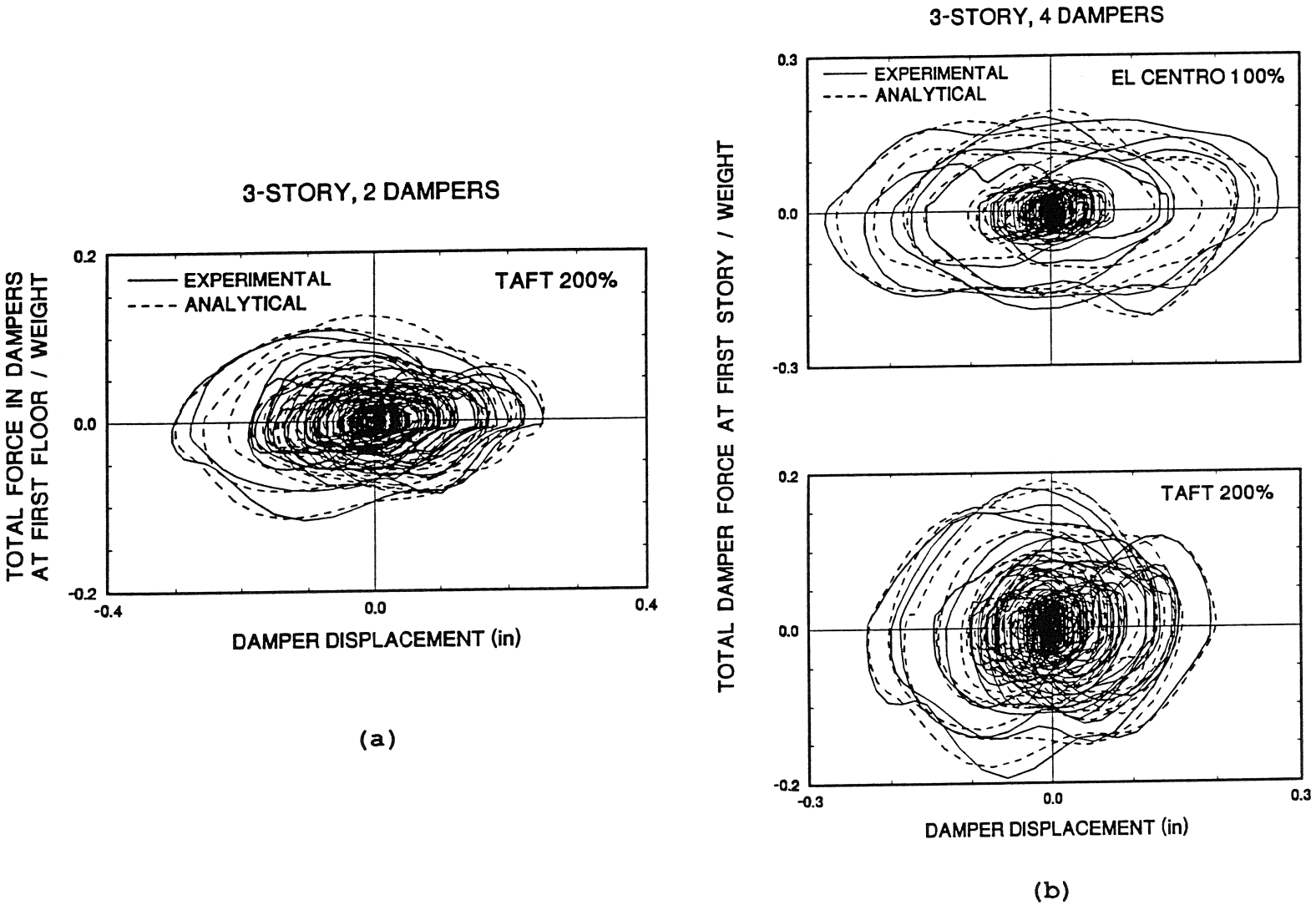

FIGURE 6-12 Comparison of Experimental and Analytical Results for the Dampers in the 3-story Structure with (a) Two Dampers and (b) Four Dampers (1 in. = 25.4 mm)

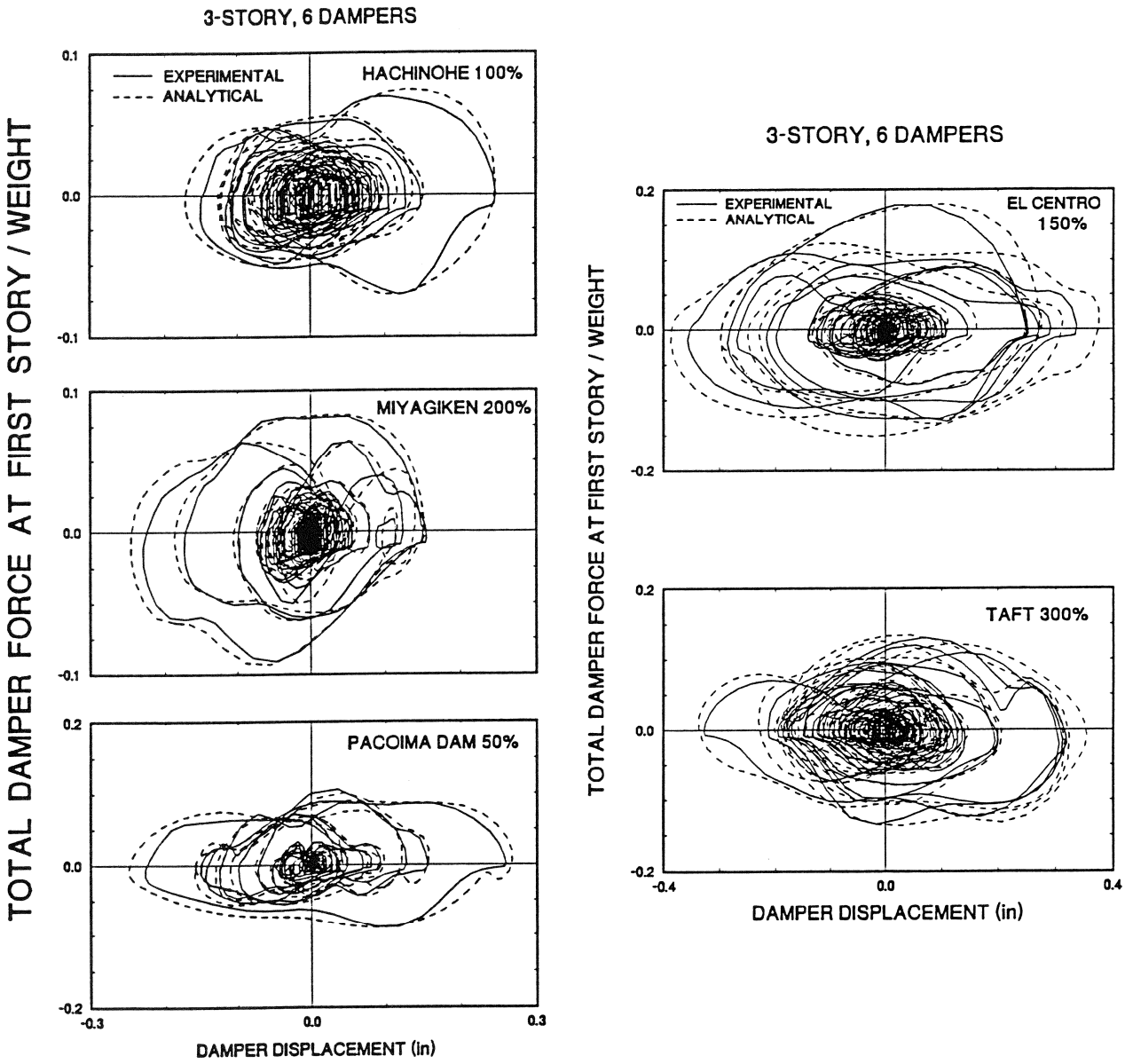

FIGURE 6-13 Comparison of Experimental and Analytical Results for the Dampers in the 3-story Structure with Six Dampers (1 in. = 25.4 mm)

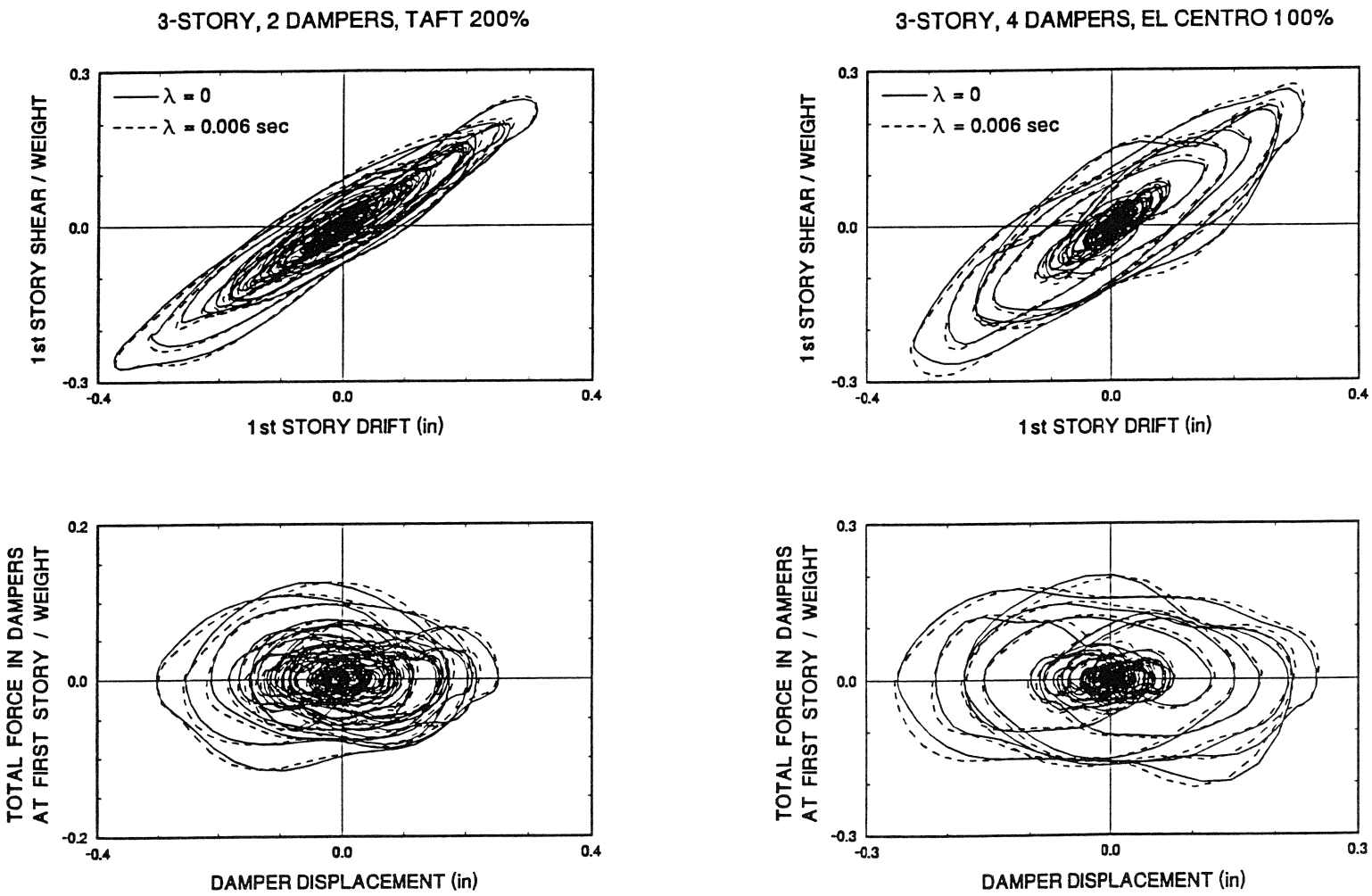

FIGURE 6-14 Comparison of Analytical Results with the Viscous (λ = 0) and Maxwell (λ = 0.006 secs) Models for the 3-story Structure with (a) Two Dampers Subjected to Taft 200% Motion and (b) Four Dampers Subjected to El Centro 100% Motion (1 in. = 25.4 mm)

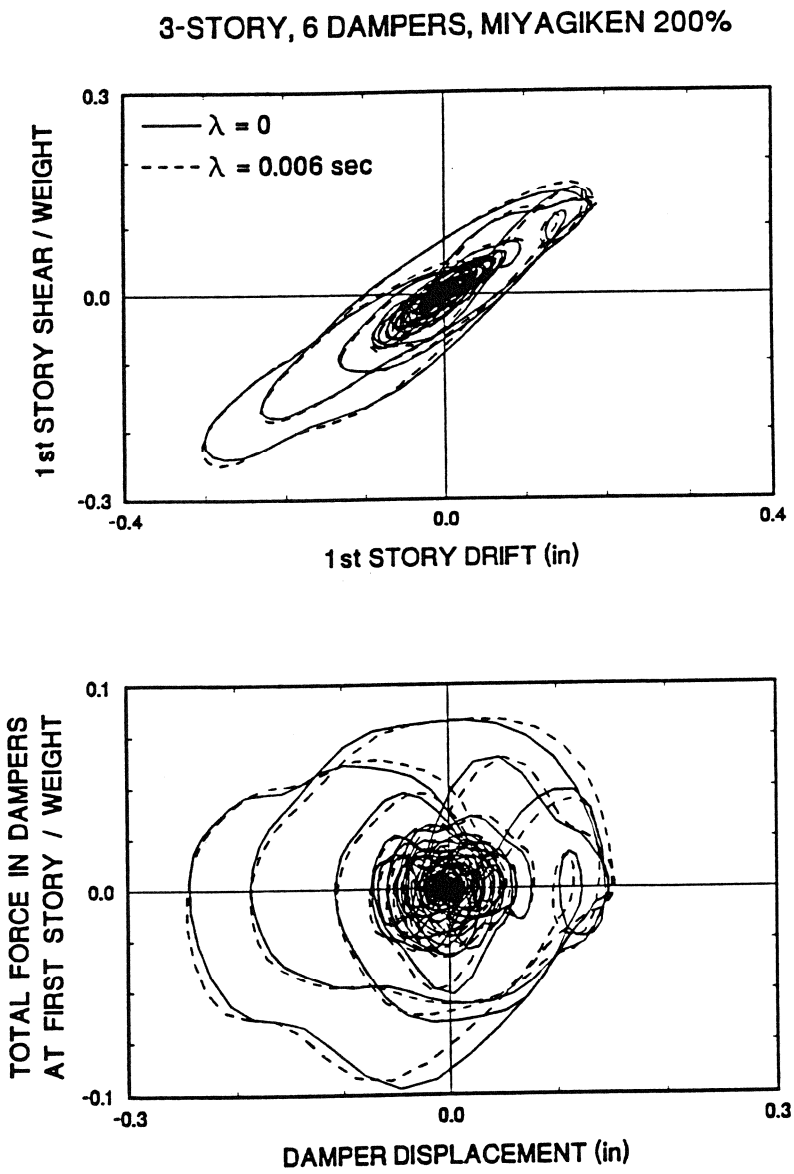

FIGURE 6-15 Comparison of Analytical Results with the Viscous (λ = 0) and Maxwell (λ = 0.006 secs) Models for the 3-story Structure with Six Dampers Subjected to Miyagiken 200% Motion (1 in. = 25.4 mm)

The application of the response spectrum analysis method requires that estimates of the structural properties are available.

6.3.1 Approximate Determination of Structural Properties

Approximate methods for the determination of the frequencies, mode shapes and damping ratios of non-classically damped structures have been successfully applied in problems involving soil-structure interaction (e.g., Novak 1983; Constantinou 1987). Veletsos (1986) presented a comprehensive treatment of the method.

The method starts with the assumption that frequencies and mode shapes of the non-classically damped structure are identical to those of the undamped structure. Typically, these quantities are determined in a standard eigenvalue analysis.

The modal damping ratios are determined from an analysis involving energy considerations. The damping ratio in the k-th mode of vibration may be expressed as

$$\xi_k = \xi_{str_k} + \frac{W_k}{4\pi L_k} \qquad (6\text{-}6)$$

where ξ_{str_k} is the damping ratio due to damping inherent to the structure, W_k is the work done by the dampers in a single cycle of motion, and L_k is the maximum strain energy. W_k may be expressed as

$$W_k = \sum_j \int_0^{T_k} P_j d(u_j - u_{j-1}) \qquad (6\text{-}7)$$

where P_j is the horizontal component of the force in the dampers at the j-th story, and u_j is the modal displacement of the j-th floor. For the case of purely viscous dampers, it can be shown that

$$P_j = C_j \cos^2\theta_j (\phi_j - \phi_{j-1}) \omega_k \cos(\omega_k t) \qquad (6\text{-}8)$$

where C_j is the combined damping coefficient of the dampers at the j-th story, θ_j is the angle of inclination of the dampers at the j-th story, ϕ_j is the modal displacement of the j-th floor in the k-th mode of vibration, and ω_k is the frequency of vibration in the k-th mode. Combining Equations 6-7 and 6-8, W_k can be written as

$$W_k = \pi \omega_k \sum_j C_j \cos^2\theta_j (\phi_j - \phi_{j-1})^2 \qquad (6\text{-}9)$$

The maximum strain energy is equal to the maximum kinetic energy, so that

$$L_k = (KE)_{MAX} = \frac{1}{2} \sum_j m_j \phi_j^2 \omega_k^2 \qquad (6\text{-}10)$$

Combining Equations 6-6, 6-9 and 6-10, the damping ratio of the structure in the k-th mode of vibration is determined to be

$$\xi_k = \xi_{str_k} + \frac{1}{2} \frac{\sum_j C_j \cos^2\theta_j (\phi_j - \phi_{j-1})^2}{\omega_k \sum_j m_j \phi_j^2} \qquad (6\text{-}11)$$

It is clear from Equation 6-11 that in order to have the greatest contribution to the modal damping ratio, the dampers should be placed at story levels where the modal interstory drift $(\phi_j - \phi_{j-1})$ is maximum.

The accuracy of the simple energy approach in determining the damping ratios of the tested structures is demonstrated in Tables 6-I and 6-II. The tables include the damping ratios calculated by the complex eigenvalue approach of Section 4 wherein the calibrated rigorous Maxwell model is utilized for the fluid dampers. The calculation was repeated by utilizing the simple viscous model and,

TABLE 6-I Comparison of Damping Ratios of One-Story Model Structure

STRUCTURE	NUMBER OF DAMPERS	RIGOROUS METHOD MAXWELL MODEL	RIGOROUS METHOD VISCOUS MODEL	ENERGY APPROACH VISCOUS MODEL
UNSTIFFENED	2	0.284	0.280	0.280
STIFFENED		0.193	0.192	0.192
UNSTIFFENED	4	0.577	0.554	0.554
STIFFENED		0.374	0.363	0.363

TABLE 6-II Comparison of Damping Ratios of 3-story Model Structure

NUMBER OF DAMPERS	RIGOROUS METHOD MAXWELL MODEL			RIGOROUS METHOD VISCOUS MODEL			ENERGY APPROACH VISCOUS MODEL		
	MODE 1	MODE 2	MODE 3	MODE 1	MODE 2	MODE 3	MODE 1	MODE 2	MODE 3
2	0.099	0.147	0.050	0.100	0.154	0.049	0.100	0.149	0.051
4	0.177	0.319	0.113	0.183	0.326	0.081	0.183	0.291	0.098
6	0.194	0.447	0.380	0.193	0.428	0.490	0.193	0.428	0.490

thus, solving exactly the eigenvalue problem of the non-classically damped structure (λ was set equal to zero). Finally, the procedure of Equation 6-11 was employed.

The results demonstrate that the damping in the fundamental mode is predicted very well by the energy approach. In addition, the energy approach provides reasonable approximations to the damping ratios of the higher modes. The error in the calculation of the higher mode damping ratios is due to neglect of the stiffening effect of the tested fluid dampers at frequencies exceeding about 4 Hz.

6.3.2 Determination of Peak Response

The determination of the peak structural response to an excitation described by a response spectrum requires that the peak response in each significant mode of vibration be evaluated first (Clough 1975). The required mode shapes, frequencies and damping ratios are determined by the procedures described in Section 6.3.1. The calculated peak modal responses are then combined by an appropriate combination rule to give estimates of the peak response.

The only complexity in the application of this approach is that of constructing high damping response spectra from the usually specified 5%-damped spectra. A recent study on this problem has been reported by Wu (1989). However, it may be appropriate to include de-amplification factors of design spectra at high damping in future design requirements of structures with supplemental damping devices. This will ensure uniformity, reasonable conservatism and avoidance of gross errors.

6.4 Comparison of Experimental, Time History, and Response Spectrum Results

Comparisons of peak response of interest in design (i.e., story shear forces and interstory drifts) are presented in Tables 6-III through 6-VI for the 3-story structure with 4 dampers subjected to the Taft 200% excitation, and for the structure with 6 dampers subjected to the Miyagiken 200%, Hachinohe 100%, and El Centro 150% excitations, respectively. The peak response is given experimentally and analytically as calculated by time history analysis and by the response spectrum approach. For the application of the response spectrum approach, the high damping displacement and acceleration spectra of Figures 3-10 to 3-14 were utilized. Interpolation was used for values of damping ratio not included in these figures.

The peak responses as determined by all four methods compare well. The prediction of story shear forces is very good but the prediction of interstory drifts is less accurate. The reader should recall that slippage occurred in the joints of the damped frame. This effect was not accounted for in the analytical models. The simple response spectrum approach yields results which are accurate enough for design purposes.

TABLE 6-III Comparison of Peak Response to Taft 200% Excitation of 3-story Structure with Four Dampers as Determined Experimentally and by Various Analytical Methods

RESPONSE	EXPERIMENTAL	TIME HISTORY, MAXWELL MODEL	TIME HISTORY, VISCOUS MODEL	RESPONSE SPECTRUM APPROACH
$\frac{\text{3rd Story Shear}}{\text{Weight}}$	0.155	0.142	0.137	0.113
$\frac{\text{2nd Story Shear}}{\text{Weight}}$	0.249	0.240	0.227	0.186
$\frac{\text{1st Story Shear}}{\text{Weight}}$	0.253	0.237	0.231	0.231
$\frac{\text{3rd Story Drift}}{\text{Height}}$ (%)	0.829	0.753	0.726	0.571
$\frac{\text{2nd Story Drift}}{\text{Height}}$ (%)	1.208	1.026	0.977	0.829
$\frac{\text{1st Story Drift}}{\text{Height}}$ (%)	0.949 (0.887) *	0.882	0.884	0.933

* = Measured from relative displacement of damper

TABLE 6-IV Comparison of Peak Response to Miyagiken 200% Excitation of 3-story Structure with Six Dampers as Determined Experimentally and by Various Analytical Methods

RESPONSE	EXPERIMENTAL	TIME HISTORY, MAXWELL MODEL	TIME HISTORY, VISCOUS MODEL	RESPONSE SPECTRUM APPROACH
$\frac{\text{3rd Story Shear}}{\text{Weight}}$	0.114	0.116	0.114	0.106
$\frac{\text{2nd Story Shear}}{\text{Weight}}$	0.202	0.204	0.197	0.178
$\frac{\text{1st Story Shear}}{\text{Weight}}$	0.254	0.250	0.241	0.221
$\frac{\text{3rd Story Drift}}{\text{Height}}$ (%)	0.610	0.583	0.586	0.540
$\frac{\text{2nd Story Drift}}{\text{Height}}$ (%)	0.963	0.859	0.858	0.788
$\frac{\text{1st Story Drift}}{\text{Height}}$ (%)	0.947 (0.890)*	0.952	0.942	0.885

* = Measured from relative displacement of damper

TABLE 6-V Comparison of Peak Response to Hachinohe 100% Excitation of 3-story Structure with Six Dampers as Determined Experimentally and by Various Analytical Methods

RESPONSE	EXPERIMENTAL	TIME HISTORY, MAXWELL MODEL	TIME HISTORY, VISCOUS MODEL	RESPONSE SPECTRUM APPROACH
$\frac{\text{3rd Story Shear}}{\text{Weight}}$	0.111	0.112	0.106	0.108
$\frac{\text{2nd Story Shear}}{\text{Weight}}$	0.201	0.195	0.186	0.185
$\frac{\text{1st Story Shear}}{\text{Weight}}$	0.256	0.250	0.243	0.229
$\frac{\text{3rd Story Drift}}{\text{Height}}$ (%)	0.575	0.566	0.558	0.563
$\frac{\text{2nd Story Drift}}{\text{Height}}$ (%)	0.963	0.837	0.825	0.828
$\frac{\text{1st Story Drift}}{\text{Height}}$ (%)	1.036 (0.957) *	0.954	0.946	0.927

* = Measured from relative displacement of damper

TABLE 6-VI Comparison of Peak Response to El Centro 150% Excitation of 3-story Structure with Six Dampers as Determined Experimentally and by Various Analytical Methods

RESPONSE	EXPERIMENTAL	TIME HISTORY, MAXWELL MODEL	TIME HISTORY, VISCOUS MODEL	RESPONSE SPECTRUM APPROACH
$\frac{\text{3rd Story Shear}}{\text{Weight}}$	0.178	0.198	0.177	0.176
$\frac{\text{2nd Story Shear}}{\text{Weight}}$	0.298	0.307	0.295	0.294
$\frac{\text{1st Story Shear}}{\text{Weight}}$	0.368	0.387	0.368	0.365
$\frac{\text{3rd Story Drift}}{\text{Height}}$ (%)	0.852	0.889	0.876	0.896
$\frac{\text{2nd Story Drift}}{\text{Height}}$ (%)	1.492	1.323	1.302	1.306
$\frac{\text{1st Story Drift}}{\text{Height}}$ (%)	1.436 (1.382) *	1.498	1.465	1.468

* = Measured from relative displacement of damper

SECTION 7
CONCLUSIONS

A combined experimental and analytical study of an energy absorbing system for structures, consisting of fluid viscous dampers, has been presented. Tests were conducted on one- and 3-story model structures with various configurations of dampers. Dampers were placed either along the entire height of the 3-story structure, or concentrated at the level of expected peak interstory drift. Tests were also conducted on the bare frame in a configuration resembling a moment resisting frame.

A comprehensive component test program on the fluid dampers was conducted. The test program evaluated the behavior of the dampers in a range of frequencies varying between essentially zero and 25 Hz, a range of amplitudes of essentially zero to 1 inch (25.4 mm), and a range of temperatures between about zero and 50°C. The component tests resulted in a database of mechanical properties which enabled the development of a rigorous mathematical model.

The mathematical model was utilized in the time history analysis of the tested structures with very good results. Furthermore, simplified models and methods of analysis were developed, evaluated and shown to produce results in good agreement with the experiments.

The important conclusions of this study are summarized below:

a) Fluid viscous dampers may be designed to exhibit a behavior which is essentially linear viscous for frequencies of motion below a certain cutoff frequency. For the tested damper this frequency was equal to about 4 Hz. Beyond this frequency the dampers exhibit viscoelastic behavior.
b) Fluid dampers may be modeled over a wide range of frequencies by the classical Maxwell model. However, since the cutoff

frequency is usually above (or they can be designed so) the frequencies of dominant modes of the structure, the dampers may be modeled as simple linear viscous dampers.

c) Temperature has a minor effect on the behavior of the tested fluid dampers. Due to a special design with a passive temperature-compensated orifice, the tested dampers exhibited variations of their damping constant from a certain value at room temperature (24°C) to +44% of that value at 0°C to -25% of that value at 50°C. This rather small change in properties over a wide range of temperatures is in sharp contrast to the extreme temperature sensitivity of viscoelastic dampers.

d) The inclusion of fluid viscous dampers in the tested structures resulted in reductions in story drifts of 30% to 70%. These reductions are comparable to those achieved by other energy dissipating systems such as viscoelastic, friction and yielding steel dampers. However, the use of fluid dampers also resulted in reductions of story shear forces by 40% to 70%, while other energy absorbing devices were incapable of achieving any significant reduction.

e) Fluid dampers are capable of achieving and surpassing the benefits offered by active control systems with the additional benefits of low cost, no requirements for power, longevity and reliability.

f) Due to their viscous nature, fluid dampers reduce drifts and thus column bending moments, while introducing additional column axial forces which are out-of-phase with the bending moments. In effect, this behavior prevents the possibility of compression failure of weak columns in retrofit applications.

g) Time history analyses of structures with added fluid dampers may be more conveniently performed by application of Discrete Fourier transform since the dampers exhibit linear behavior. Such analyses were performed for the tested structure with the results being in good agreement with the results of the experiments.

h) A simplified method for calculating the modal characteristics of structures with added fluid dampers was developed and verified. The method was used to obtain estimates of peak response of the tested structures by utilizing the response spectrum approach. The obtained results demonstrated that the simplified method is sufficiently accurate for design purposes.

SECTION 8
REFERENCES

Aiken, I.D. and Kelly, J.M. (1988). "Experimental Study of Friction Damping for Steel Frame Structures." Proc. PVP Conference, ASME, Pittsburgh, PA, Vol. 133, 95-100.

Aiken, I.D. and Kelly, J.M. (1990). "Earthquake Simulator Testing and Analytical Studies of Two Energy-Absorbing Systems for Multistory Structures" Report No. UCB/EERC-90/03, University of California, Berkeley.

Arima, F., Miyazaki, M., Tanaka, H. and Yamazaki, Y. (1988). "A Study on Building with Large Damping using Viscous Damping Walls." Proc., 9th World Conference on Earthquake Engineering, Tokyo-Kyoto, Japan, 5, 821-826.

Bird, R.B., Armstrong, R.C. and Hassager, O. (1987). Dynamics of Polymeric Liquids, J. Wiley and Sons, New York, NY.

British Standards Institution - BSI (1979). "Commentary on Corrosion at Bimetallic Contacts and its Alleviation." Standard PD 6484:1979, London, U.K.

Buckle, I.G. and Mayes, R.L. (1990). "Seismic Isolation History, Application, and Performance - a World View." Earthquake Spectra, 6(2), 161-201.

Chang, K.C., Soong, T.T., Oh, S-T. and Lai, M.L. (1991). "Seismic Response of a 2/5 Scale Steel Structure with Added Viscoelastic Dampers." Report No. NCEER-91-0012, National Center for Earthquake Engineering Research, Buffalo, NY.

Chung, L.L., Lin, R.C., Soong, T.T. and Reinhorn, A.M. (1989). "Experimental Study of Active Control of MDOF Seismic Structures." J. Engrg. Mech., ASCE, 115(8), 1609-1627.

Clements, E.W. (1972). "Shipboard Shock and Navy Devices for its Simulation." Report NRL 7396, Naval Research Laboratory, Washington, DC.

Clough, R.W. and Penzien, J. (1975). Dynamics of Structures, McGraw-Hill, New York.

Constantinou, M.C. (1987). "A Simplified Analysis Procedure for Base-Isolated Structures on Flexible Foundation." Earthquake Engrg. Struct. Dyn., 15, 963-983.

Constantinou, M.C., Reinhorn, A.M., Mokha, A. and Watson, R. (1991a). "Displacement Control Device for Base-isolated Bridges." Earthquake Spectra, 7(2), 179-200.

Constantinou, M.C., Kartoum, A., Reinhorn, A.M. and Bradford, P. (1991b). "Experimental and Theoretical Study of a Sliding Isolation System for Bridges." Report No. NCEER 91-0027, National Center for Earthquake Engineering Research, Buffalo, NY.

Filiatrault, A. and Cherry, S. (1985). "Performance Evaluation of Friction Damped Braced Steel Frames under Simulated Earthquake Loads." Report of Earthquake Engineering Research Laboratory, University of British Columbia, Vancouver, Canada.

Fitzgerald, T.F., Anagnos, T., Goodson, M. and Zsutty, T. (1989). "Slotted Bolted Connections in Aseismic Design of Concentrically Braced Connections." Earthquake Spectra, 5(2), 383-391.

Fujita, T. (editor) (1991). "Seismic Isolation and Response Control for Nuclear and Non-nuclear Structures." Special Issue for the Exhibition of the 11th International Conference on Structural Mechanics in Reactor Technology, SMiRT 11, Tokyo, Japan.

Harris, C.M. (1987). Shock and Vibration Handbook, McGraw-Hill, New York, NY.

Hsu, S-Y. and Fafitis, A. (1992). "Seismic Analysis Design of Frames with Viscoelastic Connections." J. Struct. Engrg., ASCE, 118(9), 2459-2474.

International Mathematical Statistical Library - IMSL (1987), Subroutine GVCRG, Houston, Texas.

Kelly, J.M., Skinner, M.S. and Beucke, K.E. (1980). "Experimental Testing of an Energy-Absorbing Base Isolation System." Report No. UCB/EERC-80/35, University of California, Berkeley.

Kelly, J.M. (1988). "Base Isolation in Japan, 1988". Report No. UCB/EERC-88/20, University of California, Berkeley.

Kelly, J.M. (1991). "Base Isolation: Origins and Development." News-Earthquake Engineering Research Center, University of California, Berkeley, Calif., 12(1), 1-3.

Lin, R.C., Liang, Z., Soong, T.T. and Zhang, R.H. (1988). "An Experimental Study of Seismic Structural Response with Added Viscoelastic Dampers." Report No. NCEER-88-0018, National Center for Earthquake Engineering Research, Buffalo, NY.

Makris, N. and Constantinou, M.C. (1991). "Fractional-Derivative Maxwell Model for Viscous Dampers." J. Struct. Engrg., ASCE, 117(9), 2708-2724.

Makris, N. and Constantinou, M.C. (1992). "Spring-Viscous Damper Systems for Combined Seismic and Vibration Isolation." Earthquake Engrg. Struct. Dyn., 21(8), 649-664.

Mayes, R.L., Jones, L.R., and Buckle, I.G. (1990). "Impediments to the Implementation of Seismic Isolation." Earthquake Spectra, 6(2), 283-296.

Mokha, A., Constantinou, M.C., Reinhorn, A.M., and Zayas, V. (1991). "Experimental Study of Friction Pendulum Isolation System." J. Struct. Engrg., ASCE, 117(4), 1201-1217.

Novak, M. and El Hifnawy, L. (1983). "Effect of Soil-Structure Interaction on Damping of Structures." Earthquake Engrg. Struct. Dyn., 11, 595-621.

Pall, A.S. and Marsh, C. (1982). "Response of Friction Damped Braced Frames." J. Struct. Engrg., ASCE, 108(6), 1313-1323.

Pall, A.S., Verganelakis, V. and Marsh, C. (1987). "Friction Dampers for Seismic Control of Concordia University Library Building." Proc. 5th Canadian Conference on Earthquake Engineering, Ottawa, Canada, 191-200.

Roeder, C.W. and Popov, E.P. (1978). "Eccentrically Braced Steel Frames for Earthquakes." J. Struct. Div., ASCE, 104(3), 391-412.

Skinner, R.I., Tyler,R.G., Heine, A.J., and Robinson, W.H. (1980). "Hysteretic Dampers for the Protection of Structures from Earthquakes." Bulletin of New Zealand National Society for Earthquake Engineering, 13(1), 22- 36.

Soong, T.T., Reinhorn, A.M. and Yang, J.N. (1987). "A Standardized Model for Structural Control Experiments and Some Experimental Results." Proc., Second International Symposium on Structural Control, 1985, Waterloo, Canada.

Soong, T.T. (1990). Active Structural Control: Theory and Practice, Longman, New York.

Tyler, R.G. (1978). "Tapered Steel Energy Dissipators for Earthquake Resistant Structures." Bulletin of New Zealand National Society for Earthquake Engineering, 11(4), 282-294.

Tyler, R.G. (1985). "Further Notes on a Steel Energy-Absorbing Element for Braced Frameworks." Bulletin of New Zealand National Society for Earthquake Engineering, 18(3), 270-279.

Uang, C-M. and Bertero, V.V. (1988). "Use of Energy as a Design Criterion in Earthquake-Resistant Design." Report No. UCB/EERC-88/18, University of California, Berkeley.

Veletsos, A.S. and Ventura, C.E. (1985). "Dynamic Analysis of Structures by the DFT Method." J. Struct. Engrg., ASCE, 111(2), 2625-2642.

Veletsos, A.S. and Ventura, C.E. (1986). "Modal Analysis of Non-Proportionally Damped Linear Systems." Earthquake Engrg. Struct. Dyn., 14, 217-243.

Whittaker, A.S., Bertero, V.V., Alonso, J.L. and Thompson, C.L. (1989). "Earthquake Simulator Testing of Steel Plate Added Damping and Stiffness Elements." Report No. UCB/EERC-89/02, University of California, Berkeley.

Wu, J. and Hanson, R. (1989). "Study of Inelastic Spectra with High Damping." J. Struct. Engrg, ASCE, 115(6), 1412-1431.

APPENDIX A

ONE-STORY TEST RESULTS

1 –STORY, NO DAMPERS, EL CENTRO 10%

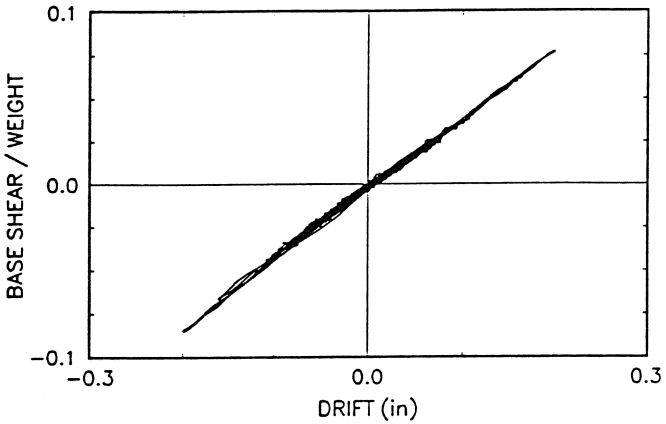

1 –STORY, NO DAMPERS, EL CENTRO 33.3%

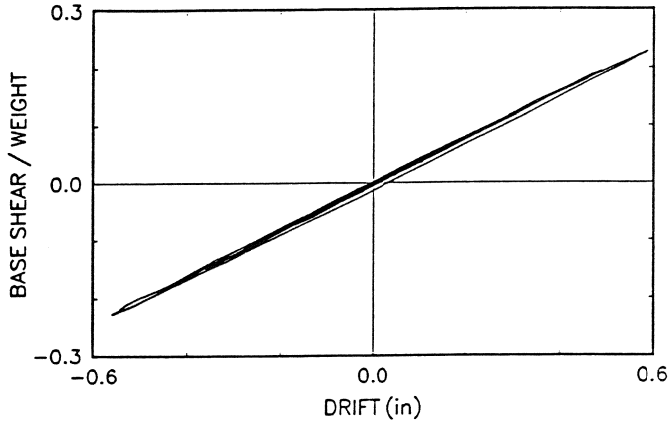

1 –STORY, NO DAMPERS, EL CENTRO 20%

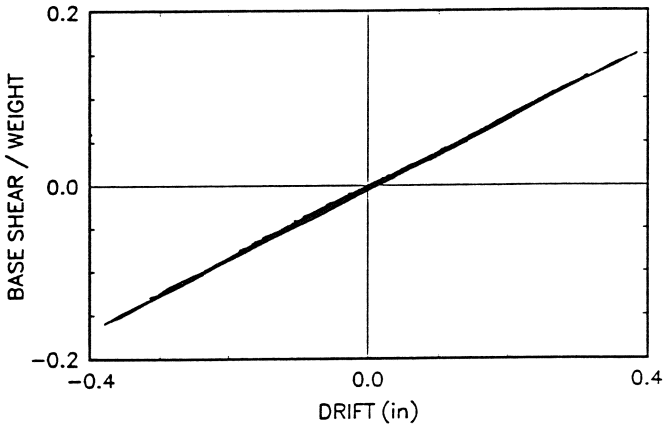

1 –STORY, NO DAMPERS, TAFT 33.3%

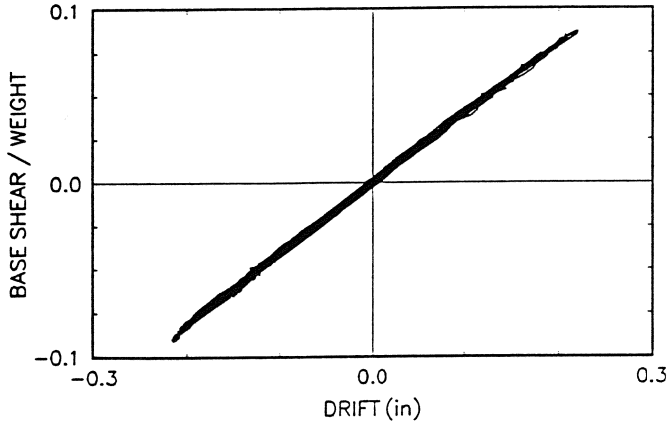

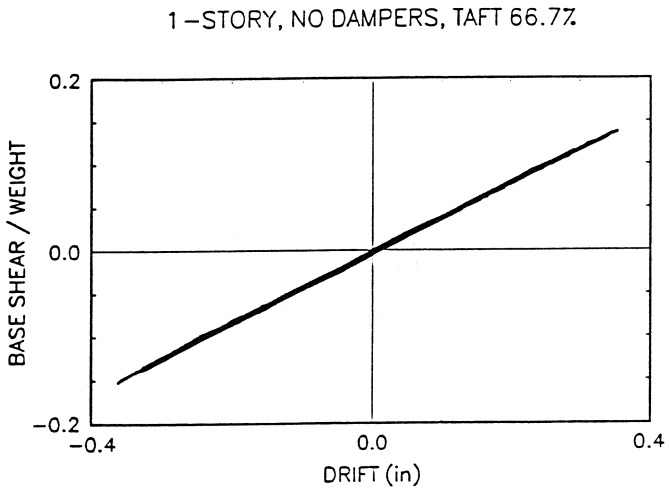
1 – STORY, NO DAMPERS, TAFT 66.7%
BASE SHEAR / WEIGHT
0.2
0.0
−0.2
−0.4
0.0
0.4
DRIFT (in)

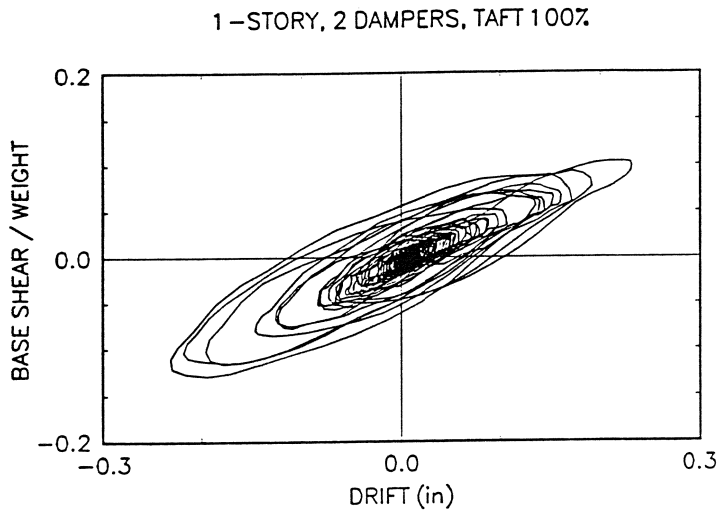
1 – STORY, 2 DAMPERS, TAFT 100%
BASE SHEAR / WEIGHT
0.2
0.0
−0.2
−0.3
0.0
0.3
DRIFT (in)

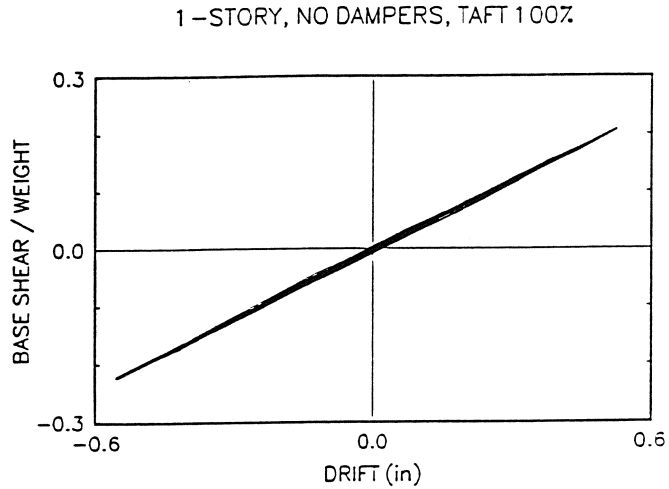
1 – STORY, NO DAMPERS, TAFT 100%
BASE SHEAR / WEIGHT
0.3
0.0
−0.3
−0.6
0.0
0.6
DRIFT (in)

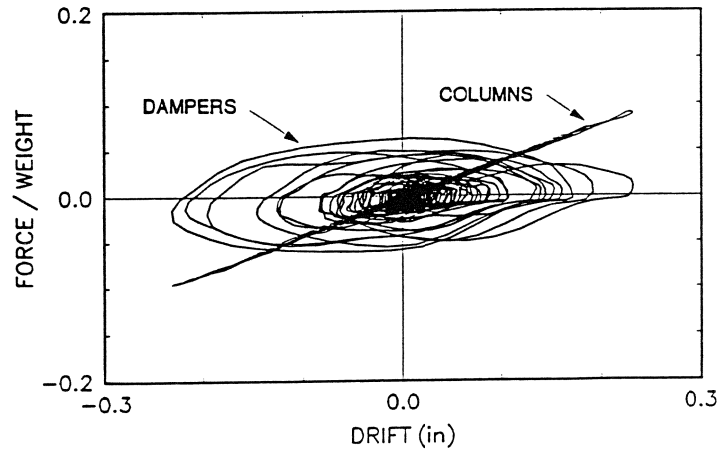
FORCE / WEIGHT
0.2
0.0
−0.2
−0.3
0.0
0.3
DRIFT (in)
DAMPERS
COLUMNS

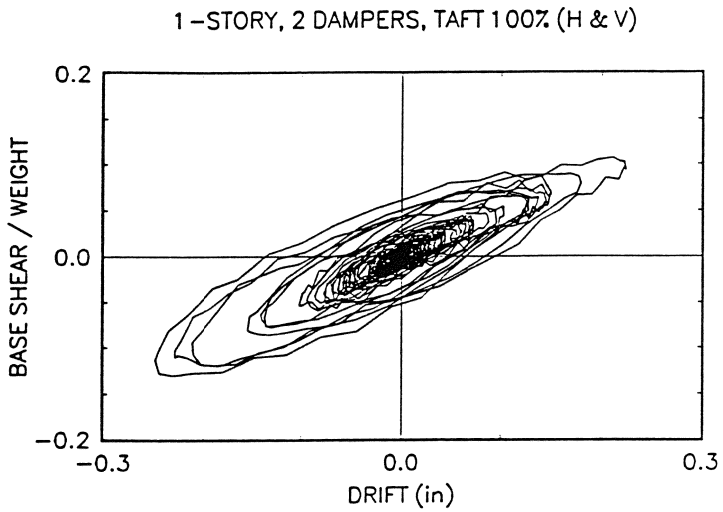
1 – STORY, 2 DAMPERS, TAFT 100% (H & V)
BASE SHEAR / WEIGHT
0.2
0.0
−0.2
−0.3
0.0
0.3
DRIFT (in)

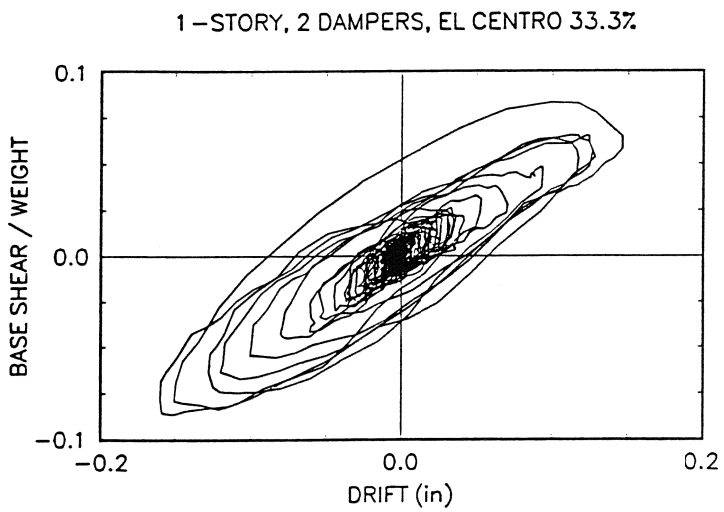
1 – STORY, 2 DAMPERS, EL CENTRO 33.3%
BASE SHEAR / WEIGHT
0.1
0.0
−0.1
−0.2
0.0
0.2
DRIFT (in)

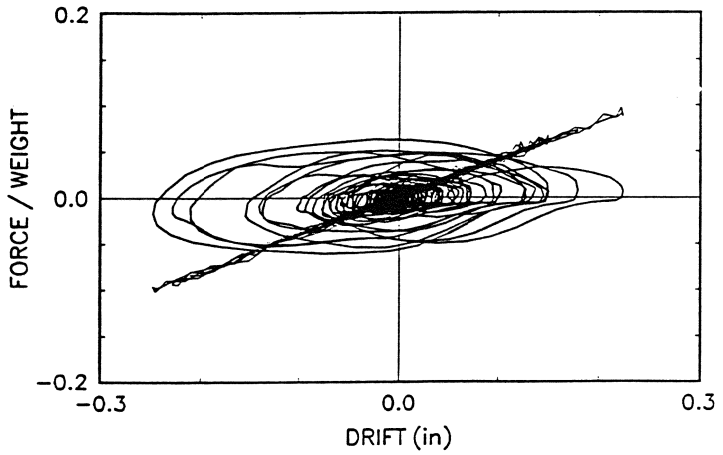
FORCE / WEIGHT
0.2
0.0
−0.2
−0.3
0.0
0.3
DRIFT (in)

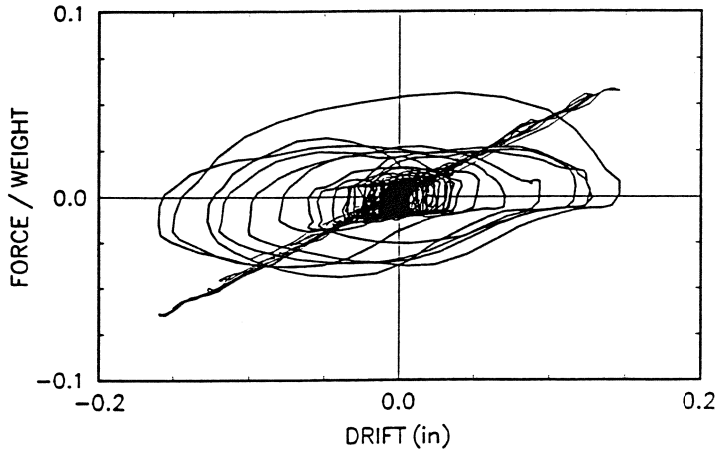
FORCE / WEIGHT
0.1
0.0
−0.1
−0.2
0.0
0.2
DRIFT (in)

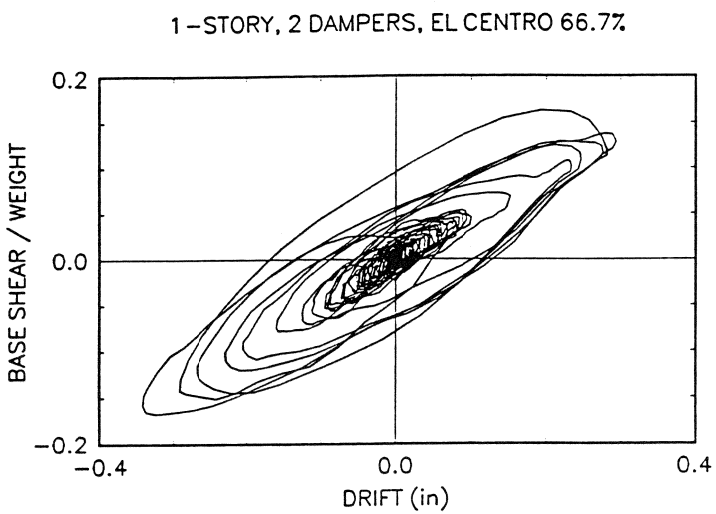
1 – STORY, 2 DAMPERS, EL CENTRO 66.7%
BASE SHEAR / WEIGHT
0.2
0.0
−0.2
−0.4
0.0
0.4
DRIFT (in)

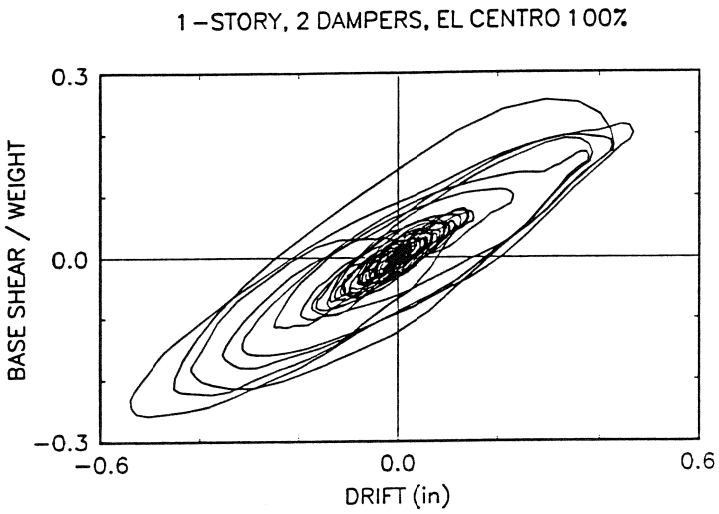
1 – STORY, 2 DAMPERS, EL CENTRO 1 00%
BASE SHEAR / WEIGHT
0.3
0.0
−0.3
−0.6
0.0
0.6
DRIFT (in)

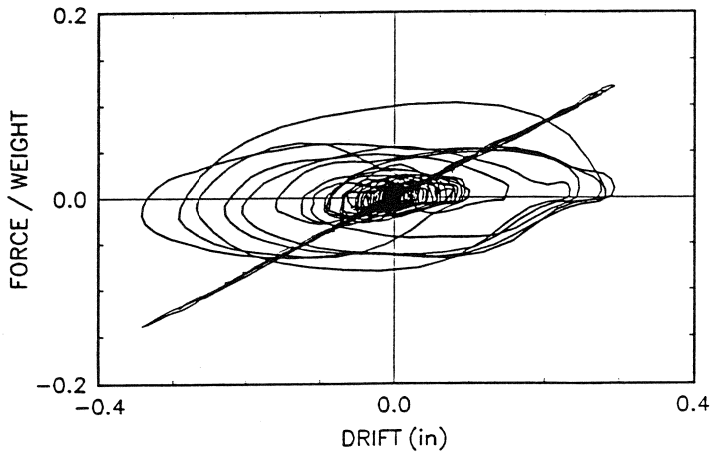
FORCE / WEIGHT
0.2
0.0
−0.2
−0.4
0.0
0.4
DRIFT (in)

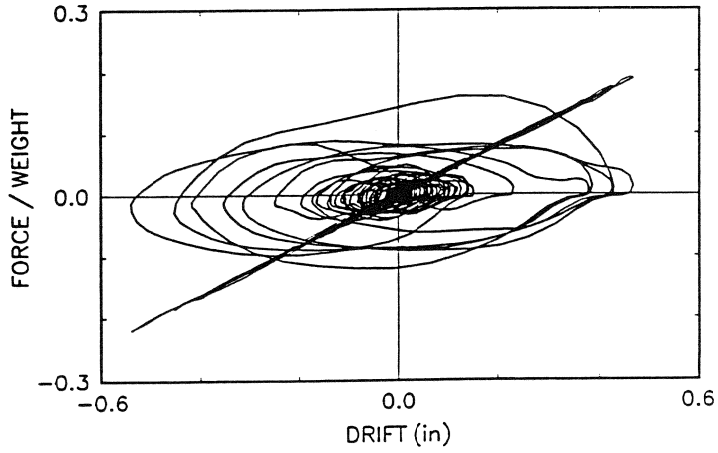
FORCE / WEIGHT
0.3
0.0
−0.3
−0.6
0.0
0.6
DRIFT (in)

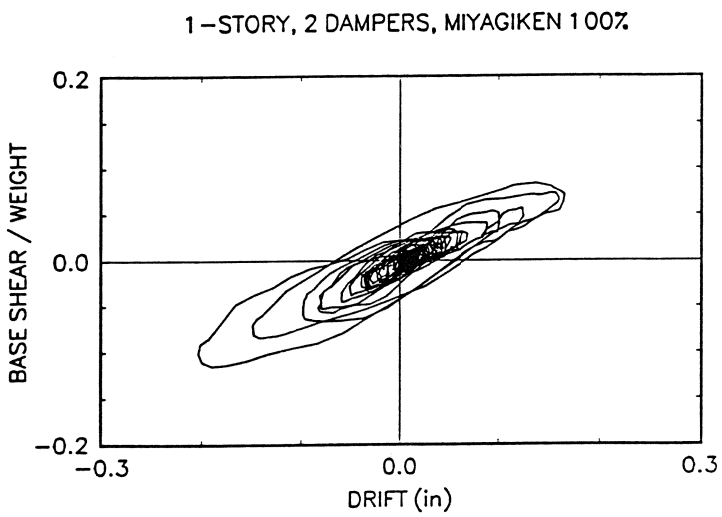
1 –STORY, 2 DAMPERS, MIYAGIKEN 100%
BASE SHEAR / WEIGHT
0.2
0.0
−0.2
−0.3
0.0
0.3
DRIFT (in)

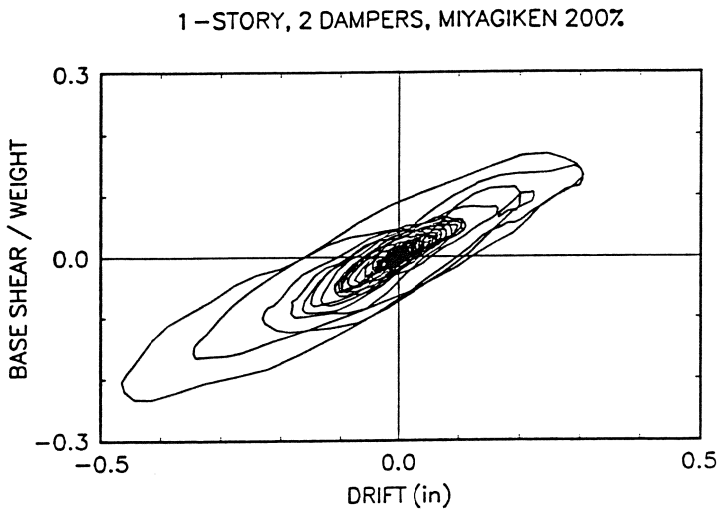
1 –STORY, 2 DAMPERS, MIYAGIKEN 200%
BASE SHEAR / WEIGHT
0.3
0.0
−0.3
−0.5
0.0
0.5
DRIFT (in)

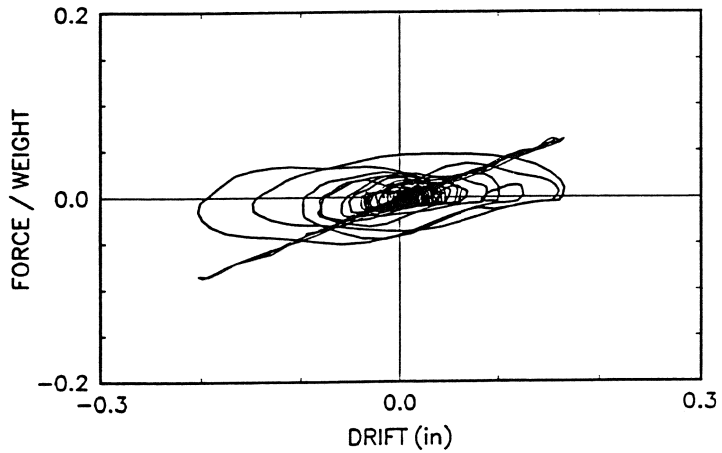
FORCE / WEIGHT
0.2
0.0
−0.2
−0.3
0.0
0.3
DRIFT (in)

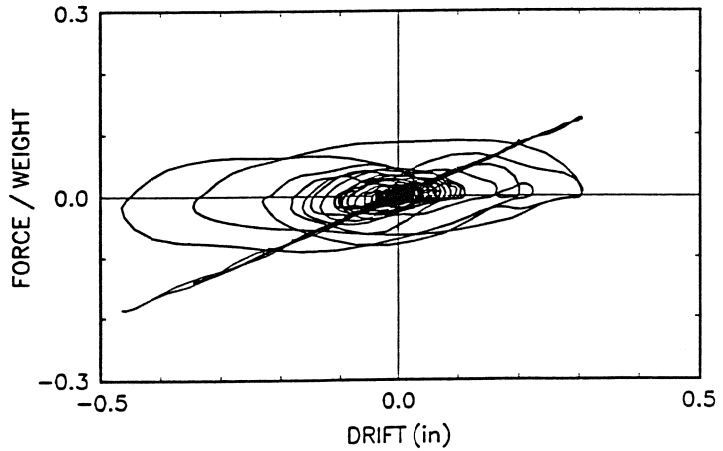
FORCE / WEIGHT
0.3
0.0
−0.3
−0.5
0.0
0.5
DRIFT (in)

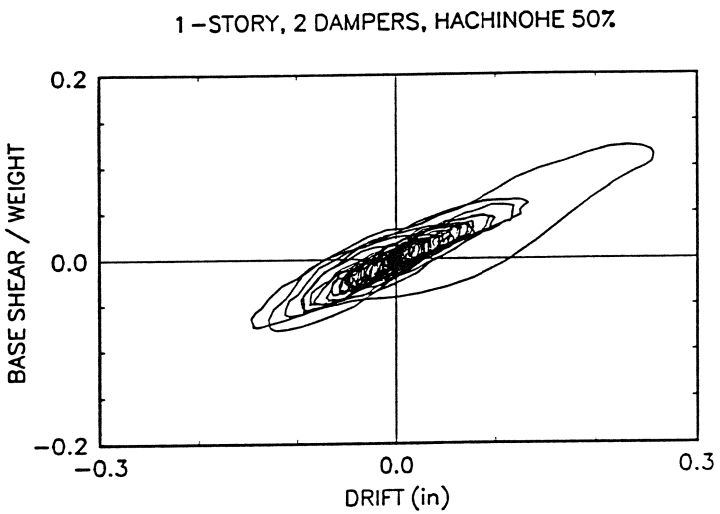
1 – STORY, 2 DAMPERS, HACHINOHE 50%
BASE SHEAR / WEIGHT
0.2
0.0
−0.2
−0.3
0.0
0.3
DRIFT (in)

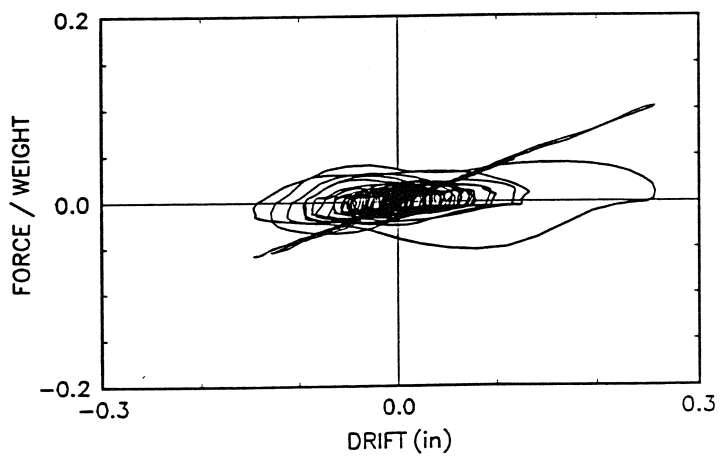
FORCE / WEIGHT
0.2
0.0
−0.2
−0.3
0.0
0.3
DRIFT (in)

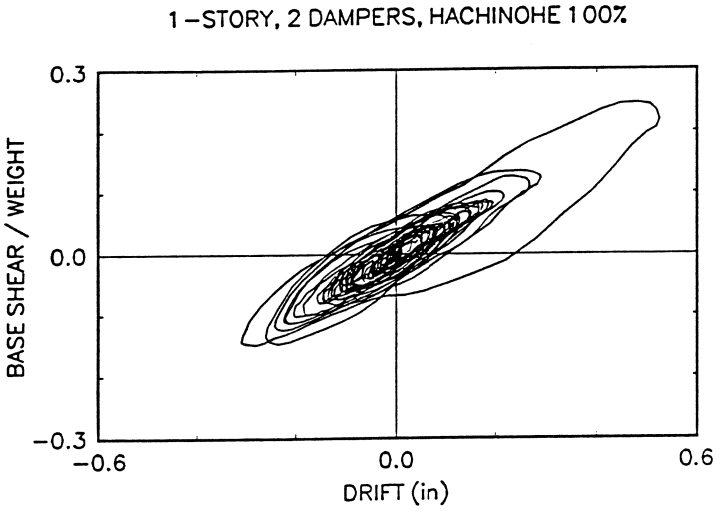
1 – STORY, 2 DAMPERS, HACHINOHE 100%
BASE SHEAR / WEIGHT
0.3
0.0
−0.3
−0.6
0.0
0.6
DRIFT (in)

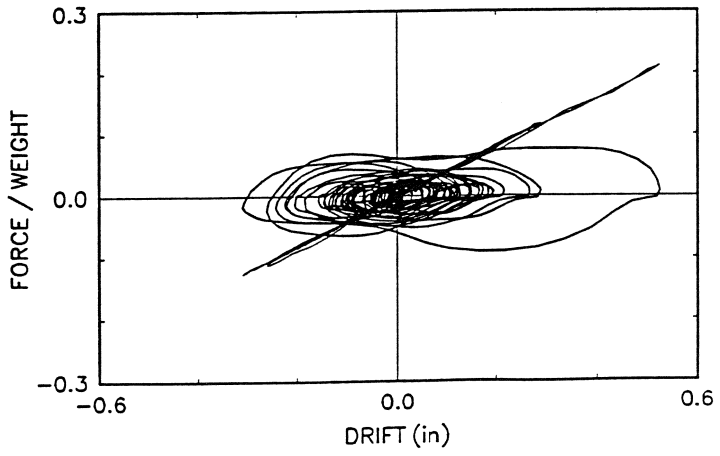
FORCE / WEIGHT
0.3
0.0
−0.3
−0.6
0.0
0.6
DRIFT (in)

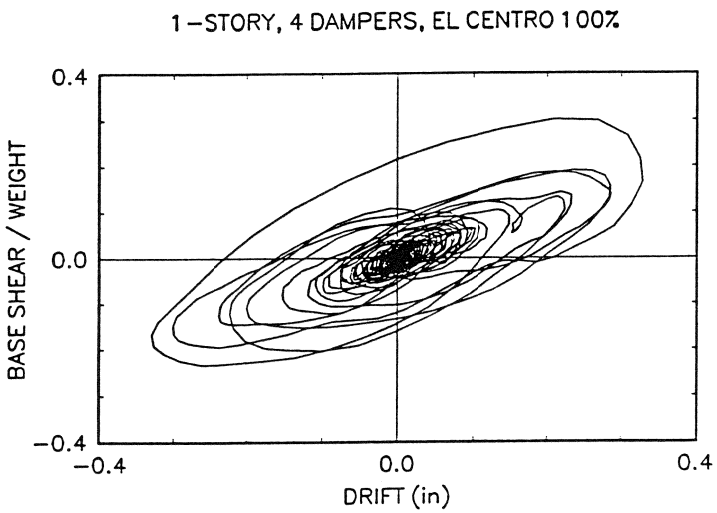
1 – STORY, 4 DAMPERS, EL CENTRO 100%
BASE SHEAR / WEIGHT
0.4
0.0
−0.4
−0.4
0.0
0.4
DRIFT (in)

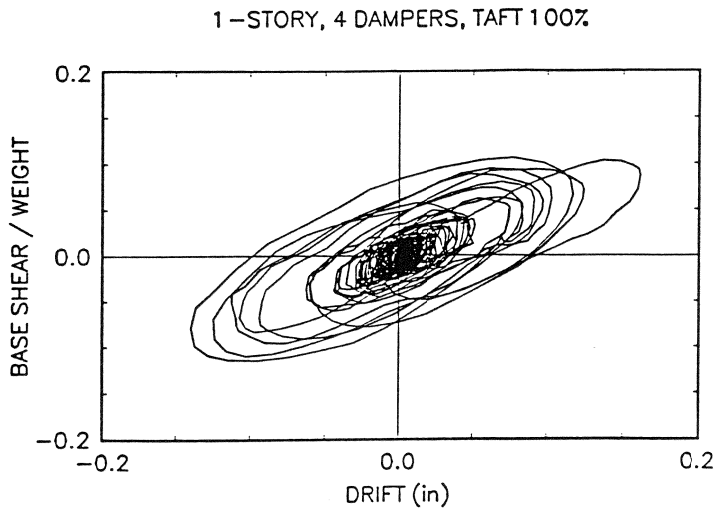
1 – STORY, 4 DAMPERS, TAFT 100%
BASE SHEAR / WEIGHT
0.2
0.0
−0.2
−0.2
0.0
0.2
DRIFT (in)

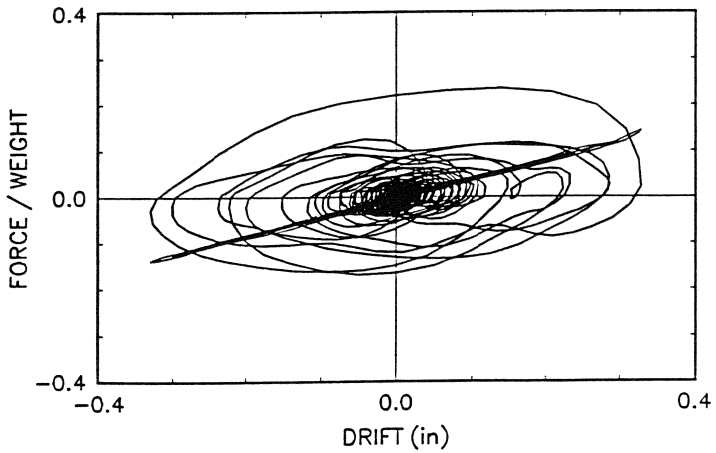
FORCE / WEIGHT
0.4
0.0
−0.4
−0.4
0.0
0.4
DRIFT (in)

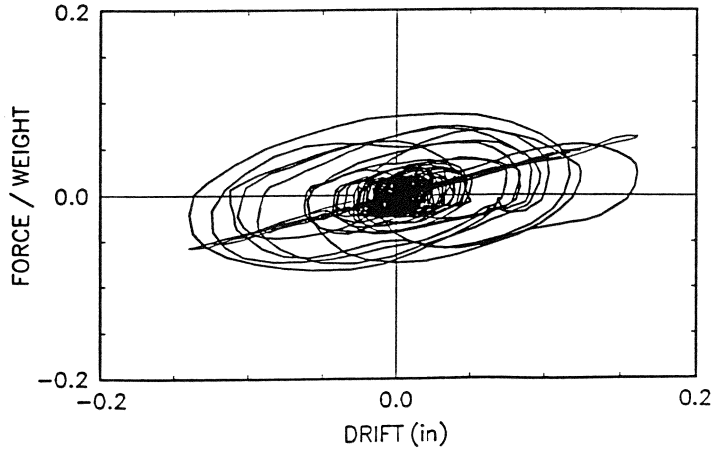
FORCE / WEIGHT
0.2
0.0
−0.2
−0.2
0.0
0.2
DRIFT (in)

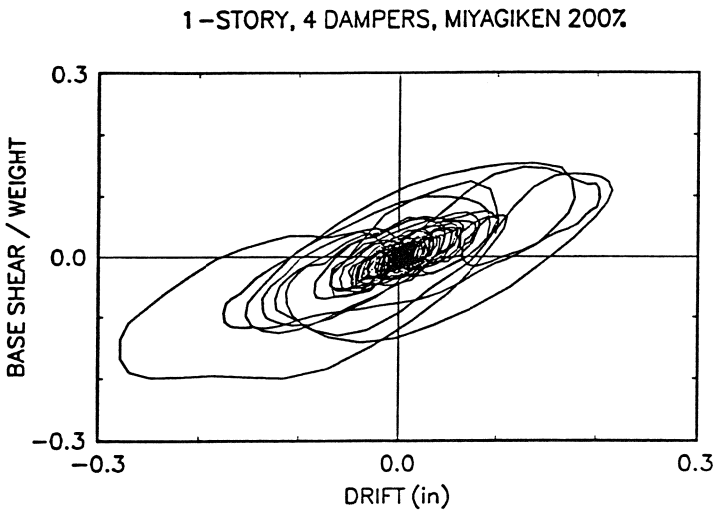
1 –STORY, 4 DAMPERS, MIYAGIKEN 200%
BASE SHEAR / WEIGHT
0.3
0.0
−0.3
−0.3
0.0
0.3
DRIFT (in)

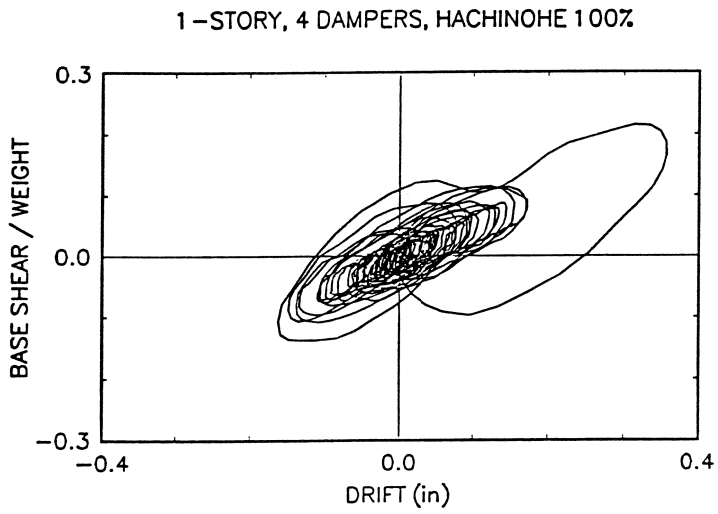
1 –STORY, 4 DAMPERS, HACHINOHE 100%
BASE SHEAR / WEIGHT
0.3
0.0
−0.3
−0.4
0.0
0.4
DRIFT (in)

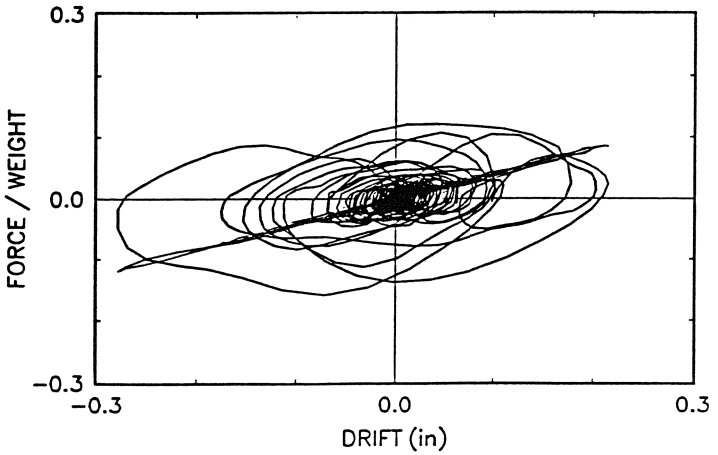
FORCE / WEIGHT
0.3
0.0
−0.3
−0.3
0.0
0.3
DRIFT (in)

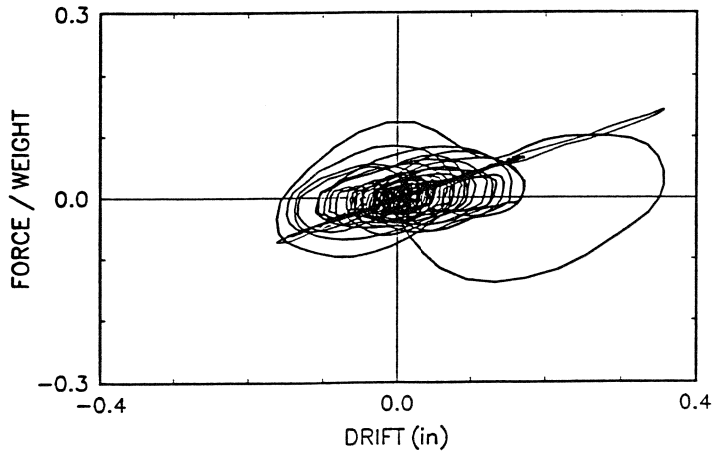
FORCE / WEIGHT
0.3
0.0
−0.3
−0.4
0.0
0.4
DRIFT (in)

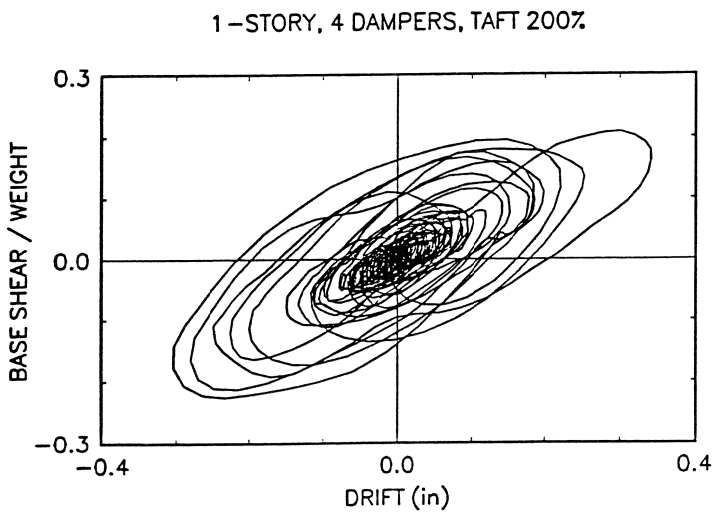
1 – STORY, 4 DAMPERS, TAFT 200%
BASE SHEAR / WEIGHT
0.3
0.0
−0.3
−0.4
0.0
0.4
DRIFT (in)

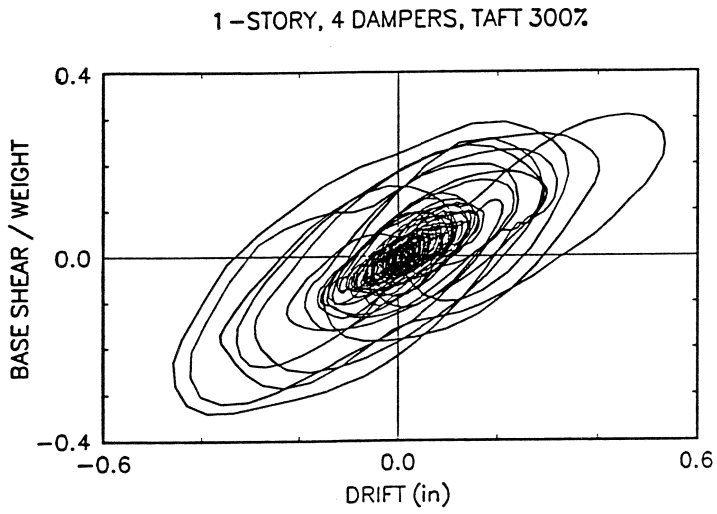
1 – STORY, 4 DAMPERS, TAFT 300%
BASE SHEAR / WEIGHT
0.4
0.0
−0.4
−0.6
0.0
0.6
DRIFT (in)

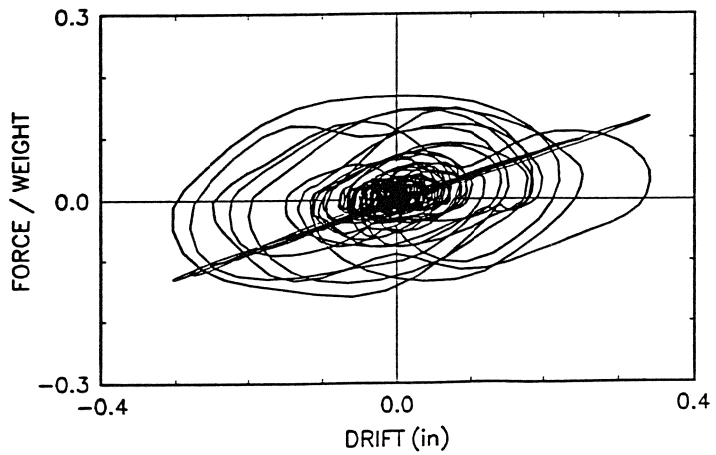
FORCE / WEIGHT
0.3
0.0
−0.3
−0.4
0.0
0.4
DRIFT (in)

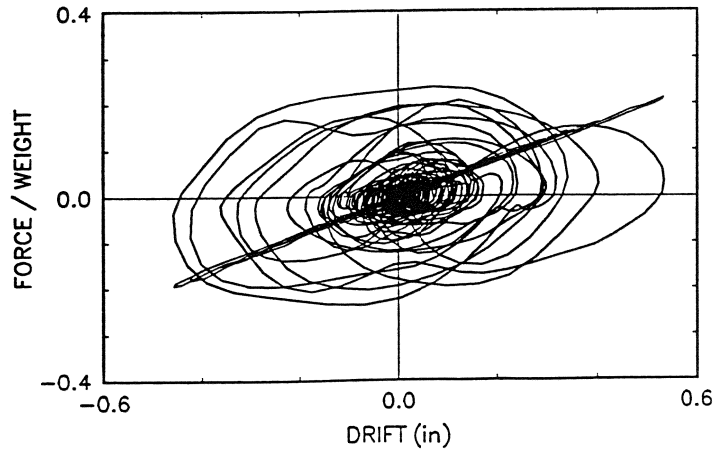
FORCE / WEIGHT
0.4
0.0
−0.4
−0.6
0.0
0.6
DRIFT (in)

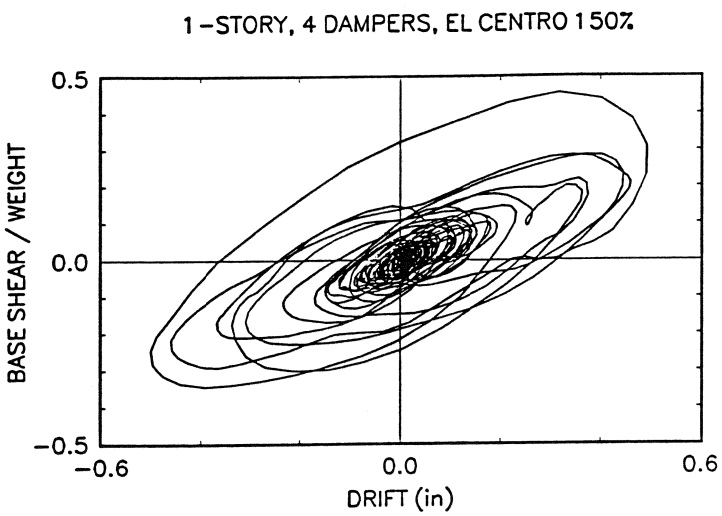
1 –STORY, 4 DAMPERS, EL CENTRO 150%
BASE SHEAR / WEIGHT
0.5
0.0
−0.5
−0.6
0.0
0.6
DRIFT (in)

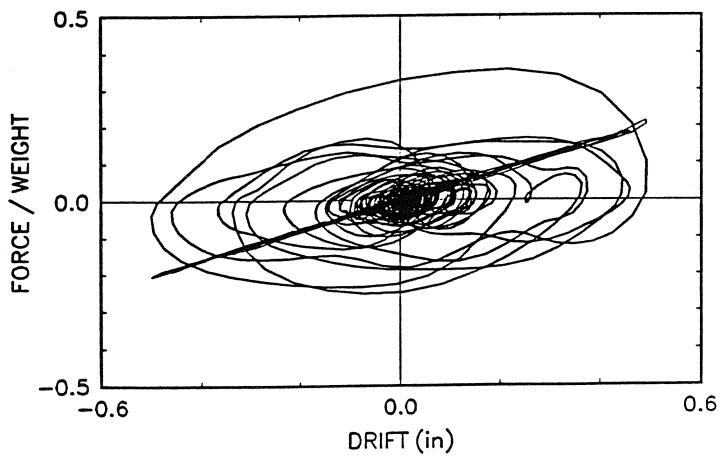
FORCE / WEIGHT
0.5
0.0
−0.5
−0.6
0.0
0.6
DRIFT (in)

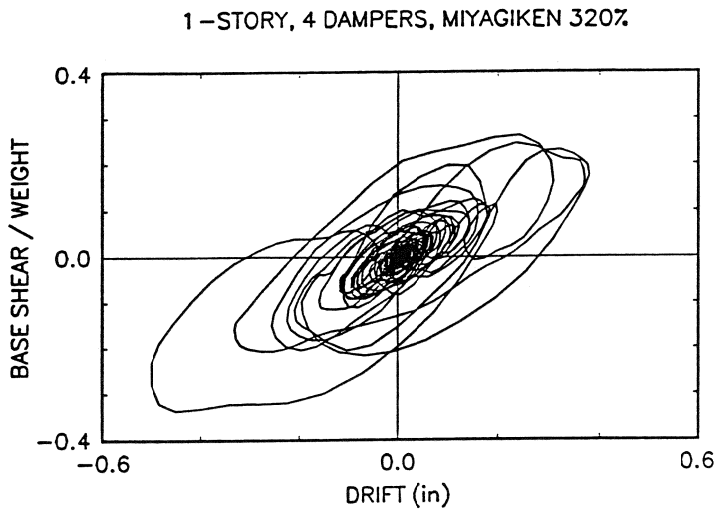
1 –STORY, 4 DAMPERS, MIYAGIKEN 320%
BASE SHEAR / WEIGHT
0.4
0.0
−0.4
−0.6
0.0
0.6
DRIFT (in)

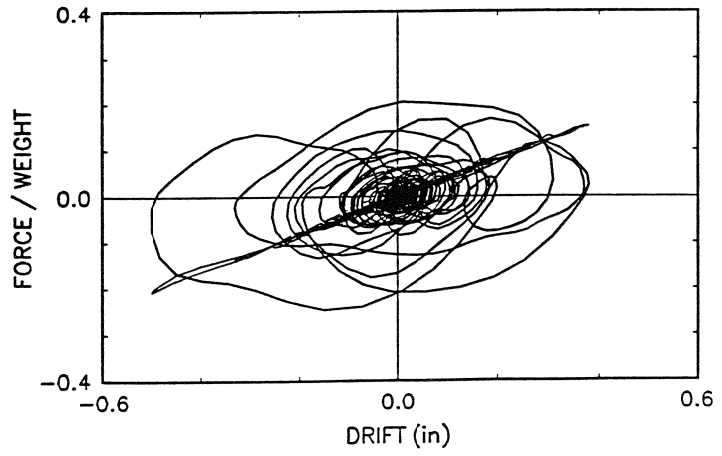
FORCE / WEIGHT
0.4
0.0
−0.4
−0.6
0.0
0.6
DRIFT (in)

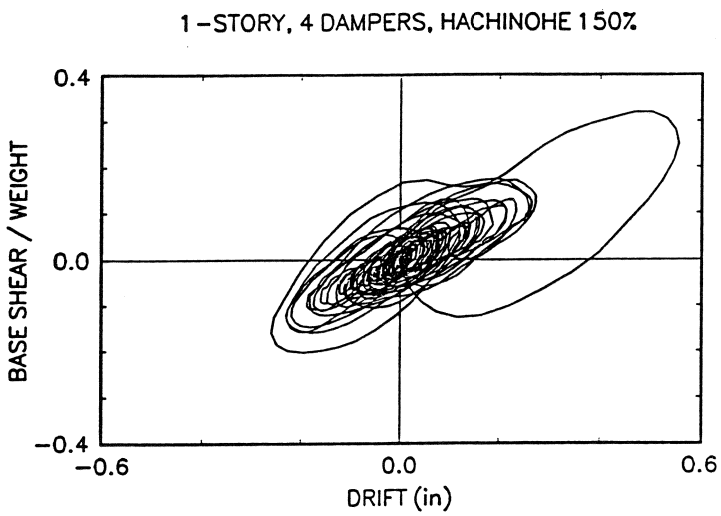
1 – STORY, 4 DAMPERS, HACHINOHE 150%
BASE SHEAR / WEIGHT
0.4
0.0
−0.4
−0.6
0.0
0.6
DRIFT (in)

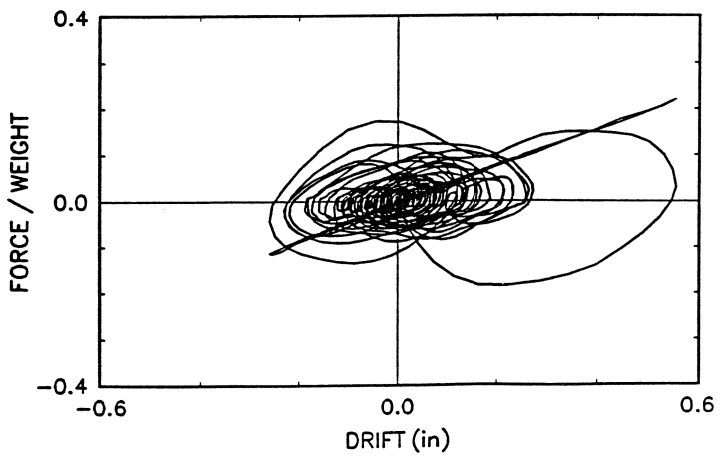
FORCE / WEIGHT
0.4
0.0
−0.4
−0.6
0.0
0.6
DRIFT (in)

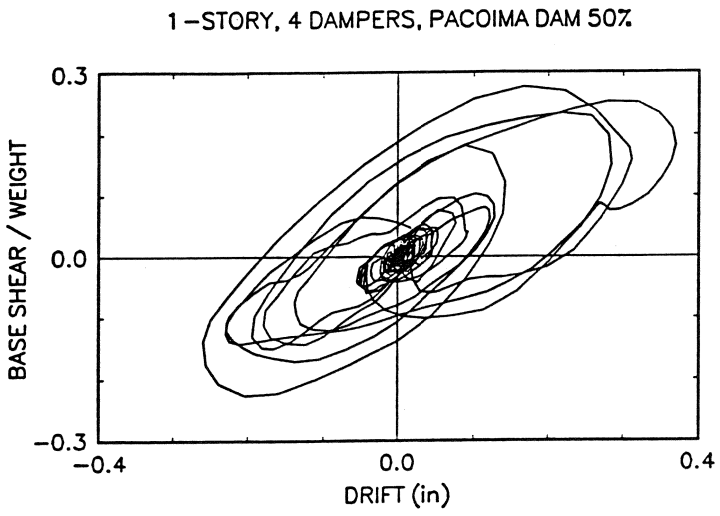
1 – STORY, 4 DAMPERS, PACOIMA DAM 50%
BASE SHEAR / WEIGHT
0.3
0.0
−0.3
−0.4
0.0
0.4
DRIFT (in)

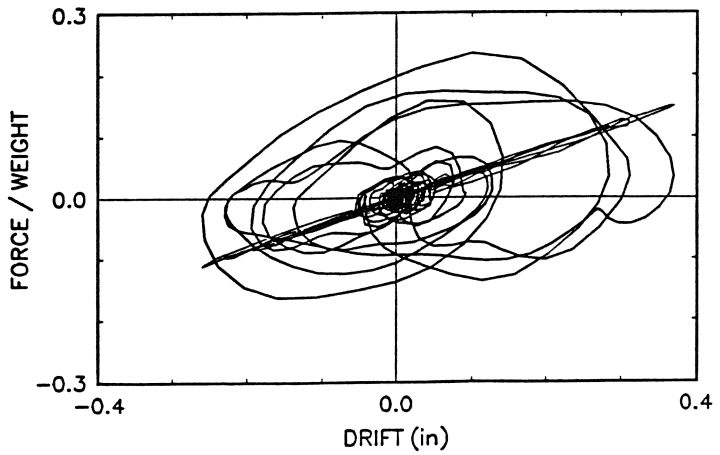
FORCE / WEIGHT
0.3
0.0
−0.3
−0.4
0.0
0.4
DRIFT (in)

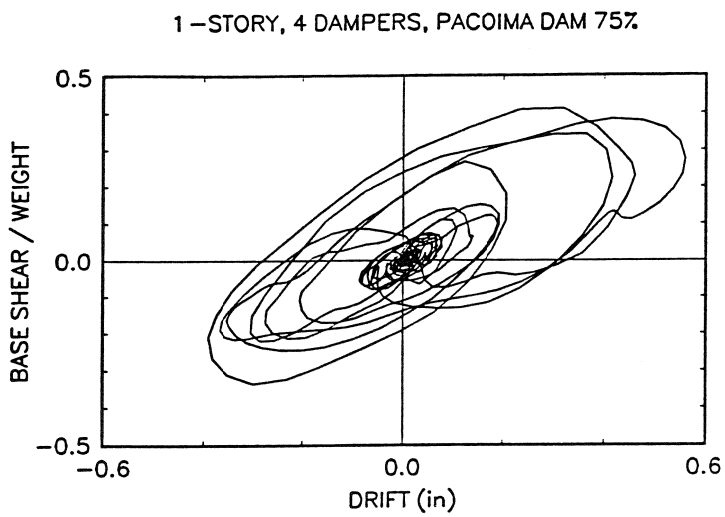
1 –STORY, 4 DAMPERS, PACOIMA DAM 75%
BASE SHEAR / WEIGHT
0.5
0.0
−0.5
−0.6
0.0
0.6
DRIFT (in)

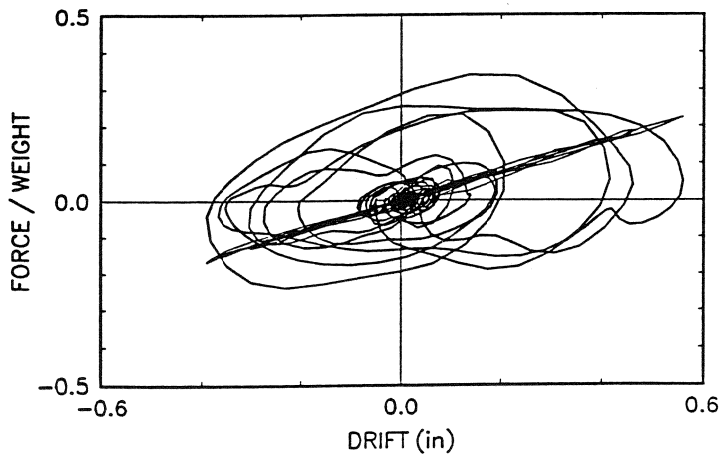
FORCE / WEIGHT
0.5
0.0
−0.5
−0.6
0.0
0.6
DRIFT (in)

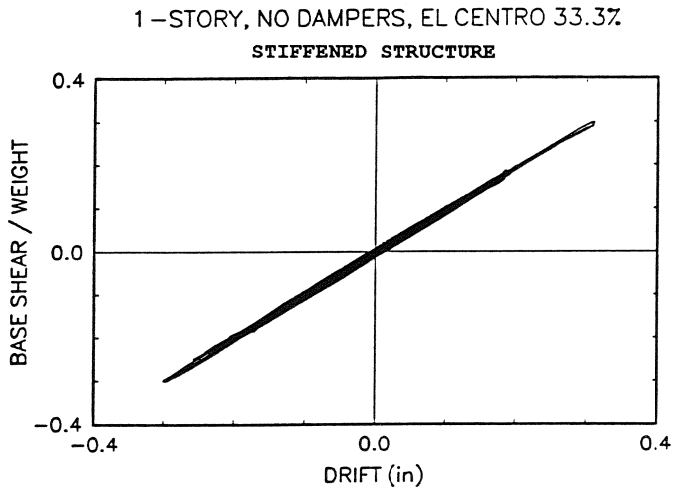
1 –STORY, NO DAMPERS, EL CENTRO 33.3%
STIFFENED STRUCTURE
BASE SHEAR / WEIGHT
0.4
0.0
−0.4
−0.4
0.0
0.4
DRIFT (in)

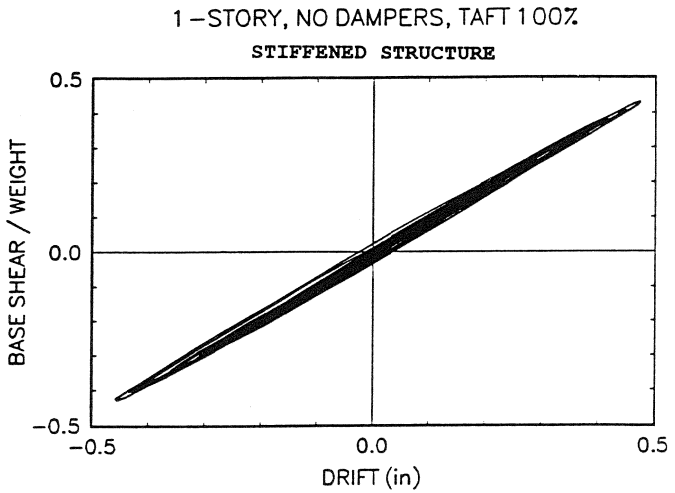
1 –STORY, NO DAMPERS, TAFT 100%
STIFFENED STRUCTURE
BASE SHEAR / WEIGHT
0.5
0.0
−0.5
−0.5
0.0
0.5
DRIFT (in)

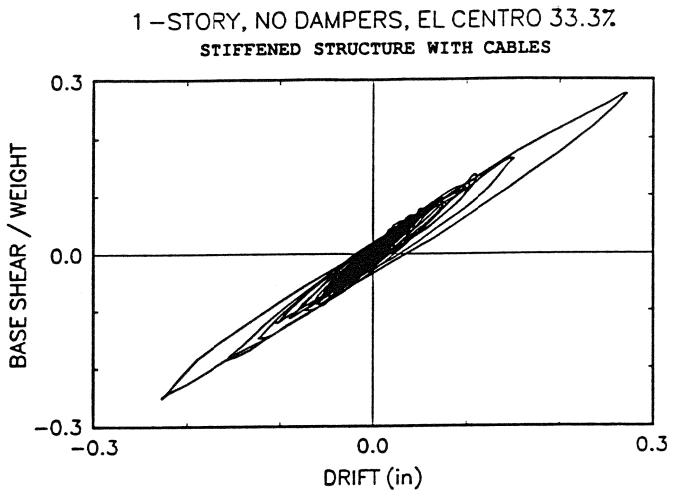
1 –STORY, NO DAMPERS, EL CENTRO 33.3%
STIFFENED STRUCTURE WITH CABLES
BASE SHEAR / WEIGHT
0.3
0.0
−0.3
−0.3
0.0
0.3
DRIFT (in)

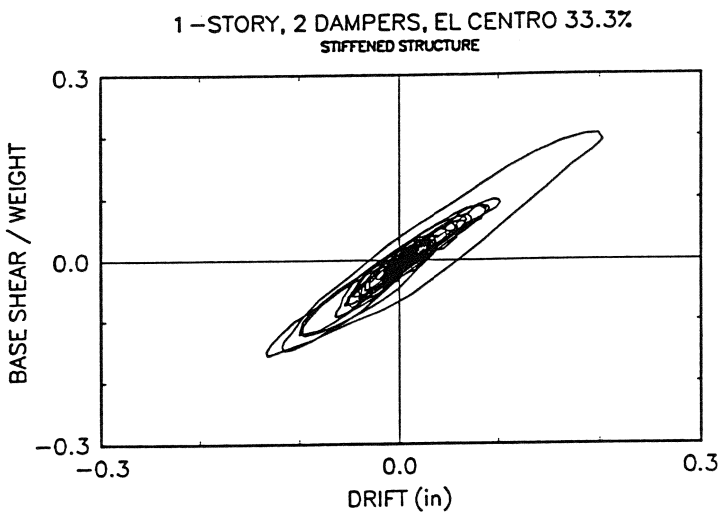
1 –STORY, 2 DAMPERS, EL CENTRO 33.3%
STIFFENED STRUCTURE
BASE SHEAR / WEIGHT
0.3
0.0
−0.3
−0.3
0.0
0.3
DRIFT (in)

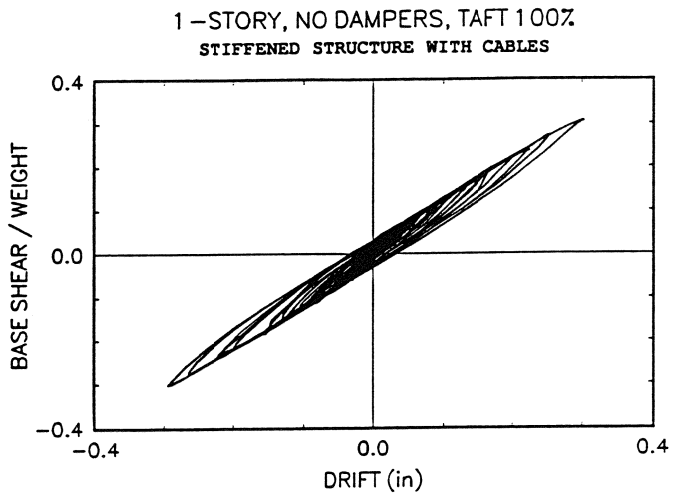
1 –STORY, NO DAMPERS, TAFT 100%
STIFFENED STRUCTURE WITH CABLES
BASE SHEAR / WEIGHT
0.4
0.0
−0.4
−0.4
0.0
0.4
DRIFT (in)

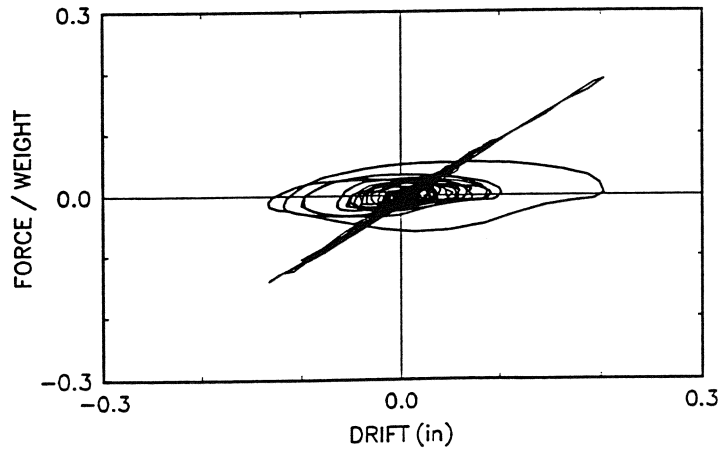
FORCE / WEIGHT
0.3
0.0
−0.3
−0.3
0.0
0.3
DRIFT (in)

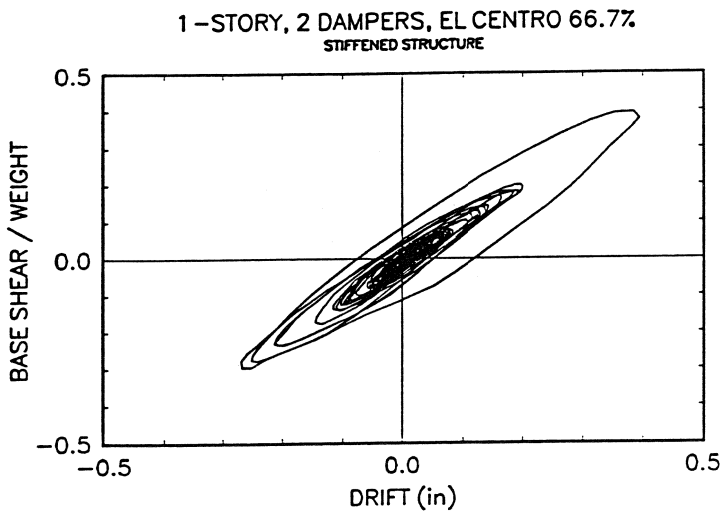
1 –STORY, 2 DAMPERS, EL CENTRO 66.7%
STIFFENED STRUCTURE
BASE SHEAR / WEIGHT
0.5
0.0
−0.5
−0.5
0.0
0.5
DRIFT (in)

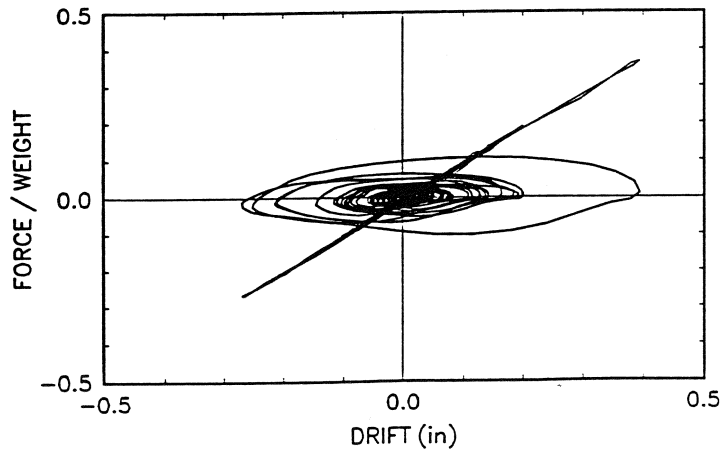
FORCE / WEIGHT
0.5
0.0
−0.5
−0.5
0.0
0.5
DRIFT (in)

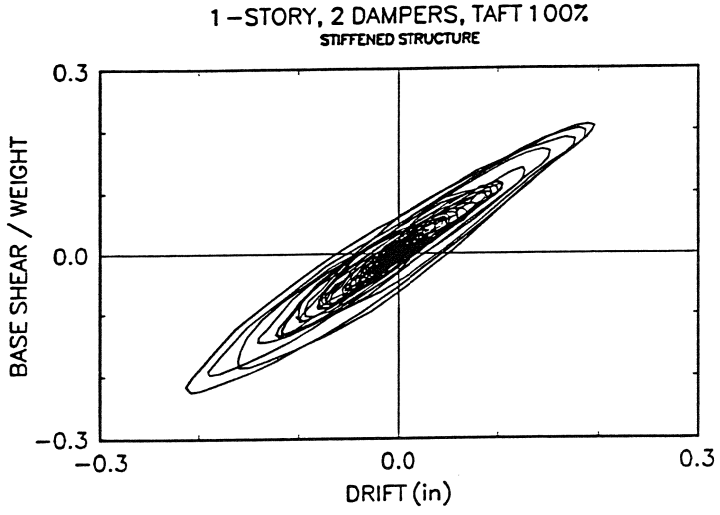
1 –STORY, 2 DAMPERS, TAFT 100%
STIFFENED STRUCTURE
BASE SHEAR / WEIGHT
0.3
0.0
−0.3
−0.3
0.0
0.3
DRIFT (in)

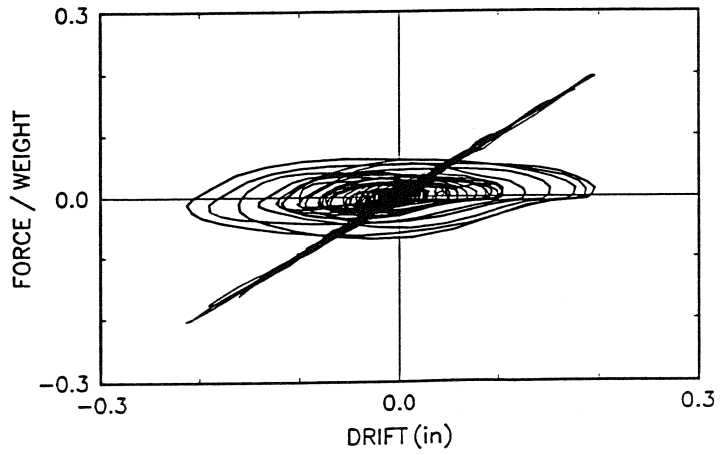
FORCE / WEIGHT
0.3
0.0
−0.3
−0.3
0.0
0.3
DRIFT (in)

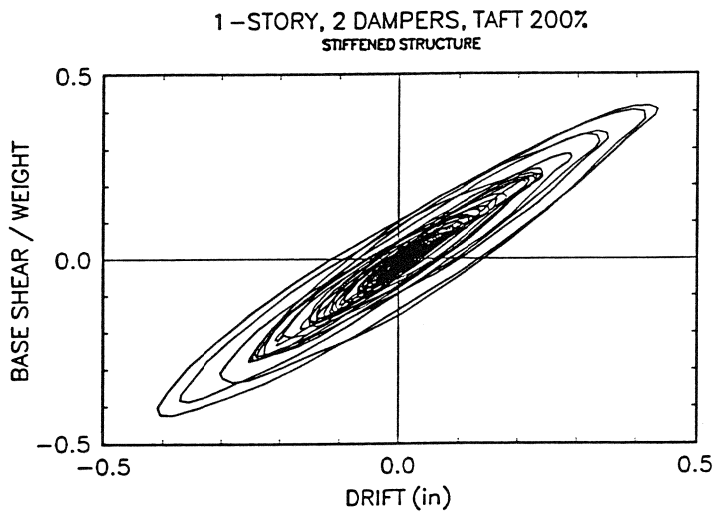
1 – STORY, 2 DAMPERS, TAFT 200%
STIFFENED STRUCTURE
BASE SHEAR / WEIGHT
0.5
0.0
−0.5
−0.5
0.0
0.5
DRIFT (in)

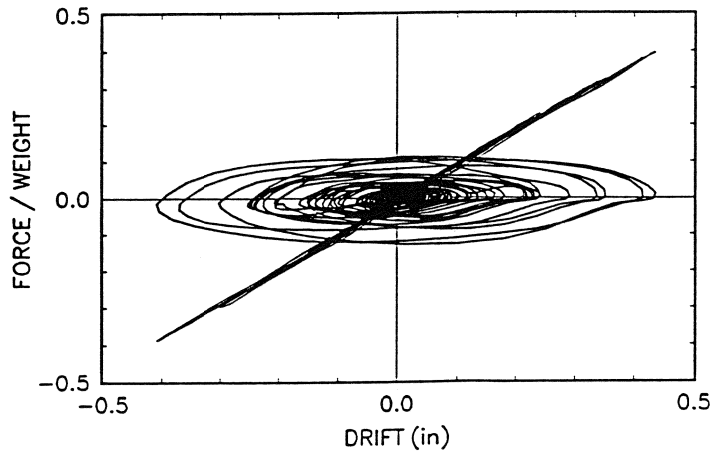
FORCE / WEIGHT
0.5
0.0
−0.5
−0.5
0.0
0.5
DRIFT (in)

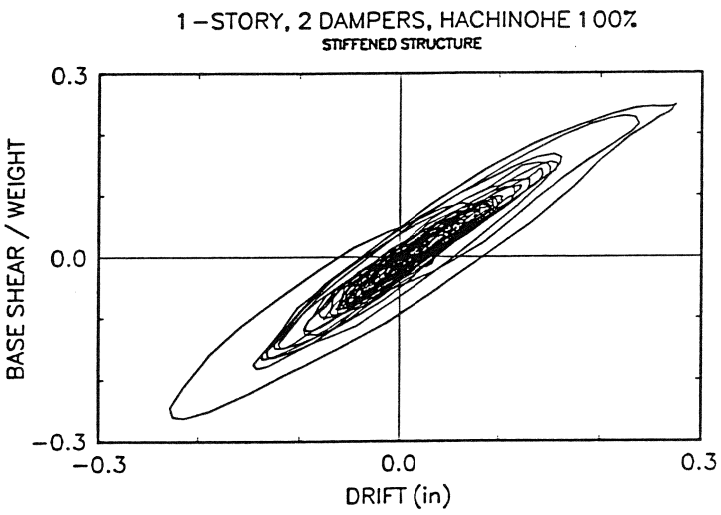
1 – STORY, 2 DAMPERS, HACHINOHE 100%
STIFFENED STRUCTURE
BASE SHEAR / WEIGHT
0.3
0.0
−0.3
−0.3
0.0
0.3
DRIFT (in)

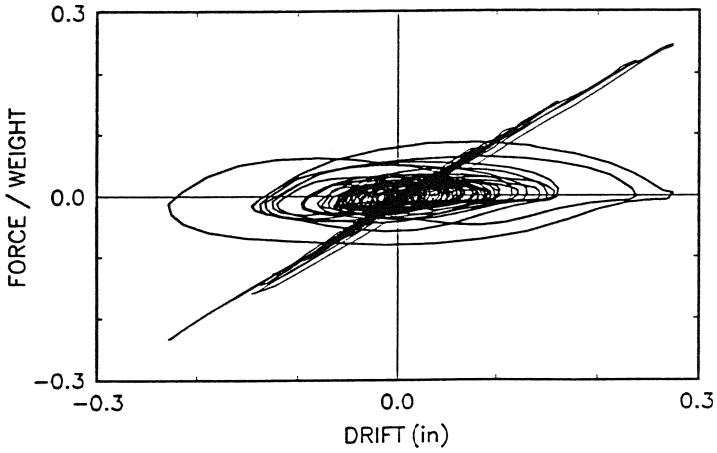
FORCE / WEIGHT
0.3
0.0
−0.3
−0.3
0.0
0.3
DRIFT (in)

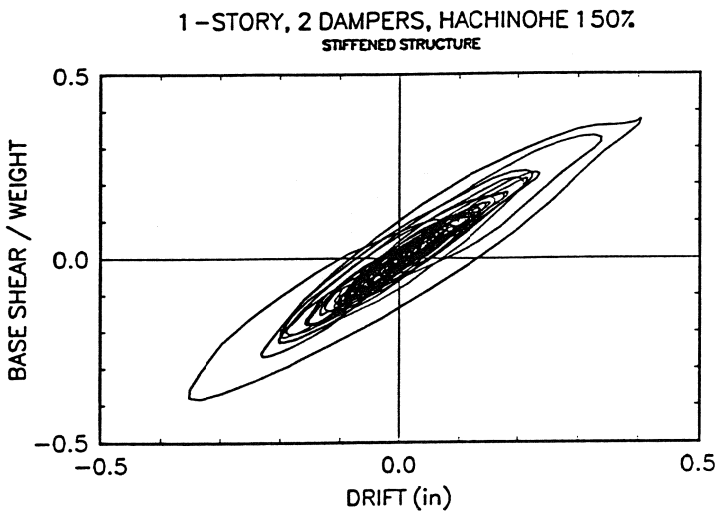
1 – STORY, 2 DAMPERS, HACHINOHE 150%
STIFFENED STRUCTURE
BASE SHEAR / WEIGHT
0.5
0.0
−0.5
−0.5
0.0
0.5
DRIFT (in)

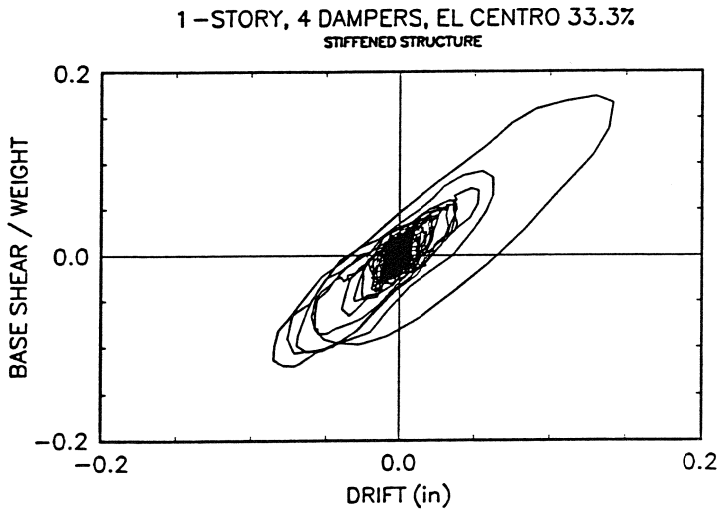
1 – STORY, 4 DAMPERS, EL CENTRO 33.3%
STIFFENED STRUCTURE
BASE SHEAR / WEIGHT
0.2
0.0
−0.2
−0.2
0.0
0.2
DRIFT (in)

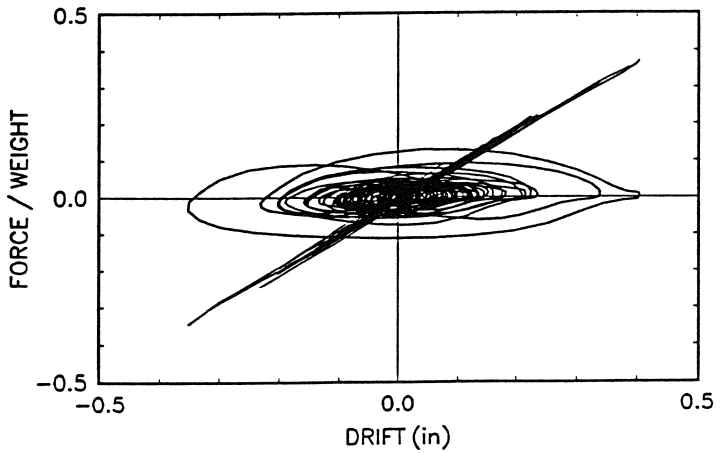
FORCE / WEIGHT
0.5
0.0
−0.5
−0.5
0.0
0.5
DRIFT (in)

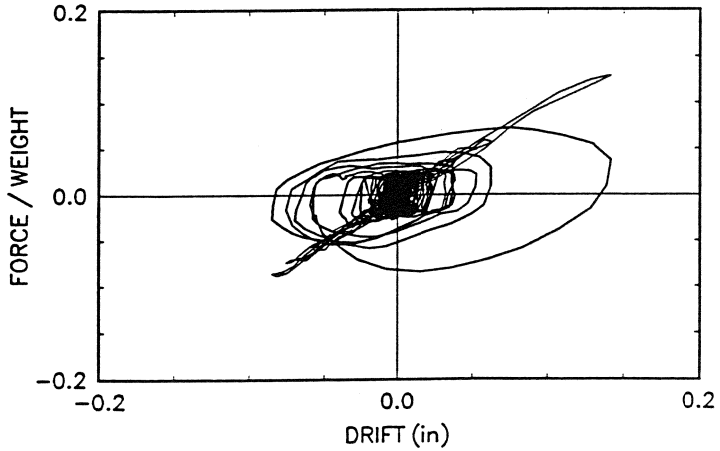
FORCE / WEIGHT
0.2
0.0
−0.2
−0.2
0.0
0.2
DRIFT (in)

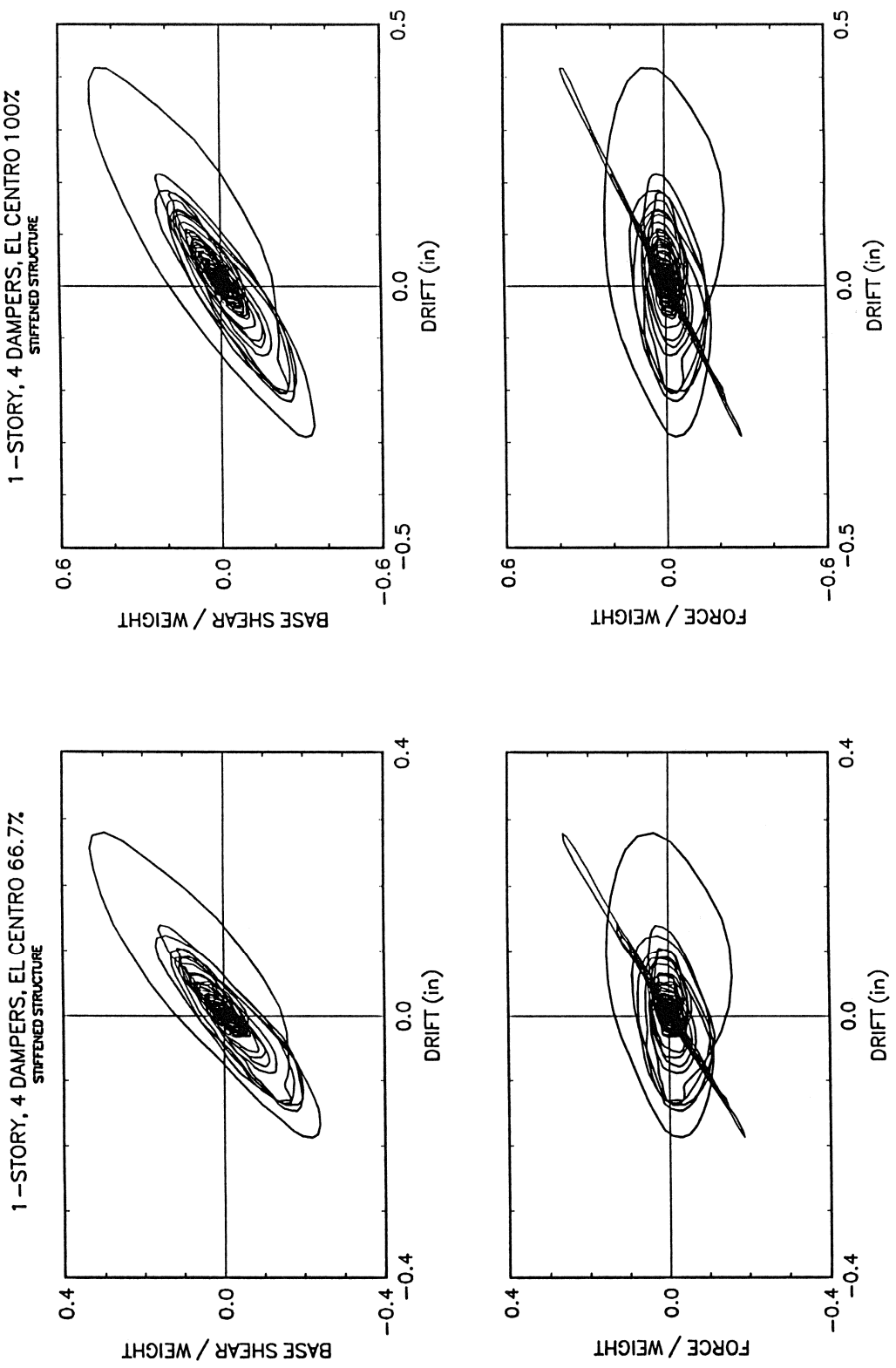
1-STORY, 4 DAMPERS, EL CENTRO 100%
STIFFENED STRUCTURE
BASE SHEAR / WEIGHT
FORCE / WEIGHT
DRIFT (in)
0.6
0.0
-0.6
0.5
0.0
-0.5
1-STORY, 4 DAMPERS, EL CENTRO 66.7%
STIFFENED STRUCTURE
BASE SHEAR / WEIGHT
FORCE / WEIGHT
DRIFT (in)
0.4
0.0
-0.4
0.4
0.0
-0.4

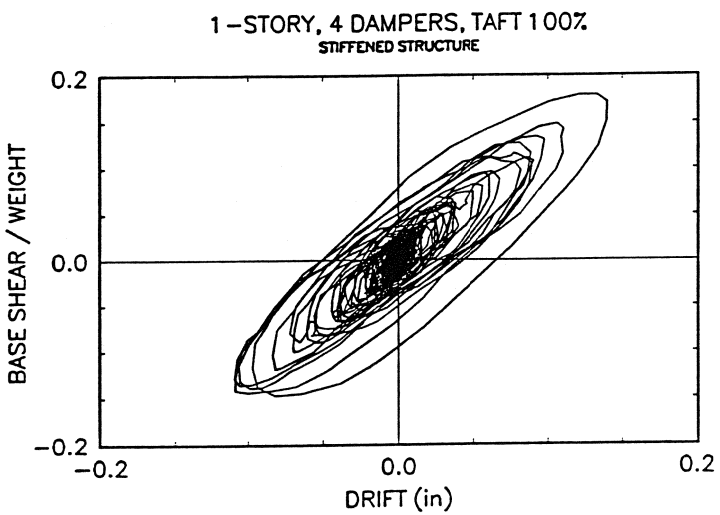
1 – STORY, 4 DAMPERS, TAFT 100%
STIFFENED STRUCTURE
BASE SHEAR / WEIGHT
0.2
0.0
−0.2
−0.2
0.0
0.2
DRIFT (in)

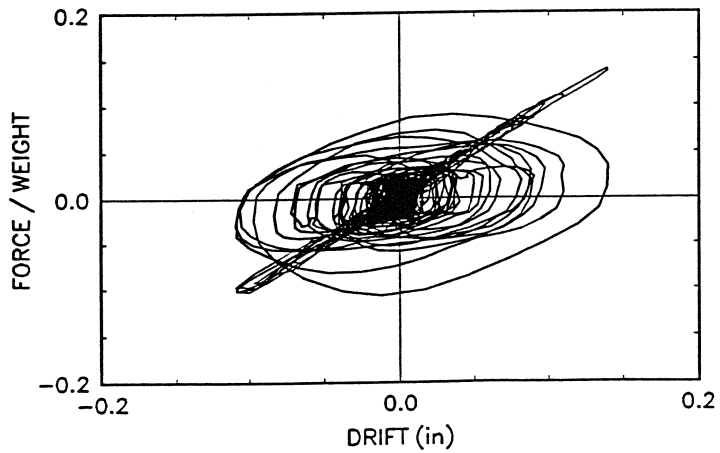
FORCE / WEIGHT
0.2
0.0
−0.2
−0.2
0.0
0.2
DRIFT (in)

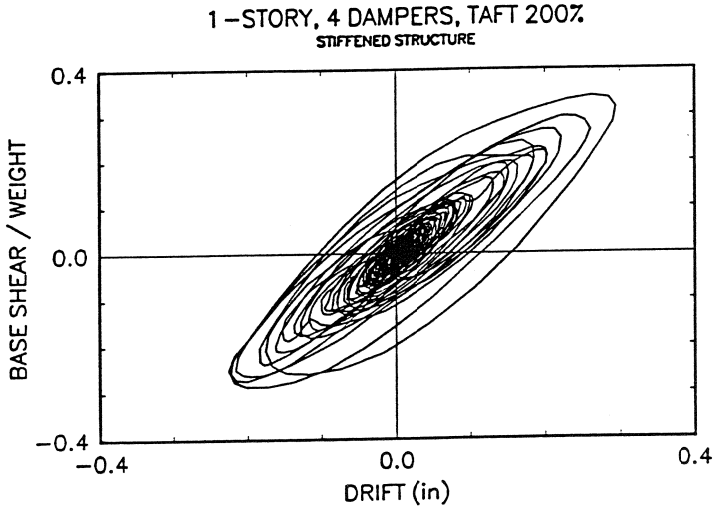
1 – STORY, 4 DAMPERS, TAFT 200%
STIFFENED STRUCTURE
BASE SHEAR / WEIGHT
0.4
0.0
−0.4
−0.4
0.0
0.4
DRIFT (in)

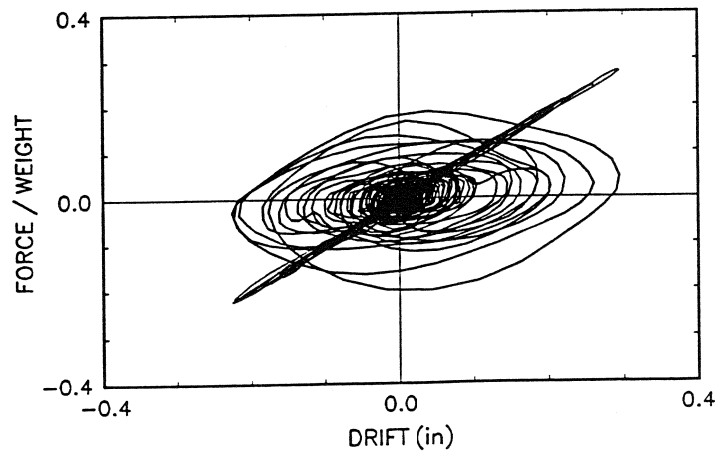
FORCE / WEIGHT
0.4
0.0
−0.4
−0.4
0.0
0.4
DRIFT (in)

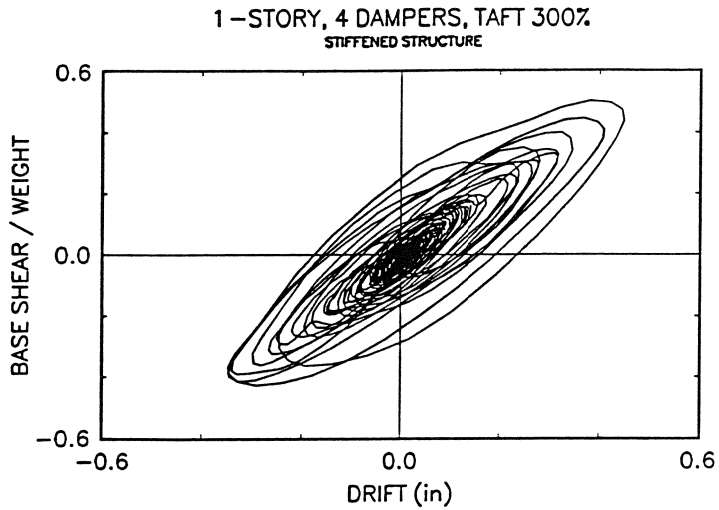
1 – STORY, 4 DAMPERS, TAFT 300%
STIFFENED STRUCTURE
BASE SHEAR / WEIGHT
0.6
0.0
−0.6
−0.6
0.0
0.6
DRIFT (in)

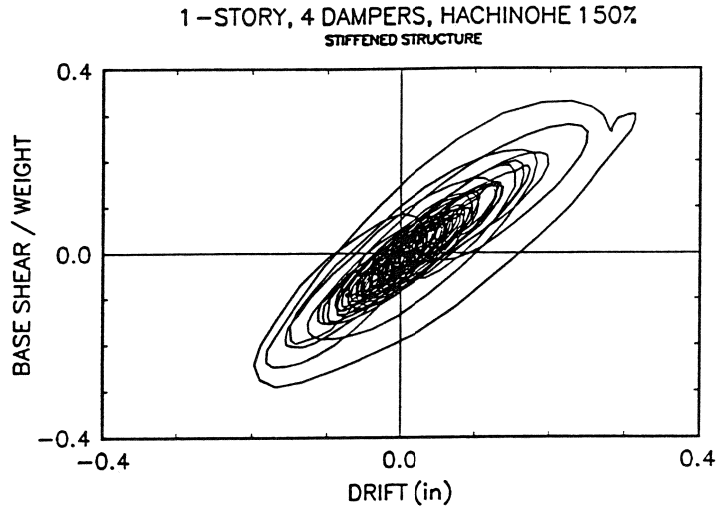
1 – STORY, 4 DAMPERS, HACHINOHE 150%
STIFFENED STRUCTURE
BASE SHEAR / WEIGHT
0.4
0.0
−0.4
−0.4
0.0
0.4
DRIFT (in)

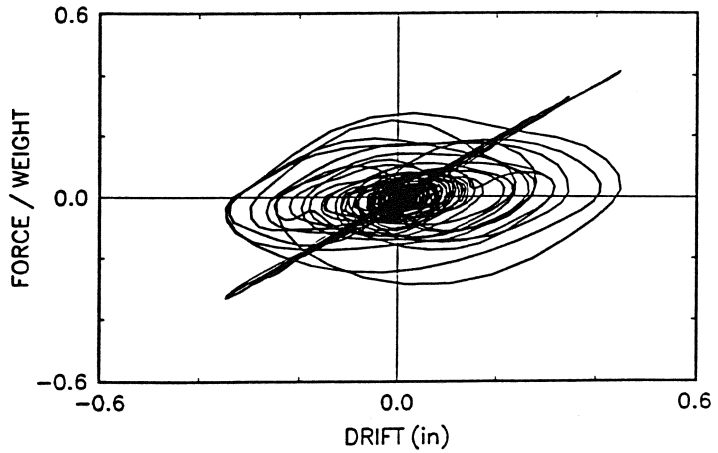
FORCE / WEIGHT
0.6
0.0
−0.6
−0.6
0.0
0.6
DRIFT (in)

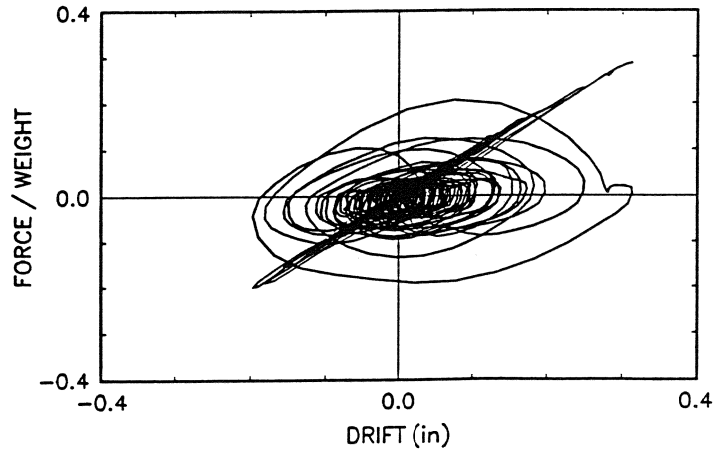
FORCE / WEIGHT
0.4
0.0
−0.4
−0.4
0.0
0.4
DRIFT (in)

APPENDIX B

THREE-STORY TEST RESULTS

3-STORY, NO DAMPERS, EL CENTRO 33.3%

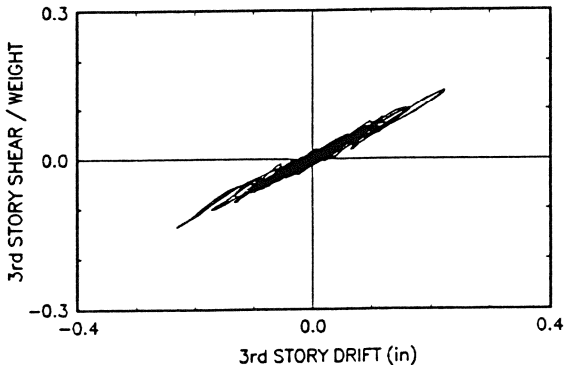

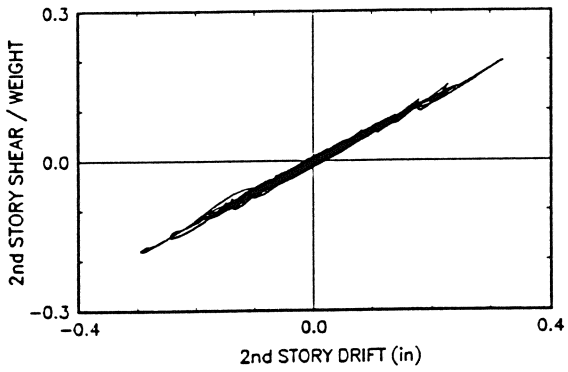

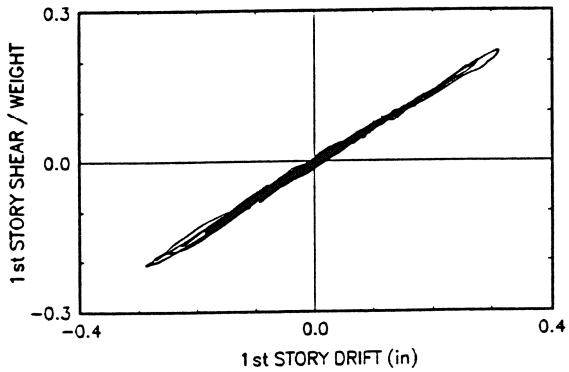

3-STORY, NO DAMPERS, EL CENTRO 50%

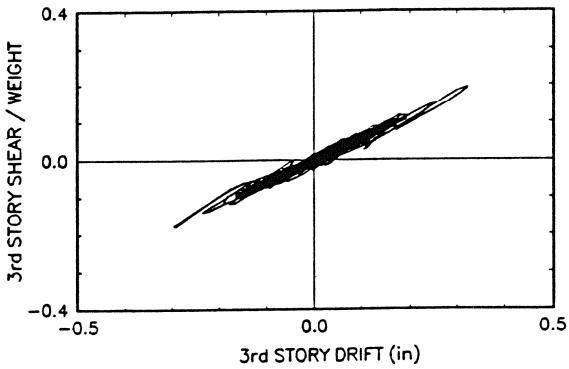

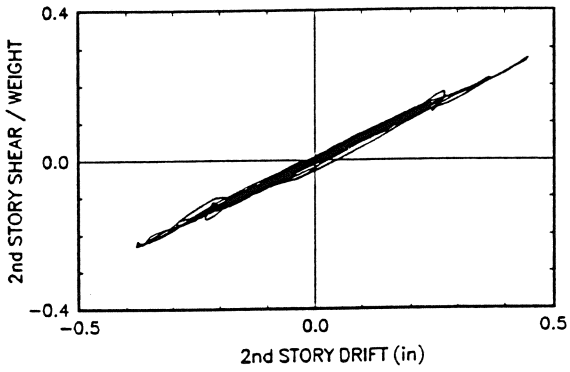

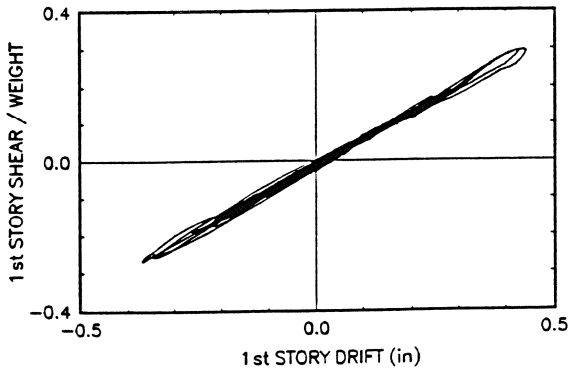

3-STORY, NO DAMPERS, TAFT 100%

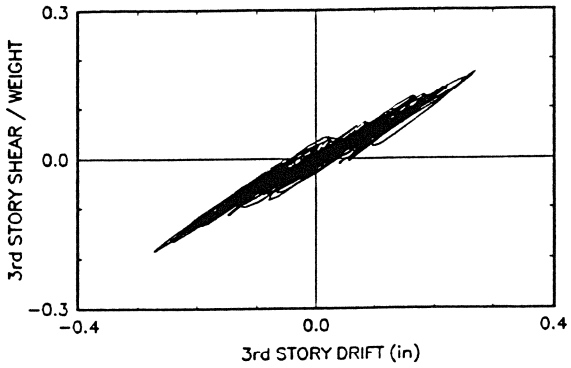

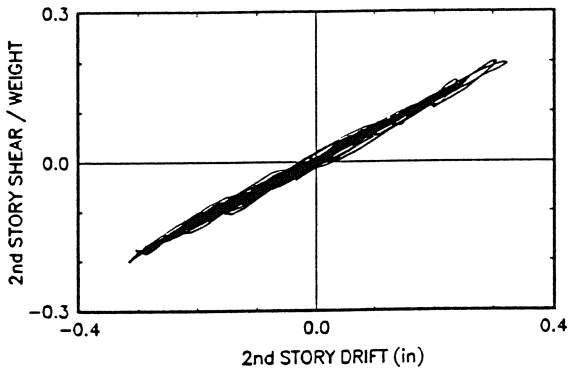

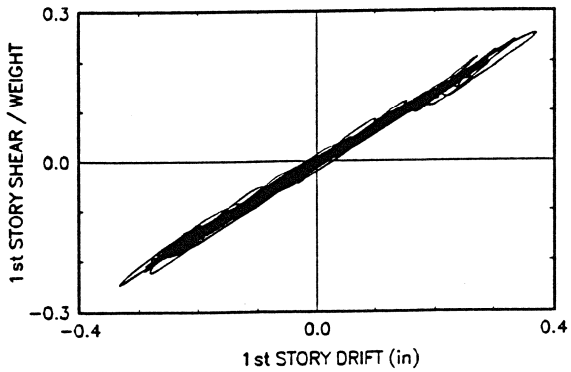

3-STORY, 6 DAMPERS, EL CENTRO 50%

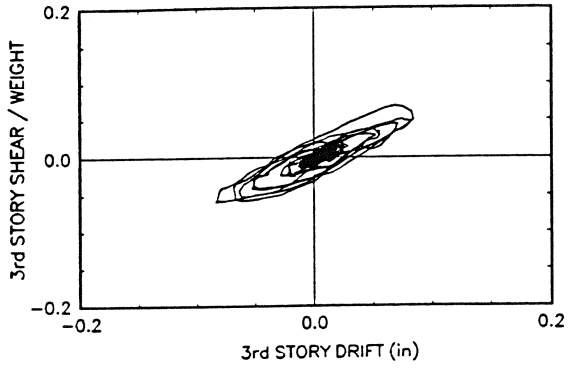

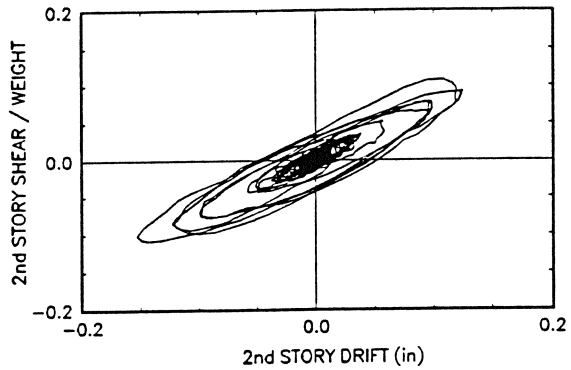

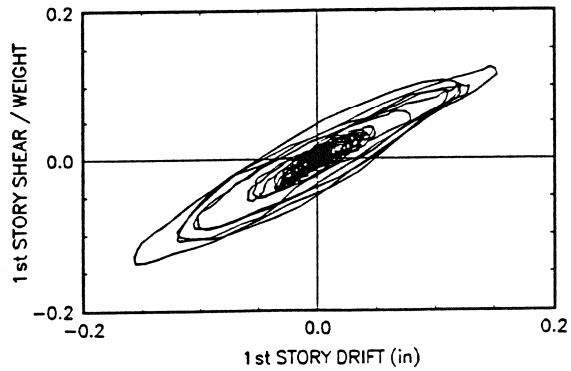

3-STORY, 6 DAMPERS, EL CENTRO 1 00%

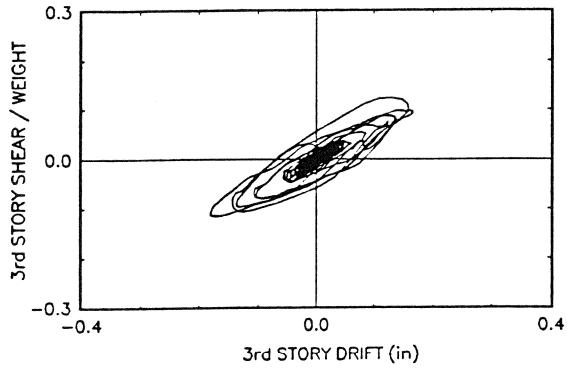

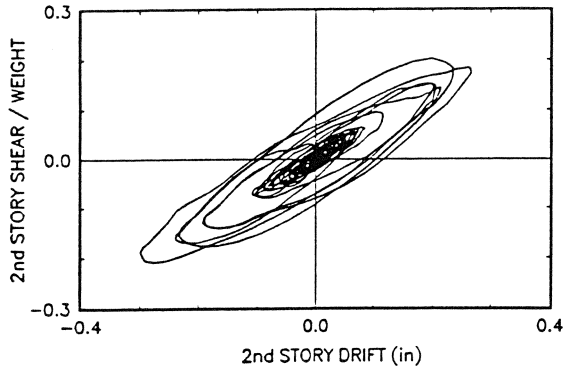

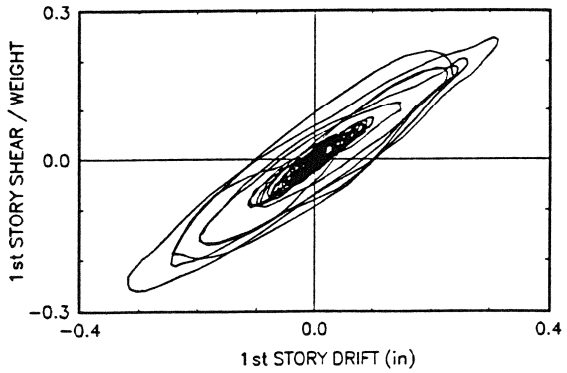

3-STORY, 6 DAMPERS, EL CENTRO 1 50%

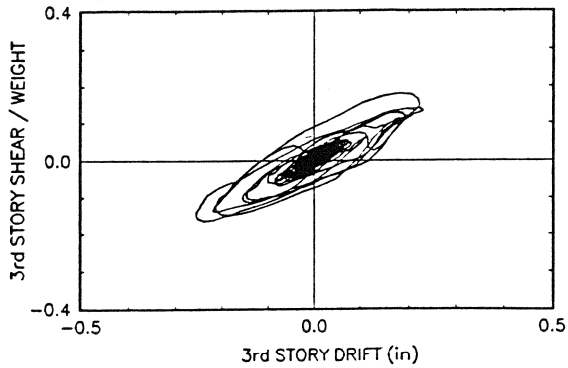

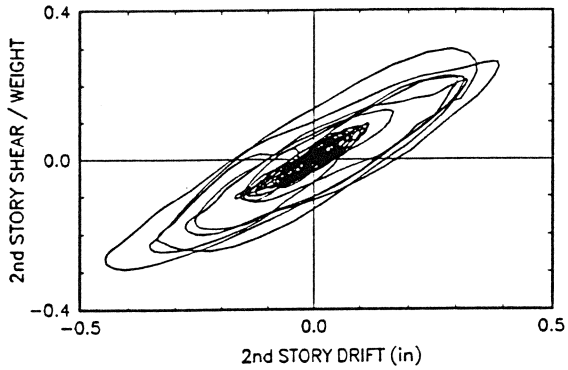

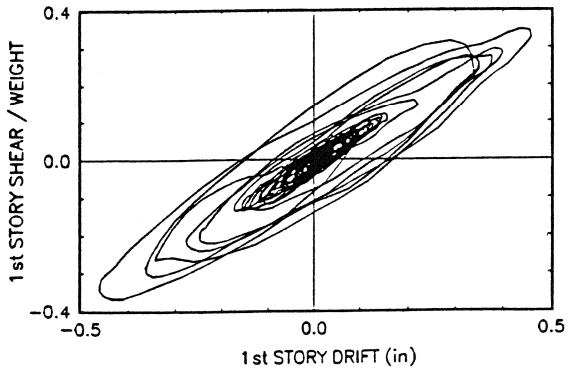

3-STORY, 6 DAMPERS, TAFT 100%

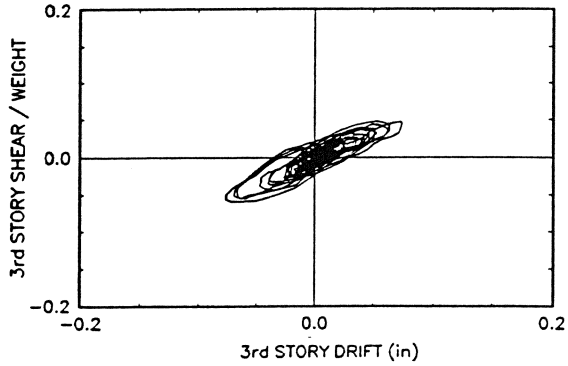

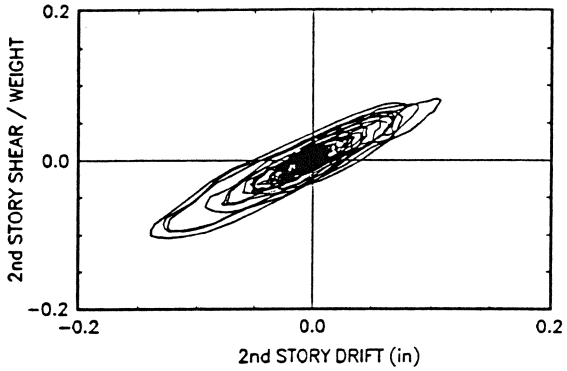

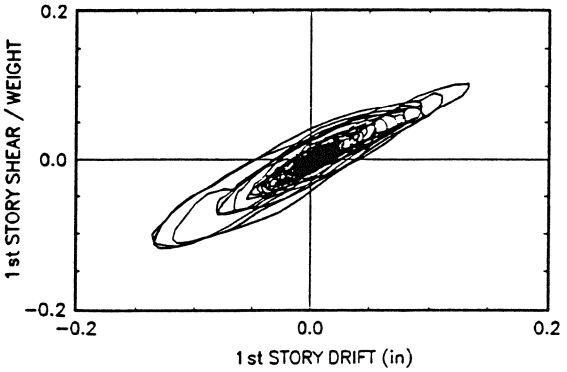

3-STORY, 6 DAMPERS, TAFT 200%

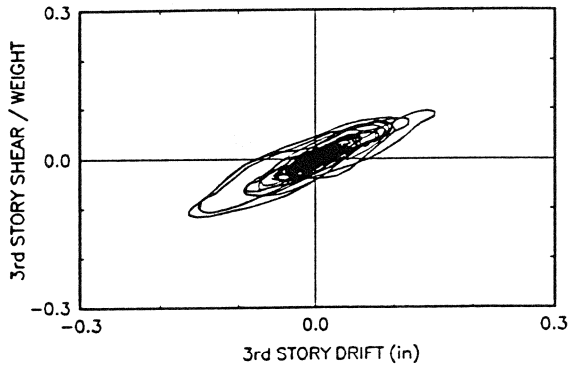

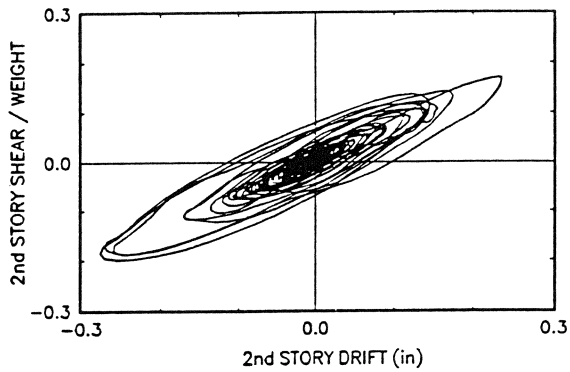

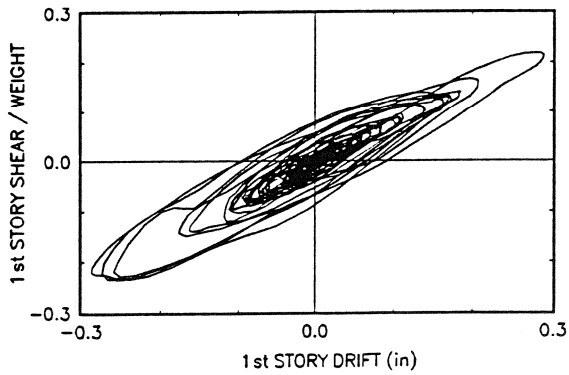

3-STORY, 6 DAMPERS, TAFT 300%

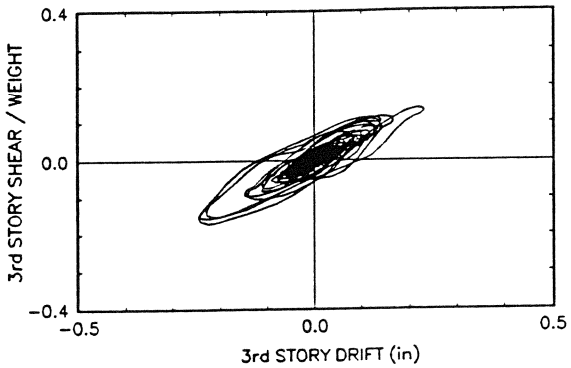

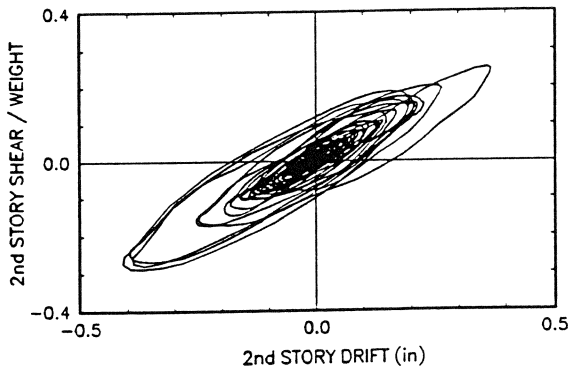

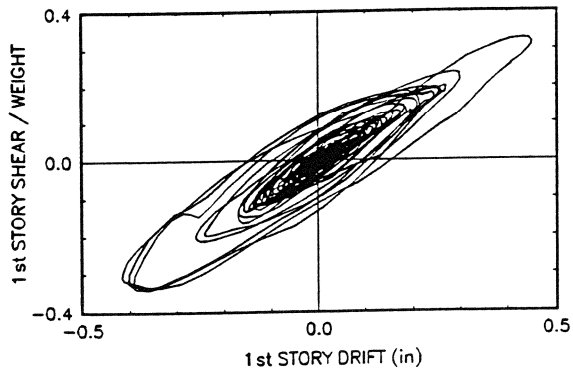

3-STORY, 6 DAMPERS, HACHINOHE 100%

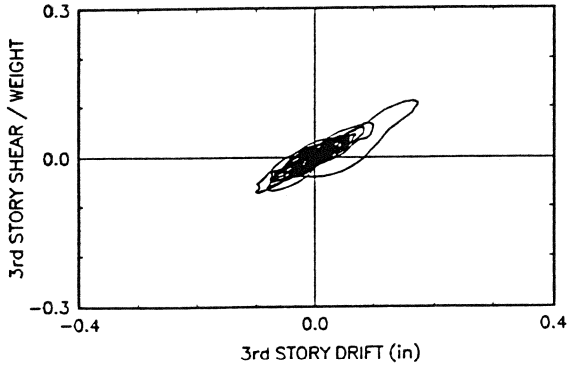

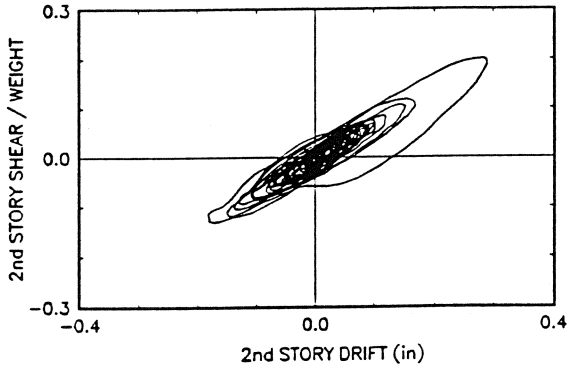

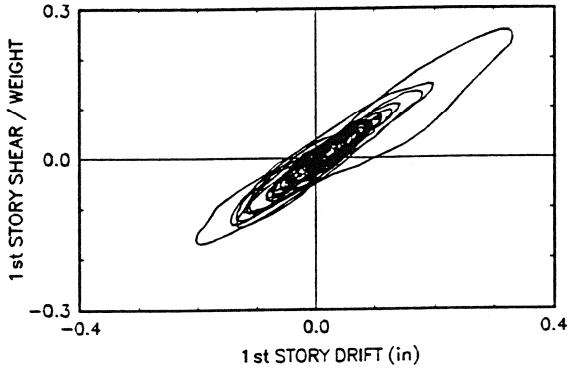

3-STORY, 6 DAMPERS, MIYAGIKEN 200%

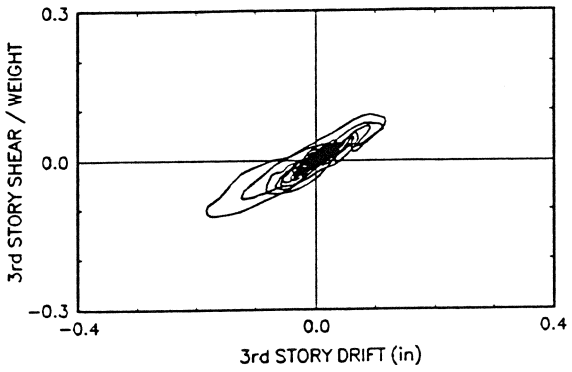

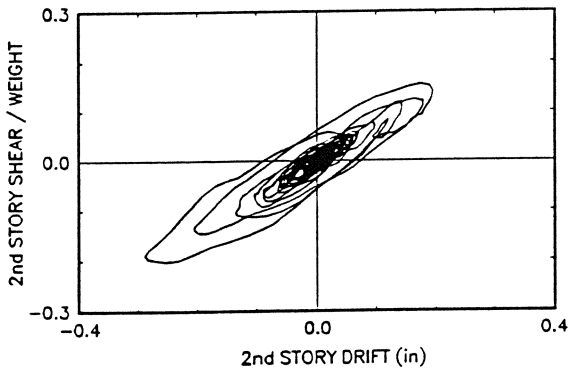

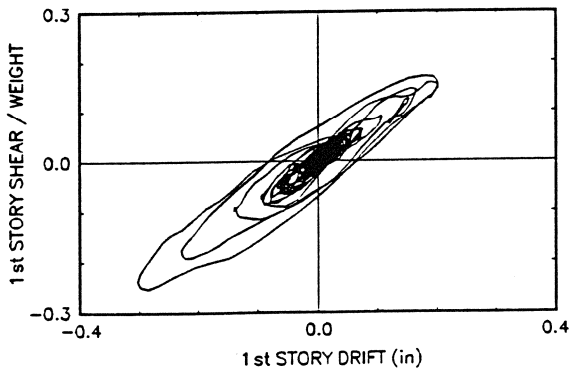

3-STORY, 6 DAMPERS, PACOIMA DAM 50%

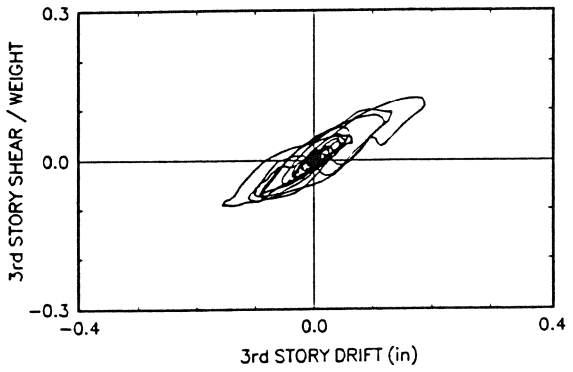

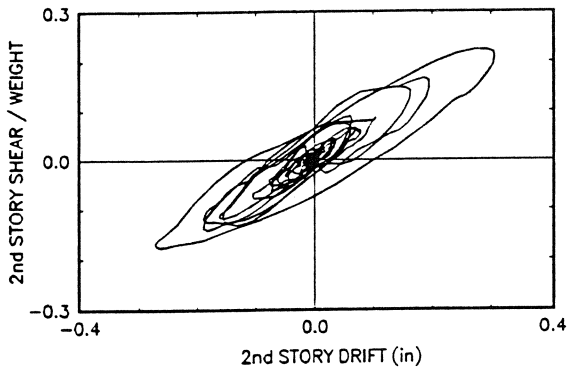

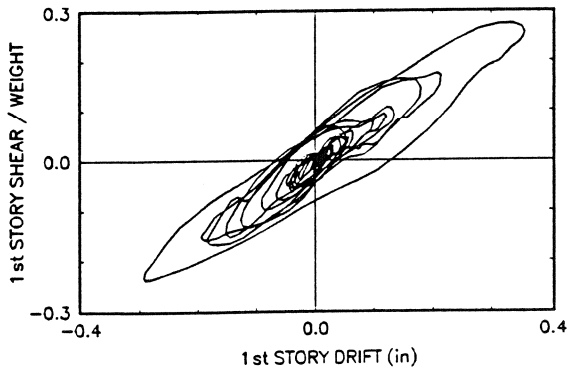

3-STORY, 6 DAMPERS, PACOIMA DAM 50% (H&V)

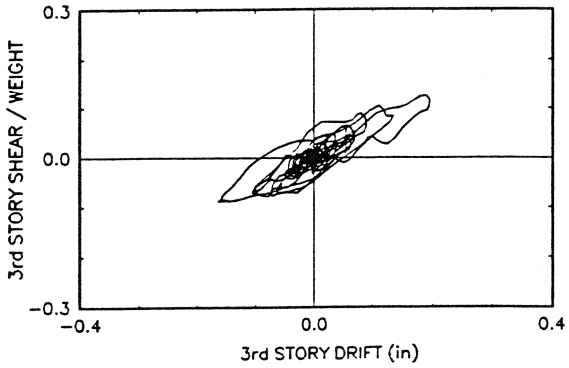

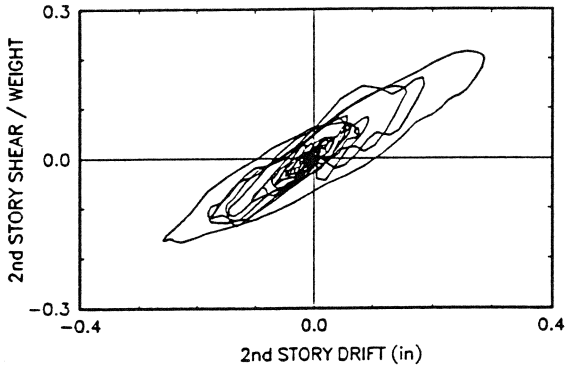

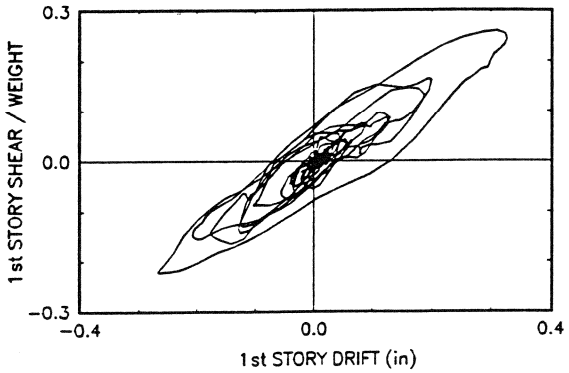

3-STORY, 6 DAMPERS, EL CENTRO 100% (H&V)

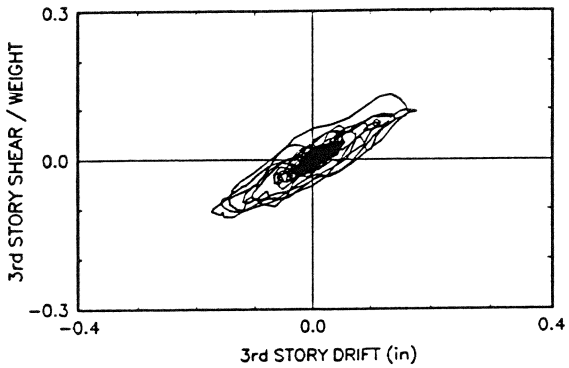

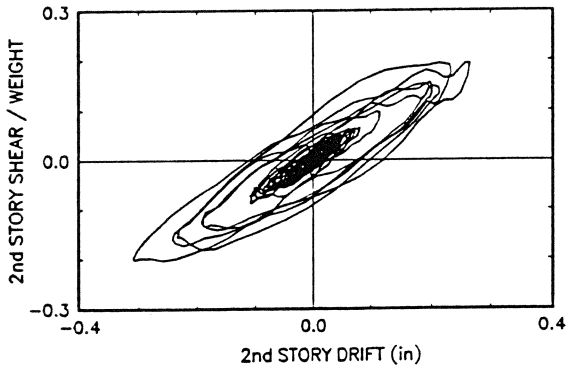

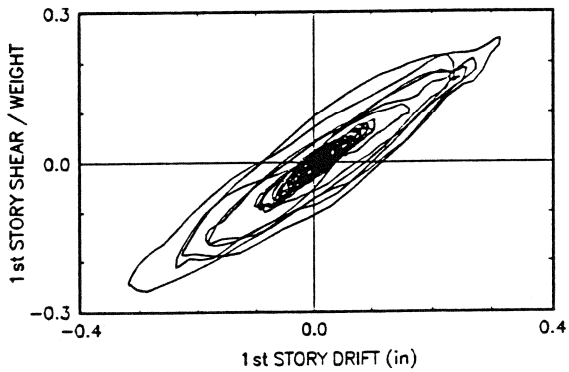

3-STORY, 6 DAMPERS, TAFT 200% (H&V)

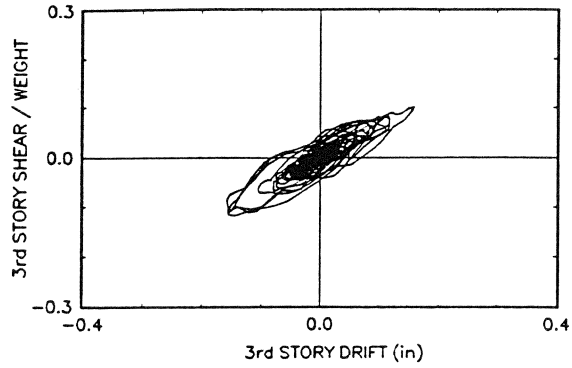

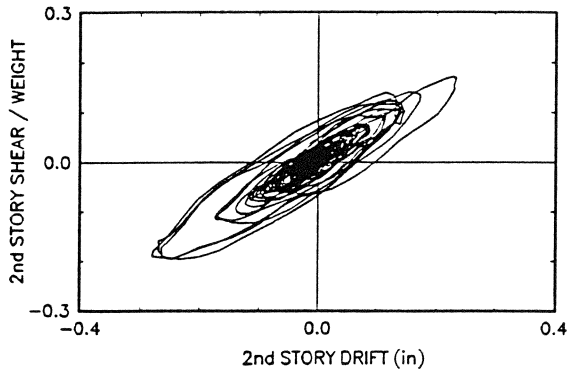

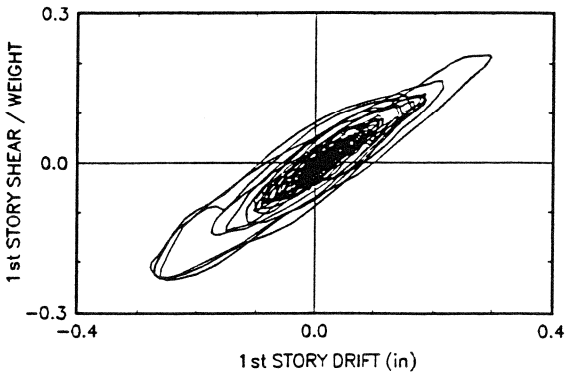

3-STORY, 2 DAMPERS, EL CENTRO 50%

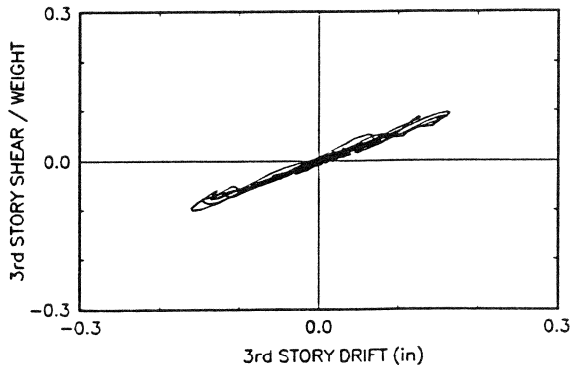

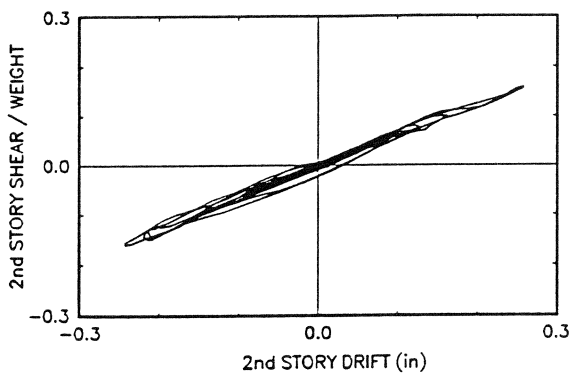

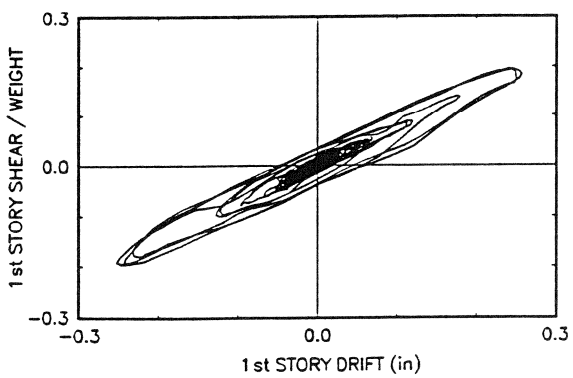

3-STORY, 2 DAMPERS, EL CENTRO 75%

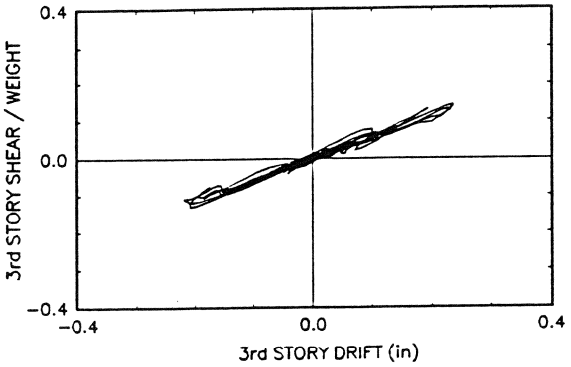

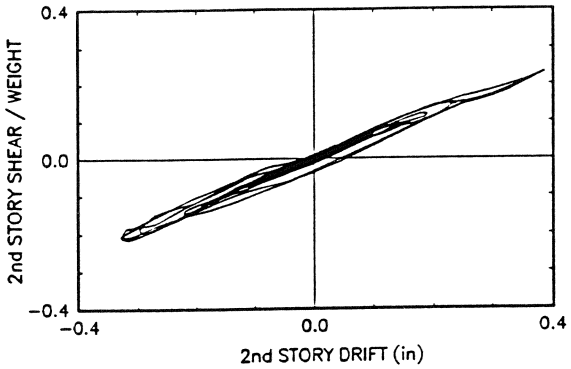

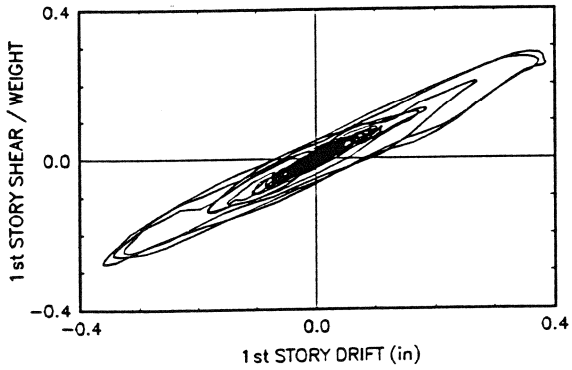

3-STORY, 2 DAMPERS, TAFT 100%

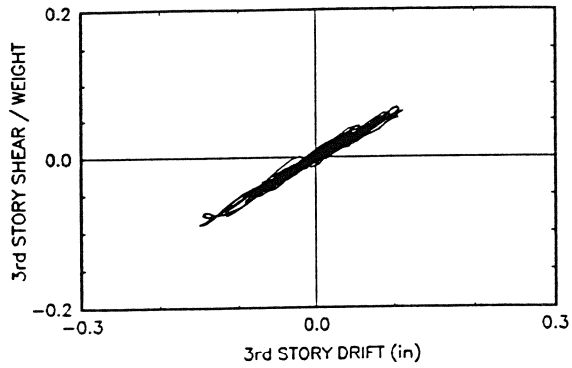

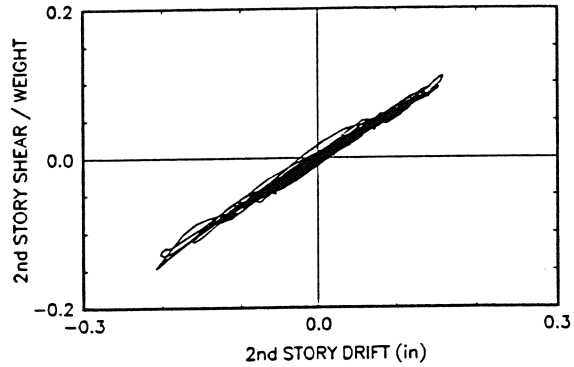

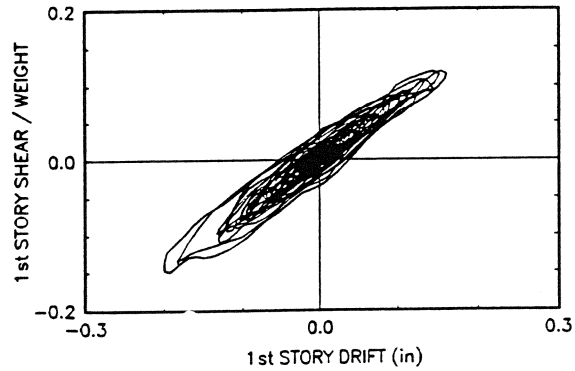

3-STORY, 2 DAMPERS, TAFT 200%

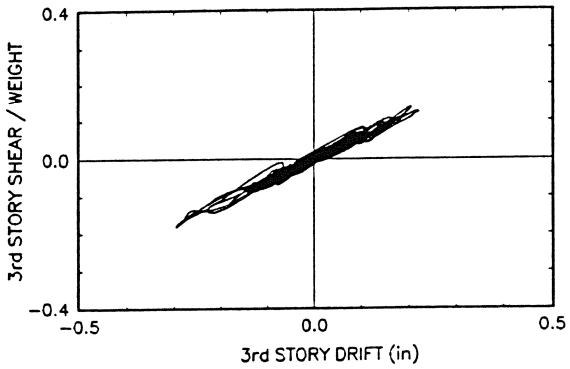

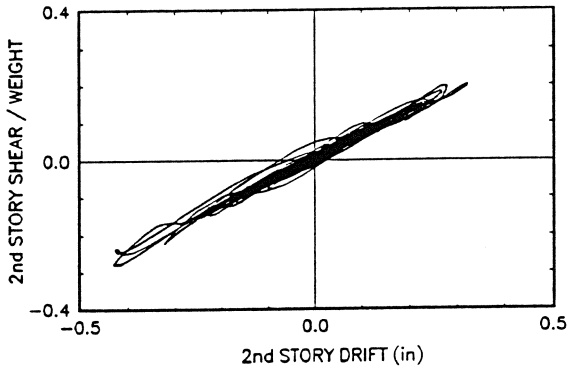

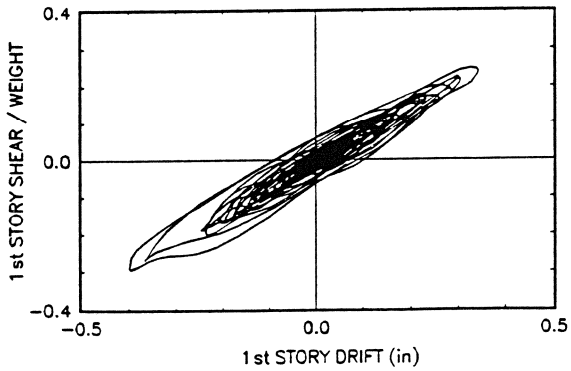

3-STORY, 4 DAMPERS, EL CENTRO 50%

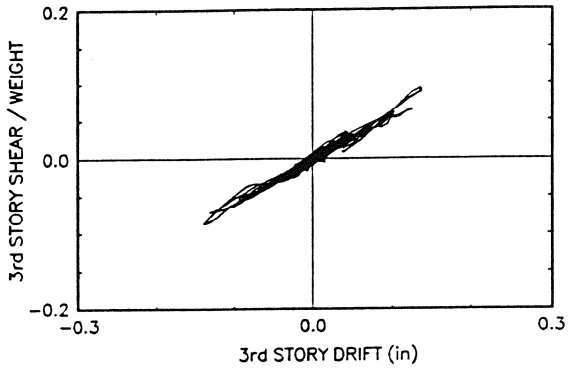

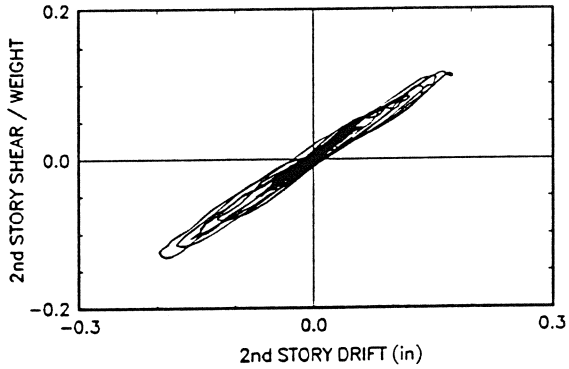

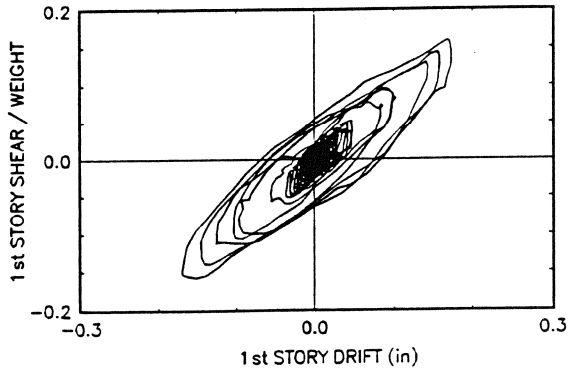

3-STORY, 4 DAMPERS, EL CENTRO 100%

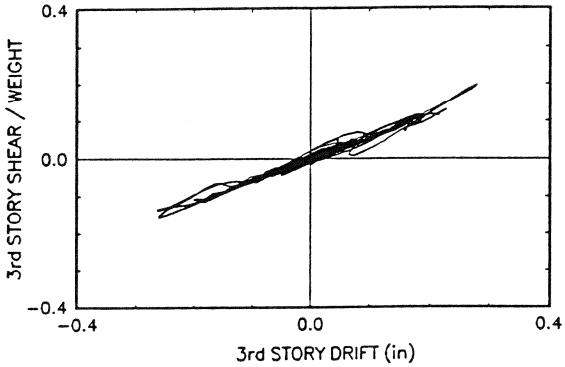

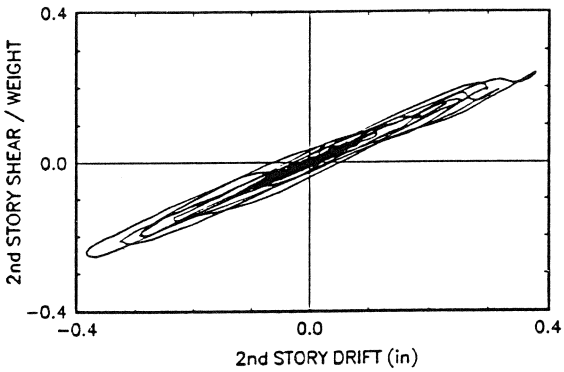

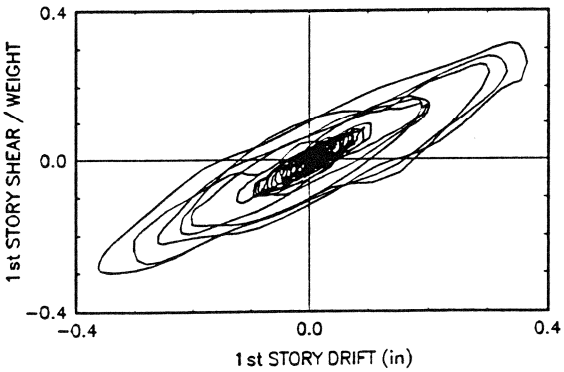

3-STORY, 4 DAMPERS, TAFT 100%

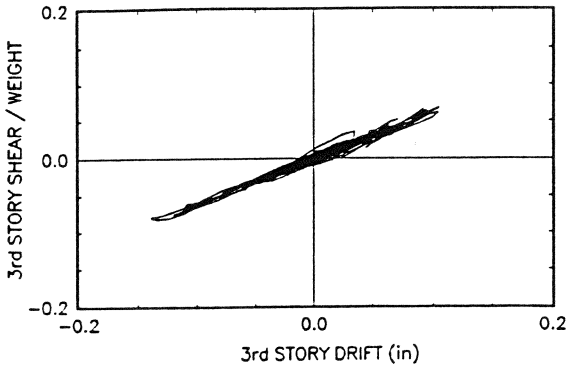

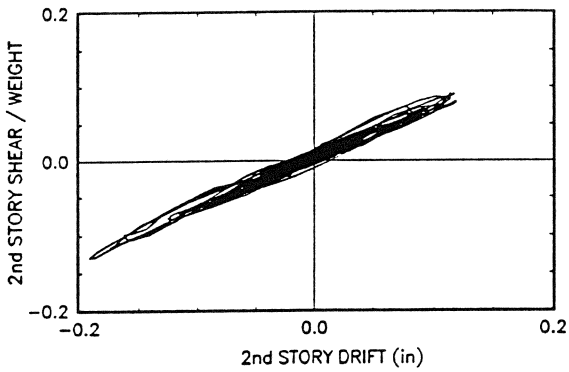

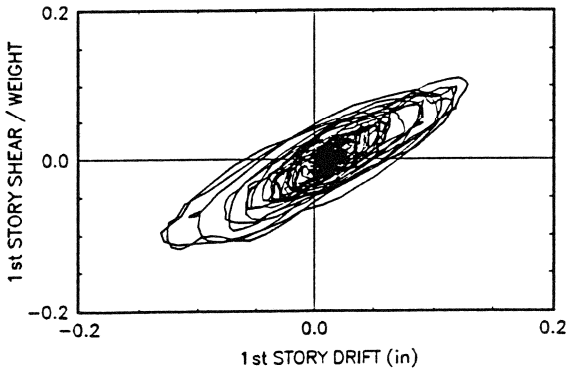

3-STORY, 4 DAMPERS, TAFT 200%

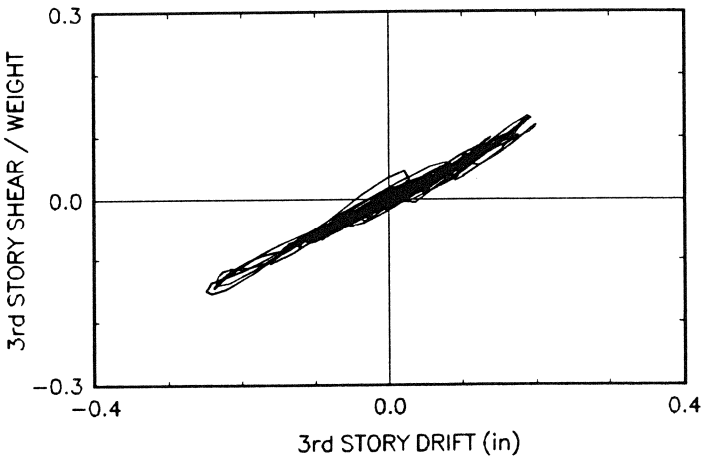

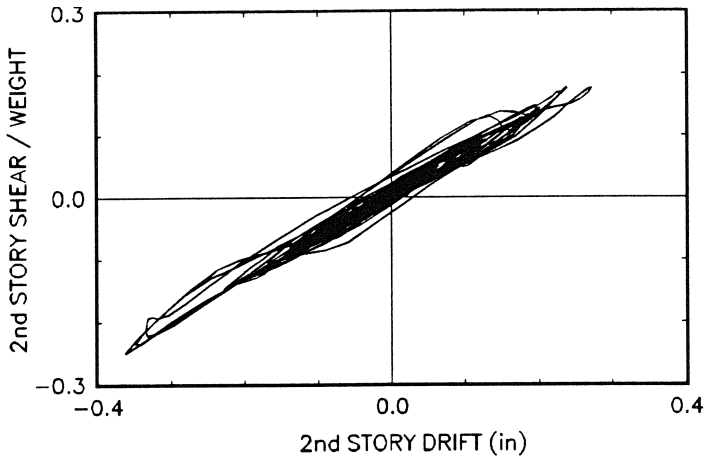

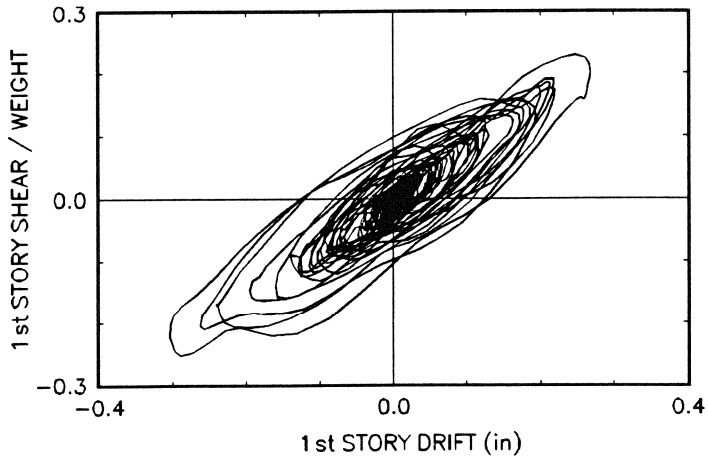

NATIONAL CENTER FOR EARTHQUAKE ENGINEERING RESEARCH
LIST OF TECHNICAL REPORTS

The National Center for Earthquake Engineering Research (NCEER) publishes technical reports on a variety of subjects related to earthquake engineering written by authors funded through NCEER. These reports are available from both NCEER's Publications Department and the National Technical Information Service (NTIS). Requests for reports should be directed to the Publications Department, National Center for Earthquake Engineering Research, State University of New York at Buffalo, Red Jacket Quadrangle, Buffalo, New York 14261. Reports can also be requested through NTIS, 5285 Port Royal Road, Springfield, Virginia 22161. NTIS accession numbers are shown in parenthesis, if available.

NCEER-87-0001 "First-Year Program in Research, Education and Technology Transfer," 3/5/87, (PB88-134275/AS).

NCEER-87-0002 "Experimental Evaluation of Instantaneous Optimal Algorithms for Structural Control," by R.C. Lin, T.T. Soong and A.M. Reinhorn, 4/20/87, (PB88-134341/AS).

NCEER-87-0003 "Experimentation Using the Earthquake Simulation Facilities at University at Buffalo," by A.M. Reinhorn and R.L. Ketter, to be published.

NCEER-87-0004 "The System Characteristics and Performance of a Shaking Table," by J.S. Hwang, K.C. Chang and G.C. Lee, 6/1/87, (PB88-134259/AS). This report is available only through NTIS (see address given above).

NCEER-87-0005 "A Finite Element Formulation for Nonlinear Viscoplastic Material Using a Q Model," by O. Gyebi and G. Dasgupta, 11/2/87, (PB88-213764/AS).

NCEER-87-0006 "Symbolic Manipulation Program (SMP) - Algebraic Codes for Two and Three Dimensional Finite Element Formulations," by X. Lee and G. Dasgupta, 11/9/87, (PB88-219522/AS).

NCEER-87-0007 "Instantaneous Optimal Control Laws for Tall Buildings Under Seismic Excitations," by J.N. Yang, A. Akbarpour and P. Ghaemmaghami, 6/10/87, (PB88-134333/AS).

NCEER-87-0008 "IDARC: Inelastic Damage Analysis of Reinforced Concrete Frame - Shear-Wall Structures," by Y.J. Park, A.M. Reinhorn and S.K. Kunnath, 7/20/87, (PB88-134325/AS).

NCEER-87-0009 "Liquefaction Potential for New York State: A Preliminary Report on Sites in Manhattan and Buffalo," by M. Budhu, V. Vijayakumar, R.F. Giese and L. Baumgras, 8/31/87, (PB88-163704/AS). This report is available only through NTIS (see address given above).

NCEER-87-0010 "Vertical and Torsional Vibration of Foundations in Inhomogeneous Media," by A.S. Veletsos and K.W. Dotson, 6/1/87, (PB88-134291/AS).

NCEER-87-0011 "Seismic Probabilistic Risk Assessment and Seismic Margins Studies for Nuclear Power Plants," by Howard H.M. Hwang, 6/15/87, (PB88-134267/AS).

NCEER-87-0012 "Parametric Studies of Frequency Response of Secondary Systems Under Ground-Acceleration Excitations," by Y. Yong and Y.K. Lin, 6/10/87, (PB88-134309/AS).

NCEER-87-0013 "Frequency Response of Secondary Systems Under Seismic Excitation," by J.A. HoLung, J. Cai and Y.K. Lin, 7/31/87, (PB88-134317/AS).

NCEER-87-0014 "Modelling Earthquake Ground Motions in Seismically Active Regions Using Parametric Time Series Methods," by G.W. Ellis and A.S. Cakmak, 8/25/87, (PB88-134283/AS).

NCEER-87-0015 "Detection and Assessment of Seismic Structural Damage," by E. DiPasquale and A.S. Cakmak, 8/25/87, (PB88-163712/AS).

NCEER-87-0016 "Pipeline Experiment at Parkfield, California," by J. Isenberg and E. Richardson, 9/15/87, (PB88-163720/AS). This report is available only through NTIS (see address given above).

NCEER-87-0017 "Digital Simulation of Seismic Ground Motion," by M. Shinozuka, G. Deodatis and T. Harada, 8/31/87, (PB88-155197/AS). This report is available only through NTIS (see address given above).

NCEER-87-0018 "Practical Considerations for Structural Control: System Uncertainty, System Time Delay and Truncation of Small Control Forces," J.N. Yang and A. Akbarpour, 8/10/87, (PB88-163738/AS).

NCEER-87-0019 "Modal Analysis of Nonclassically Damped Structural Systems Using Canonical Transformation," by J.N. Yang, S. Sarkani and F.X. Long, 9/27/87, (PB88-187851/AS).

NCEER-87-0020 "A Nonstationary Solution in Random Vibration Theory," by J.R. Red-Horse and P.D. Spanos, 11/3/87, (PB88-163746/AS).

NCEER-87-0021 "Horizontal Impedances for Radially Inhomogeneous Viscoelastic Soil Layers," by A.S. Veletsos and K.W. Dotson, 10/15/87, (PB88-150859/AS).

NCEER-87-0022 "Seismic Damage Assessment of Reinforced Concrete Members," by Y.S. Chung, C. Meyer and M. Shinozuka, 10/9/87, (PB88-150867/AS). This report is available only through NTIS (see address given above).

NCEER-87-0023 "Active Structural Control in Civil Engineering," by T.T. Soong, 11/11/87, (PB88-187778/AS).

NCEER-87-0024 "Vertical and Torsional Impedances for Radially Inhomogeneous Viscoelastic Soil Layers," by K.W. Dotson and A.S. Veletsos, 12/87, (PB88-187786/AS).

NCEER-87-0025 "Proceedings from the Symposium on Seismic Hazards, Ground Motions, Soil-Liquefaction and Engineering Practice in Eastern North America," October 20-22, 1987, edited by K.H. Jacob, 12/87, (PB88-188115/AS).

NCEER-87-0026 "Report on the Whittier-Narrows, California, Earthquake of October 1, 1987," by J. Pantelic and A. Reinhorn, 11/87, (PB88-187752/AS). This report is available only through NTIS (see address given above).

NCEER-87-0027 "Design of a Modular Program for Transient Nonlinear Analysis of Large 3-D Building Structures," by S. Srivastav and J.F. Abel, 12/30/87, (PB88-187950/AS).

NCEER-87-0028 "Second-Year Program in Research, Education and Technology Transfer," 3/8/88, (PB88-219480/AS).

NCEER-88-0001 "Workshop on Seismic Computer Analysis and Design of Buildings With Interactive Graphics," by W. McGuire, J.F. Abel and C.H. Conley, 1/18/88, (PB88-187760/AS).

NCEER-88-0002 "Optimal Control of Nonlinear Flexible Structures," by J.N. Yang, F.X. Long and D. Wong, 1/22/88, (PB88-213772/AS).

NCEER-88-0003 "Substructuring Techniques in the Time Domain for Primary-Secondary Structural Systems," by G.D. Manolis and G. Juhn, 2/10/88, (PB88-213780/AS).

NCEER-88-0004 "Iterative Seismic Analysis of Primary-Secondary Systems," by A. Singhal, L.D. Lutes and P.D. Spanos, 2/23/88, (PB88-213798/AS).

NCEER-88-0005 "Stochastic Finite Element Expansion for Random Media," by P.D. Spanos and R. Ghanem, 3/14/88, (PB88-213806/AS).

NCEER-88-0006 "Combining Structural Optimization and Structural Control," by F.Y. Cheng and C.P. Pantelides, 1/10/88, (PB88-213814/AS).

NCEER-88-0007 "Seismic Performance Assessment of Code-Designed Structures," by H.H-M. Hwang, J-W. Jaw and H-J. Shau, 3/20/88, (PB88-219423/AS).

NCEER-88-0008 "Reliability Analysis of Code-Designed Structures Under Natural Hazards," by H.H-M. Hwang, H. Ushiba and M. Shinozuka, 2/29/88, (PB88-229471/AS).

NCEER-88-0009 "Seismic Fragility Analysis of Shear Wall Structures," by J-W Jaw and H.H-M. Hwang, 4/30/88, (PB89-102867/AS).

NCEER-88-0010 "Base Isolation of a Multi-Story Building Under a Harmonic Ground Motion - A Comparison of Performances of Various Systems," by F-G Fan, G. Ahmadi and I.G. Tadjbakhsh, 5/18/88, (PB89-122238/AS).

NCEER-88-0011 "Seismic Floor Response Spectra for a Combined System by Green's Functions," by F.M. Lavelle, L.A. Bergman and P.D. Spanos, 5/1/88, (PB89-102875/AS).

NCEER-88-0012 "A New Solution Technique for Randomly Excited Hysteretic Structures," by G.Q. Cai and Y.K. Lin, 5/16/88, (PB89-102883/AS).

NCEER-88-0013 "A Study of Radiation Damping and Soil-Structure Interaction Effects in the Centrifuge," by K. Weissman, supervised by J.H. Prevost, 5/24/88, (PB89-144703/AS).

NCEER-88-0014 "Parameter Identification and Implementation of a Kinematic Plasticity Model for Frictional Soils," by J.H. Prevost and D.V. Griffiths, to be published.

NCEER-88-0015 "Two- and Three- Dimensional Dynamic Finite Element Analyses of the Long Valley Dam," by D.V. Griffiths and J.H. Prevost, 6/17/88, (PB89-144711/AS).

NCEER-88-0016 "Damage Assessment of Reinforced Concrete Structures in Eastern United States," by A.M. Reinhorn, M.J. Seidel, S.K. Kunnath and Y.J. Park, 6/15/88, (PB89-122220/AS).

NCEER-88-0017 "Dynamic Compliance of Vertically Loaded Strip Foundations in Multilayered Viscoelastic Soils," by S. Ahmad and A.S.M. Israil, 6/17/88, (PB89-102891/AS).

NCEER-88-0018 "An Experimental Study of Seismic Structural Response With Added Viscoelastic Dampers," by R.C. Lin, Z. Liang, T.T. Soong and R.H. Zhang, 6/30/88, (PB89-122212/AS). This report is available only through NTIS (see address given above).

NCEER-88-0019 "Experimental Investigation of Primary - Secondary System Interaction," by G.D. Manolis, G. Juhn and A.M. Reinhorn, 5/27/88, (PB89-122204/AS).

NCEER-88-0020 "A Response Spectrum Approach For Analysis of Nonclassically Damped Structures," by J.N. Yang, S. Sarkani and F.X. Long, 4/22/88, (PB89-102909/AS).

NCEER-88-0021 "Seismic Interaction of Structures and Soils: Stochastic Approach," by A.S. Veletsos and A.M. Prasad, 7/21/88, (PB89-122196/AS).

NCEER-88-0022 "Identification of the Serviceability Limit State and Detection of Seismic Structural Damage," by E. DiPasquale and A.S. Cakmak, 6/15/88, (PB89-122188/AS). This report is available only through NTIS (see address given above).

NCEER-88-0023 "Multi-Hazard Risk Analysis: Case of a Simple Offshore Structure," by B.K. Bhartia and E.H. Vanmarcke, 7/21/88, (PB89-145213/AS).

NCEER-88-0024 "Automated Seismic Design of Reinforced Concrete Buildings," by Y.S. Chung, C. Meyer and M. Shinozuka, 7/5/88, (PB89-122170/AS). This report is available only through NTIS (see address given above).

NCEER-88-0025 "Experimental Study of Active Control of MDOF Structures Under Seismic Excitations," by L.L. Chung, R.C. Lin, T.T. Soong and A.M. Reinhorn, 7/10/88, (PB89-122600/AS).

NCEER-88-0026 "Earthquake Simulation Tests of a Low-Rise Metal Structure," by J.S. Hwang, K.C. Chang, G.C. Lee and R.L. Ketter, 8/1/88, (PB89-102917/AS).

NCEER-88-0027 "Systems Study of Urban Response and Reconstruction Due to Catastrophic Earthquakes," by F. Kozin and H.K. Zhou, 9/22/88, (PB90-162348/AS).

NCEER-88-0028 "Seismic Fragility Analysis of Plane Frame Structures," by H.H-M. Hwang and Y.K. Low, 7/31/88, (PB89-131445/AS).

NCEER-88-0029 "Response Analysis of Stochastic Structures," by A. Kardara, C. Bucher and M. Shinozuka, 9/22/88, (PB89-174429/AS).

NCEER-88-0030 "Nonnormal Accelerations Due to Yielding in a Primary Structure," by D.C.K. Chen and L.D. Lutes, 9/19/88, (PB89-131437/AS).

NCEER-88-0031 "Design Approaches for Soil-Structure Interaction," by A.S. Veletsos, A.M. Prasad and Y. Tang, 12/30/88, (PB89-174437/AS). This report is available only through NTIS (see address given above).

NCEER-88-0032 "A Re-evaluation of Design Spectra for Seismic Damage Control," by C.J. Turkstra and A.G. Tallin, 11/7/88, (PB89-145221/AS).

NCEER-88-0033 "The Behavior and Design of Noncontact Lap Splices Subjected to Repeated Inelastic Tensile Loading," by V.E. Sagan, P. Gergely and R.N. White, 12/8/88, (PB89-163737/AS).

NCEER-88-0034 "Seismic Response of Pile Foundations," by S.M. Mamoon, P.K. Banerjee and S. Ahmad, 11/1/88, (PB89-145239/AS).

NCEER-88-0035 "Modeling of R/C Building Structures With Flexible Floor Diaphragms (IDARC2)," by A.M. Reinhorn, S.K. Kunnath and N. Panahshahi, 9/7/88, (PB89-207153/AS).

NCEER-88-0036 "Solution of the Dam-Reservoir Interaction Problem Using a Combination of FEM, BEM with Particular Integrals, Modal Analysis, and Substructuring," by C-S. Tsai, G.C. Lee and R.L. Ketter, 12/31/88, (PB89-207146/AS).

NCEER-88-0037 "Optimal Placement of Actuators for Structural Control," by F.Y. Cheng and C.P. Pantelides, 8/15/88, (PB89-162846/AS).

NCEER-88-0038 "Teflon Bearings in Aseismic Base Isolation: Experimental Studies and Mathematical Modeling," by A. Mokha, M.C. Constantinou and A.M. Reinhorn, 12/5/88, (PB89-218457/AS). This report is available only through NTIS (see address given above).

NCEER-88-0039 "Seismic Behavior of Flat Slab High-Rise Buildings in the New York City Area," by P. Weidlinger and M. Ettouney, 10/15/88, (PB90-145681/AS).

NCEER-88-0040 "Evaluation of the Earthquake Resistance of Existing Buildings in New York City," by P. Weidlinger and M. Ettouney, 10/15/88, to be published.

NCEER-88-0041 "Small-Scale Modeling Techniques for Reinforced Concrete Structures Subjected to Seismic Loads," by W. Kim, A. El-Attar and R.N. White, 11/22/88, (PB89-189625/AS).

NCEER-88-0042 "Modeling Strong Ground Motion from Multiple Event Earthquakes," by G.W. Ellis and A.S. Cakmak, 10/15/88, (PB89-174445/AS).

NCEER-88-0043 "Nonstationary Models of Seismic Ground Acceleration," by M. Grigoriu, S.E. Ruiz and E. Rosenblueth, 7/15/88, (PB89-189617/AS).

NCEER-88-0044 "SARCF User's Guide: Seismic Analysis of Reinforced Concrete Frames," by Y.S. Chung, C. Meyer and M. Shinozuka, 11/9/88, (PB89-174452/AS).

NCEER-88-0045 "First Expert Panel Meeting on Disaster Research and Planning," edited by J. Pantelic and J. Stoyle, 9/15/88, (PB89-174460/AS).

NCEER-88-0046 "Preliminary Studies of the Effect of Degrading Infill Walls on the Nonlinear Seismic Response of Steel Frames," by C.Z. Chrysostomou, P. Gergely and J.F. Abel, 12/19/88, (PB89-208383/AS).

NCEER-88-0047 "Reinforced Concrete Frame Component Testing Facility - Design, Construction, Instrumentation and Operation," by S.P. Pessiki, C. Conley, T. Bond, P. Gergely and R.N. White, 12/16/88, (PB89-174478/AS).

NCEER-89-0001 "Effects of Protective Cushion and Soil Compliancy on the Response of Equipment Within a Seismically Excited Building," by J.A. HoLung, 2/16/89, (PB89-207179/AS).

NCEER-89-0002 "Statistical Evaluation of Response Modification Factors for Reinforced Concrete Structures," by H.H-M. Hwang and J-W. Jaw, 2/17/89, (PB89-207187/AS).

NCEER-89-0003 "Hysteretic Columns Under Random Excitation," by G-Q. Cai and Y.K. Lin, 1/9/89, (PB89-196513/AS).

NCEER-89-0004 "Experimental Study of 'Elephant Foot Bulge' Instability of Thin-Walled Metal Tanks," by Z-H. Jia and R.L. Ketter, 2/22/89, (PB89-207195/AS).

NCEER-89-0005 "Experiment on Performance of Buried Pipelines Across San Andreas Fault," by J. Isenberg, E. Richardson and T.D. O'Rourke, 3/10/89, (PB89-218440/AS).

NCEER-89-0006 "A Knowledge-Based Approach to Structural Design of Earthquake-Resistant Buildings," by M. Subramani, P. Gergely, C.H. Conley, J.F. Abel and A.H. Zaghw, 1/15/89, (PB89-218465/AS).

NCEER-89-0007 "Liquefaction Hazards and Their Effects on Buried Pipelines," by T.D. O'Rourke and P.A. Lane, 2/1/89, (PB89-218481).

NCEER-89-0008 "Fundamentals of System Identification in Structural Dynamics," by H. Imai, C-B. Yun, O. Maruyama and M. Shinozuka, 1/26/89, (PB89-207211/AS).

NCEER-89-0009 "Effects of the 1985 Michoacan Earthquake on Water Systems and Other Buried Lifelines in Mexico," by A.G. Ayala and M.J. O'Rourke, 3/8/89, (PB89-207229/AS).

NCEER-89-R010 "NCEER Bibliography of Earthquake Education Materials," by K.E.K. Ross, Second Revision, 9/1/89, (PB90-125352/AS).

NCEER-89-0011 "Inelastic Three-Dimensional Response Analysis of Reinforced Concrete Building Structures (IDARC-3D), Part I - Modeling," by S.K. Kunnath and A.M. Reinhorn, 4/17/89, (PB90-114612/AS).

NCEER-89-0012 "Recommended Modifications to ATC-14," by C.D. Poland and J.O. Malley, 4/12/89, (PB90-108648/AS).

NCEER-89-0013 "Repair and Strengthening of Beam-to-Column Connections Subjected to Earthquake Loading," by M. Corazao and A.J. Durrani, 2/28/89, (PB90-109885/AS).

NCEER-89-0014 "Program EXKAL2 for Identification of Structural Dynamic Systems," by O. Maruyama, C-B. Yun, M. Hoshiya and M. Shinozuka, 5/19/89, (PB90-109877/AS).

NCEER-89-0015 "Response of Frames With Bolted Semi-Rigid Connections, Part I - Experimental Study and Analytical Predictions," by P.J. DiCorso, A.M. Reinhorn, J.R. Dickerson, J.B. Radziminski and W.L. Harper, 6/1/89, to be published.

NCEER-89-0016 "ARMA Monte Carlo Simulation in Probabilistic Structural Analysis," by P.D. Spanos and M.P. Mignolet, 7/10/89, (PB90-109893/AS).

NCEER-89-P017 "Preliminary Proceedings from the Conference on Disaster Preparedness - The Place of Earthquake Education in Our Schools," Edited by K.E.K. Ross, 6/23/89.

NCEER-89-0017 "Proceedings from the Conference on Disaster Preparedness - The Place of Earthquake Education in Our Schools," Edited by K.E.K. Ross, 12/31/89, (PB90-207895). This report is available only through NTIS (see address given above).

NCEER-89-0018 "Multidimensional Models of Hysteretic Material Behavior for Vibration Analysis of Shape Memory Energy Absorbing Devices, by E.J. Graesser and F.A. Cozzarelli, 6/7/89, (PB90-164146/AS).

NCEER-89-0019 "Nonlinear Dynamic Analysis of Three-Dimensional Base Isolated Structures (3D-BASIS)," by S. Nagarajaiah, A.M. Reinhorn and M.C. Constantinou, 8/3/89, (PB90-161936/AS). This report is available only through NTIS (see address given above).

NCEER-89-0020 "Structural Control Considering Time-Rate of Control Forces and Control Rate Constraints," by F.Y. Cheng and C.P. Pantelides, 8/3/89, (PB90-120445/AS).

NCEER-89-0021 "Subsurface Conditions of Memphis and Shelby County," by K.W. Ng, T-S. Chang and H-H.M. Hwang, 7/26/89, (PB90-120437/AS).

NCEER-89-0022 "Seismic Wave Propagation Effects on Straight Jointed Buried Pipelines," by K. Elhmadi and M.J. O'Rourke, 8/24/89, (PB90-162322/AS).

NCEER-89-0023 "Workshop on Serviceability Analysis of Water Delivery Systems," edited by M. Grigoriu, 3/6/89, (PB90-127424/AS).

NCEER-89-0024 "Shaking Table Study of a 1/5 Scale Steel Frame Composed of Tapered Members," by K.C. Chang, J.S. Hwang and G.C. Lee, 9/18/89, (PB90-160169/AS).

NCEER-89-0025 "DYNA1D: A Computer Program for Nonlinear Seismic Site Response Analysis - Technical Documentation," by Jean H. Prevost, 9/14/89, (PB90-161944/AS). This report is available only through NTIS (see address given above).

NCEER-89-0026 "1:4 Scale Model Studies of Active Tendon Systems and Active Mass Dampers for Aseismic Protection," by A.M. Reinhorn, T.T. Soong, R.C. Lin, Y.P. Yang, Y. Fukao, H. Abe and M. Nakai, 9/15/89, (PB90-173246/AS).

NCEER-89-0027 "Scattering of Waves by Inclusions in a Nonhomogeneous Elastic Half Space Solved by Boundary Element Methods," by P.K. Hadley, A. Askar and A.S. Cakmak, 6/15/89, (PB90-145699/AS).

NCEER-89-0028 "Statistical Evaluation of Deflection Amplification Factors for Reinforced Concrete Structures," by H.H.M. Hwang, J-W. Jaw and A.L. Ch'ng, 8/31/89, (PB90-164633/AS).

NCEER-89-0029 "Bedrock Accelerations in Memphis Area Due to Large New Madrid Earthquakes," by H.H.M. Hwang, C.H.S. Chen and G. Yu, 11/7/89, (PB90-162330/AS).

NCEER-89-0030 "Seismic Behavior and Response Sensitivity of Secondary Structural Systems," by Y.Q. Chen and T.T. Soong, 10/23/89, (PB90-164658/AS).

NCEER-89-0031 "Random Vibration and Reliability Analysis of Primary-Secondary Structural Systems," by Y. Ibrahim, M. Grigoriu and T.T. Soong, 11/10/89, (PB90-161951/AS).

NCEER-89-0032 "Proceedings from the Second U.S. - Japan Workshop on Liquefaction, Large Ground Deformation and Their Effects on Lifelines, September 26-29, 1989," Edited by T.D. O'Rourke and M. Hamada, 12/1/89, (PB90-209388/AS).

NCEER-89-0033 "Deterministic Model for Seismic Damage Evaluation of Reinforced Concrete Structures," by J.M. Bracci, A.M. Reinhorn, J.B. Mander and S.K. Kunnath, 9/27/89.

NCEER-89-0034 "On the Relation Between Local and Global Damage Indices," by E. DiPasquale and A.S. Cakmak, 8/15/89, (PB90-173865).

NCEER-89-0035 "Cyclic Undrained Behavior of Nonplastic and Low Plasticity Silts," by A.J. Walker and H.E. Stewart, 7/26/89, (PB90-183518/AS).

NCEER-89-0036 "Liquefaction Potential of Surficial Deposits in the City of Buffalo, New York," by M. Budhu, R. Giese and L. Baumgrass, 1/17/89, (PB90-208455/AS).

NCEER-89-0037 "A Deterministic Assessment of Effects of Ground Motion Incoherence," by A.S. Veletsos and Y. Tang, 7/15/89, (PB90-164294/AS).

NCEER-89-0038 "Workshop on Ground Motion Parameters for Seismic Hazard Mapping," July 17-18, 1989, edited by R.V. Whitman, 12/1/89, (PB90-173923/AS).

NCEER-89-0039 "Seismic Effects on Elevated Transit Lines of the New York City Transit Authority," by C.J. Costantino, C.A. Miller and E. Heymsfield, 12/26/89, (PB90-207887/AS).

NCEER-89-0040 "Centrifugal Modeling of Dynamic Soil-Structure Interaction," by K. Weissman, Supervised by J.H. Prevost, 5/10/89, (PB90-207879/AS).

NCEER-89-0041 "Linearized Identification of Buildings With Cores for Seismic Vulnerability Assessment," by I-K. Ho and A.E. Aktan, 11/1/89, (PB90-251943/AS).

NCEER-90-0001 "Geotechnical and Lifeline Aspects of the October 17, 1989 Loma Prieta Earthquake in San Francisco," by T.D. O'Rourke, H.E. Stewart, F.T. Blackburn and T.S. Dickerman, 1/90, (PB90-208596/AS).

NCEER-90-0002 "Nonnormal Secondary Response Due to Yielding in a Primary Structure," by D.C.K. Chen and L.D. Lutes, 2/28/90, (PB90-251976/AS).

NCEER-90-0003 "Earthquake Education Materials for Grades K-12," by K.E.K. Ross, 4/16/90, (PB91-113415/AS).

NCEER-90-0004 "Catalog of Strong Motion Stations in Eastern North America," by R.W. Busby, 4/3/90, (PB90-251984)/AS.

NCEER-90-0005 "NCEER Strong-Motion Data Base: A User Manual for the GeoBase Release (Version 1.0 for the Sun3)," by P. Friberg and K. Jacob, 3/31/90 (PB90-258062/AS).

NCEER-90-0006 "Seismic Hazard Along a Crude Oil Pipeline in the Event of an 1811-1812 Type New Madrid Earthquake," by H.H.M. Hwang and C-H.S. Chen, 4/16/90(PB90-258054).

NCEER-90-0007 "Site-Specific Response Spectra for Memphis Sheahan Pumping Station," by H.H.M. Hwang and C.S. Lee, 5/15/90, (PB91-108811/AS).

NCEER-90-0008 "Pilot Study on Seismic Vulnerability of Crude Oil Transmission Systems," by T. Ariman, R. Dobry, M. Grigoriu, F. Kozin, M. O'Rourke, T. O'Rourke and M. Shinozuka, 5/25/90, (PB91-108837/AS).

NCEER-90-0009 "A Program to Generate Site Dependent Time Histories: EQGEN," by G.W. Ellis, M. Srinivasan and A.S. Cakmak, 1/30/90, (PB91-108829/AS).

NCEER-90-0010 "Active Isolation for Seismic Protection of Operating Rooms," by M.E. Talbott, Supervised by M. Shinozuka, 6/8/9, (PB91-110205/AS).

NCEER-90-0011 "Program LINEARID for Identification of Linear Structural Dynamic Systems," by C-B. Yun and M. Shinozuka, 6/25/90, (PB91-110312/AS).

NCEER-90-0012 "Two-Dimensional Two-Phase Elasto-Plastic Seismic Response of Earth Dams," by A.N. Yiagos, Supervised by J.H. Prevost, 6/20/90, (PB91-110197/AS).

NCEER-90-0013 "Secondary Systems in Base-Isolated Structures: Experimental Investigation, Stochastic Response and Stochastic Sensitivity," by G.D. Manolis, G. Juhn, M.C. Constantinou and A.M. Reinhorn, 7/1/90, (PB91-110320/AS).

NCEER-90-0014 "Seismic Behavior of Lightly-Reinforced Concrete Column and Beam-Column Joint Details," by S.P. Pessiki, C.H. Conley, P. Gergely and R.N. White, 8/22/90, (PB91-108795/AS).

NCEER-90-0015 "Two Hybrid Control Systems for Building Structures Under Strong Earthquakes," by J.N. Yang and A. Danielians, 6/29/90, (PB91-125393/AS).

NCEER-90-0016 "Instantaneous Optimal Control with Acceleration and Velocity Feedback," by J.N. Yang and Z. Li, 6/29/90, (PB91-125401/AS).

NCEER-90-0017 "Reconnaissance Report on the Northern Iran Earthquake of June 21, 1990," by M. Mehrain, 10/4/90, (PB91-125377/AS).

NCEER-90-0018 "Evaluation of Liquefaction Potential in Memphis and Shelby County," by T.S. Chang, P.S. Tang, C.S. Lee and H. Hwang, 8/10/90, (PB91-125427/AS).

NCEER-90-0019 "Experimental and Analytical Study of a Combined Sliding Disc Bearing and Helical Steel Spring Isolation System," by M.C. Constantinou, A.S. Mokha and A.M. Reinhorn, 10/4/90, (PB91-125385/AS).

NCEER-90-0020 "Experimental Study and Analytical Prediction of Earthquake Response of a Sliding Isolation System with a Spherical Surface," by A.S. Mokha, M.C. Constantinou and A.M. Reinhorn, 10/11/90, (PB91-125419/AS).

NCEER-90-0021 "Dynamic Interaction Factors for Floating Pile Groups," by G. Gazetas, K. Fan, A. Kaynia and E. Kausel, 9/10/90, (PB91-170381/AS).

NCEER-90-0022 "Evaluation of Seismic Damage Indices for Reinforced Concrete Structures," by S. Rodriguez-Gomez and A.S. Cakmak, 9/30/90, PB91-171322/AS).

NCEER-90-0023 "Study of Site Response at a Selected Memphis Site," by H. Desai, S. Ahmad, E.S. Gazetas and M.R. Oh, 10/11/90, (PB91-196857/AS).

NCEER-90-0024 "A User's Guide to Strongmo: Version 1.0 of NCEER's Strong-Motion Data Access Tool for PCs and Terminals," by P.A. Friberg and C.A.T. Susch, 11/15/90, (PB91-171272/AS).

NCEER-90-0025 "A Three-Dimensional Analytical Study of Spatial Variability of Seismic Ground Motions," by L-L. Hong and A.H.-S. Ang, 10/30/90, (PB91-170399/AS).

NCEER-90-0026 "MUMOID User's Guide - A Program for the Identification of Modal Parameters," by S. Rodriguez-Gomez and E. DiPasquale, 9/30/90, (PB91-171298/AS).

NCEER-90-0027 "SARCF-II User's Guide - Seismic Analysis of Reinforced Concrete Frames," by S. Rodriguez-Gomez, Y.S. Chung and C. Meyer, 9/30/90, (PB91-171280/AS).

NCEER-90-0028 "Viscous Dampers: Testing, Modeling and Application in Vibration and Seismic Isolation," by N. Makris and M.C. Constantinou, 12/20/90 (PB91-190561/AS).

NCEER-90-0029 "Soil Effects on Earthquake Ground Motions in the Memphis Area," by H. Hwang, C.S. Lee, K.W. Ng and T.S. Chang, 8/2/90, (PB91-190751/AS).

NCEER-91-0001 "Proceedings from the Third Japan-U.S. Workshop on Earthquake Resistant Design of Lifeline Facilities and Countermeasures for Soil Liquefaction, December 17-19, 1990," edited by T.D. O'Rourke and M. Hamada, 2/1/91, (PB91-179259/AS).

NCEER-91-0002 "Physical Space Solutions of Non-Proportionally Damped Systems," by M. Tong, Z. Liang and G.C. Lee, 1/15/91, (PB91-179242/AS).

NCEER-91-0003 "Seismic Response of Single Piles and Pile Groups," by K. Fan and G. Gazetas, 1/10/91, (PB92-174994/AS).

NCEER-91-0004 "Damping of Structures: Part 1 - Theory of Complex Damping," by Z. Liang and G. Lee, 10/10/91, (PB92-197235/AS).

NCEER-91-0005 "3D-BASIS - Nonlinear Dynamic Analysis of Three Dimensional Base Isolated Structures: Part II," by S. Nagarajaiah, A.M. Reinhorn and M.C. Constantinou, 2/28/91, (PB91-190553/AS).

NCEER-91-0006 "A Multidimensional Hysteretic Model for Plasticity Deforming Metals in Energy Absorbing Devices," by E.J. Graesser and F.A. Cozzarelli, 4/9/91, (PB92-108364/AS).

NCEER-91-0007 "A Framework for Customizable Knowledge-Based Expert Systems with an Application to a KBES for Evaluating the Seismic Resistance of Existing Buildings," by E.G. Ibarra-Anaya and S.J. Fenves, 4/9/91, (PB91-210930/AS).

NCEER-91-0008 "Nonlinear Analysis of Steel Frames with Semi-Rigid Connections Using the Capacity Spectrum Method," by G.G. Deierlein, S-H. Hsieh, Y-J. Shen and J.F. Abel, 7/2/91, (PB92-113828/AS).

NCEER-91-0009 "Earthquake Education Materials for Grades K-12," by K.E.K. Ross, 4/30/91, (PB91-212142/AS).

NCEER-91-0010 "Phase Wave Velocities and Displacement Phase Differences in a Harmonically Oscillating Pile," by N. Makris and G. Gazetas, 7/8/91, (PB92-108356/AS).

NCEER-91-0011 "Dynamic Characteristics of a Full-Size Five-Story Steel Structure and a 2/5 Scale Model," by K.C. Chang, G.C. Yao, G.C. Lee, D.S. Hao and Y.C. Yeh," 7/2/91.

NCEER-91-0012 "Seismic Response of a 2/5 Scale Steel Structure with Added Viscoelastic Dampers," by K.C. Chang, T.T. Soong, S-T. Oh and M.L. Lai, 5/17/91 (PB92-110816/AS).

NCEER-91-0013 "Earthquake Response of Retaining Walls; Full-Scale Testing and Computational Modeling," by S. Alampalli and A-W.M. Elgamal, 6/20/91, to be published.

NCEER-91-0014 "3D-BASIS-M: Nonlinear Dynamic Analysis of Multiple Building Base Isolated Structures," by P.C. Tsopelas, S. Nagarajaiah, M.C. Constantinou and A.M. Reinhorn, 5/28/91, (PB92-113885/AS).

NCEER-91-0015 "Evaluation of SEAOC Design Requirements for Sliding Isolated Structures," by D. Theodossiou and M.C. Constantinou, 6/10/91, (PB92-114602/AS).

NCEER-91-0016 "Closed-Loop Modal Testing of a 27-Story Reinforced Concrete Flat Plate-Core Building," by H.R. Somaprasad, T. Toksoy, H. Yoshiyuki and A.E. Aktan, 7/15/91, (PB92-129980/AS).

NCEER-91-0017 "Shake Table Test of a 1/6 Scale Two-Story Lightly Reinforced Concrete Building," by A.G. El-Attar, R.N. White and P. Gergely, 2/28/91, (PB92-222447/AS).

NCEER-91-0018 "Shake Table Test of a 1/8 Scale Three-Story Lightly Reinforced Concrete Building," by A.G. El-Attar, R.N. White and P. Gergely, 2/28/91.

NCEER-91-0019 "Transfer Functions for Rigid Rectangular Foundations," by A.S. Veletsos, A.M. Prasad and W.H. Wu, 7/31/91, to be published.

NCEER-91-0020 "Hybrid Control of Seismic-Excited Nonlinear and Inelastic Structural Systems," by J.N. Yang, Z. Li and A. Danielians, 8/1/91, (PB92-143171/AS).

NCEER-91-0021 "The NCEER-91 Earthquake Catalog: Improved Intensity-Based Magnitudes and Recurrence Relations for U.S. Earthquakes East of New Madrid," by L. Seeber and J.G. Armbruster, 8/28/91, (PB92-176742/AS).

NCEER-91-0022 "Proceedings from the Implementation of Earthquake Planning and Education in Schools: The Need for Change - The Roles of the Changemakers," by K.E.K. Ross and F. Winslow, 7/23/91, (PB92-129998/AS).

NCEER-91-0023 "A Study of Reliability-Based Criteria for Seismic Design of Reinforced Concrete Frame Buildings," by H.H.M. Hwang and H-M. Hsu, 8/10/91, (PB92-140235/AS).

NCEER-91-0024 "Experimental Verification of a Number of Structural System Identification Algorithms," by R.G. Ghanem, H. Gavin and M. Shinozuka, 9/18/91, (PB92-176577/AS).

NCEER-91-0025 "Probabilistic Evaluation of Liquefaction Potential," by H.H.M. Hwang and C.S. Lee," 11/25/91, (PB92-143429/AS).

NCEER-91-0026 "Instantaneous Optimal Control for Linear, Nonlinear and Hysteretic Structures - Stable Controllers," by J.N. Yang and Z. Li, 11/15/91, (PB92-163807/AS).

NCEER-91-0027 "Experimental and Theoretical Study of a Sliding Isolation System for Bridges," by M.C. Constantinou, A. Kartoum, A.M. Reinhorn and P. Bradford, 11/15/91, (PB92-176973/AS).

NCEER-92-0001 "Case Studies of Liquefaction and Lifeline Performance During Past Earthquakes, Volume 1: Japanese Case Studies," Edited by M. Hamada and T. O'Rourke, 2/17/92, (PB92-197243/AS).

NCEER-92-0002 "Case Studies of Liquefaction and Lifeline Performance During Past Earthquakes, Volume 2: United States Case Studies," Edited by T. O'Rourke and M. Hamada, 2/17/92, (PB92-197250/AS).

NCEER-92-0003 "Issues in Earthquake Education," Edited by K. Ross, 2/3/92, (PB92-222389/AS).

NCEER-92-0004 "Proceedings from the First U.S. - Japan Workshop on Earthquake Protective Systems for Bridges," 2/4/92, to be published.

NCEER-92-0005 "Seismic Ground Motion from a Haskell-Type Source in a Multiple-Layered Half-Space," A.P. Theoharis, G. Deodatis and M. Shinozuka, 1/2/92, to be published.

NCEER-92-0006 "Proceedings from the Site Effects Workshop," Edited by R. Whitman, 2/29/92, (PB92-197201/AS).

NCEER-92-0007 "Engineering Evaluation of Permanent Ground Deformations Due to Seismically-Induced Liquefaction," by M.H. Baziar, R. Dobry and A-W.M. Elgamal, 3/24/92, (PB92-222421/AS).

NCEER-92-0008 "A Procedure for the Seismic Evaluation of Buildings in the Central and Eastern United States," by C.D. Poland and J.O. Malley, 4/2/92, (PB92-222439/AS).

NCEER-92-0009 "Experimental and Analytical Study of a Hybrid Isolation System Using Friction Controllable Sliding Bearings," by M.Q. Feng, S. Fujii and M. Shinozuka, 5/15/92.

NCEER-92-0010 "Seismic Resistance of Slab-Column Connections in Existing Non-Ductile Flat-Plate Buildings," by A.J. Durrani and Y. Du, 5/18/92.

NCEER-92-0011 "The Hysteretic and Dynamic Behavior of Brick Masonry Walls Upgraded by Ferrocement Coatings Under Cyclic Loading and Strong Simulated Ground Motion," by H. Lee and S.P. Prawel, 5/11/92, to be published.

NCEER-92-0012 "Study of Wire Rope Systems for Seismic Protection of Equipment in Buildings," by G.F. Demetriades, M.C. Constantinou and A.M. Reinhorn, 5/20/92.

NCEER-92-0013 "Shape Memory Structural Dampers: Material Properties, Design and Seismic Testing," by P.R. Witting and F.A. Cozzarelli, 5/26/92.

NCEER-92-0014 "Longitudinal Permanent Ground Deformation Effects on Buried Continuous Pipelines," by M.J. O'Rourke, and C. Nordberg, 6/15/92.

NCEER-92-0015 "A Simulation Method for Stationary Gaussian Random Functions Based on the Sampling Theorem," by M. Grigoriu and S. Balopoulou, 6/11/92, (PB93-127496/AS).

NCEER-92-0016 "Gravity-Load-Designed Reinforced Concrete Buildings: Seismic Evaluation of Existing Construction and Detailing Strategies for Improved Seismic Resistance," by G.W. Hoffmann, S.K. Kunnath, J.B. Mander and A.M. Reinhorn, 7/15/92, to be published.

NCEER-92-0017 "Observations on Water System and Pipeline Performance in the Limón Area of Costa Rica Due to the April 22, 1991 Earthquake," by M. O'Rourke and D. Ballantyne, 6/30/92, (PB93-126811/AS).

NCEER-92-0018 "Fourth Edition of Earthquake Education Materials for Grades K-12," Edited by K.E.K. Ross, 8/10/92.

NCEER-92-0019 "Proceedings from the Fourth Japan-U.S. Workshop on Earthquake Resistant Design of Lifeline Facilities and Countermeasures for Soil Liquefaction," Edited by M. Hamada and T.D. O'Rourke, 8/12/92.

NCEER-92-0020 "Active Bracing System: A Full Scale Implementation of Active Control," by A.M. Reinhorn, T.T. Soong, R.C. Lin, M.A. Riley, Y.P. Wang, S. Aizawa and M. Higashino, 8/14/92, (PB93-127512/AS).

NCEER-92-0021 "Empirical Analysis of Horizontal Ground Displacement Generated by Liquefaction-Induced Lateral Spreads," by S.F. Bartlett and T.L. Youd, 8/17/92, to be published.

NCEER-92-0022 "IDARC Version 3.0: Inelastic Damage Analysis of Reinforced Concrete Structures," by S.K. Kunnath, A.M. Reinhorn and R.F. Lobo, 8/31/92, to be published.

NCEER-92-0023 "A Semi-Empirical Analysis of Strong-Motion Peaks in Terms of Seismic Source, Propagation Path and Local Site Conditions, by M. Kamiyama, M.J. O'Rourke and R. Flores-Berrones, 9/9/92.

NCEER-92-0024 "Seismic Behavior of Reinforced Concrete Frame Structures with Nonductile Details, Part I: Summary of Experimental Findings of Full Scale Beam-Column Joint Tests," by A. Beres, R.N. White and P. Gergely, 9/30/92, to be published.

NCEER-92-0025 "Experimental Results of Repaired and Retrofitted Beam-Column Joint Tests in Lightly Reinforced Concrete Frame Buildings," by A. Beres, S. El-Borgi, R.N. White and P. Gergely, 10/29/92, to be published.

NCEER-92-0026 "A Generalization of Optimal Control Theory: Linear and Nonlinear Structures," by J.N. Yang, Z. Li and S. Vongchavalitkul, 11/2/92.

NCEER-92-0027 "Seismic Resistance of Reinforced Concrete Frame Structures Designed Only for Gravity Loads: Part I - Design and Properties of a One-Third Scale Model Structure," by J.M. Bracci, A.M. Reinhorn and J.B. Mander, 12/1/92, to be published.

NCEER-92-0028 "Seismic Resistance of Reinforced Concrete Frame Structures Designed Only for Gravity Loads: Part II - Experimental Performance of Subassemblages," by L.E. Aycardi, J.B. Mander and A.M. Reinhorn, 12/1/92, to be published.

NCEER-92-0029 "Seismic Resistance of Reinforced Concrete Frame Structures Designed Only for Gravity Loads: Part III - Experimental Performance and Analytical Study of a Structural Model," by J.M. Bracci, A.M. Reinhorn and J.B. Mander, 12/1/92, to be published.

NCEER-92-0030 "Evaluation of Seismic Retrofit of Reinforced Concrete Frame Structures: Part I - Experimental Performance of Retrofitted Subassemblages," by D. Choudhuri, J.B. Mander and A.M. Reinhorn, 12/8/92, to be published.

NCEER-92-0031 "Evaluation of Seismic Retrofit of Reinforced Concrete Frame Structures: Part II - Experimental Performance and Analytical Study of a Retrofitted Structural Model," by J.M. Bracci, A.M. Reinhorn and J.B. Mander, 12/8/92, to be published.

NCEER-92-0032 "Experimental and Analytical Investigation of Seismic Response of Structures with Supplemental Fluid Viscous Dampers," by M.C. Constantinou and M.D. Symans, 12/21/92.

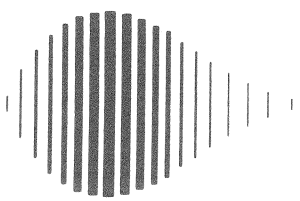

National Center for Earthquake Engineering Research
State University of New York at Buffalo